

# Development of New Adaptive Control Strategies for a Two-Link Flexible Manipulator

Santanu Kumar Pradhan



**Department of Electrical Engineering  
National Institute of Technology Rourkela  
Rourkela-769008, Orissa, India**

# Development of New Adaptive Control Strategies for a Two-Link Flexible Manipulator

*Thesis submitted in partial fulfillment  
of the requirement for the degree of*

Doctor of Philosophy

*in*

Electrical Engineering

*By*

Santanu Kumar Pradhan  
(Roll: 509EE106)

*under the guidance of*

Prof. Bidyadhar Subudhi



**Department of Electrical Engineering  
National Institute of Technology Rourkela  
April 2013**



Department of Electrical Engineering  
**National Institute of Technology Rourkela**  
Rourkela-769008, Orissa, India

## **Certificate**

This is to certify that the thesis entitled *Development of New Adaptive Control Strategies for a Two-Link Flexible Manipulator* by *Santanu Kumar Pradhan* is a record of an original research work carried out by him under my supervision and guidance in partial fulfillment of the requirements for the award of the degree of Doctor of Philosophy in Electrical Engineering during 2009-2012 in the Department of Electrical Engineering, National Institute of Technology (NIT), Rourkela. Neither this thesis nor any part of it has been submitted for any degree or academic award elsewhere.

**Dr. Bidyadhar Subudhi**

Professor

Electrical Engineering Department

Place: NIT Rourkela

Date:

*To my mother, and*

*In memory of my father*

*Sri Sraban Kumar Pradhan*

## Acknowledgement

My heartfelt gratitude first goes to my supervisor, Prof. Bidyadhar Subudhi, who introduced me to the control and robotics area, and guided me through every stage of my study and research. He also made a considerable effort to improve my written English.

I would like to thank Head of Department Prof. A. K. Panda, Prof. S. Das, Prof. D. P. Mohapatra, Prof. K. B. Mohanthy and Prof. Sandip Ghosh for their helpful and stimulating comments and suggestions in the final stages of this thesis.

I thank to all my friends for being there whenever I needed them.

I must acknowledge the academic resource that I have got from NIT, Rourkela giving me a comfortable and active environment for pursuing my research.

I would like to thank my mother and my sister for their support, endurance and endless encouragement for pursuing my research.

Finally, I particularly would like to record my warmest feelings of thanks to my wife and my son *Sidharth* who have endured a lot by tolerating my negligence of them during my research. I will remain deeply and greatly indebted and grateful to them.

*Santanu Kumar Pradhan*

## **Abstract**

Manipulators with thin and light weight arms or links are called as Flexible-Link Manipulators (FLMs). FLMs offer several advantages over rigid-link manipulators such as achieving high-speed operation, lower energy consumption, and increase in payload carrying capacity and find applications where manipulators are to be operated in large workspace like assembly of free-flying space structures, hazardous material management from safer distance, detection of flaws in large structure like airplane and submarines. However, designing a feedback control system for a flexible-link manipulator is challenging due the system being non-minimum phase, under-actuated and non-collocated. Further difficulties are encountered when such manipulators handle unknown payloads. Overall deflection of the flexible manipulator are governed by the different vibrating modes (excited at different frequencies) present along the length of the link. Due to change in payload, the flexible modes (at higher frequencies) are excited giving rise to uncertainties in the dynamics of the FLM. To achieve effective tip trajectory tracking whilst quickly suppressing tip deflections when the FLM carries varying payloads adaptive control is necessary instead of fixed gain controller to cope up with the changing dynamics of the manipulator. Considerable research has been directed in the past to design adaptive controllers based on either linear identified model of a FLM or error signal driven intelligent supervised learning e.g. neural network, fuzzy logic and hybrid neuro-fuzzy. However, the dynamics of the FLM being nonlinear there is a scope of exploiting nonlinear modeling approach to design adaptive controllers. The objective of the thesis is to design advanced adaptive control strategies for a two-link flexible manipulator (TLFM) to control the tip trajectory tracking and its deflections while handling unknown payloads.

To achieve tip trajectory control and simultaneously suppressing the tip deflection quickly when subjected to unknown payloads, first a direct adaptive control (DAC) is proposed. The proposed DAC uses a Lyapunov based nonlinear adaptive control scheme ensuring overall system stability for the control of TLFM. For the developed control laws, the stability proof of the closed-loop system is also presented. The design of this DAC involves choosing a control law with tunable TLFM parameters, and then an adaptation law is developed using the closed loop error dynamics. The performance of the developed controller is then compared with that of a fuzzy learning based adaptive controller (FLAC). The FLAC consists of three major components namely a fuzzy logic controller, a reference model and a learning mechanism. It utilizes a learning mechanism, which automatically adjusts the rule base of the fuzzy controller so that the closed loop performs according to the user defined reference model containing information of the desired behavior of the controlled system.

Although the proposed DAC shows better performance compared to FLAC but it suffers from the complexity of formulating a multivariable regressor vector for the TLFM. Also, the adaptive mechanism for parameter updates of both the DAC and FLAC depend upon feedback error based supervised learning. Hence, a reinforcement learning (RL) technique is employed to derive an adaptive controller for the TLFM. The new reinforcement learning based adaptive control (RLAC) has an advantage that it attains optimal control adaptively in on-line. Also, the performance of the RLAC is compared with that of the DAC and FLAC.

In the past, most of the indirect adaptive controls for a FLM are based on linear identified model. However, the considered TLFM dynamics is highly nonlinear. Hence, a nonlinear autoregressive moving average with exogenous input (NARMAX) model based new Self-Tuning Control (NMSTC) is proposed. The proposed adaptive controller uses a multivariable

Proportional Integral Derivative (PID) self-tuning control strategy. The parameters of the PID are adapted online using a nonlinear autoregressive moving average with exogenous-input (NARMAX) model of the TLFM. Performance of the proposed NMSTC is compared with that of RLAC.

The proposed NMSTC law suffers from over-parameterization of the controller. To overcome this a new nonlinear adaptive model predictive control using the NARMAX model of the TLFM (NMPC) developed next. For the proposed NMPC, the current control action is obtained by solving a finite horizon open loop optimal control problem on-line, at each sampling instant, using the future predicted model of the TLFM. NMPC is based on minimization of a set of predicted system errors based on available input-output data, with some constraints placed on the projected control signals resulting in an optimal control sequence. The performance of the proposed NMPC is also compared with that of the NMSTC.

Performances of all the developed algorithms are assessed by numerical simulation in MATLAB/SIMULINK environment and also validated through experimental studies using a physical TLFM set-up available in Advanced Control and Robotics Research Laboratory, National Institute of Technology Rourkela. It is observed from the comparative assessment of the performances of the developed adaptive controllers that proposed NMPC exhibits superior performance in terms of accurate tip position tracking (steady state error  $\approx 0.01^\circ$ ) while suppressing the tip deflections (maximum amplitude of the tip deflection  $\approx 0.1$  mm) when the manipulator handles variation in payload (increased payload of 0.3 kg).

The adaptive control strategies proposed in this thesis can be applied to control of complex flexible space shuttle systems, long reach manipulators for hazardous waste management from safer distance and for damping of oscillations for similar vibration systems.



# Contents

<b>Acknowledgement</b>	iii
<b>Abstract</b>	iv
<b>List of figures</b>	xiii
<b>List of tables</b>	xxiii
<b>Acronyms</b>	xxv
<b>1 Introduction.....</b>	<b>1</b>
1.1 Background.....	2
1.2 Literature Survey on Adaptive Control of Flexible Manipulators.....	5
1.2.1 Self-tuning Adaptive Control .....	5
1.2.2 Model Reference Adaptive Control .....	8
1.2.3 Lyapunov based Robust Adaptive Control .....	9
1.2.4 Adaptive Input Shaping.....	10
1.2.5 Intelligent Controllers based on Soft Computing Techniques .....	11
1.3 Motivation of the Present Work.....	17
1.4 Objective of the Thesis .....	18
1.5 Thesis Organization .....	19

<b>2 Dynamic Modeling of a Two-link Flexible Manipulator.....</b>	<b>21</b>
2.1 Introduction.....	22
2.2 Experimental Set-up.....	23
2.2.1 Hardware Components .....	24
2.2.2 Software Components .....	27
2.3 Description of the Two-Link Flexible Manipulator.....	28
2.4 Dynamic Model of the Two-Link Flexible Manipulator .....	29
2.5 Model Validation .....	34
2.6 Results and Discussions.....	34
2.7 Chapter Summary .....	40
<b>3 Direct Adaptive Control of a Two-link Flexible Manipulator.....</b>	<b>41</b>
3.1 Introduction.....	42
3.2 Direct Adaptive Control .....	42
3.3 Fuzzy Learning based Adaptive Control .....	46
3.3.1 The Fuzzy Controller.....	47
3.3.2 Reference Model .....	55
3.3.3 Learning Mechanism.....	55
3.4 Results and Discussions.....	57
3.4.1 Simulation Results for an initial payload of 0.157 kg.....	58
3.4.2 Simulation Results for an additional payload of 0.3 kg .....	64

3.4.3 Experimental Results for an initial payload of 0.157 kg .....	71
3.4.4 Experimental Results for an additional payload of 0.3 kg .....	77
3.5 Chapter Summary .....	84
<b>4 Reinforcement Learning based Adaptive Control of a Two-link Flexible Manipulator....</b>	<b>85</b>
4.1 Introduction.....	86
4.2 Reinforcement Learning based Adaptive Controller .....	88
4.2.1 Actor Critic Block .....	89
4.2.2 Critic weight update using proposed reinforcement learning algorithm .....	92
4.2.3 Actor weight update using gradient based estimator and the proposed reinforcement learning algorithm.....	95
4.2.4 Convergence analysis of the critic weights using the proposed reinforcement learning algorithm .....	96
4.3 Results and Discussions.....	99
4.3.1 Simulation Results for an initial payload of 0.157 kg.....	100
4.3.2 Simulation Results for an additional payload of 0.3 kg .....	106
4.3.3 Experimental Results for an initial payload of 0.157 kg.....	113
4.3.4 Experimental Results for an additional payload of 0.3 kg .....	120
4.4 Chapter Summary .....	127
<b>5Self-Tuning Control of a Two-link Flexible Manipulator using NARMAX model .....</b>	<b>128</b>
5.1 Introduction.....	129
5.2 Identification of the TLFM dynamics using NARMAX model .....	131

5.3 Self-Tuning Control using NARMAX model.....	134
5.4 Results and Discussions.....	138
5.4.1 Simulation Results for an initial payload of 0.157 kg.....	138
5.4.2 Simulation Results for an additional payload of 0.3 kg .....	142
5.4.3 Experimental Results for an initial payload of 0.157 kg.....	151
5.4.4 Experimental Results for an additional payload of 0.3 kg .....	157
5.5 Chapter Summary .....	164
<b>6 Nonlinear Adaptive Model Predictive Control of a Two-link Flexible Manipulator using NARMAX model.....</b>	<b>166</b>
6.1 Introduction.....	167
6.2 Nonlinear Adaptive Model Predictive Control using NARMAX model.....	168
6.3 Results and Discussions.....	173
6.3.1 Simulation Results for an initial payload of 0.157 kg.....	173
6.3.2 Simulation Results for an additional payload of 0.3 kg .....	179
6.3.3 Experimental Results for an initial payload of 0.157 kg.....	186
6.3.4 Experimental Results for an additional payload of 0.3 kg .....	192
6.4 Chapter Summary .....	199
<b>7 Conclusion and Suggestions for Future Work .....</b>	<b>201</b>
7.1 Summary of the Thesis Work .....	202
7.2 Thesis Contribution.....	205

7.3 Suggestions for Future Work .....	206
7.3.1 Adaptive Iterative Learning Control for a TLFM .....	206
7.3.2 Adaptive Visual-Servo Control for a TLFM.....	207
<b>Publications .....</b>	<b>208</b>
<b>Appendix A: Dynamic Equations of the TLFM using AMM method.....</b>	<b>210</b>
<b>References .....</b>	<b>215</b>

# List of Figures

1.1 Flexible modes of the FLM with initial payload .....	4
1.2 Flexible modes of the FLM with an additional payload .....	4
2.1 Photograph of the experimental set-up of the TLFM .....	24
2.2 Schematic of the experimental set-up showing each hardware and payload arrangement .....	25
2.3 Interfacing of signals for the TLFM set-up .....	27
2.4 Schematic diagram of a planar TLFM .....	28
2.5 Three different boundary conditions (a) Clamped-free, (b) Clamped-inertia and (c) Pinned .....	30
2.6 Torque profiles-1 for (joint-1) . .....	35
2.7 Torque profiles-1 for (joint-2) . .....	35
2.8 Joint-1 position: Torque profiles-1 .....	36
2.9 Joint-2 position: Torque profiles-1 .....	36
2.10 Link-2 tip deflection: Torque profiles-1 .....	37
2.11 Torque profiles-2 for (joint-1) .....	38
2.12 Torque profiles-2 for (joint-2) .....	38
2.13 Joint-1 position: Torque profiles-2 .....	39

2.14 Joint-2 position: Torque profiles-2 .....	39
2.15 Link-2 tip deflection: Torque profiles-2 .....	40
3.1 Direct adaptive control structure.....	43
3.2 Fuzzy logic based adaptive controller for TLFM .....	47
3.3 Membership function for Link-1 inputs $e_1$ and $\Delta e_1$ .....	48
3.4 Membership function for outputs $\tau_1$ and $\tau_2$ .....	48
3.5 Membership function for Link-2 inputs $e_2$ , $\Delta e_1$ and $\Delta e_2$ .....	48
3.6 Simulation results (time domain) for link-1 tip deflection performances (0.157 kg): DAC and FLAC .....	59
3.7 Simulation results (time domain) for link-2 tip deflection performances (0.157 kg) DAC and FLAC .....	59
3.8 Simulation results (time domain) for tip trajectory tracking errors (Link-1) (0.157 kg) DAC and FLAC.....	60
3.9 Simulation results (time domain) for tip trajectory tracking errors (Link-2) (0.157 kg): DAC and FLAC.....	60
3.10 Simulation results (time domain) for torque profiles (joint-1) (0.157 kg): DAC and FLAC	61
3.11 Simulation results (time domain) for torque profiles (joint-2) (0.157 kg): DAC and FLAC	61
3.12 Simulation results (frequency domain) link-1 tip deflection performances (0.157 kg): DAC and FLAC.....	62

3.13 Simulation results (frequency domain) for link-2 tip deflection performances (0.157 kg).....	63
3.14 Simulation results (frequency domain) for tip trajectory tracking errors (Link-1) (0.157 kg) DAC and FLAC .....	63
3.15 Simulation results (frequency domain) for tip trajectory tracking errors (Link-2) (0.157 kg): DAC and FLAC .....	64
3.16 Simulation results (time domain) for link-1 tip deflection performances (0.457 kg): DAC and FLAC.....	66
3.17 Simulation results (time domain) for link-1 tip deflection performances (0.457 kg): DAC and FLAC.....	66
3.18 Simulation results (time domain) for tip trajectory tracking errors (Link-1) (0.457 kg) DAC and FLAC.....	67
3.19 Simulation results (time domain) for tip trajectory tracking errors (Link-2) (0.457 kg) DAC and FLAC.....	67
3.20 Simulation results (time domain) for torque profiles (joint-1) (0.457 kg): DAC and FLAC	68
3.21 Simulation results (time domain) for torque profiles (joint-2) (0.457 kg): DAC and FLAC	68
3.22 Simulation results (frequency domain) for link-1 tip deflection performances (0.457 kg): DAC and FLAC .....	69
3.23 Simulation results (frequency domain) for link-1 tip deflection performances (0.457 kg): DAC and FLAC .....	69



3.24 Simulation results (frequency domain) for tip trajectory tracking errors (Link-1) (0.457 kg)	
DAC and FLAC .....	70
3.25 Simulation results (frequency domain) for tip trajectory tracking errors (Link-2) (0.457 kg)	
DAC and FLAC .....	70
3.26 Experiment results (time domain) for link-1 tip deflection performances (0.157 kg): DAC	
and FLAC.....	72
3.27 Experiment results (time domain) for link-2 tip deflection performances (0.157 kg): DAC	
and FLAC.....	73
3.28 Experiment results (time domain) for tip trajectory tracking errors (Link-1) (0.157 kg):	
DAC and FLAC .....	73
3.29 Experiment results (time domain) for tip trajectory tracking errors (Link-2) (0.157 kg):	
DAC and FLAC .....	74
3.30 Experiment results (time domain) for torque profiles (joint-1) (0.157 kg): DAC and FLAC	74
3.31 Experiment results (time domain) for torque profiles (joint-2) (0.157 kg): DAC and FLAC	75
3.32 Experiment results (frequency domain) for link-1 tip deflection performances (0.157 kg):	
DAC and FLAC .....	75
3.33 Experiment results (frequency domain) for link-2 tip deflection performances (0.157 kg):	
DAC and FLAC .....	76
3.34 Experiment results (frequency domain) for tip trajectory tracking errors (Link-1) (0.157 kg):	
DAC and FLAC .....	76

3.35 Experiment results (frequency domain) for tip trajectory tracking errors (Link-2) (0.157 kg): DAC and FLAC .....	77
3.36 Experiment results (time domain) for link-1 tip deflection performances (0.457 kg): DAC and FLAC.....	78
3.37 Experiment results (time domain) for link-2 tip deflection performances (0.457 kg): DAC and FLAC.....	78
3.38 Experiment results (time domain) for Tip trajectory tracking errors (Link-1) (0.457 kg): DAC and FLAC .....	79
3.39 Experiment results (time domain) for tip trajectory tracking errors (Link-2) (0.457 kg): DAC and FLAC .....	79
3.40 Experiment results (time domain) for torque profiles (joint-1) (0.457 kg): DAC and FLAC	80
3.41 Experiment results (time domain) for torque profiles (joint-2) (0.457 kg): DAC and FLAC	80
3.42 Experiment results (frequency domain) for link-1 tip deflection performances (0.457 kg): DAC and FLAC .....	82
3.43 Experiment results (frequency domain) for link-2 tip deflection performances (0.457 kg): DAC and FLAC .....	82
3.44 Experiment results (frequency domain) for Tip trajectory tracking errors (Link-1) (0.457 kg): DAC and FLAC.....	83
3.45 Experiment results (frequency domain) for tip trajectory tracking errors (Link-2) (0.457 kg): DAC and FLAC .....	83

4.1 Structure of reinforcement learning based adaptive control for a TLFM .....	88
4.2 Actor-Critic based Reinforcement learning .....	90
4.3 Simulation results (time domain) for tip trajectory tracking errors (Link-1) (0.157 kg): DAC, FLAC and RLAC .....	101
4.4 Simulation results (time domain) for tip trajectory tracking errors (Link-2) (0.157 kg): DAC, FLAC and RLAC .....	102
4.5 Simulation results (time domain) for comparison of link-1 tip deflection performances (Link-1) (0.157 kg): DAC, FLAC and RLAC .....	102
4.6 Simulation results (time domain) for comparison of link-2 tip deflection performances (Link-1) (0.157 kg): DAC, FLAC and RLAC .....	103
4.7 Simulation results (time domain) for torque profiles (joint-1) (Link-1) (0.157 kg): DAC, FLAC and RLAC .....	103
4.8 Simulation results (time domain) for torque profiles (joint-2) (Link-1) (0.157 kg): DAC, FLAC and RLAC .....	104
4.9 Simulation results (frequency domain) for tip trajectory tracking errors (Link-1) (0.157 kg): DAC, FLAC and RLAC .....	104
4.10 Simulation results (frequency domain) for tip trajectory tracking errors (Link-2) (0.157 kg): DAC, FLAC and RLAC .....	105
4.11 Simulation results (frequency domain) for comparison of link-1 tip deflection performances (Link-1) (0.157 kg): DAC, FLAC and RLAC .....	105

4.12 Simulation results (frequency domain) for comparison of link-2 tip deflection performances (Link-1) (0.157 kg): DAC, FLAC and RLAC .....	106
4.13 Simulation results (time domain) for tip trajectory tracking errors (Link-1) (0.457 kg): DAC, FLAC and RLAC .....	108
4.14 Simulation results (time domain) for tip trajectory tracking errors (Link-2) (0.457 kg): DAC, FLAC and RLAC .....	108
4.15 Simulation results (time domain) for comparison of link-1 tip deflection performances (Link-1) (0.457 kg): DAC, FLAC and RLAC .....	109
4.16 Simulation results (time domain) for comparison of link-2 tip deflection performances (Link-1) (0.457 kg): DAC, FLAC and RLAC .....	109
4.17 Simulation results (time domain) for torque profiles (joint-1) (0.457 kg): DAC, FLAC and RLAC .....	110
4.18 Simulation results (time domain) for torque profiles (joint-2) (0.457 kg): DAC, FLAC and RLAC .....	110
4.19 Simulation results for adaptation of the actor and critic weights to optimal values .....	111
4.20 Simulation results (frequency domain) for tip trajectory tracking errors (Link-1) (0.457 kg): DAC, FLAC and RLAC .....	111
4.21 Simulation results (frequency domain) for tip trajectory tracking errors (Link-2) (0.457 kg): DAC, FLAC and RLAC .....	112
4.22 Simulation results (frequency domain) for comparison of link-1 tip deflection performances (Link-1) (0.457 kg): DAC, FLAC and RLAC .....	112

4.23 Simulation results (frequency domain) for comparison of link-2 tip deflection performances (Link-1) (0.457 kg): DAC, FLAC and RLAC .....	113
4.24 Experiment results (time domain) for tip trajectory tracking errors (Link-1) (0.157 kg): DAC, FLAC and RLAC .....	115
4.25 Experiment results (time domain) for tip trajectory tracking errors (Link-2) (0.157 kg): DAC, FLAC and RLAC .....	115
4.26 Experiment results (time domain) for comparison of link-1 tip deflection performances (0.157 kg): DAC, FLAC and RLAC.....	116
4.27 Experiment results (time domain) for comparison of link-2 tip deflection performances (0.157 kg): DAC, FLAC and RLAC.....	116
4.28 Experiment results (time domain) for torque profiles (joint-1) (0.157 kg): DAC, FLAC and RLAC .....	117
4.29 Experiment results (time domain) for torque profiles (joint-2) (0.157 kg): DAC, FLAC and RLAC .....	117
4.30 Experiment results (frequency domain) for tip trajectory tracking errors (Link-1) (0.157 kg): DAC, FLAC and RLAC .....	118
4.31 Experiment results (frequency domain) for tip trajectory tracking errors (Link-2) (0.157 kg): DAC, FLAC and RLAC .....	118
4.32 Experiment results (frequency domain) for comparison of link-1 tip deflection performances (0.157 kg): DAC, FLAC and RLAC.....	119

4.33 Experiment results (frequency domain) for comparison of link-2 tip deflection performances (0.157 kg): DAC, FLAC and RLAC .....	119
4.34 Experiment results (time domain) for tip trajectory tracking errors (Link-1) (0.457 kg): DAC, FLAC and RLAC .....	120
4.35 Experiment results (time domain) for tip trajectory tracking errors (Link-2) (0.457 kg): DAC, FLAC and RLAC .....	121
4.36 Experiment results (time domain) for comparison of link-1 tip deflection performances (0.457 kg): DAC, FLAC and RLAC.....	121
4.37 Experiment results (time domain) for comparison of link-2 tip deflection performances (0.457 kg): DAC, FLAC and RLAC.....	122
4.38 Experiment results (time domain) for torque profiles (joint-1) (0.457 kg): DAC, FLAC and RLAC .....	122
4.39 Experiment results (time domain) for torque profiles (joint-2) (0.457 kg): DAC, FLAC and RLAC .....	123
4.40 Experimental results for adaptation of the actor and critic weights to optimal values .....	123
4.41 Experiment results (frequency domain) for tip trajectory tracking errors (Link-1) (0.457 kg): DAC, FLAC and RLAC .....	124
4.42 Experiment results (frequency domain) for tip trajectory tracking errors (Link-2) (0.457 kg): DAC, FLAC and RLAC .....	124
4.43 Experiment results (frequency domain) for comparison of link-1 tip deflection performances (0.457 kg): DAC, FLAC and RLAC.....	125

4.44 Experiment results (time domain) for comparison of link-1 tip deflection performances (0.457 kg): DAC, FLAC and RLAC .....	125
5.1 Structure of the NARMAX model of a planar TLFM .....	132
5.2 Structure for estimation of NARMAX parameters for TLFM.....	132
5.3 Structure of the NMSTC controller .....	136
5.4 Algorithm for NMSTC .....	137
5.5 Simulation results (time domain) for comparison of link-1 tip deflection performances (0.157 kg): RLAC and NMSTC .....	139
5.6 Simulation results (time domain) for comparison of link-2 tip deflection performances (0.157 kg): RLAC and NMSTC .....	140
5.7 Simulation results (time domain) tip trajectory tracking errors (Link-1) (0.157 kg): RLAC and NMSTC .....	140
5.8 Simulation results (time domain) for tip trajectory tracking errors (Link-2) (0.157 kg): RLAC and NMSTC .....	141
5.9 Simulation results (time domain) for torque profiles (joint-1) (0.157 kg): RLAC and NMSTC	141
5.10 Simulation results (time domain) for torque profiles (joint-2) (0.157 kg): RLAC and NMSTC.....	142
5.11 Simulation results (frequency domain) for comparison of link-1 tip deflection performances (0.157 kg): RLAC and NMSTC.....	142

5.12 Simulation results (frequency domain) for comparison of link-2 tip deflection performances (0.157 kg): RLAC and NMSTC.....	143
5.13 Simulation results (frequency domain) tip trajectory tracking errors (Link-1) (0.157 kg): RLAC and NMSTC .....	143
5.14 Simulation results (frequency domain) for tip trajectory tracking errors (Link-2) (0.157 kg): RLAC and NMSTC .....	144
5.15 Simulation results (time domain) for comparison of link-1 tip deflection performances (0.457 kg): RLAC and NMSTC.....	145
5.16 Simulation results (time domain) for comparison of link-2 tip deflection performances (0.457 kg): RLAC and NMSTC.....	145
5.17 Simulation results (time domain) for tip trajectory tracking errors (Link-1) (0.457 kg): RLAC and NMSTC .....	146
5.18 Simulation results (time domain) for tip trajectory tracking errors (Link-2) (0.457 kg): RLAC and NMSTC .....	146
5.19 Simulation results (time domain) for torque profiles (joint-1) (0.457 kg): RLAC and NMSTC.....	147
5.20 Simulation results (time domain) for torque profiles (joint-2) (0.457 kg): RLAC and NMSTC.....	147
5.21 Simulation results (frequency domain) for comparison of link-1 tip deflection performances (0.457 kg): RLAC and NMSTC.....	148



5.22 Simulation results (frequency domain) for comparison of link-2 tip deflection performances (0.457 kg): RLAC and NMSTC.....	148
5.23 Simulation results (frequency domain) for tip trajectory tracking errors (Link-1) (0.457 kg): RLAC and NMSTC .....	149
5.24 Simulation results (frequency domain) for tip trajectory tracking errors (Link-2) (0.457 kg): RLAC and NMSTC .....	149
5.25 Experimental results (time domain) for comparison of link-1 tip deflection performances (0.157 kg): RLAC and NMSTC.....	152
5.26 Experimental results (time domain) for comparison of link-2 tip deflection performances (0.157 kg): RLAC and NMSTC.....	152
5.27 Experimental results (time domain) for tip trajectory tracking errors (Link-1) (0.157 kg): RLAC and NMSTC .....	153
5.28 Experimental results (time domain) for tip trajectory tracking errors (Link-2) (0.157 kg): RLAC and NMSTC .....	153
5.29 Experimental results (time domain) for torque profiles (joint-1) (0.157 kg): RLAC and NMSTC) .....	154
5.30 Experimental results (time domain) for torque profiles (joint-2) (0.157 kg): RLAC and NMSTC.....	154
5.31 Experimental results (frequency domain) for comparison of link-1 tip deflection performances (0.157 kg): RLAC and NMSTC.....	155

5.32 Experimental results (frequency domain) for comparison of link-2 tip deflection performances (0.157 kg): RLAC and NMSTC .....	156
5.33 Experimental results (frequency domain) for tip trajectory tracking errors (Link-1) (0.157 kg): RLAC and NMSTC .....	156
5.34 Experimental results (frequency domain) for tip trajectory tracking errors (Link-2) (0.157 kg): RLAC and NMSTC .....	157
5.35 Experimental results (time domain) for comparison of link-1 tip deflection performances (0.457 kg): RLAC and NMSTC.....	158
5.36 Experimental results (time domain) for comparison of link-2 tip deflection performances (0.457 kg): RLAC and NMSTC.....	158
5.37 Experimental results (time domain) for tip trajectory tracking errors (Link-1) (0.457 kg): RLAC and NMSTC .....	160
5.38 Experimental results (time domain) for tip trajectory tracking errors (Link-2) (0.457 kg): RLAC and NMSTC .....	160
5.39 Experimental results (time domain) for torque profiles (joint-1) (0.457 kg): RLAC and NMSTC.....	161
5.40 Experimental results (time domain) for torque profiles (joint-2) (0.457 kg): RLAC and NMSTC.....	161
5.41 Experimental results (frequency domain) for comparison of link-1 tip deflection performances (0.457 kg): RLAC and NMSTC.....	162

5.42 Experimental results (frequency domain) for comparison of link-2 tip deflection performances (0.457 kg): RLAC and NMSTC .....	162
5.43 Experimental results (frequency domain) for tip trajectory tracking errors (Link-1) (0.457 kg): RLAC and NMSTC .....	163
5.44 Experimental results (frequency domain) for tip trajectory tracking errors (Link-2) (0.457 kg): RLAC and NMSTC .....	163
6.1 Basic Nonlinear model predictive control concept .....	168
6.1 Structure of the proposed adaptive NMPC .....	169
6.3 Algorithm for proposed adaptive NMPC .....	172
6.4 Simulation results (time domain) for comparison of link-1 tip deflection performances (0.157 kg): NMSTC and NMMPC .....	174
6.5 Simulation results (time domain) for comparison of link-2 tip deflection performances (0.157 kg): NMSTC and NMMPC .....	174
6.6 Simulation results (time domain) for tip trajectory tracking errors (Link-1) (0.157 kg): NMSTC and NMMPC .....	175
6.7 Simulation results (time domain) for tip trajectory tracking errors (Link-2) (0.157 kg): NMSTC and NMMPC .....	175
6.8 Simulation results (time domain) for torque profiles (joint-1) (0.157 kg): NMSTC and NMMPC .....	176

6.9 Simulation results (time domain) for torque profiles (joint-2) (0.157 kg): NMSTC and NMMPC.....	176
6.10 Simulation results (frequency domain) for comparison of link-1 tip deflection performances (0.157 kg): NMSTC and NMMPC .....	177
6.11 Simulation results (frequency domain) for comparison of link-2 tip deflection performances (0.157 kg): NMSTC and NMMPC .....	178
6.12 Simulation results (frequency domain) for tip trajectory tracking errors (Link-1) (0.157 kg): NMSTC and NMMPC .....	178
6.13 Simulation results (frequency domain) for tip trajectory tracking errors (Link-2) (0.157 kg): NMSTC and NMMPC .....	179
6.14 Simulation results (time domain) for comparison of link-1 tip deflection performances (0.457 kg): NMSTC and NMMPC .....	180
6.15 Simulation results (time domain) for comparison of link-2 tip deflection performances (0.457 kg): NMSTC and NMMPC .....	181
6.16 Simulation results (time domain) for tip trajectory tracking errors (Link-1) (0.457 kg): NMSTC and NMMPC .....	181
6.17 Simulation results (time domain) for tip trajectory tracking errors (Link-2) (0.457 kg): NMSTC and NMMPC .....	182
6.18 Simulation results (time domain) for torque profiles (joint-1) (0.457 kg): NMSTC and NMMPC.....	182

6.19 Simulation results (time domain) for torque profiles (joint-2) (0.457 kg): NMSTC and NMMPC.....	183
6.20 Simulation results (frequency domain) for comparison of link-1 tip deflection performances (0.457 kg): NMSTC and NMMPC .....	184
6.21 Simulation results (frequency domain) for comparison of link-2 tip deflection performances (0.457 kg): NMSTC and NMMPC .....	185
6.22 Simulation results (frequency domain) for tip trajectory tracking errors (Link-1) (0.457 kg): NMSTC and NMMPC .....	185
6.23 Simulation results (frequency domain) for tip trajectory tracking errors (Link-2) (0.457 kg): NMSTC and NMMPC .....	186
6.24 Experimental results (time domain) for comparison of link-1 tip deflection performances (0.157 kg): NMSTC and NMMPC .....	187
6.25 Experimental results (time domain) for comparison of link-2 tip deflection performances (0.157 kg): NMSTC and NMMPC .....	188
6.26 Experimental results (time domain) for tip trajectory tracking errors (Link-1) (0.157 kg): NMSTC and NMMPC .....	188
6.27 Experimental results (time domain) for tip trajectory tracking errors (Link-2) (0.157 kg): NMSTC and NMMPC .....	189
6.28 Experimental results (time domain) for torque profiles (joint-1) (0.157 kg): NMSTC and NMMPC.....	189

6.29 Experimental results (time domain) for torque profiles (joint-2) (0.157 kg): NMSTC and NMMPC.....	190
6.30 Experimental results (frequency domain) for comparison of link-1 tip deflection performances (0.157 kg): NMSTC and NMMPC.....	190
6.31 Experimental results (frequency domain) for comparison of link-2 tip deflection performances (0.157 kg): NMSTC and NMMPC.....	191
6.32 Experimental results (frequency domain) for tip trajectory tracking errors (Link-1) (0.157 kg): NMSTC and NMMPC.....	191
6.33 Experimental results (frequency domain) for tip trajectory tracking errors (Link-2) (0.157 kg): NMSTC and NMMPC.....	192
6.34 Experimental results (time domain) for comparison of link-1 tip deflection performances (0.457 kg): NMSTC and NMMPC .....	193
6.35 Experimental results (time domain) for comparison of link-2 tip deflection performances (0.457 kg): NMSTC and NMMPC .....	194
6.36 Experimental results (time domain) for tip trajectory tracking errors (Link-1) (0.457 kg): NMSTC and NMMPC .....	194
6.37 Experimental results (time domain) for tip trajectory tracking errors (Link-2) (0.457 kg): NMSTC and NMMPC .....	195
6.38 Experimental results (time domain) for torque profiles (joint-1) (0.457 kg): NMSTC and NMMPC.....	195

6.39 Experimental results (time domain) for torque profiles (joint-2) (0.457 kg): NMSTC and NMMPC.....	196
6.40 Experimental results (frequency domain) for comparison of link-1 tip deflection performances (0.457 kg): NMSTC and NMMPC.....	197
6.41 Experimental results (frequency domain) for comparison of link-2 tip deflection performances (0.457 kg): NMSTC and NMMPC.....	198
6.42 Experimental results (frequency domain) for tip trajectory tracking errors (Link-1) (0.457 kg): NMSTC and NMMPC.....	198
6.43 Experimental results (frequency domain) for tip trajectory tracking errors (Link-2) (0.457 kg): NMSTC and NMMPC.....	199

# List of Tables

2.1 Physical Parameters of the TLFM .....	27
3.1 Link-1 Rule Base of the TLFM .....	50
3.2 Link-2 Rule Base of the TLFM when $\Delta e_{2=}$ (NB).....	51
3.3 Link-2 Rule Base of the TLFM when $\Delta e_{2=}$ (NM).....	52
3.4 Link-2 Rule Base of the TLFM when $\Delta e_{2=}$ (NS) .....	52
3.5 Link-2 Rule Base of the TLFM when $\Delta e_{2=}$ (ZE) .....	53
3.6 Link-2 Rule Base of the TLFM when $\Delta e_{2=}$ (PS).....	53
3.7 Link-2 Rule Base of the TLFM when $\Delta e_{2=}$ (PM).....	54
3.8 Link-2 Rule Base of the TLFM when $\Delta e_{2=}$ (PB) .....	54
3.9 Controller Parameters for TLFM .....	58
4.1 Proposed RLS-ET-AM algorithm.....	96
4.2 Controller Parameters for RLAC .....	99
5.1 Comparison of simulation results for the controllers (RLAC and NMSTC).....	150
5.2 Comparison of experimental results for the controllers (RLAC and NMSTC).....	164



6.1 Comparison of simulation results for the controllers (NMPC and NMSTC) .....	183
6.2 Comparison of experimental results for the controllers (NMPC and NMSTC) .....	197

# Acronyms

- AMM: Assume Mode Method
- ARX: Autoregressive with Exogenous
- ARMAX: Autoregressive with Moving Average and Exogenous Input
- DAC: Direct adaptive control
- DAQ: Data acquisitions
- FEM: Finite element method
- FLC: Fuzzy logic controller
- FLM: Flexible-link manipulator
- HFNC: Hybrid Fuzzy Neuro Control
- MPC: Model Predictive Control
- MRAC: Model Reference Adaptive Control
- NARMAX: Nonlinear Autoregressive with Moving Average and Exogenous Input
- NMPC: Nonlinear Model Predictive Control
- NMSTC: NARMAX Model based Self-Tuning Control
- NN: Neural Network
- PD: Proportional Derivative
- PID: Proportional Integral Derivative
- RL: Reinforcement Learning
- RLAC: Reinforcement Learning based Adaptive Control
- RLS: Recursive Least Square

- STC: Self-Tuning Control
- TLFM: Two-Link Flexible Manipulator
- ZOH: Zero-Order Hold

# Chapter 1

## Introduction

The Chapter is organized as follows. *Section 1.1* gives a background of a flexible-link manipulator highlighting its applications, advantages over rigid-link manipulators and control complexities associated with these robots are also illustrated. *Section 1.2* presents a literature survey on the adaptive control strategies of flexible-link manipulators. Motivation of the present work is given in *Section 1.3*. Objective of the thesis are presented in *Section 1.4*. Finally, the organization of the thesis is presented in *Section 1.5*.

## 1.1. Background

Rigid-link manipulators are usually made of strong materials consequently, the manipulator is heavy. Also, the rigid structures require a large power to operate since the dynamics is sluggish and slow. These drawbacks are avoided by making the links light. Manipulators constructed with light and thin links/arms are called as flexible-link manipulators (FLMs). Due to lightweight, these manipulators exhibit many advantages such as achieving high-speed operation, lower energy consumption, and increase in payload carrying capacity over their rigid counterparts. FLMs are preferred in applications requiring large workspace where rigid ones may not be suitable, for example assembly of free-flying space structures and hazardous material management from safer distance [1]. Research on flexible manipulators is motivating and interesting due to the fact that field of robotics and automation has advanced significantly in recent years, driven by industrial requirements for quicker response times and lower power consumption. These demands have led to changes in robot arm design, using lightweight materials and modifying the physical configuration of a robot such that the links are longer and thinner. The FLMs have also several other potential applications in space exploration. In space robotics, it is in particular emphasized to use FLMs that are suitable to move pay-loads and to carry out specialized jobs (Shuttle Manipulator that is used to help the Astronauts during extra vehicular activities). Also, use of light weight flexible structured robots in space is necessary when the weight of the robots is a concern to prevent unnecessary energy consumption and to achieve higher payload-to-mass ratio.

Tip position control of a FLM is challenging due to distributed link flexibility, which makes the system non-minimum phase, under-actuated and infinite dimensional [2]. But controlling a

flexible manipulator is more difficult compared to a rigid one. The control complexities are as follows. The motion control of flexible manipulators is difficult owing to occurrence of oscillation due to flexibility distributed along the links and thus it is difficult to achieve accuracy in positioning of the end-effector. It may be noted that if one applies the control design for a rigid-manipulator to a FLM, it may lead to nonlinear control spill over into the flexible modes causing poor performance and instability. Thus, applying rigid-link manipulator control strategies to flexible robots (elasticity in both links and joints) may lead to significant deflections and the endpoint/tip/end-effector oscillates around the desired path. Thus, the static deflections could lead to non-zero values of the tip deflections due to these flexibilities. Therefore, to improve tip trajectory tracking and dynamic response near the target point, the elastic properties of the manipulator have to be taken into account when developing a control strategy for this class of robots. Tip trajectory tracking control of flexible manipulators is also difficult owing to the non-minimum phase problems due to non-collocation of actuator torques at the base of the manipulator and sensor at the end-effector. But in space applications, the use of non-collocated servo-control is essential for any automated satellite servicing module. As the manipulator is expected to maneuver with unanticipated payload at the end-effector, thus payload variability is also an important concern. Further, due to sudden change in payload, there may be large variation in manipulator parameters and that in turn adds further complexities to the FLM dynamics. It can be observed from Fig.1.1 and Fig.1.2 that due to change in payload, the rigid modes remain unchanged whereas there is a large variation in the shape of the flexible modes. Thus it becomes very difficult to control a FLM under variable payload condition using conventional fixed gain controllers. Hence, the torque applied to the actuators of a FLM to control the tip position and its deflection with changes in payload should be adaptive in nature.

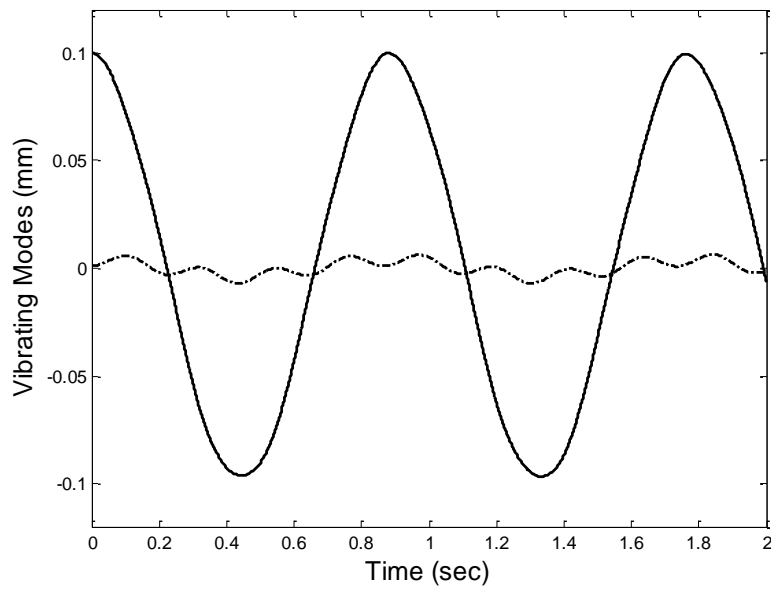


Fig.1.1 Flexible modes of the FLM with initial payload

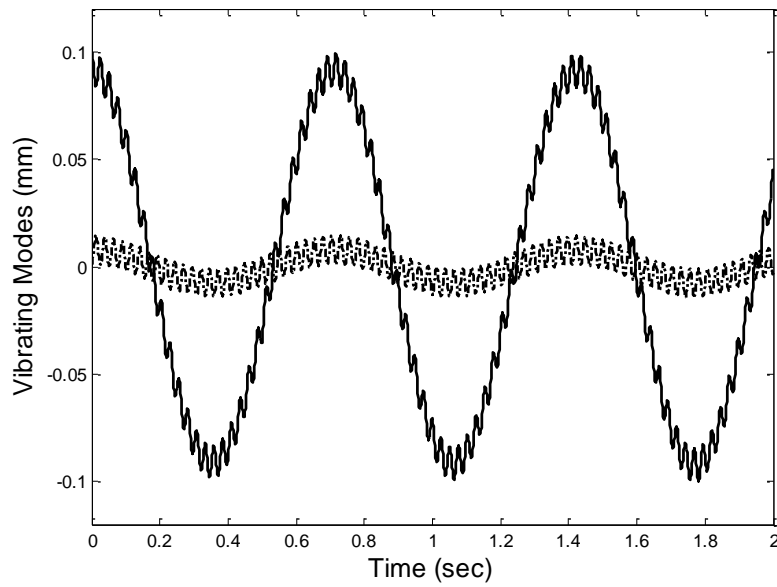


Fig.1.2 Flexible modes of the FLM with an additional payload

The controller is to be designed such that the effect of change in payload will be incorporated in the control parameter using an adaptive mechanism.

## 1.2. Literature Survey on Adaptive Control for Flexible-Link

### Manipulator

A number of approaches in the past have been reported on the development of different adaptive controller strategies for control of the tip position and its deflections of a FLM under different uncertainties for instance changes in payload and friction etc. The reported adaptive control schemes can be broadly categorized into following types: i) Self-tuning control, ii) Model reference adaptive control, iii) Lyapunov based Robust adaptive control, iv) Adaptive input shaping control, and v) Intelligent control based on neural network (NN), fuzzy logic control (FLC) and neuro-fuzzy control. This section reviews the various results obtained using different adaptive control schemes to control tip position and its deflections when a FLM handles variable payload at its tip. Several observations are made the reported approaches on adaptive control of a FLM, these are i) control structure adopted, ii) control law formation, iii) choice of control parameter updated and iv) choice of parameter adaptation law.

#### 1.2.1. Self-tuning control for a FLM

A self-tuning controller (STC) has three main elements namely a control law generator, an *on-line* dynamic FLM parameter estimator that uses measured system output and input values and an algorithm that relates the *on-line* estimated parameters and control parameters. The trade-off between choices of control law, manner in which the self-tuning control law is derived, choice of the FLM parameters to be estimated and its governing adaptation rule decides the performance



of the STC for a FLM. There have been numerous attempts since last two decades to design an efficient STC law for a FLM by many researchers for example; a STC for a two-link flexible manipulator with a flexible fore-arm has been reported in [3], where the unknown parameters of the model were estimated using an autoregressive exogenous (ARX) model of the manipulator. In [4], a frequency domain model of the single-link flexible manipulator is employed to design a proportional derivative based STC. A STC for a single-link and two-link flexible manipulator is designed to control the tip position using a time domain transfer function model in the presence of joint friction and changes in payload in [5] and [6] respectively. A nonlinear STC for a two-link flexible manipulator is presented in [7] while handling unknown payload. In [8] a digital STC for a robotic manipulator with a sliding flexible link is presented. The most important feature of the STC is its capability to vary the order of the control law adaptively. Order of the control law is varied using a lattice filter via adaptive parameter estimation. A STC is proposed for a single-link flexible manipulator with unknown load in [9]. The STC scheme reported in [9] essentially comprises a least-squares identification algorithm and a self-tuning pole placement controller. An adaptive control scheme for the tip position control of a single-link flexible manipulator handling unknown changing loads and its experimental verification is presented in [10]. The scheme essentially comprises a least squares identification algorithm and a self-tuning pole placement controller. The controller uses a recursive algorithm which constrains the control signal not to respond immediately to any sudden changes in the control gains due to changes in the parameter estimate vector. A self-tuning approach to computed torque control of a two link flexible manipulator has been proposed in [11] in which gains  $K_p$ ,  $K_d$  and  $K_i$  of the STC are adopted by using neural networks. The learning method developed in the proposed STC not only adjusts the connection weights of the NN with change in payloads but simultaneously damps the

tip vibration. An effective method for controlling flexible-link robot developed and demonstrated experimentally for end- point controller under high-frequency uncertainties in the plant and parametric uncertainties of the payload in [12]. The methodology is to design a controller that is robust to the high-frequency uncertainties, and adapt to the parametric uncertainties. Robustness to the high-frequency uncertainties is obtained using LQG control with frequency weighting of the cost function. Real time identification is effectively merged with the robust control in a self-tuning regulator approach to adapt to the parametric uncertainties of the payload. In [13], an adaptive augmented state feedback control approach to end-effector tracking of two-link flexible manipulator is presented. The highly nonlinear dynamic model of flexible manipulator has been linearized around a set of nominal operating points first. Two disturbance variables, which present the unmodeled dynamics of the manipulator, are proposed. The un-measurable disturbance variables are on-line adaptively estimated by employing a recursive filter. In [14], a STC has been developed for a discrete-time model of a single-link flexible manipulator when subjected to unknown payload. The unknown payload is then identified by using a regressor form of the system dynamics and the multi-output recursive-least-square (RLS) algorithm. Indirect adaptive control method to control single-link lightweight flexible manipulators in the presence of payload changes is presented in [15]. The overall control scheme proposed consists of three nested control loops. Once the friction and other nonlinear effects have been compensated, the inner loop is designed to give a fast motor response. The middle loop simplifies the dynamics of the system and reduces its transfer function to a double integrator. A fractional derivative controller is used to shape the outer loop into the form of a fractional order integrator. In [16] and [17], a STC comprising of a fast *on-line* closed-loop identification method

combined with an output-feedback controller of the generalized proportional integral (GPI) type for the control is presented for a flexible robotic arm.

### 1.2.2. Model reference adaptive control for a FLM

In model reference adaptive control (MRAC), the closed loop performs according to the user defined reference model containing information of the desired behavior of the controlled system. Based on a MRAC approach, a robust controller for a one link flexible arm moving along a pre-defined trajectory while subjected to handle unknown in payloads is proposed in [18]. In order to satisfy the perfect model following conditions, a linearized model of the FLM system is chosen. In [19], a discrete-time MRAC has been proposed for a flexible-link manipulator assuming as rigid model with collocated actuators and sensors. In [20], a nonlinear extension of MRAC technique to guide a double arm non-linearizable robot manipulator with flexible links, driven by actuators collocated with joints subject to uncertain payload and inertia is presented. The objective is to track a given simple nonlinear, rigid but compatible dynamical model in real, possibly stipulated time and within stipulated degree of accuracy of convergence, while avoiding collision of the arms. Fuzzy logic based MRAC has been proposed in [21]. MRAC gives satisfactory performance in case of a single-link flexible manipulator, whereas in case of more degrees of freedom (multi-link flexible manipulator), the nonlinear coupling terms in the joint variables (which are not present in the one link case) become dominant, particularly at high speed, and control performance may be degraded. Also, the choice of the reference model for a FLM dynamics is very difficult. Hence, MRAC based adaptive control design for a FLM is not popular.

### 1.2.3. Lyapunov based Robust adaptive control

A nonlinear adaptive control for a FLM has been employed in [22]. The nonlinear model of the FLM is based on a quasi-static approximation which consists of the transports subsystem and the motor equations are corrected for the elastic compliance. The adaptive control scheme presented in the paper exploits the fact that unknown parameters appear linear in dynamic equations as coefficients of known functions. The motor controller updates all unknown rigid manipulator parameters as well as elastic parameters and ensures global asymptotic stability of the tracking errors with all signals in the system remaining bounded. In [23], adaptive control law has been presented for the motion control of flexible manipulators. Asymptotical stability of the closed-loop system has been ensured by using the well-known Lyapunov theory. For preventing the observation spillover problem, a second-order analog filter in the strain gauge amplifier and a first order digital filter in the state measurement were also incorporated. In [24], an adaptive control algorithm for a single flexible link robot with a payload mass at the link's free-end is proposed. The proposed dynamic model takes into account the nonlinearities, the actuator hub dynamics, and the payload mass dynamics. The control objective is to regulate the link displacement while driving the hub position to a desired set-point. A Lyapunov-based design procedure has been employed to develop a model-based control law which fulfills the control objectives. The adaptive control strategy is composed of a boundary control torque applied to the actuator hub and a boundary control force at the link's free-end. A robust sliding mode adaptive control scheme for a flexible link robotic manipulator is presented in [25]. The design has considered the flexible dynamics as a singular perturbed system with a slow (rigid) sub systems and a fast (flexible) systems. These subsystems are separately controlled. The slow control was

achieved by means of a robust sliding adaptive approach. The flexible dynamics was controlled using  $H^\infty$  technique, which successfully handles the interaction between the slow and fast subsystems. A nonlinear adaptive and robust controller for a two-link flexible robot arm is developed in [26]. A dynamic state feedback controller is used to achieve robust regulation of the rigid modes as well as suppression of elastic vibrations. In [27], an adaptive-robust control scheme was applied to control the three axes maneuver of a flexible satellite. This controller successfully suppresses the vibrations of the flexible appendages. The piezoelectric layers were attached to the appendages and worked as actuators. The proposed adaptive-robust method is a combination of adaptive and robust controllers, and performs well in the presence of parameter uncertainty and disturbance. Advantage of these nonlinear adaptive controllers is that they provide closed-loop stability of FLMs through the nonlinear model based approach. However there lies great deal of computational complexity and presence of unmolded dynamics.

#### 1.2.4. Adaptive input shaping

An adaptive input shaper is a particular case of a finite impulse response filter that obtains the command reference by adaptively convolving the desired trajectory with a sequence of impulses [28]. An adaptive precompensation scheme is suggested in [29] which is implemented by combining a frequency domain identification scheme that is used to estimate the modal frequencies on-line. The combined adaptive input shaping scheme provides the most rapid slew that results in a vibration-free output for a single-link flexible manipulator. Adaptive input precompensators in conjunction with nonlinear controllers for multi-link flexible manipulators are presented in [30]. This is achieved by estimating the time of application of the impulses for on-line preshaping and in the case of payload uncertainty, estimation of the payload and real-

time adjustment of the nonlinear inner-loop based controller. In [31], an adaptive robust control approach is presented by combining the input shaping technique with sliding-mode control to reduce the residual vibration. In [32], a time-delay command shaping filter using a commuted shaping order approach is proposed, which leads to the development of a simple and effective adaptive command shaping technique for both single and multi-mode cases. The adaptive filter coefficients leaving fixed the number of impulses and the time delay to completely cancel the residual vibration of the given system. The work proposed in [33] describes a practical approach to investigate and develop a hybrid iterative learning control scheme with input shaping for a single-link flexible manipulator. An adaptive controller has been designed in two phases for a FLM in [34]. In which collocated position controller on the basis of a proportional-derivative feedback control technique is developed first and then an adaptive command-filter vibration controller is developed based on the dominant vibration modes of the system and placed inside the position control loop. In [35], an adaptive input shaping technique is used to control a FLM. A frequency domain identification scheme is proposed to adjust time separation of shaper impulses. This method requires a little knowledge of the FLM dynamics and is directly applicable to multimode systems, which would introduce considerable complications for identification-based schemes. Adaptive pre input shaping is an open-loop adaptive control. Major drawback of these schemes is that it does not incorporate the FLM dynamics to design the control law, hence fails to adapt when there are on-line parametric uncertainties.

#### 1.2.5. Intelligent control based on Soft-computing techniques

Soft computing techniques (Neural Network (NN), Fuzzy Logic Control (FLC) and Hybrid fuzzy-neuro control (HFNC)) have been exploited by several researchers to develop intelligent

control strategies for FLMs. It is well known that neural networks can be trained for achieving good control performances of a system without having an accurate model [36-38]. Practical implementation of a NN tracking controller on a single-link flexible manipulator is proposed in [39]. The NN controller is composed of an outer PD tracking loop, a singular perturbation inner loop for stabilization of the fast flexible-mode dynamics, and an NN inner loop used to feedback linearize the slow pointing dynamics. No off-line training or learning is needed for the NN. In [40], a NN-based controller for tip position tracking of flexible-link manipulators. The controllers are designed by utilizing the modified output re-definition approach. Four different neural network schemes are proposed. The first two schemes are developed by using a modified version of the ‘feedback error-learning’ approach to learn the inverse dynamics of the flexible manipulator. In the third scheme, the controller is designed based on tracking the hub position while controlling the elastic deflection at the tip. In the fourth scheme which employs two neural networks, the first network (referred to as the ‘output neural network’) is responsible for specifying an appropriate output for ensuring minimum phase behavior of the system. The second neural network is responsible for implementing an inverse dynamics controller. In [41] an intelligent-based control strategy for tip position tracking control of a single-link flexible manipulator is presented. The well-known inverse dynamics control strategy for rigid-link manipulators is used to design two feed-forward neural networks (NNs) are proposed to learn the nonlinearities of the flexible arm associated with the inverse dynamics controller. In [42], a neural network approach is presented for the motion control of constrained flexible manipulators, where both the contact force exerted by the flexible manipulator and the position of the end-effector contacting with a surface are controlled. Experimental results involving the control of a manipulator with one flexible link, using a conventional nonlinear harmonic drive actuator is

shown in [43], where, an adaptive control law is developed for compensating the nonlinear friction by using NNs. In [44], combined sliding mode control (SMC)-neural network (NN) approach has been employed to design a tracking control of a flexible-link manipulator. The chattering phenomenon in conventional SMC is eliminated by incorporating a saturation function in the proposed controller, and the computation burden caused by model dynamics is reduced by applying a two-layer NN with an analytical approximated upper bound, which is used to implement the uncertain function describing the FLM dynamics. A NN-based intelligent adaptive controller that introduces a new concept of intelligent supervisory loop is proposed in [45]. The scheme consists of an on-line radial basis-function NN (RBFNN) in parallel with a model reference adaptive controller (MRAC) and uses a growing dynamic RBFNN to augment MRAC. Updation of the RBFNN width, center, and weight characteristics is performed such that error reduction and improved tracking accuracy are accomplished. In [46], a scheme of multiple neural networks (MNNs) with a new strategy of combination is proposed. This combination can obtain an accumulative learning: the knowledge is increased by gradually adding more neural networks to the system. This scheme is applied to flexible link control via feedback-error-learning strategy, which is known as multi-network-feedback-error-learning. Three different neural control approaches are used to control a flexible manipulator. Advantage of a using NN based adaptive control is that it can approximate the complex nonlinear dynamics of the FLM under uncertainties, but it also suffers from prior tuning of its neural weights via a learning mechanism driven by a cost function.

Fuzzy logic uses human experience in developing control law which relies mainly on the experience of the designer when dealing with a particular system. The fuzzy logic technique has also been exploited for designing controllers for single-link flexible manipulators in [47].



Moudgal et al. in [21] proposed two FLC schemes for a two-link flexible manipulator namely, an uncoupled FLC and a coupled FLC. They showed that the coupled FLC outperformed the uncoupled one by compensating inter-action between the two flexible links. However, the coupled FLC involved more tuning factors and a huge rule base. In [48], an adaptive fuzzy controller for flexible link robot arm is derived. The design technique is a hybrid scheme involving both frequency and time domain techniques. The eigenvalues of the open loop plant can be estimated through application of a frequency domain based identification algorithm. The region of the eigenvalue space, within which the system operates, is partitioned into fuzzy cells. Membership functions are assigned to the fuzzy sets of the eigenvalue universe of discourse. The degree of uncertainty on the estimated eigenvalues is encountered through these membership functions. The knowledge data base consists of feedback gains required to place the closed loop poles at predefined locations. A rule based controller infers the control input variable weighting each with the value of the membership functions at the identified eigenvalue. A fuzzy logic using the singular perturbation approach for flexible-link robot arm control is proposed in [49]. To reduce the spillover effect, a singular perturbation approach has been exploited to derive the slow and fast subsystems. A composite control design is then adopted by superimposing both slow and fast subsystem controllers. The fast-subsystem controller damps out the vibration of the flexible structure by the linear quadratic regulator (LQR) approach. The slow-subsystem controller is a fuzzy controller that accomplishes the trajectory tracking. To guarantee the stability of the internal dynamics a boundary-layer correction based on singular perturbations has been added. In [50], a fuzzy logic controllers has been designed with a less number of membership functions (MFs) using a heuristic approach for high tracking precision and fast execution time control of a two-link flexible space robot. In [51], an adaptive fuzzy output

feedback approach is proposed for a single-link robotic manipulator coupled to a brushed direct current (DC) motor with a non-rigid joint. The controller is designed to compensate for the nonlinear dynamics associated with the mechanical subsystem and the electrical subsystems while only requiring the measurements of link position. Using fuzzy logic systems to approximate the unknown nonlinearities, an adaptive fuzzy filter observer is designed to estimate the immeasurable states. By combining the adaptive backstepping and dynamic surface control (DSC) techniques, an adaptive fuzzy output feedback control approach is developed. Stability proof of the overall closed-loop system is given via the Lyapunov direct method. In spite of numerous advantages fuzzy logic based adaptive controller for a FLM suffer from the need of expert rule base.

Subsequently, soft computing methods such as fuzzy logic and neural networks techniques were used to develop of hybrid fuzzy neural control schemes [52-53]. The above Hybrid fuzzy-neuro control (HFNC) scheme generates control actions combining contributions from both a fuzzy controller and a neural controller. The primary loop of the proposed HFNC contains a fuzzy controller and a neural network controller in the secondary loop to compensate for the coupling effects due to the rigid and flexible motion along with the inter-link coupling. A composite control using hierarchical fuzzy logic technique together has been used in [54] to control a flexible manipulator. A neuro-fuzzy controller has been used as a nonlinear compensator for a flexible four-link manipulator in [55]. Two classes of neuro-fuzzy models, the Takagi–Sugeno fuzzy model and the rectangular local linear model network have been applied for designing feed-forward controllers to compensate the nonlinearities (change in payload and joint friction). The first model incorporates expert-based fuzzy rules into the controller, whereas the second model structure automatically partitions the input space. An adaptation algorithm is

developed to train the controller in order to stabilize the whole system. Design and properties of an intelligent optimal control for a nonlinear flexible robot arm that is driven by a permanent-magnet synchronous servo motor is proposed in [56]. The intelligent optimal control system a fuzzy neural network controller is used to learn a nonlinear function in the optimal control law, and a robust controller is designed to compensate the approximation error. A simple adaptive algorithm is proposed by the authors to adjust the uncertain bound in the robust controller avoiding the chattering phenomena. The control laws of the intelligent optimal control system are derived in the sense of optimal control technique and Lyapunov stability analysis, so that system-tracking stability can be guaranteed in the closed-loop system. Design and implementation of active vibration control based on fuzzy logic and NNs is used in [57]. The proposed controller dampens the end-point vibration in a single-link flexible manipulator mounted on a two degrees-of-freedom platform. The inputs to the FLC are the angular position of the hub and the end point deflection of the flexible beam. A NN predicting the deflection was obtained using a set of three strain gauge pairs mounted on the beam and a linear-variable differential transformer placed at the tip. It also discusses how to build the rule base for the flexible beam based on the relation between the angular displacement of the hub and the end-point deflection, as well as the approach that was used to develop the NN model. Active vibration control of a single-link flexible beam using intelligent learning algorithm based on Adaptive neuro-fuzzy inference system (ANFIS) is proposed in [58].

### 1.3. Motivation of the present work

Intelligent controllers based on neural networks (NN) consume considerable amount of time for training. While the performance of a fuzzy logic controller (FLC) depends on the rules, and formulating appropriate rules is difficult. Also, the intelligent controllers using NN, FL and hybrid neuro-fuzzy based adaptive controllers (HNFAC) for a FLM are based on supervised learning [39]-[44], where the learning is driven by an error signal (difference between desired and current response). A learning method called reinforcement learning (RL), which occurs when an agent learns behavior through trial-and-error interaction with the environment based on “reinforcement” signals from the environment [59] can be introduced to design an adaptive controller for a FLM. The benefits of RL based adaptive control are that it generates adaptive optimal control *online*. Also, in past RL has been applied successfully for many complex systems such as an acrobat, elevator dispatching, dynamic cellular channel allocation and inverted pendulum etc. [60]. Hence, there is an immediate motivation to design a real-time adaptive controller based on RL technique.

A lot of research has been directed in the past to design an indirect adaptive controller for a FLM are based on linear identified model [46-49]. The limitation of such methods is that a linear model is considered to estimate the two-link flexible manipulator (TLFM) dynamics which is complex and nonlinear. Thus, there is a motivation to propose a nonlinear identified model based adaptive controller which will capture the change in TLFM dynamics due to change in payload and it will be incorporated in the tuning of the controller parameters adaptively. There is an opportunity to design a nonlinear adaptive controller using nonlinear autoregressive moving average with exogenous input (NARMAX) model of the TLFM. Also, there are some initiatives

in past to design a predictive controller for FLM, but either they consider a linear model or there is lack of adaptive tuning of control parameters in real-time. Hence a nonlinear adaptive model predictive control based on NARMAX model can be developed for the TLFM.

## 1.4. Objectives of the Thesis

The objectives of the thesis are as follows.

- To derive a mathematical model of a physical TLFM set-up and to validate the obtained model and later which model will be used for developing the adaptive controllers.
- To design and implement a direct adaptive controller (DAC) and a fuzzy learning based adaptive controller (FLAC) for controlling the tip trajectory while suppressing its deflection when subjected to handle varying payloads for a TLFM.
- To exploit reinforcement learning (RL) technique for designing a new RL based adaptive controller (RLAC) to control the tip trajectory and its deflection when subjected to handle varying payloads and compare its performances by numerical simulation and experimental validation with that of DAC and FLAC.
- To design a new self-tuning PID control by exploiting the NARMAX model (NMSTC) of the TLFM such that good tip trajectory tracking performance be achieved while quickly suppressing its deflection with varying payloads and to compare its performance with that of the RLAC.
- To design a new nonlinear adaptive model predictive control (NMPC) based on NARMAX model of the TLFM and study its performance in controlling the tip trajectory and its deflection while the end effector is subjected to carry payloads.

## 1.5. Thesis Organization

**Chapter 1** gives an overview of a flexible-link manipulator highlighting its applications and advantages over rigid-link manipulators. The control complexities associated with these robots are also illustrated. A literature survey on the adaptive control strategies of flexible-link manipulators is presented. Motivation and objectives of the thesis are described also given. Subsequently the thesis organization is presented.

**Chapter 2** develops a mathematical model of a physical two-link flexible manipulator (TLFM) available in Advanced Control and Robotics Research Laboratory, National Institute of Technology Rourkela. The resulting mathematical model will be used for development of different adaptive controllers in subsequent Chapters. The dynamic equations of the studied TLFM are derived. The resulting mathematical model is validated using open-loop response obtained from the experiment and simulation.

**Chapter 3** develops a direct adaptive controller (DAC) for achieving the tip trajectory tracking and damping its deflection while the TLFM is subjected to carry different payloads. The performances of the developed controller are then compared with that of a fuzzy learning based adaptive controller (FLAC). These two adaptive controllers are implemented on both the developed mathematical model of the TLFM and on the physical TLFM as described in Chapter 2. The simulation and experimental results show that DAC performs better than FLAC.

**Chapter 4** describes the development of a real-time adaptive controller for the TLFM by exploiting reinforcement learning (RL) technique. The proposed reinforcement learning based adaptive controller (RLAC) along with its actor-critic block and critic weights convergence are reported. Tip trajectory tracking and suppression of tip deflection performances of the proposed

RLAC are compared with that of a DAC and a FLAC developed in Chapter 3. The simulation and experimental results show that RLAC outperforms DAC and FLAC in terms of tip trajectory tracking and suppression of tip deflections.

**Chapter 5** develops a nonlinear autoregressive moving average with exogenous-input (NARMAX) model of the TLFM. Subsequently, a NARMAX model based multivariable PID self-tuning control (NMSTC) strategy is developed. The parameters of the PID are adapted *on-line* using the NARMAX model of the TLFM. NMSTC is applied to the developed mathematical model and to the physical set-up. The results envisage that NMSTC shows better performance (tip trajectory tracking and suppression of tip deflections) compared to RLAC developed in Chapter 4 while subjected to an unknown payload.

**Chapter 6** provides a NARMAX model-based nonlinear adaptive model predictive control (NMPC) strategy. The nonlinear predicted model is based on the NARMAX model is derived in Chapter 5. NMPC is applied to the developed mathematical model and to the physical TLFM set-up. The simulation and experimental results show that the tip trajectory tracking and suppression of tip deflections while subjected to an unknown payload are minimized compared to NMSTC proposed in Chapter 5.

**Chapter 7** summarizes the work described in the thesis. This chapter also includes a brief note on scope of further research that can be pursued in future as extension of this thesis work.

**Appendix A** provides details of the dynamic equations of the TLFM obtained using AMM method described in Chapter 2.

## Chapter 2

# Experimental Set-up of a Two-Link Flexible Manipulator and its Modeling

In this chapter, a mathematical model for a two-link flexible manipulator (TLFM) available in Advanced Control and Robotics Research Lab., National Institute of Technology Rourkela is developed. This model will be used for development of different adaptive controllers in subsequent Chapters. Section 2.2 presents the hardware and software details of the experimental TLFM set-up. The dynamic equations of this physical TLFM are derived in Section 2.3. The derivation for the dynamic model of studied TLFM is given in Section 2.4. Finally in Section 2.5, the obtained mathematical model is validated using open-loop response of the physical robot exciting with different bang-bang torque signals.



## 2.1. Introduction

Unlike rigid manipulators, the dynamics of FLMs possess mechanical flexibilities in the links. Link flexibility is a consequence of the lightweight constructional feature in manipulator arms that are designed to operate at high speed with low inertia [61-64]. Thus, FLM undergo two types of motion, i.e. rigid and flexible motion. Because of the interaction of these motions, the resulting dynamic equations of FLM are highly complex and in turn, the control task becomes more challenging compared to that for rigid robots. Therefore, a first step towards designing an efficient control strategy for these manipulators must be aimed at developing accurate dynamic models that can characterize the above flexibilities along with the rigid dynamics. Because of the distributed link flexure, the dynamics of FLM is difficult than rigid ones. Due to the distributed link flexure, the dynamics of the FLM becomes distributed parameter system. A number of approaches to model such distributed parameter system has been reported in literature. Modeling of the flexible robots using both assumed mode method (AMM) and finite element methods (FEM) are very efficient approaches as these method model the distributed link flexure with good accuracy. In [65], the dynamics of a single-link flexible manipulator using Lagrange's equation and the AMM was studied. A nonlinear model of flexible link is derived and then linearized it to design a linear controller design in [66]. A complete nonlinear model for a single flexible link robot using AMM model is also carried out by Luca and Siciliano in [67]. Their work is concerned with different modes of vibration and an inversion controller design based on the AMM. They have also extended the model to the two link flexible manipulator in [68] and same work has been again extended with payload variation by Ahmad [69].

Therefore in this *Chapter* the dynamic equations of a TLFM are derived using Lagrangian dynamics and AMM model. The links are modeled using Euler-Bernoulli's beam equation. The following assumptions are made in order to simplify the TLFM dynamics for the development of a dynamic model of the TLFM [70]:

- Each link is assumed to be long and slender. Therefore, transverse shear and the rotary inertia effects are negligible.
- The motion of each link is assumed to be in the horizontal plane.
- Links are considered to have constant cross-sectional area and uniform material properties, i.e. with constant mass density and Young's modulus, etc.
- Motion of the links can have deformations in the horizontal direction only.

## 2.2. Experimental set-up of the TLFM

In this section, the experimental flexible robot hardware set-up with the sensors, actuators, and digital processor etc. are described in detail. This set up is manufactured by m/s Quanser pvt. Ltd., USA. The set-up has two links and two joints and an end effector to carry payload. There is an arrangement available for connecting payload at the end effector. The photograph of the experimental set-up is shown in Fig.2.1. The hardware and software components for the experimental set-up are described next.

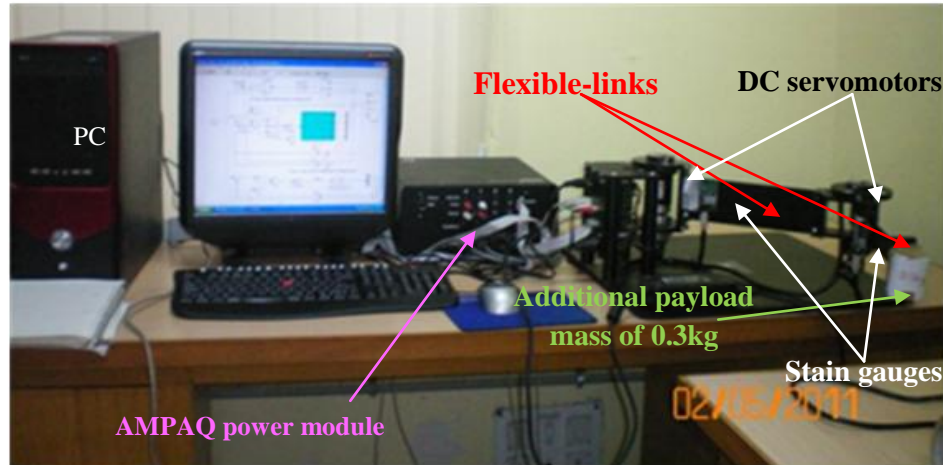


Fig.2.1 Photograph of the experimental set-up of the TLFM

### 2.2.1. Hardware Components

The hardware components of the TLFM experimental set-up are shown in Fig.2.2 which constitute of a data acquisition board, two-channel linear current amplifier, a personal computer (PC) with Intel(R) core (TM) 2 DUO E7400 processor and operates at 2.8 GHz clock cycle., an interface board, a two-link flexible manipulator with digital optical encoders and two strain gauges at the base of each link. TLFM is provided with one pair of flexible links. This pair is made of one three-inch wide steel beam and another beam which is one-and-a-half-inch wide. Data acquisition board (DAQ) provides two Analog-to-Digital (A/D) converters on board. Each A/D converter handles four channels, for a total of 8 single-ended analog inputs. Each A/D samples signal from all four channels simultaneously and holds the sampled signals while it converts the analog value to a 14-bit digital code. Each channel includes anti-aliasing filtering and input protection against electrostatic discharge (ESD) and improper connections. The input voltage ranges from -10V to +10V. Also there are two 12-bit digital-to-analog (D/A) converters on board. Each D/A converter outputs four channels, for a total of 8 analog outputs. The D/A

converters are double buffered, so new output values can be preloaded in to the D/A converters, and all analog outputs updated simultaneously. DAQ board has 32 channels of digital input-output (I/O). The channels are individually programmable as an input or an output port. All 32 channels may be read or written simultaneously.

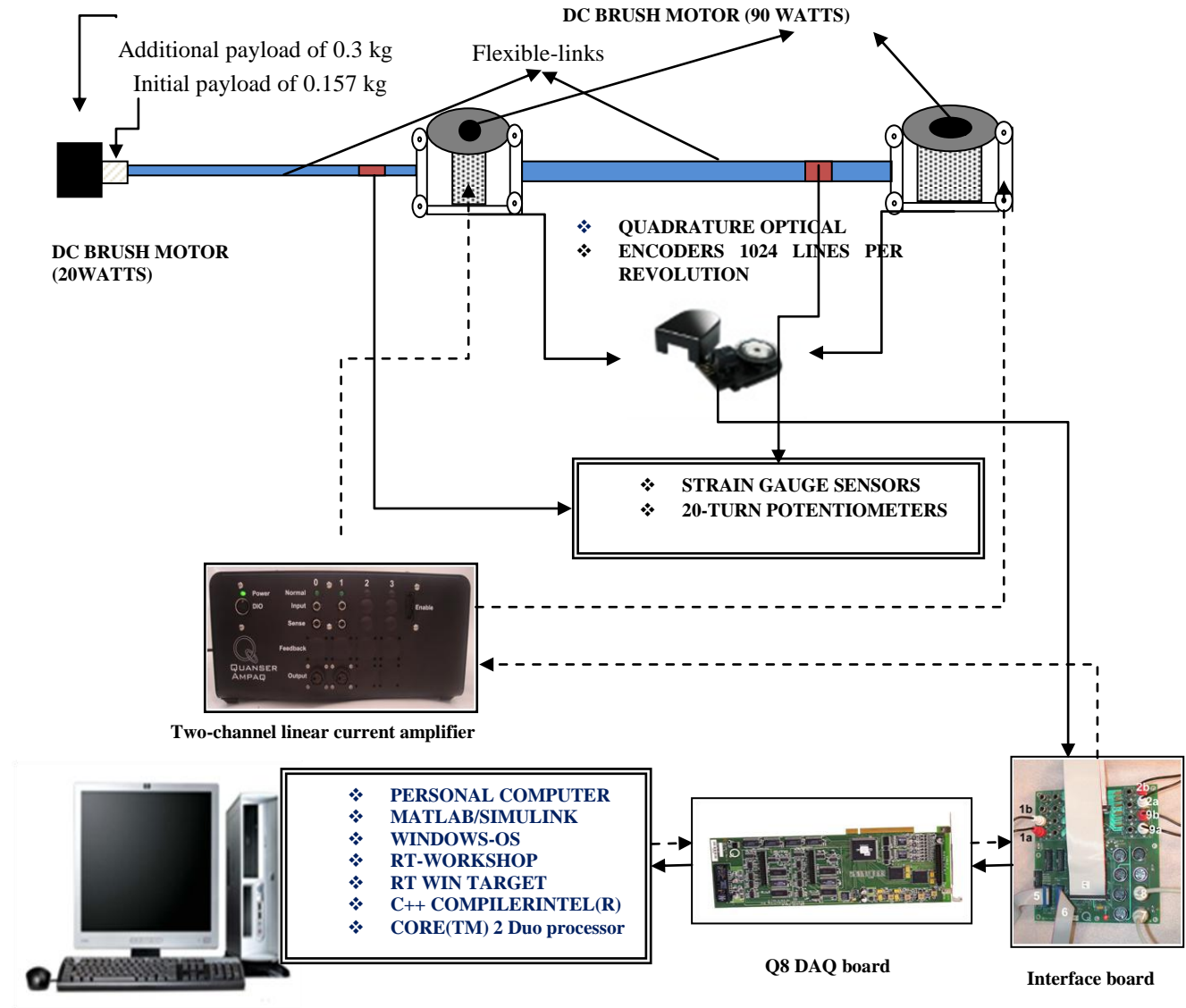


Fig.2.2 Schematic of the experimental set-up showing each hardware and payload arrangement

The outputs are TTL and CMOS compatible [71]. DAQ board contains four encoder chips, for position measurement each handles two channels, for a total of 8 encoder inputs. All four encoder chips can be accessed in a single 32-bit operation, and both channels can be accessed at the same time per chip. Hence, all eight encoder inputs may be processed simultaneously. There are two 32-bit general purpose counters on the DAQ board which can be used as PWM outputs with 30 ns resolution. For example, each counter can generate a 10-bit, 16 kHz, PWM signal. The TLFM is driven by two DC servo motors located at the bottom of the hub and between the joint of two links. They are permanent magnet, brush type DC servo motors which generate a torque  $\tau_i = K_t I_i(t)$ , where  $I_i(t)$  is motor current for  $i^{\text{th}}$  joint whereas  $K_{t1} = 0.119\text{Nm/A}$  and  $K_{t2} = 0.0234\text{Nm/A}$ . Since the motors are high-speed and relatively low-torque actuators, they are coupled to the joints through a harmonic drive speed increaser with a gear ratio of 1:100 and 1:50 for joint-1 and joint-2 respectively. They facilitate in increase in the speed of the motors, needed to accelerate the links. The optical incremental encoder is attached to the DC servo motor making the hub position  $\theta_i$  digitally available. This digital signal is decoded through an integrated circuitry on the interface board for feeding back. In addition to 32 digital I/O channels, the DAQ board has four additional channels for special two digital inputs and two digital outputs. One strain gauge sensor to measure the bending deformation of the link is mounted at the clamped base of each flexible link. Each strain gauge sensor is connected to its own signal conditioning and amplifier board. The amplifier board is equipped with two 20-turn potentiometers.

Physical parameters of the experimental TLFM together with its drive mechanism are given in Table 2.1.

Table 2.1: Physical Parameters of the TLFM

Parameter	Link-1	Link-2
Link length	0.201m	0.2m
Elasticity	$2.0684 \times 10^{11} (\text{N/m}^2)$	$2.0684 \times 10^{11} (\text{N/m}^2)$
Rotor moment of Inertia	$6.28 \times 10^{-6} (\text{kg m}^2)$	$1.03 \times 10^{-6} (\text{kg m}^2)$
Drive moment of Inertia	$7.361 \times 10^{-4} (\text{kg m}^2)$	$44.55 \times 10^{-6} (\text{kg m}^2)$
Link moment of Inertia	$0.17043 (\text{kg m}^2)$	$0.0064387 (\text{kg m}^2)$
Gear ratio	100	50
Maximum Rotation	(+/-90, +/-90)deg.	(+/-90, +/-90)deg.
Drive Torque constant	0.119(Nm/A)	0.0234(Nm/A)

### 2.2.2. Software Components

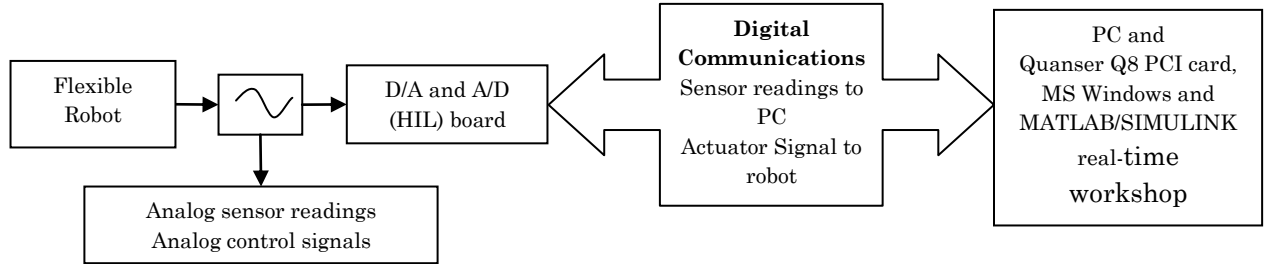


Fig.2.3 Interfacing of signals for the TLFM set-up.

Fig.2.3 shows the interfacing of signals for the TLFM set-up which works on MS Windows operating system with the MATLAB/SIMULINK 2007a software. There is a provision of real-time target logic code builder to interface the SIMULINK model [72]. The MATLAB code for controller is built up in the real-time set up by using the real-time target logic code in C language. The PC program written in Matlab uses C language as an user interface program for the host PC.

which starts up the DAQ board to interact with it and with the user. This program calls functions from the High Level Language Interface (provided by the DAQ board).

### 2.3. Description of the TLFM

The schematic diagram of a planar TLFM is shown in Fig.2.4, where  $\tau_i$  is the actuated torque of the  $i^{\text{th}}$  link,  $\theta_i$  is the joint angle of the  $i^{\text{th}}$  joint and  $d_i(l_i, t)$  represents the deflection along  $i^{\text{th}}$  link. The outer free end of the TLFM is attached with payload mass  $M_p$ .  $(X_i, Y_i)$  is the rigid body co-ordinate frame associate with  $i^{\text{th}}$  link and  $(\hat{X}_i, \hat{Y}_i)$  is flexible moving co-ordinate frame. The rigid body motion is described by the  $\theta_i$  is the joint angle and transversal flexible motion is due to  $d_i(l_i, t)$ . The dynamic model of the TLFM is derived by first utilizing the Euler-Bernoulli beam theory to obtain a partial differential equation with the corresponding boundary conditions representing the motion of the links.

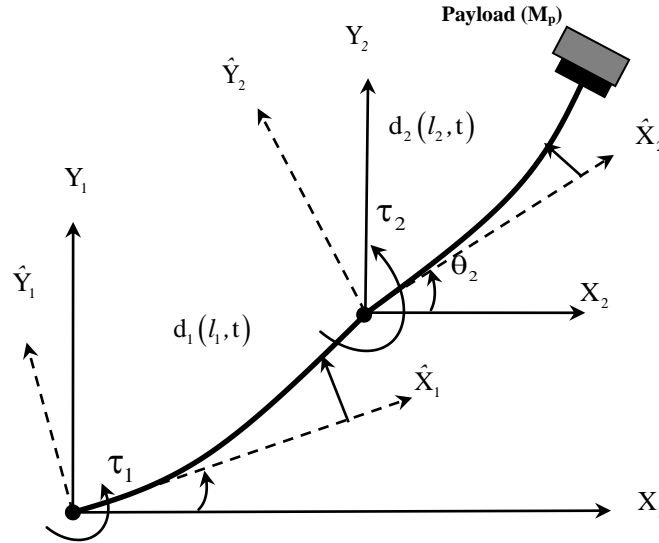


Fig.2.4 Schematic diagram of a planar TLFM

## 2.4. Dynamic model of the TLFM

Then, considering the system energy, the Lagrangian formulation approach along with the assumed modes method the dynamics of the TLFM are derived. The dynamic model is developed to reveal the dynamic behavior of the system using the Lagrangian approach which is defined as

$$\frac{d}{dt} \frac{\partial L}{\partial \dot{q}_i} - \frac{\partial L}{\partial q_i} = \tau_i \quad (2.1)$$

where

$L = (K_T)_i - (U_T)_i$  : Lagrangian expressed as difference between total kinetic energy  $K_T$  and total potential energy  $U_T$  of the TLFM.

$\tau_i$  : Generalized force at the  $i^{\text{th}}$  joint.

$q_i$  : Generalized coordinate of the  $i^{\text{th}}$  link.

The generalized coordinate's  $q_i$  comprise of joint angles, joint velocities and modal coordinates. The total kinetic energy of the  $i^{\text{th}}$  link can be expressed as  $K_{T_i} = (\text{Total kinetic energy due to } i^{\text{th}} \text{ joint}) + (\text{Total kinetic energy due to } i^{\text{th}} \text{ link}) + (\text{Total kinetic energy due to payload } M_p)$  and in absence of gravity. The Links are modeled as Euler-Bernoulli beams with deformation  $d_i(l, t)$  satisfying the  $i^{\text{th}}$  link partial differential equation

$$(EI)_i \frac{\partial^4 d_i(l, t)}{\partial l_i^4} + \rho_i \frac{\partial^2 d_i(l, t)}{\partial t_i^2} = 0 \quad (2.2)$$

where



- $\rho_i$  : Density of the  $i^{\text{th}}$  link ( $i=1, 2$ ).
- $d_i(l_i, t)$  : Deflection of the  $i^{\text{th}}$  link.
- $(EI)_i$  : Flexural rigidity of the  $i^{\text{th}}$  link.
- $l_i$  : Length of the  $i^{\text{th}}$  link.
- $t$  : Time.

A solution of equation (2.3) can be obtained by applying proper boundary conditions at the base and at the end of each link. The three boundary conditions are shown in Fig.2.5 where, Fig.2.5 (a) shows the clamped-free boundary condition i.e. one end is blocked in both angular and vertical direction and the other end is free. The next boundary condition is the clamped-inertia (Fig.2.5 (b)), i.e. one end is blocked clamped-free case but the other end carries and inertia load. The last boundary condition i.e. pinned is shown in Fig.2.5 (c). Inertia-Inertia (often referred to as the pseudo pinned) and, it is locked in the vertical direction but free to move in the angular direction with the help of a rotary actuator mounted on the base that did not provide a torque to the link.

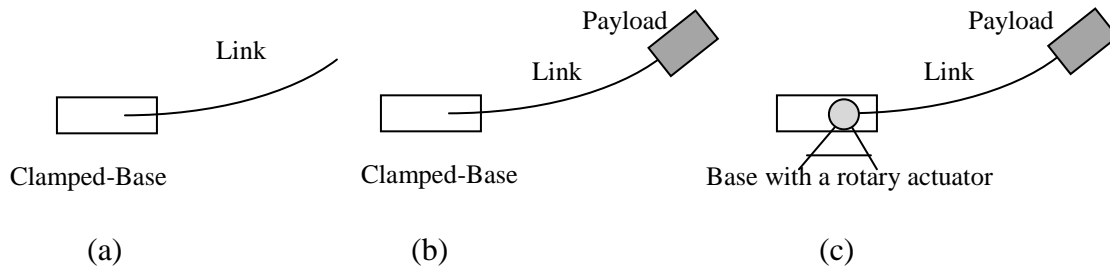


Fig.2.5 Three different boundary conditions (a) Clamped-free, (b) Clamped-inertia (c) Pinned

Considering that each link is clamped at the and mass of the link is negligible compared to the mass of the payload, it can be found that

$$\begin{aligned} (EI)_i \frac{\partial^2 d_i(l_i, t)}{\partial l_i^2} &= -J_{eqi} \frac{d^2}{dt^2} \left( \frac{\partial d_i(l_i, t)}{\partial l_i} \right) \\ (EI)_i \frac{\partial^3 d_i(l_i, t)}{\partial l_i^3} &= M_{eqi} \frac{d^2}{dt^2} (d_i(l_i, t)) \end{aligned} \quad (2.3)$$

where  $J_{eqi}$  and  $M_{eqi}$  are mass and moment of inertia at the end of  $i^{th}$  link. Since, (2.3) is a partial differential equation with respect to time and space coordinate. A finite dimensional expression for the link flexibility  $d_i(l_i, t)$  of  $i^{th}$  link can be represented using an assume mode method (AMM) [81] as

$$d_i(l_i, t) = \sum_{j=1}^n \varphi_{ij}(l_i) \delta_{ij}(t) \quad (2.4)$$

where

- $\varphi_{ij}$  :  $j^{th}$  mode shapes (spatial coordinate) of the  $i^{th}$  link.
- $\delta_{ij}$  :  $j^{th}$  modal coordinates (time coordinate) of the  $i^{th}$  link.
- $n$  : Number of assume modes.

Putting the expression for link flexibility  $d_i(l_i, t)$  given in (2.5) to (2.1) a general solution is derived, which is a product of time harmonic function of the form

$$\delta_{ij}(t) = e^{j\omega_{ij} t} \quad (2.5)$$

and of a space eigen function of the form

$$\begin{aligned} \varphi_i(l_i) &= C_{1,i} \sin(\beta_i, l_i) + C_{2,i} \cos(\beta_i, l_i) + C_{3,i} \sinh(\beta_i, l_i) \\ &\quad + C_{4,i} \cosh(\beta_i, l_i) \end{aligned} \quad (2.6)$$

where  $\omega_i$  natural frequency of the  $i^{\text{th}}$  link and  $\beta_i^4 = \omega_i^4 \rho_i / (EI)_i$ . By applying the boundary condition given in Fig.2.5 (a) the constant coefficients in (2.6) can be determined as

$$C_{3,i} = -C_{1,i}, \quad C_{4,i} = -C_{2,i}, \quad (2.7)$$

and from Fig.2.5 (b),one gets

$$\left[ f(\beta_i, L_i) \right] \begin{bmatrix} C_{1,i} \\ C_{2,i} \end{bmatrix} = 0 \quad (2.8)$$

Putting (2.7) in (2.6) and solving (2.8), one obtains the first  $m$  positive roots which in turn gives values of  $\beta_i$ . Hence, a finite solution to the link deformation as well as to (2.2) is obtained. As a result, using the initial Lagrangian equation in (2.1) a matrix representation for the dynamic model of the TLFM is (see Appendix A for further details)

$$\mathbf{M}(\theta_i, \delta_i) \begin{bmatrix} \ddot{\theta}_i \\ \ddot{\delta}_i \end{bmatrix} + \begin{bmatrix} \mathbf{c}_1(\theta_i, \delta_i, \dot{\theta}_i, \dot{\delta}_i) \\ \mathbf{c}_2(\theta_i, \delta_i, \dot{\theta}_i, \dot{\delta}_i) \end{bmatrix} + \mathbf{K} \begin{bmatrix} 0 \\ \delta_i \end{bmatrix} + \mathbf{D} \begin{bmatrix} 0 \\ \dot{\delta}_i \end{bmatrix} = \begin{bmatrix} \tau_i \\ 0 \end{bmatrix} \quad (2.9)$$

where

- $\tau_i$  : Actuated torque of the  $i^{\text{th}}$  link ( $i=1, 2$ ).
- $\theta_i, \dot{\theta}_i$  : Joint angle and velocity of the  $i^{\text{th}}$  joint.
- $\delta_i, \dot{\delta}_i$  : Modal displacement and velocity of the  $i^{\text{th}}$  link.
- $\mathbf{M}$  : Inertia matrix.
- $\mathbf{c}_1, \mathbf{c}_2$  : Vectors containing of Coriolis and Centrifugal forces.
- $\mathbf{K}$  : Stiffness matrix
- $\mathbf{D}$  : Damping matrix.

The TLFM dynamics (2.10) can be rewritten in state space form as

$$\dot{x} = f_i(x) + g_i(x)u_i \quad (2.10)$$

with  $x$  as the state vector i.e.  $x = [\theta_i, \dot{\theta}_i, \delta_i, \dot{\delta}_i]^T$

$$\text{and } f_i(x) = \mathbf{M}(\theta_i, \delta_i)^{-1} \left( - \begin{bmatrix} \mathbf{c}_1(\theta_i, \delta_i, \dot{\theta}_i, \dot{\delta}_i) \\ \mathbf{c}_2(\theta_i, \delta_i, \dot{\theta}_i, \dot{\delta}_i) \end{bmatrix} - \mathbf{K} \begin{bmatrix} 0 \\ \delta_i \end{bmatrix} - \mathbf{D} \begin{bmatrix} 0 \\ \dot{\delta}_i \end{bmatrix} \right)$$

$$g_i(x) = \mathbf{M}(\theta_i, \delta_i)^{-1}$$

and  $u_i = \begin{bmatrix} \tau_i \\ 0 \end{bmatrix}$   $\delta_i$  and  $\dot{\delta}_i$  being the modal displacement and modal velocity for the  $i^{\text{th}}$  link

respectively. It is known from [73-76] transfer function from the torque input to the tip position output of a FLM is, in general, nonminimum phase. For a feedback controller, the nonminimum phase property hinders perfect asymptotic tracking of a desired tip trajectory. Thus for perfect tip trajectory tracking, the TLFM should be minimum phase. The minimum phase property may be achieved by output redefinition [77, 41] or splitting the dynamics of the TLFM into two time scale by using singular perturbation method [78]. The actual output vector  $y_{pi}$  is considered as the output for  $i^{\text{th}}$  link instead of  $\theta_i$  to avoid the difficulty of non-minimum phase behavior of the TLFM. Assuming that beam deflection is usually small with respect to link length, from Fig.2.4 the output is redefined as

$$y_{pi} = \theta_i + \left[ \frac{d_i(l_i, t)}{l_i} \right] \quad (2.11)$$

where  $d_i(l_i, t)$  is the link flexibility of  $i^{\text{th}}$  link, whose expression is given in (2.5).

## 2.5. Model validation

To validate the correctness of the dynamic equations of the TLFM derived in *Section 2.3*, it is excited by different bang-bang input torque signals. Bang-Bang input torque signal is chosen because in order to excite all the flexible modes as well as coupling terms. The open-loop responses of both physical and derived model of the TLFM are validated by comparing joint-1 position, joint-2 position and link-2 tip deflection of the TLFM.

## 2.6. Results and Discussions

To extract the open loop response of the developed mathematical model of the TLFM in eq. (2.9), numerical simulation has been performed using MATLAB/SIMULINK<sup>®</sup> software. The bang-bang torque profiles applied to the TLFM are shown in Fig.2.6 and Fig.2.7 is symmetric and their values are 0.042 Nm for joint-1 and 0.008 Nm for joint-2 respectively. In Fig.2.8, the joint-1 position is shown for which it is seen that the joint responses have a maximum amplitude of  $10^\circ$  and minimum amplitude of  $-5^\circ$ . The joint-2 position response is shown in Fig. 2.9. The maximum and minimum joint-position responses observed for joint-2 are  $9.8^\circ$  and  $-4^\circ$  respectively. In Fig.2.10 link-2 tip deflection trajectory response obtained from experiments are compared with that of obtained from simulation are shown. Fig.2.10 shows that the maximum deflection of 1.2 mm is noted in case of experimental results while, the simulation model shows maximum deflection of 1 mm.

From Fig.2.8-Fig.2.10 it can be verified that the derived dynamic equation approximates the dynamics of the physical set up.

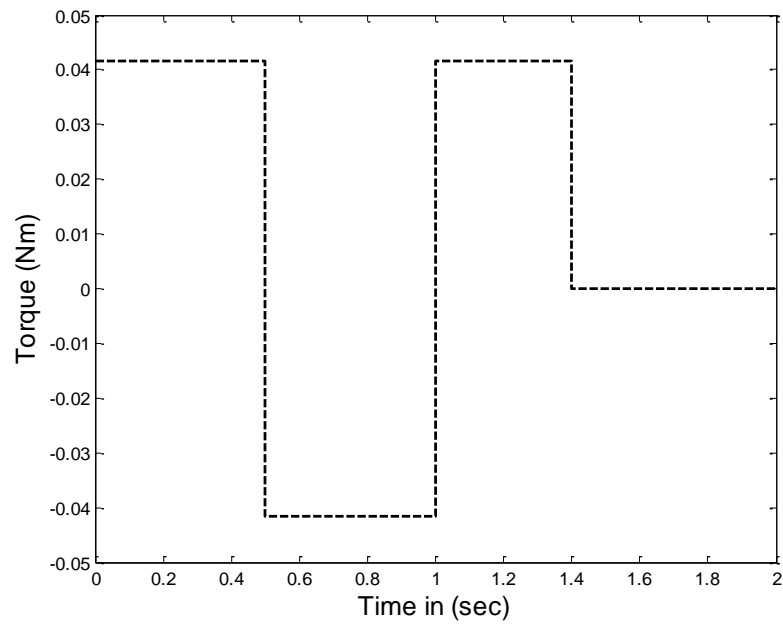


Fig.2.6 Torque profiles-1 for (joint-1)

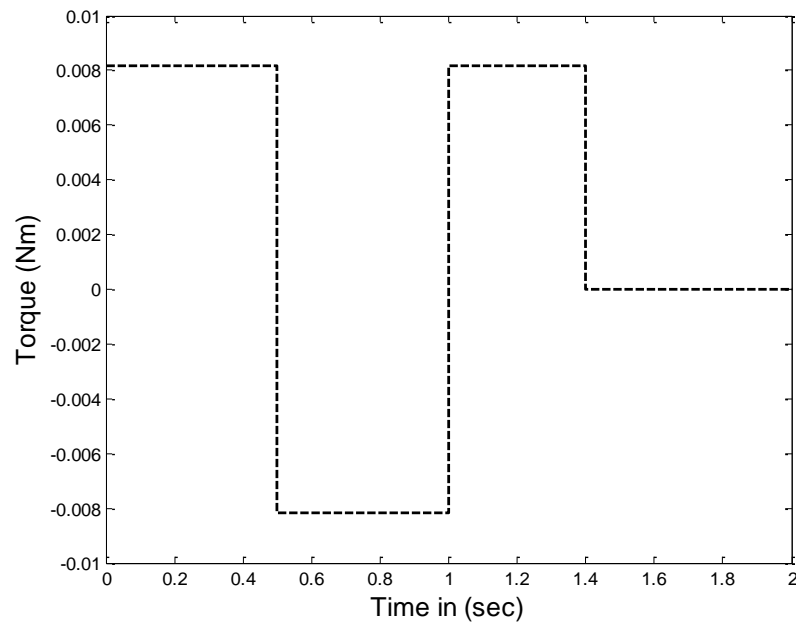


Fig.2.7 Torque profiles-1 for (joint-2)

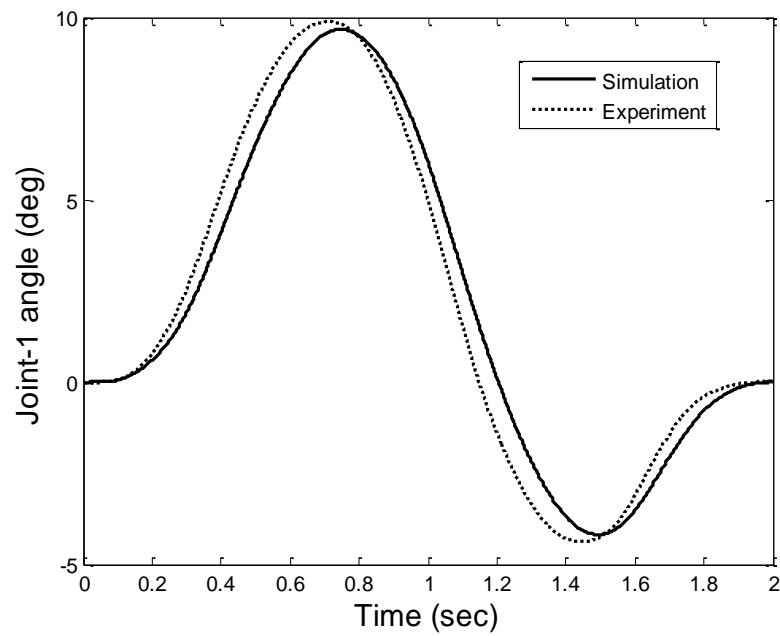


Fig.2.8 Joint-1 position: Torque profiles-1

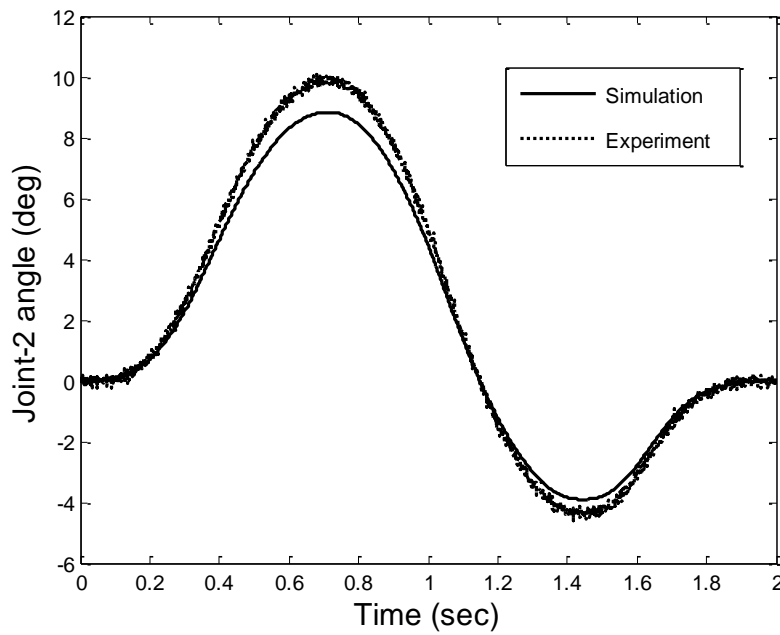


Fig.2.9 Joint-2 position: Torque profiles-1

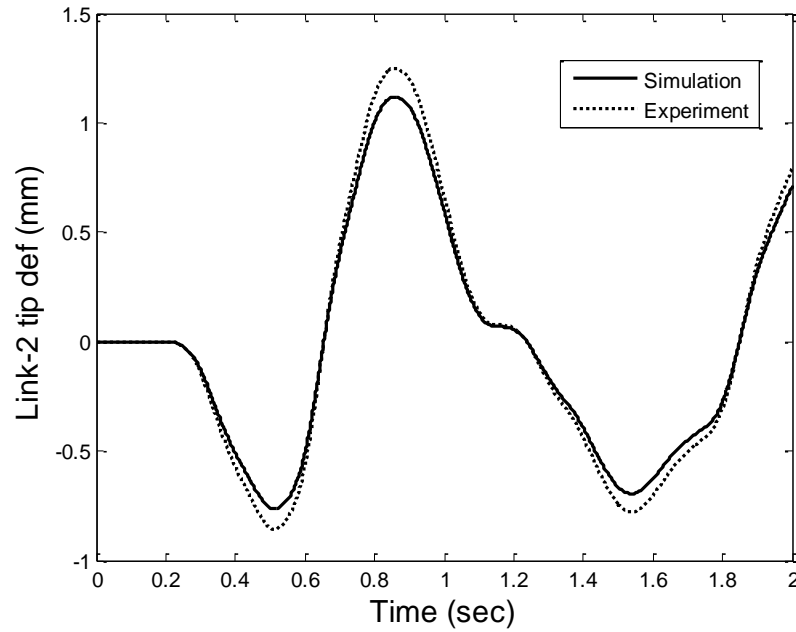


Fig.2.10 Link-2 tip deflection: Torque profiles-1

To further validate the proposed model a different bang-bang torque signal is applied to both the actuators. Fig.2.11 and Fig.2.12 show the torque profile-2 for joint -1 and joint-2 respectively. The responses for joint-1 position are shown in Fig.2.13 for joint-2 position in Fig.2.14 and link-2 tip deflections are given in Fig.2.15. Fig.2.13 shows joint-1 position response, which show maximum amplitude of  $5^\circ$  and minimum amplitude of  $-10^\circ$ . The maximum and minimum joint-position responses observed for joint-2 are  $5.2^\circ$  and  $-10^\circ$  respectively as shown in Fig.2.14. In Fig.2.15 link-2 tip deflection trajectory response obtained from experiments are compared with that of obtained from simulation are shown. Fig.2.15 shows that the maximum deflection of 1 mm is observed in case of experimental results while, the simulation model shows maximum deflection of 0.85 mm.



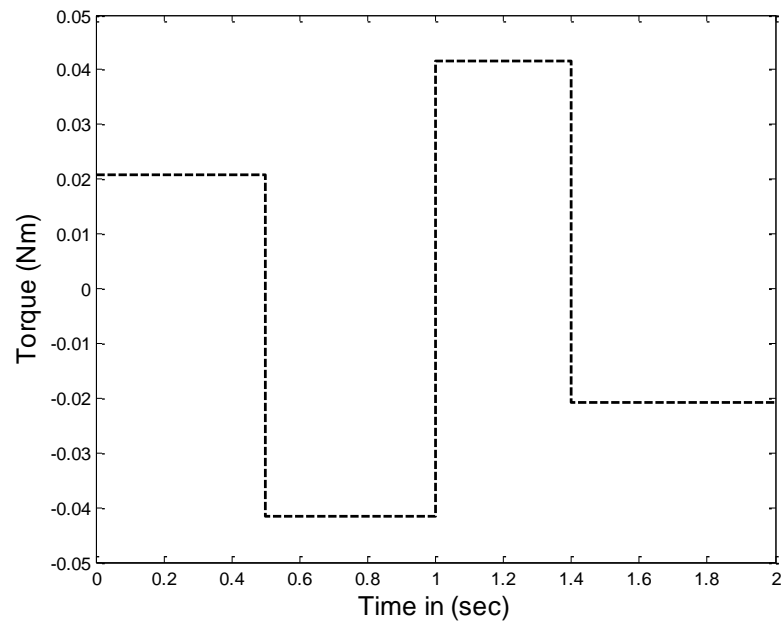


Fig.2.11 Torque profiles-2 for (joint-1)

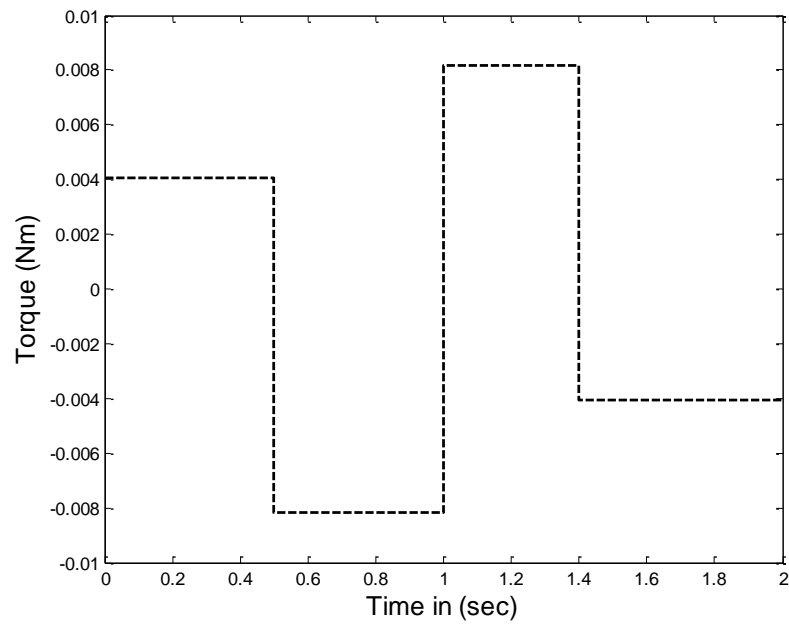


Fig.2.12 Torque profiles-2 for (joint-2)

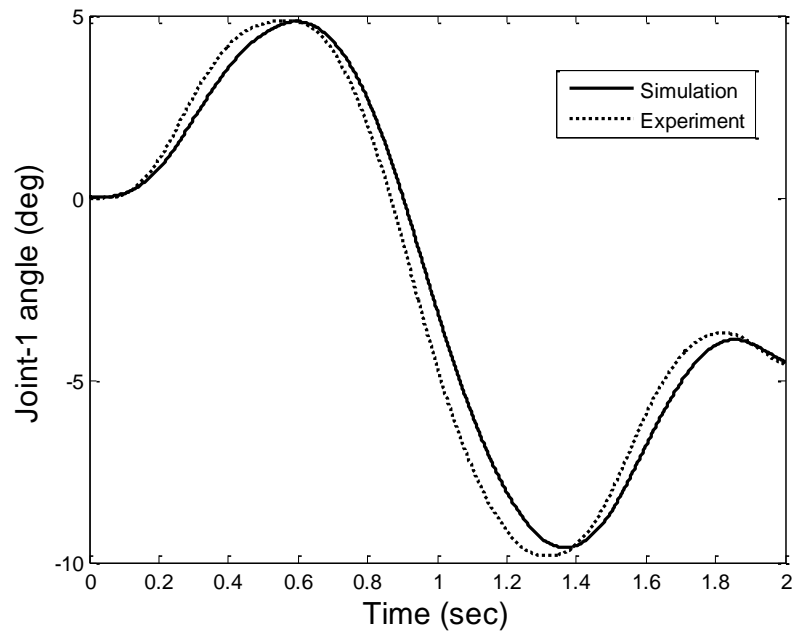


Fig.2.13 Joint-1 position: Torque profiles-2

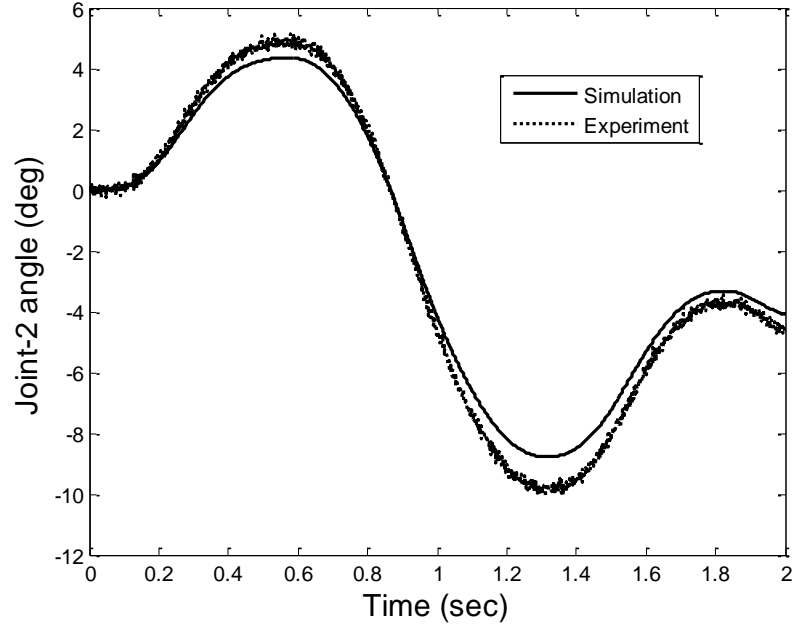


Fig.2.14 Joint-2 position: Torque profiles-2

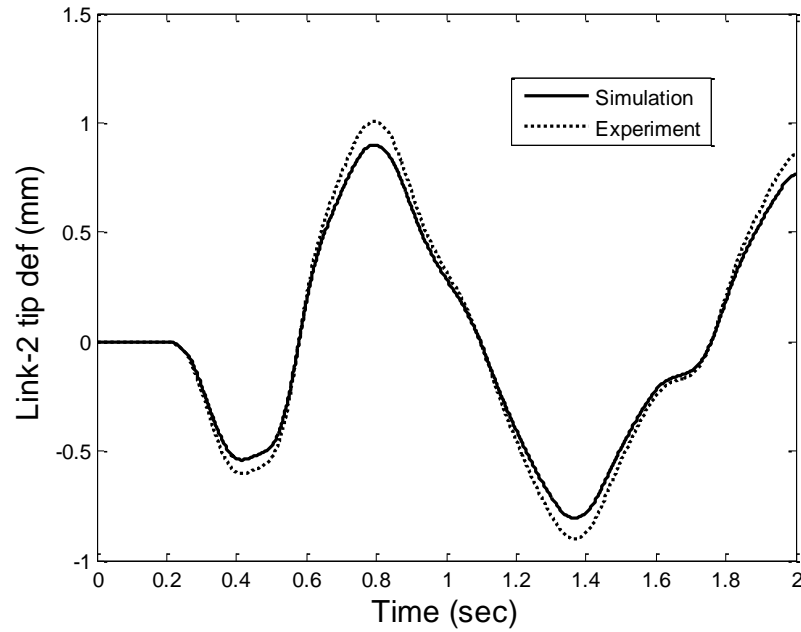


Fig.2.15 Link-2 tip deflection: Torque profiles-2

## 2.7. Chapter Summary

The chapter described the software and hardware components of the experimental two-link flexible manipulator (TLFM) set-up. The dynamic equations of the physical TLFM have been derived which will be used in subsequent chapters for realization of new adaptive control algorithms for the TLFM. The dynamic equations of the TLFM are obtained using Lagrangian dynamics and assume mode method. Also, the derived mathematical model has been validated using open loop responses such as joint position, tip deflection of the physical TLFM when excited by different bang-bang input torque signals. From the results obtained, it is confirmed that the model obtained is appropriate enough to represent physical TLFM.

## Chapter 3

# Direct Adaptive Control of a Two-Link Flexible Manipulator

In this Chapter, a direct adaptive control (DAC) is developed to control the tip position while simultaneously suppressing its deflection for the two-link flexible manipulator (TLFM) when subjected to carry different payloads. The performance of the developed controller is then compared with a fuzzy learning based adaptive controller (FLAC). FLAC is chosen for comparisons, since fuzzy logic is an intelligent rules based method that uses human experience in the control law, which relies mainly on the experience of the designer. The chapter is organized as follows. *Section 3.2* presents the design of a direct adaptive controller. The design of the fuzzy learning based adaptive control is described in *Section 3.3*. These two adaptive controllers namely DAC and FLAC are simulated using the mathematical model derived in

*Chapter 2* and the real-time implementations of these control algorithms were performed on a physical TLFM. The obtained simulation and experimental results are analyzed in *Section 3.4*.

### 3.1 Introduction

As discussed in introduction (*Chapter 1*), controlling a flexible-link manipulator is difficult owing to distributed link flexibility which makes this type of manipulator system dynamics under-actuated and non-collocated [78]. Further, control of a flexible-link manipulator becomes more challenging when it has to handle variable payloads. In order to achieve good tip trajectory tracking while suppressing tip deflection with varied payloads, adaptive control should be employed, which can provide appropriate control torques to the actuators to achieve the above two-control tasks (good tip trajectory tracking and suppression of tip deflection).

In this thesis a Lyapunov based adaptive control scheme assuring system stability has been proposed for the control of a TLFM. For the developed control laws, the stability proof of the overall system is also given. The design of this direct adaptive controller involves in choosing a control law with tunable TLFM parameters and then an adaptation law is to be developed using the closed loop error dynamics. The objective of this chapter is to develop a direct adaptive control law such that even there is a change in TLFM dynamics due to payload variation, good tip trajectory tracking along with suppression of tip deflection can be achieved.

### 3.2 Direct adaptive control (DAC)

The structure of the direct adaptive control for a TLFM is shown in Fig.3.1. An adaptive scheme is then developed to cope up with the parametric uncertainty due to change in payload. The adaptive controller proposed here is a direct adaptive controller, in the sense that parameter

adaptation mechanism is driven directly by the motion tracking error whereas in case of indirect adaptive control the control parameters are updated using the online estimated FLM parameters. The direct adaptive control law is derived as follows. Define  $\mathbf{a}$  as a vector containing the parameters of the TLFM given by

$$\mathbf{a} = [J_{l1}J_{l2}J_{h1}J_{h2}m_{1eq}m_{2eq}m_c]^T$$

with parameters  $\mathbf{a}$  defined as

- $a_1$  : Link-1 inertia.
- $a_2$  : Link-2 inertia.
- $a_3$  : Hub-1 inertia.
- $a_4$  : Hub-2 inertia.
- $a_5$  : Link-1 equivalent mass
- $a_6$  : Link-2 equivalent mass
- $a_7$  : Total coupling mass between the links

The choice of vector  $\mathbf{a}$  is made so as to keep the number of manipulator parameter to minimum.

Let  $\hat{\mathbf{a}}$  be the estimate of  $\mathbf{a}$ .

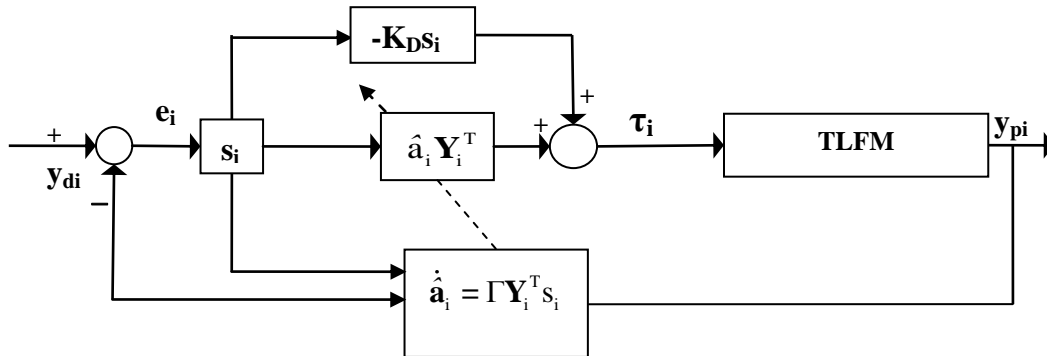


Fig.3.1 Direct adaptive control structure

Then, the TLFM dynamics (2.7) can be written in the linear parameterized form as

$$\tau_i = \tilde{\mathbf{a}} \left[ Y \left( y_p, \dot{y}_p, \dot{y}_r, \ddot{y}_r \right) \right]^T \quad (3.1)$$

With  $\tilde{\mathbf{a}}$  being parameter estimation error and the regressor vector  $Y(\cdot)$  in (3.1) consist of the tip position  $y_p$ , tip velocity and relative error  $y_r$  defined as

$$y_r = \dot{y}_p - \Lambda e \quad (3.2)$$

where

$\Lambda$  : Positive definite matrix.

$e$  : Tip trajectory error ( $\theta_d - y_p$ )

The adaptive control law for TLFM system is derived as suggested in [79] as

$$\tau_i = \tilde{\mathbf{a}} \left[ Y \left( y, \dot{y}, \dot{y}_r, \ddot{y}_r \right) \right]^T - K_D s_i \quad (3.3)$$

where  $K_D$  is the positive definite matrix and vector  $s_i$  is a measure of tracking accuracy of the  $i^{\text{th}}$  link and is defined as

$$s_i = \dot{e}_i + \Lambda e_i = \dot{y}_{p_i} + \Lambda y_{r_i} \quad (3.4)$$

The parameter adaptation rule is given by

$$\dot{\tilde{\mathbf{a}}} = -\Gamma \mathbf{Y}^T \mathbf{s} \quad (3.5)$$

where  $\Gamma$  is a symmetric positive definite matrix. A nonlinear adaptive control law given in (3.3) with the adaption law in (3.5) will provide the desired tip trajectory tracking under payload variation. To prove closed-loop stability of the proposed nonlinear adaptive controller, we define a Lyapunov candidate function,  $V(t)$  as

$$\mathbf{V}(t) = \frac{1}{2} \left[ \mathbf{s}^T \mathbf{M} \mathbf{s} + \tilde{\mathbf{a}}^T \Gamma^{-1} \tilde{\mathbf{a}} \right] \quad (3.6)$$

where  $\mathbf{M}$  be the inertia matrix in and  $\Gamma$  is a symmetric positive definite matrix. Differentiating (3.6) with respect to time leads to

$$\dot{\mathbf{V}}(t) = \mathbf{s}^T [\mathbf{M}\ddot{\mathbf{y}} - \mathbf{M}\ddot{\mathbf{y}}_r] + \frac{1}{2} \mathbf{s}^T \dot{\mathbf{M}} \mathbf{s} + \tilde{\mathbf{a}}^T \Gamma^{-1} \dot{\tilde{\mathbf{a}}} \quad (3.7)$$

Substituting for  $\mathbf{M}\ddot{\mathbf{y}}$  from the TLFM dynamics (2.7) and using the linear parameterization of the TLFM dynamics in (3.1), one obtains

$$\dot{\mathbf{V}}(t) = \mathbf{s}^T [\boldsymbol{\tau} - \mathbf{a} \mathbf{Y}^T] + \tilde{\mathbf{a}}^T \Gamma^{-1} \dot{\tilde{\mathbf{a}}} \quad (3.8)$$

Substituting the adaptive control law  $\boldsymbol{\tau} = \hat{\mathbf{a}} \mathbf{Y}^T - \mathbf{K}_D \mathbf{s}$  into (3.5) gives

$$\begin{aligned} \dot{\mathbf{V}}(t) &= \mathbf{s}^T [\hat{\mathbf{a}} \mathbf{Y}^T - \mathbf{K}_D \mathbf{s} - \mathbf{a} \mathbf{Y}^T] + \tilde{\mathbf{a}}^T \Gamma^{-1} \dot{\tilde{\mathbf{a}}} \\ &= \mathbf{s}^T [(\mathbf{a} - \hat{\mathbf{a}}) \mathbf{Y}^T - \mathbf{K}_D \mathbf{s}] + \tilde{\mathbf{a}}^T \Gamma^{-1} \dot{\tilde{\mathbf{a}}} \\ &= \mathbf{s}^T [\tilde{\mathbf{a}} \mathbf{Y}^T - \mathbf{K}_D \mathbf{s}] + \tilde{\mathbf{a}}^T \Gamma^{-1} \dot{\tilde{\mathbf{a}}} \\ &= -\mathbf{s}^T \mathbf{K}_D \mathbf{s} + \tilde{\mathbf{a}}^T [\Gamma^{-1} \dot{\tilde{\mathbf{a}}} \mathbf{Y}^T \mathbf{s}] \end{aligned} \quad (3.9)$$

the parameter adaptation rule  $\dot{\tilde{\mathbf{a}}} = -\Gamma \mathbf{Y}^T \mathbf{s}$  is used which leads to

$$\dot{\mathbf{V}}(t) = -\mathbf{s}^T \mathbf{K}_D \mathbf{s} \leq 0 \quad (3.10)$$

It can be seen from (3.10) that for some positive values of  $\mathbf{K}_D$ ,  $\mathbf{s}$  converges to zero. An explicit form of the control law for the  $i^{\text{th}}$  link in terms of parameter vector  $\mathbf{a}$  is given by

$$\begin{aligned} \tau_1 &= a_1 Y_{11} + a_3 Y_{12} + a_4 Y_{13} + a_5 Y_{14} + a_6 Y_{15} + a_7 Y_{16} - K_D s_1 \\ \tau_2 &= a_2 Y_{21} + a_3 Y_{22} + a_5 Y_{23} + a_6 Y_{24} + a_7 Y_{25} - K_D s_2 \end{aligned} \quad (3.12)$$



where  $Y_{ij}$  are the  $ij^{\text{th}}$  element of regressor vectors for  $i=1,2$  and  $j=1,2\cdots 7$ . The adaptation law can be explicitly written as

$$\begin{aligned}\dot{\hat{\mathbf{a}}}_1 &= -\Gamma_1 Y_{11} s_1, \quad \dot{\hat{\mathbf{a}}}_4 = -\Gamma_4 (Y_{13} s_1), \quad \dot{\hat{\mathbf{a}}}_2 = -\Gamma_2 Y_{21} s_2, \\ \dot{\hat{\mathbf{a}}}_5 &= -\Gamma_5 (Y_{14} s_1 + Y_{23} s_2), \quad \dot{\hat{\mathbf{a}}}_3 = -\Gamma_3 (Y_{12} s_1 + Y_{22} s_2), \\ \dot{\hat{\mathbf{a}}}_6 &= -\Gamma_6 (Y_{15} s_1 + Y_{24} s_2), \quad \dot{\hat{\mathbf{a}}}_7 = -\Gamma_7 (Y_{16} s_1 + Y_{25} s_2)\end{aligned}\tag{3.13}$$

The feedback gain matrix  $K_D$  and the adaptation gain matrix  $\Gamma$  are diagonal as defined below  $\Gamma = \text{diag}(\Gamma_1, \Gamma_2, \Gamma_3, \Gamma_4, \Gamma_5, \Gamma_6, \Gamma_7)$  and  $K_D = \text{diag}(K_{D1}, K_{D2})$ . To test the performances of the DAC with change in payload, it is compared with that of the FLAC which is discussed in the next *Section*.

### 3.3 Fuzzy learning based adaptive control (FLAC)

It is observed from Chapter 2 that the dynamics of the TLFM is highly nonlinear due to distributed-link flexure. Further uncertainties lie in the dynamics of a TLFM when it has to operate under variable payloads by exciting its infinite modes along the links. Because when payload is attached to a FLM its flexible modes get excited. Ideally infinite numbers of modes are necessary to represent the dynamics of a FLM. But for controller realization higher modes are truncated. This also gives rise to uncertain FLM dynamics. Fuzzy logic being a suitable candidate for controlling uncertain systems it is applied to develop an adaptive controller in this section. The proposed fuzzy logic based adaptive controller (FLAC) utilizes a learning mechanism which automatically adjusts the rule base of the controller so that the closed loop performs according to the user defined reference model containing information of the desired behavior of the TLFM.



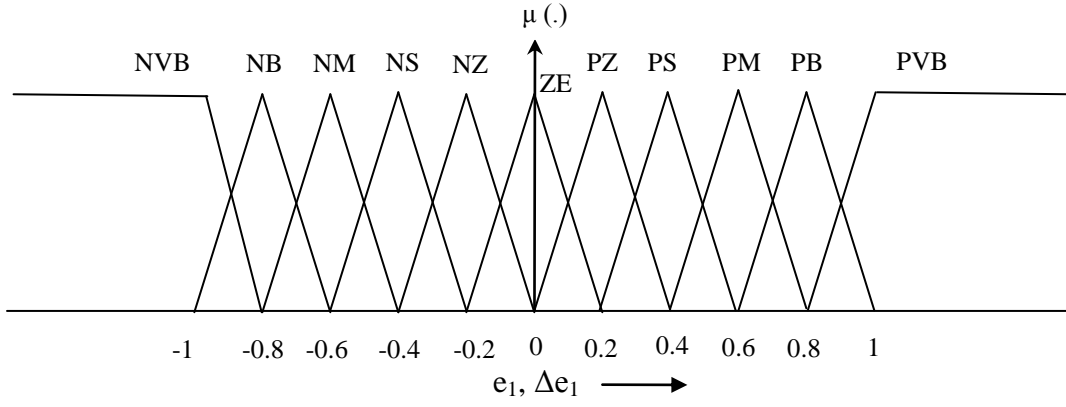


Fig.3.3 Membership function for Link-1 inputs  $e_1$  and  $\Delta e_1$

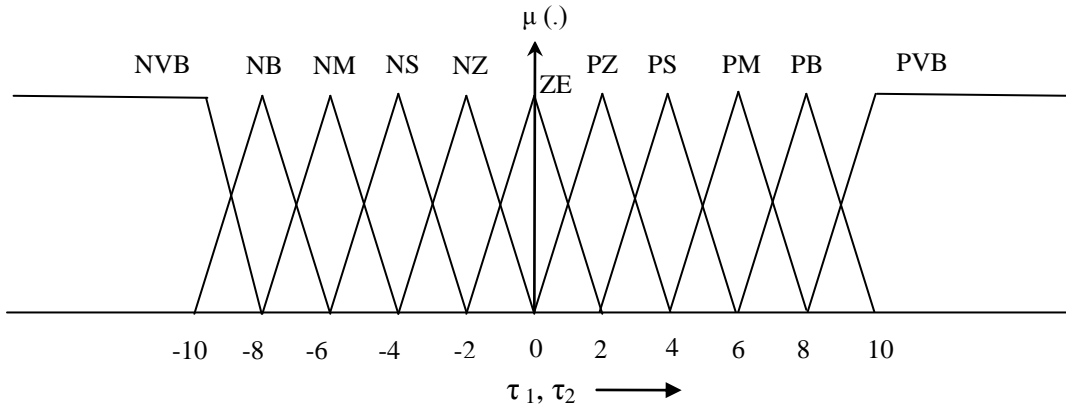


Fig.3.4 Membership function for outputs  $\tau_1$  and  $\tau_2$

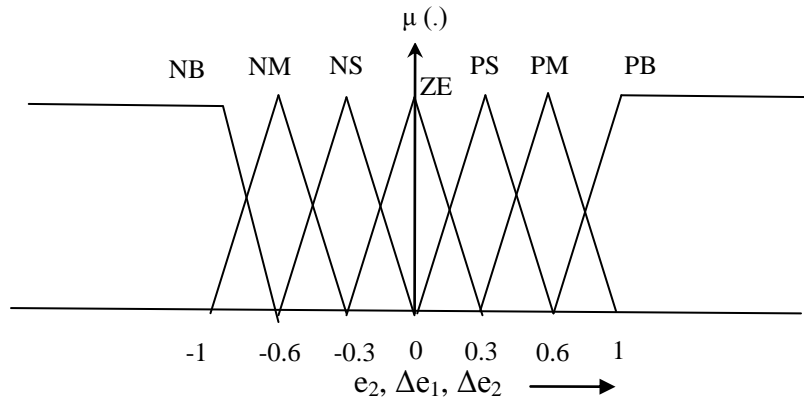


Fig.3.5 Membership function for Link-2 inputs  $e_2$ ,  $\Delta e_1$  and  $\Delta e_2$

For link-1, after observing the open-loop and closed-loop response one get the input universe of discourse chosen to be  $[-1, 1]$ . The output universe of course is chosen as  $[-10, +10]$  Nm so that the link motion be kept within reasonable limit. A fuzzy rule-base is formulated using the following constraints. For link-1, if there is a positive error i.e.  $e_1$ , and a positive change in error  $\Delta e_1$ , then the controller will input a positive torque  $\tau_{FLAC1}$  for this situation, so that the link is not properly aligned but is moving in the proper direction. As the error and the acceleration decrease, the controller applies smaller torque to avoid overshoot. The rule-base array used for the link-1 controller is shown in Table 3.1. The rule-base is an  $11 \times 11$  array, as there are 11 fuzzy sets on the input universes of discourse for link-1. The top most row shows the indices for the eleven fuzzy sets for the link-1 change in error input  $\Delta e_1$  and the column at extreme left shows the indices for the eleven fuzzy sets for the link-1 position error input  $e_1$ . The rule base used for the link-1 fuzzy term set for the input variables  $e_1$  and  $\Delta e_1$  and output variable was  $\tau_{FLAC1}$  assumed to have same cardinality of 11 as:  $F = \{PVB, PB, PM, PS, PZ, ZE, NZ, NS, NM, NB, NVB\}$ , where NVB, NB, NM, NS, NZ, ZE, PZ, PS, PM and PB denote Negative Very Big, Negative Big, Negative Medium, Negative Small, Negative Zero, Zero, Positive Zero, Positive Small, Positive Medium and Positive Big respectively. The body of the array shows the indices  $i^{th}$  link for  $\tau_{FLACi}$  in fuzzy implications of the form

$$\text{If } \langle e_i \text{ and } \Delta e_i \rangle \text{ Then } \langle \tau_{FLACi} \rangle$$

Similarly rules were derived for the link-2, although it should be noted that the link-2 FLC involves the change in error ( $\Delta e_1$ ) of the first link. Therefore, the rule base is a three-dimensional array. There are three inputs and, to keep the rule base to a reasonable size, 7 fuzzy sets were used for the inputs  $e_2$ ,  $\Delta e_1$  and  $\Delta e_2$  and output  $\tau_{FLAC2}$  such that  $F = \{PB, PM, PS, ZE, NS, NM, NB\}$ , where NB, NM, NS, ZE, PS, PM and PB denote Negative Big, Negative Medium, Negative Small, Zero, Positive Small, Positive Medium and Positive Big respectively.

Negative Small, Zero, Positive Small. Table 3.2-3.8 depict a three dimensional rule-base for link-2.

Table 3.1: Link-1 Rule Base of the TLFM

<b>Torque</b>	<b><math>\Delta e_1</math></b>										
<b><math>e_1</math></b>	<b>NVB</b>	<b>NB</b>	<b>NM</b>	<b>NS</b>	<b>NZ</b>	<b>ZE</b>	<b>PZ</b>	<b>PS</b>	<b>PM</b>	<b>PB</b>	<b>PVB</b>
<b>NVB</b>	NVB	NVB	NVB	NB	NB	NM	NM	NS	NS	NZ	ZE
<b>NB</b>	NVB	NVB	NB	NB	NB	NM	NS	NS	NZ	ZE	PZ
<b>NM</b>	NVB	NB	NB	NM	NM	NS	NS	NZ	ZE	PZ	PS
<b>NS</b>	NB	NB	NM	NM	NM	NS	NZ	ZE	PZ	PS	PS
<b>NZ</b>	NB	NM	NM	NS	NS	NZ	ZE	PZ	PS	PS	PM
<b>ZE</b>	NB	NM	NS	NS	ZE	ZE	ZE	PZ	PS	PM	PB
<b>PZ</b>	NM	NS	NS	NZ	ZE	PZ	PS	PS	PM	PM	PB
<b>PS</b>	NS	NS	NZ	ZE	PZ	PS	PS	PM	PM	PB	PVB
<b>PM</b>	NS	NZ	ZE	NS	PS	PS	PM	PM	PB	PB	PVB
<b>PB</b>	NZ	ZE	PZ	NM	PS	PM	PM	PB	PB	PVB	PVB
<b>PVB</b>	ZE	PZ	PS	PB	PM	PM	PB	PB	PVB	PVB	PVB

Table 3.5 represents the case when the  $\Delta e_2=0$  from the shoulder link is zero and is the center of the rule-base (the body of the table denotes the indices  $m$ ) for  $\tau_{FLAC2}$ . Tables 3.2-3.4 are for the case when the change in error for link-2 tip position error i.e.  $\Delta e_2$  is negative and Table 3.6-3.8 are for the case where change in error for link-2 tip position error i.e.  $\Delta e_2$  is positive. The central portion (portion where  $\Delta e_2$  is zero or small) of the rule base makes use of the entire output

universe of discourse. As one move away from the center of the rule base (to the region where the link-2 tip position error is large), only a small portion of the output universe of discourse is used to keep the output of the controller small. Thus tip position error of the link-1 is dependent on the  $\Delta e_2$  from the link-2 tip position. The tip position error of the link-2 is decreased if the  $\Delta e_2$  is large and is increased as the  $\Delta e_2$  decreases. The FLC designed above is incorporated with an adaptive mechanism which automatically adjusts the knowledge base of the fuzzy controller so that the closed-loop system performs according to the specifications given by the reference model.

Table 3.2: Link-2 Rule Base of the TLFM when  $\Delta e_2 = (\text{NB})$ 

<b>Torque</b>	<b><math>\Delta e_2</math></b>						
<b><math>e_1</math></b>	<b>NB</b>	<b>NM</b>	<b>NS</b>	<b>ZE</b>	<b>PS</b>	<b>PM</b>	<b>PB</b>
<b>NB</b>	NB	NB	NB	NM	NM	NS	ZE
<b>NM</b>	NB	NB	NM	NS	NS	ZE	PS
<b>NS</b>	NB	NM	NM	NS	ZE	PS	PS
<b>ZE</b>	NM	NM	NS	ZE	PS	PM	PM
<b>PS</b>	NM	NS	ZE	PS	PS	PM	PM
<b>PM</b>	NS	ZE	PS	PS	PM	PM	PM
<b>PB</b>	ZE	PS	PS	PM	NM	PM	PB

Table 3.3: Link-2 Rule Base of the TLFM when  $\Delta e_2 = (NM)$ 

Torque	$\Delta e_2$						
$e_1$	NB	NM	NS	ZE	PS	PM	PB
NB	NB	NB	NB	NM	NM	NS	ZE
NM	NB	NB	NM	NS	NS	ZE	PS
NS	NB	NM	NM	NS	ZE	PS	PS
ZE	NM	NM	NS	ZE	PS	PM	PM
PS	NM	NS	ZE	PS	PS	PM	PM
PM	NS	ZE	PS	PS	PM	PM	PM
PB	ZE	PS	PS	PM	PM	PM	PB

Table 3.4: Link-2 Rule Base of the TLFM when  $\Delta e_2 = (NS)$ 

Torque	$\Delta e_2$						
$e_1$	NB	NM	NS	ZE	PS	PM	PB
NB	NB	NB	NB	NB	NM	NS	ZE
NM	NB	NM	NM	NM	NS	ZE	PS
NS	NM	NM	NM	NS	ZE	PS	PS
ZE	NM	NM	ZE	ZE	ZE	PS	PM
PS	NM	NS	ZE	PS	PM	PM	PB
PM	NS	ZE	PS	PM	PB	PB	PB
PB	ZE	PS	PM	PM	PB	PB	PB

Table 3.5: Link-2 Rule Base of the TLFM when  $\Delta e_2 = (ZE)$ 

<b>Torque</b>	<b><math>\Delta e_2</math></b>						
<b><math>e_1</math></b>	<b>NB</b>	<b>NM</b>	<b>NS</b>	<b>ZE</b>	<b>PS</b>	<b>PM</b>	<b>PB</b>
<b>NB</b>	NB	NB	NB	NB	NB	NM	ZE
<b>NM</b>	NB	NB	NB	NB	NS	ZE	PS
<b>NS</b>	NB	NM	NM	NS	ZE	PS	PM
<b>ZE</b>	NM	NS	ZE	ZE	ZE	PS	PM
<b>PS</b>	NM	NS	ZE	PS	PM	PM	PB
<b>PM</b>	NS	ZE	PM	PM	PB	PB	PB
<b>PB</b>	ZE	PS	PM	PB	PB	PB	PB

Table 3.6: Link-2 Rule Base of the TLFM when  $\Delta e_2 = (PS)$ 

<b>Torque</b>	<b><math>\Delta e_2</math></b>						
<b><math>e_1</math></b>	<b>NB</b>	<b>NM</b>	<b>NS</b>	<b>ZE</b>	<b>PS</b>	<b>PM</b>	<b>PB</b>
<b>NB</b>	NB	NB	NB	NM	NM	NS	ZE
<b>NM</b>	NB	NB	NM	NM	NS	ZE	PS
<b>NS</b>	NB	NM	NM	NS	ZE	PS	PM
<b>ZE</b>	NM	NS	ZE	ZE	ZE	PS	PM
<b>PS</b>	NM	NS	ZE	PS	NM	PB	PB
<b>PM</b>	NS	ZE	PS	PM	NB	PB	PB
<b>PB</b>	ZE	PS	PM	PB	NB	PB	PB



Table 3.7: Link-2 Rule Base of the TLFM when  $\Delta e_2 = (\text{PM})$ 

<b>Torque</b>	<b><math>\Delta e_2</math></b>						
<b><math>e_1</math></b>	<b>NB</b>	<b>NM</b>	<b>NS</b>	<b>ZE</b>	<b>PS</b>	<b>PM</b>	<b>PB</b>
<b>NB</b>	NB	NM	NM	NS	NS	NS	ZE
<b>NM</b>	NB	NM	NM	NS	NS	ZE	PS
<b>NS</b>	NM	NM	NS	NS	ZE	PS	PM
<b>ZE</b>	NM	NS	NS	ZE	PS	PS	PM
<b>PS</b>	NS	NS	ZE	PS	PS	PM	PB
<b>PM</b>	NS	ZE	PS	PS	PM	PB	PB
<b>PB</b>	ZE	PS	PM	PM	PB	PB	PB

Table 3.8: Link-2 Rule Base of the TLFM when  $\Delta e_2 = (\text{PB})$ 

<b>Torque</b>	<b><math>\Delta e_2</math></b>						
<b><math>e_1</math></b>	<b>NB</b>	<b>NM</b>	<b>NS</b>	<b>ZE</b>	<b>PS</b>	<b>PM</b>	<b>PB</b>
<b>NB</b>	NM	NM	NM	NS	NS	NS	ZE
<b>NM</b>	NM	NM	NS	NS	NS	ZE	PS
<b>NS</b>	NM	NM	NS	NS	ZE	PS	PM
<b>ZE</b>	NM	NS	NS	ZE	PS	PS	PM
<b>PS</b>	NS	NS	ZE	PS	PS	PM	PM
<b>PM</b>	NS	ZE	PS	PS	PM	PM	PB
<b>PB</b>	ZE	PS	PS	PM	PM	PB	PB

Now, fuzzy sets for both link-1 and link-2 FLC are all initially centered at zero resulting in rule-bases filled with zeros. This implies that the fuzzy controller by itself has no knowledge about how to control the plant. As the algorithm executes, the output fuzzy sets are rearranged by the learning mechanism, filling up the rule-base. For instance, once a desired trajectory is commanded the learning mechanism described below will move the centers of the activated rules away from zero and begin to synthesize the fuzzy controller.

### 3.3.2 Reference model

Through reference model, the desired closed-loop system behavior is specified. It is used to characterize closed-loop specifications such as rise-time, overshoot, and settling time. The performance of the overall system is computed with respect to the reference model by generating error signals between the reference model output and the plant outputs. The choice of the reference model is very important as it dictates the FLAC to perform in the desired manner.

### 3.3.3 Learning mechanism

Learning Mechanism performs the function of modifying the knowledge base (made by observing data from the controlled process, the reference model, and the fuzzy controller) of the fuzzy controller so that the closed loop system behaves as the reference model. The learning block constitutes a fuzzy inverse model and a knowledge base modifier. These are explained next.

The fuzzy inverse model takes input as  $\mathbf{e}_{mi}$  (error between the current closed loop TLFM behavior from the specified behavior of the reference model reference model for  $i^{\text{th}}$  link) and gives output  $\mathbf{p}_i$  (factor by which change is necessary in the TLFM inputs for  $i^{\text{th}}$  joint). The design

of the fuzzy inverse model requires the knowledge of the closed loop on-line TLFM tip position error profile and change in error profile. Fuzzy inverse model accomplishes two works i) it initially synthesizes the direct fuzzy controller by also using information gathered during on-line operation, and ii) subsequent tuning of the fuzzy controller by using on-line information about plant behavior changes. The rule bases of the fuzzy inverse model are same as fuzzy control block and they are given. Fuzzy inverse model rules capture knowledge such as: i) if the position error  $e_{mi} = y_{mi} - y_{pi}$  is small, but the link is moving in the correct direction to reduce this error, then a smaller change (or no change) is made to the direct fuzzy controller than if the link is moving to increase the  $e_{mi}$ ; and ii) if the  $e_{mi}$  is large, then the fuzzy controller must be adjusted to avoid overshoot.

Next, given the information about the necessary changes in the control input (fuzzy inverse model output) as expressed by the vector  $p_i$ , the knowledge base modifier changes the knowledge base of the fuzzy controller so that the previously applied control action will be modified by the amount  $p_i$ . Hence, the knowledge base modifier performs the function of modifying the fuzzy controller so that the better payload adaptability can be achieved for a TLFM. By modifying the fuzzy controller's knowledge base we may force the fuzzy controller to produce a desired output. It is important to note that our rule-base modification procedure implements a form of local learning and hence utilizes memory. In other words, different parts of the rule-base are "filled in" based on different operating conditions for the system, and when one area of the rule-base is updated, other rules are not affected. Hence, the controller adapts to change in payload and also remembers how it has adapted to past situations. Knowledge-base modification is achieved by shifting the centers of the rules (initialized at zero) that were "on" during the previous control action by the amount  $p_i$  for the  $i^{th}$  link.

Suppose we have the fuzzy inverse model output  $\mathbf{p}_i = \mathbf{p}_0$  (is the amount by which the rule base will be modified) indicating that the value of the output to the plant ( $\tau_{\text{FLAC}i} + \mathbf{p}_0$ ) to improve performance instead of  $\tau_{\text{FLAC}i}$ . The knowledge-base modification procedure consists of two steps: i) determine the rules that are “on,” i.e., the rules that produced the previous control action and, ii) modify the entries in the knowledge-base array for those rules by the amount  $\mathbf{p}_i$ . The entries of the rule base are modified by shifting the center of the fuzzy rule base using the following rule [21].

### 3.4 Results and Discussions

The numerical simulations of the DAC and FLAC have been performed using MATLAB/SIMULINK<sup>®</sup>. To validate the tip trajectory tracking performances of these controllers, the desired trajectory vector for two the joints,  $\theta_{di}(t)$   $i=1,2$  is chosen as

$$\theta_{d_i}(t) = \theta_0(t) + \left[ 6 \frac{t^5}{t_d^5} - 15 \frac{t^4}{t_d^4} + 10 \frac{t^3}{t_d^3} \right] (\theta_f(t) - \theta_0(t)) \quad (3.14)$$

where  $\theta_{di}(t) = [\theta_{d1}, \theta_{d2}]^T$ ,  $\theta_d(0) = \{0,0\}$  are the initial positions of the links and  $\theta_f(0) = \{\pi/4, \pi/6\}$  are the final positions for link-1 and link-2,  $t_d$  is the time taken to reach the final positions which is taken 4 sec. The physical parameters of the studied TLFM are given in chapter 2 (Table 2.1) and the controller parameters for FLAC and DAC are given in Table 3.9. Here to keep the model simple a first order system is taken as a reference model. The reference model is taken as  $\frac{5}{s+5}$  for both the links [21].

Table 3.9: Controller Parameters for TLFM

Sl. No.	Type of Controller	Controller Parameters
1.	DAC	$\Gamma = \text{diag}([20, 0.2, 0.5, 0.2, 20, 50, 10])$ , $\Lambda = 0.5$ , $K_{D1}=20$ and $K_{D2}=15$
2.	FLAC	$k_{11}=0.5$ , $k_{12}= 1.25$ , $k_{21}=0.75$ , $k_{22}= 2.25$ (Scaling gains for TLFM) $k_{11}=0.5$ , $g_{12}= 1.25$ , $k_{21}=0.75$ , $k_{22}= 2.25$ (Scaling gains for Learning Mechanism).

#### 3.4.1 Simulation results for an initial payload of 0.157 kg

Simulation results after comparing the performances exhibited by two adaptive control schemes (FLAC and DAC) while carrying a 0.157 kg payload are shown in Fig.3.6-3.11. Fig. 3.6 and Fig. 3.7 show the tip deflection trajectories for link-1 and link-2 carrying 0.157 kg of payload. From these figures it is seen that the FLAC suppresses the tip deflection faster compared to the DAC by damping it within 4sec.

Fig.3.8 and Fig.3.9 show the tip trajectory tracking error curves for link-1 and link-2 respectively. From Fig. 3.8, it is seen that there exists a tracking error  $0.4^\circ$  in case of the FLAC and  $1^\circ$  in case of DAC for link-1. Link-2 tracking error profiles in Fig. 3.9 reveal that the tracking errors of  $0.3^\circ$  and  $0.4^\circ$  for DAC and FLAC respectively.

Fig. 3.10 and Fig. 3.11 show the control torque profiles generated by DAC and FLAC for joint-1 and joint-2 respectively. From Fig. 3.10 and Fig. 3.11, it is seen that the control input generated by the FLAC becomes zero compared to DAC for link-1 and link-2 when the desired tip position is tracked. But, it is observed that the FLAC control signal exhibits some amount of chattering compared to DAC.

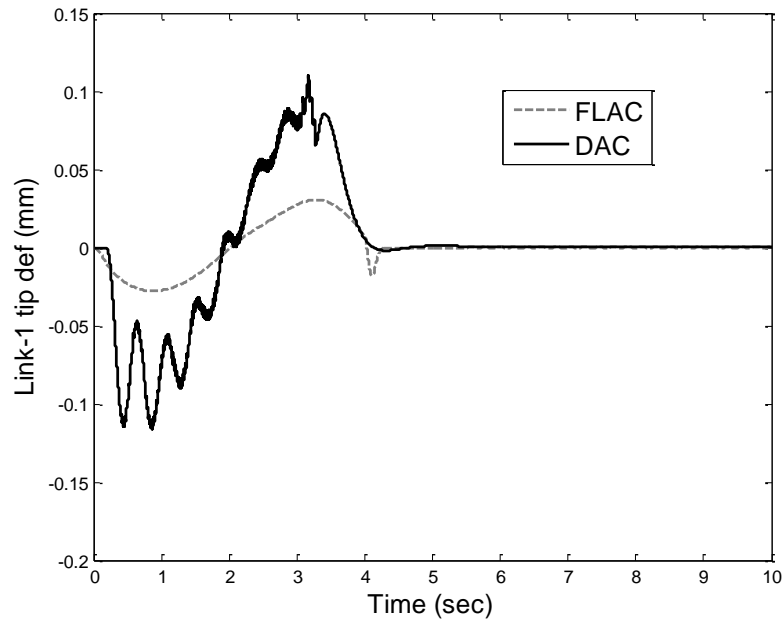


Fig.3.6 Simulation results (time domain) for link-1 tip deflection performances (0.157 kg): DAC and FLAC

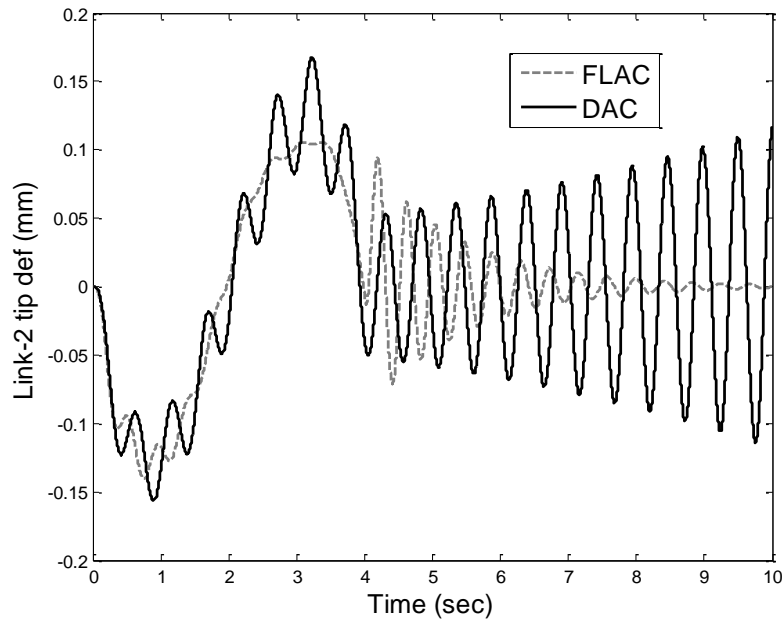


Fig.3.7 Simulation results (time domain) for link-2 tip deflection performances (0.157 kg) DAC and FLAC

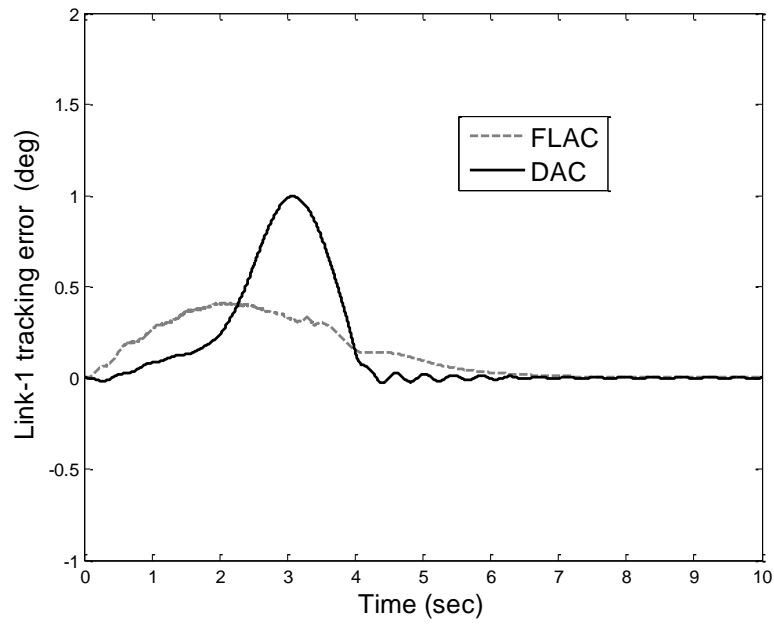


Fig.3.8 Simulation results (time domain) for tip trajectory tracking errors (Link-1) (0.157 kg)

DAC and FLAC

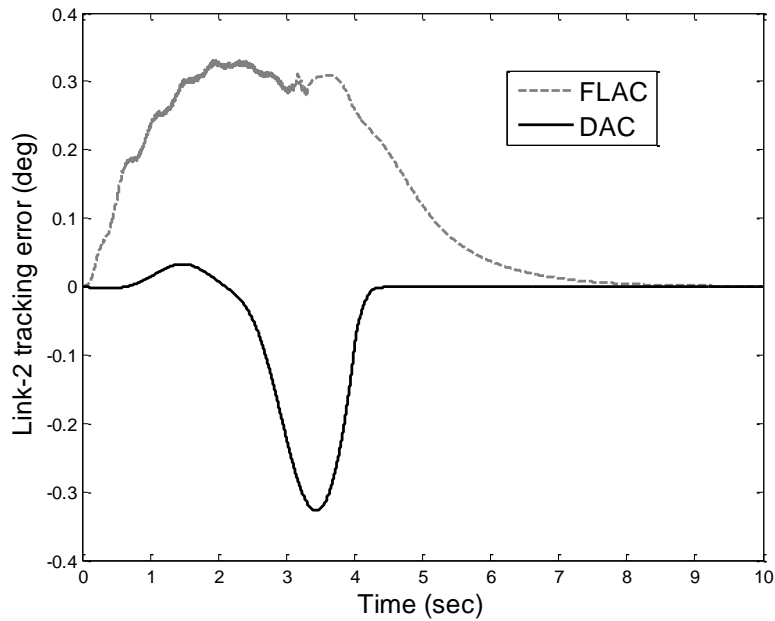


Fig.3.9 Simulation results (time domain) for tip trajectory tracking errors (Link-2) (0.157 kg):

DAC and FLAC

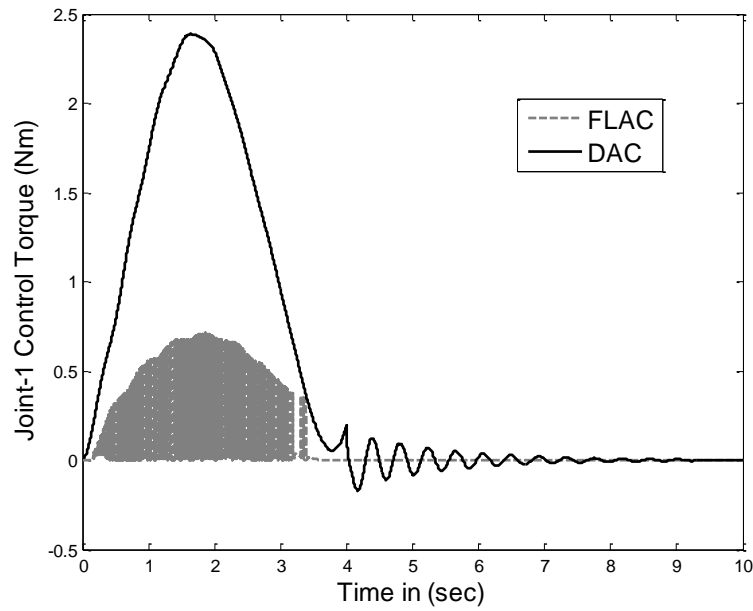


Fig.3.10 Simulation results (time domain) for torque profiles (joint-1) (0.157 kg): DAC and  
FLAC

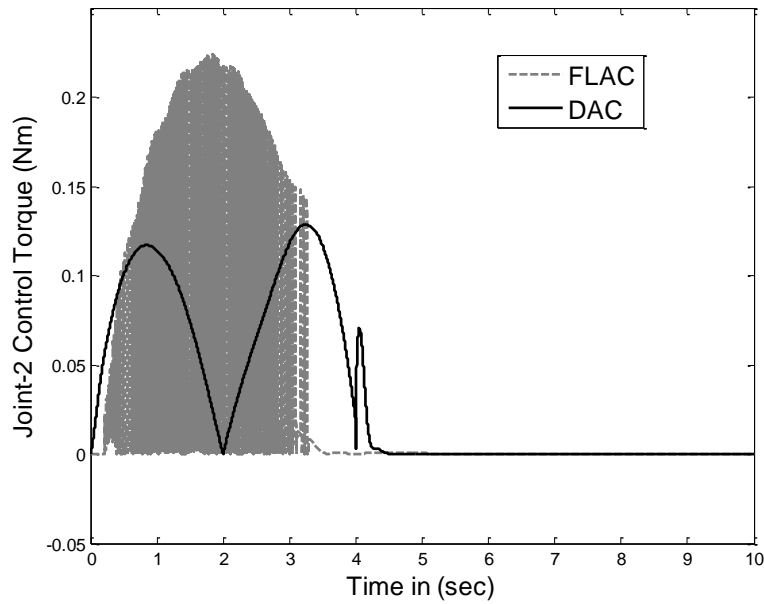


Fig.3.11 Simulation results (time domain) for torque profiles (joint-2) (0.157 kg): DAC and  
FLAC



In addition to time-domain analysis, frequency domain representations of the various controller performances were carried out plotting the power spectral densities versus frequencies of different signals such the deflection and tracking errors. Figs. 3.12 to 3.15 show the PSDs of the for tip deflections of link-1 and link-2 and tip trajectory tracking errors of both links. From Fig. 3.12 it is observed that in case of FLAC the average power of the PSD is -22dB less compared to that of the DAC for link-1, thus it is concluded that the modes are less excited hence, and there is reduction in vibration in case of FLAC compared to DAC for link-1. Similarly for link-2 in Fig. 3.13, the average power for the FLAC is -45dB less compared to that of the DAC showing less excitation to the link-2 modes by FLAC resulting reduced vibration. The average power of the tip trajectory error is calculated from its PSDs in Fig. 3.14 and Fig. 3.15 respectively, and it was found that there is a considerable reduction in average power i.e. -6dB and 21.4dB for link-1 and link-2 respectively in case of FLAC compared to DAC.

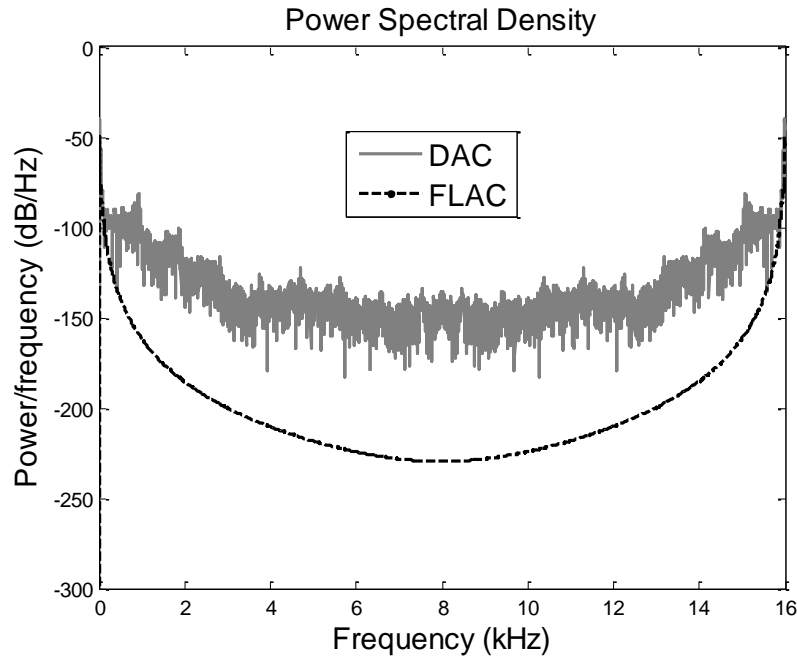


Fig.3.12 Simulation results (frequency domain) link-1 tip deflection performances (0.157 kg):  
DAC and FLAC

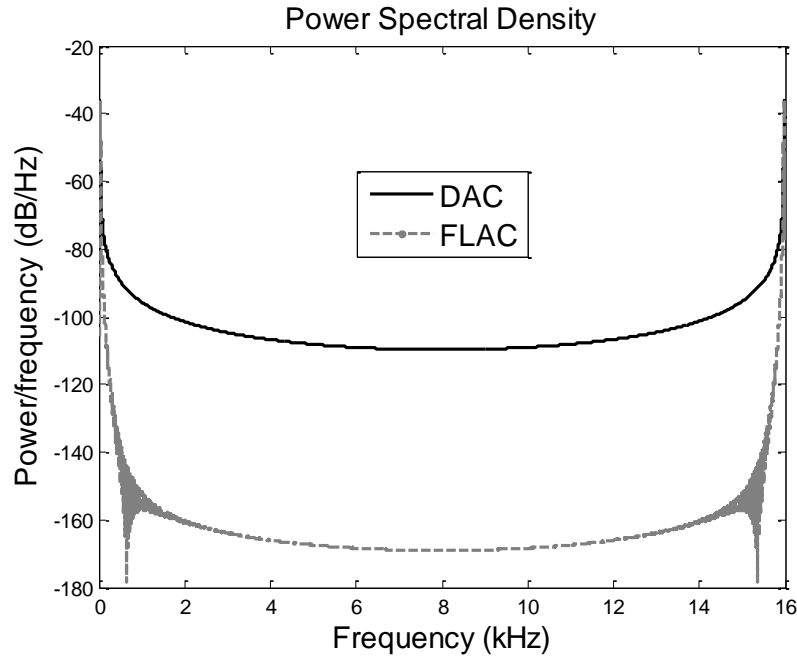


Fig.3.13 Simulation results (frequency domain) for link-2 tip deflection performances (0.157 kg)

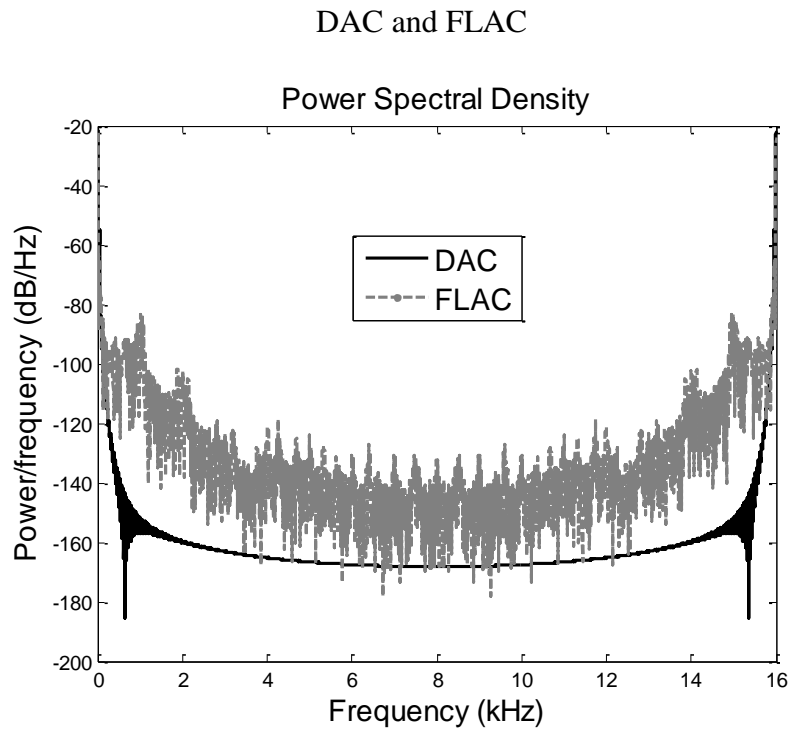


Fig.3.14 Simulation results (frequency domain) for tip trajectory tracking errors (Link-1) (0.157 kg) DAC and FLAC

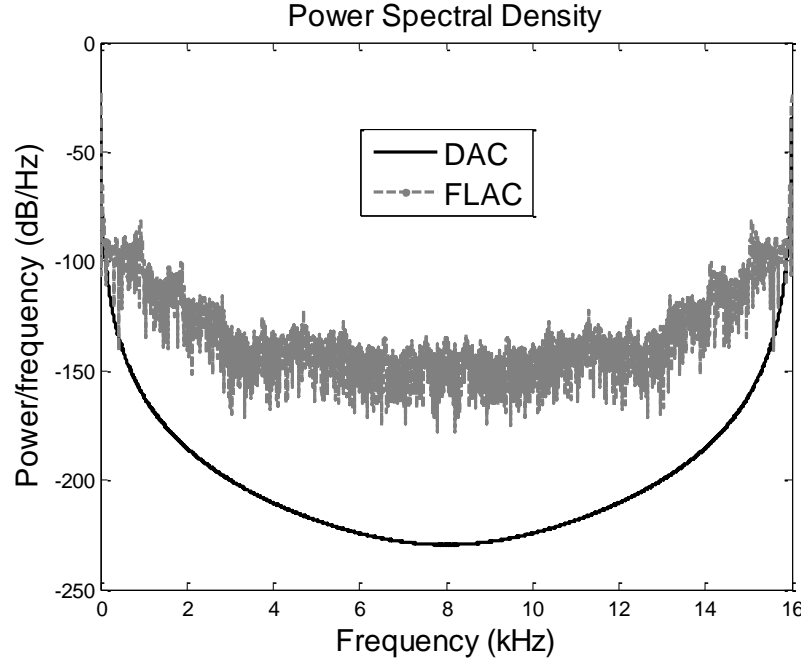


Fig.3.15 Simulation results (frequency domain) for tip trajectory tracking errors (Link-2) (0.157 kg): DAC and FLAC

### 3.4.2 Simulation results for an additional payload of 0.3 kg

Next, the payload mass of the end-effector of the TLFM is varied by an additional payload of 0.3 kg to the existing initial payload of 0.157 kg making the overall payload 0.457 kg. Performances of three controllers FLAC and DAC for 0.457 kg payload were compared in Fig. 3.16-3.21. Fig.3.16 and Fig.3.17 depict the deflection trajectory for link-1 and link-2. From Fig.3.16, it is seen that tip deflection is maximum (0.5 mm) in case of FLAC compared to DAC (0.1 mm) when a payload of 0.457 kg is attached to link-1.

From Fig.3.17, it is seen that the tip deflection trajectories for link-2 is more oscillatory when carrying 0.457 kg of payload in case of DAC compared to FLAC. From Fig.3.18, it can be seen that the time evolution of the error trajectory achieved by employing DAC has yielded maximum

value ( $1^\circ$ ) compared to the FLAC ( $0.4^\circ$ ). Thus a conclusion can be drawn that under additional payload FLAC successfully damps the tip deflections more efficiently compared to DAC.

Fig.3.19 shows that FLAC has yielded ( $0.12^\circ$ ) value compared to the DAC controllers. Joint torque signals generated from DAC and FLAC are compared in Fig.3.20 and Fig.3.21. Torque profiles for joint-1 generated by employing the two controllers are shown in Fig.3.20, and that for joint-2 is shown in Fig.3.21. The joint torque control input for joint-1 obtained by DAC reaches to a maximum value (2.5 Nm) at 2 sec when the tip reaches to the final position at 4 sec the control input reduces to 0.5 Nm. In case of FLAC where control input reaches to a maximum value (0.5 Nm) at 2 sec and 0.15 Nm. From Fig.3.21, the joint control torque signals generated by DAC and FLAC for link-2 have maximum values of 1.3 Nm and 0.2 Nm respectively. Further, the frequency domain analysis was carried out by plotting the PSDs of the link deflections and tracking errors. From Fig. 3.22, it can be observed that the average power of FLAC is -12dB less compared to DAC for link-1, which signifies that there is a reduction in vibration compared to FLAC. Fig. 3.23 shows the average power for the FLAC is -45dB less compared to DAC in case of link-2 tip deflection, i.e. FLAC exhibits less average power at same particular frequency. Thus, it can be concluded that with FLAC, the link vibration is effectively suppressed compared to DAC. The average power of the tip trajectory error is calculated from its PSDs in Fig. 3.24 and Fig. 3.25 respectively, and it was found that there is a considerable reduction in average power of -5dB and -4dB for link-1 and link-2, respectively, in case of FLAC compared to DAC.

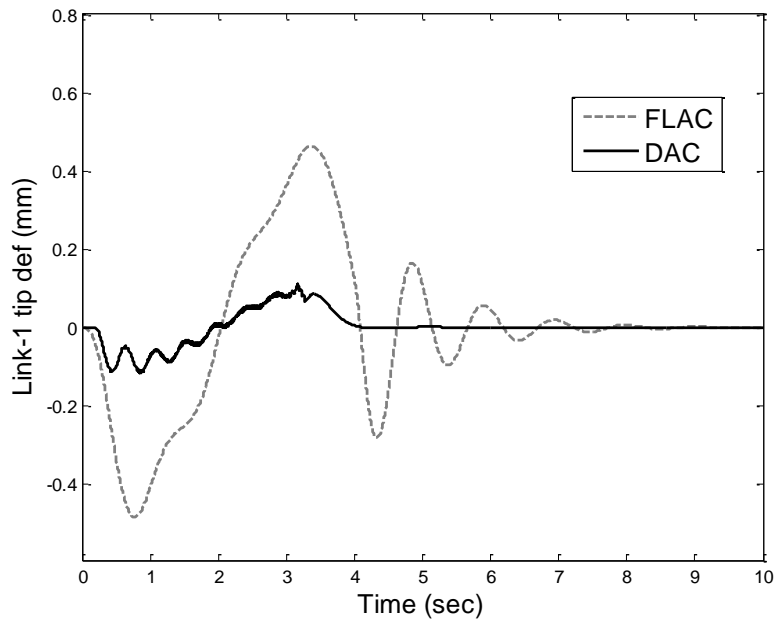


Fig.3.16 Simulation results (time domain) for link-1 tip deflection performances (0.457 kg):

DAC and FLAC

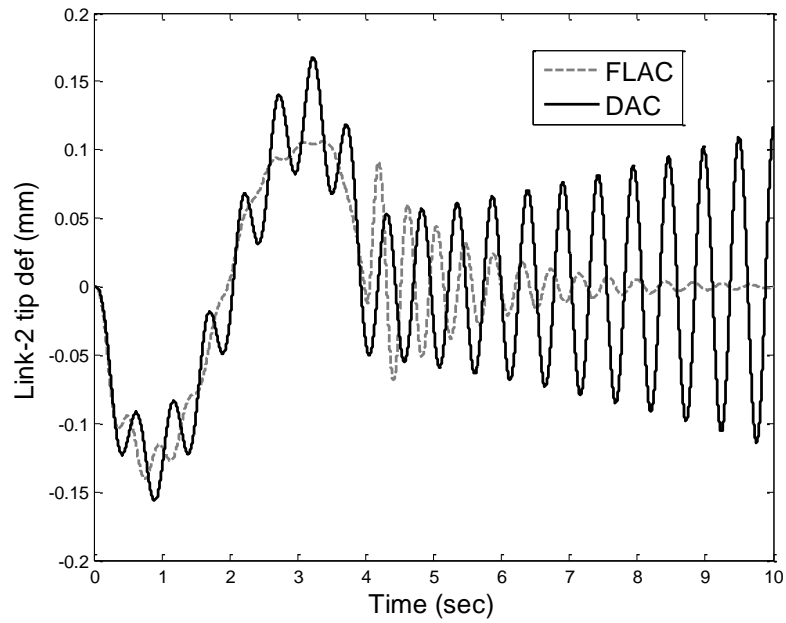


Fig.3.17 Simulation results (time domain) for link-1 tip deflection performances (0.457 kg):

DAC and FLAC

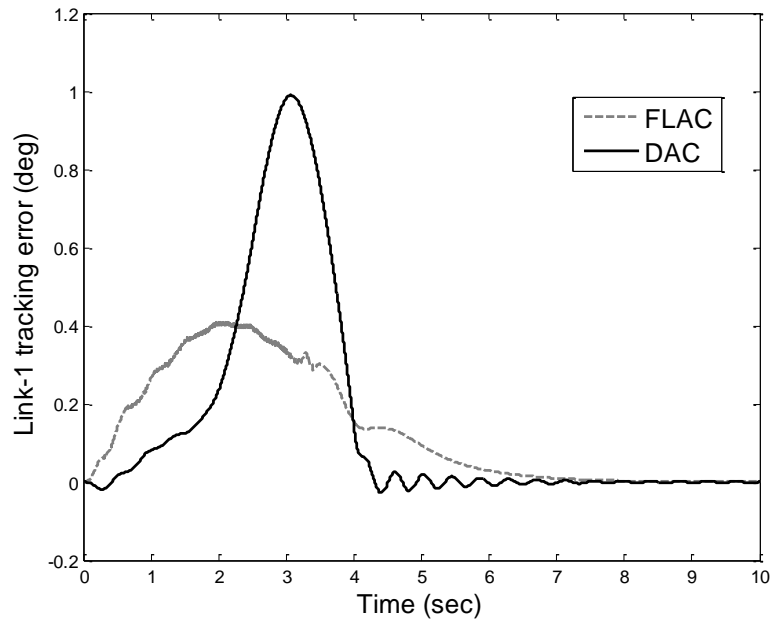


Fig.3.18 Simulation results (time domain) for tip trajectory tracking errors (Link-1) (0.457 kg)

DAC and FLAC

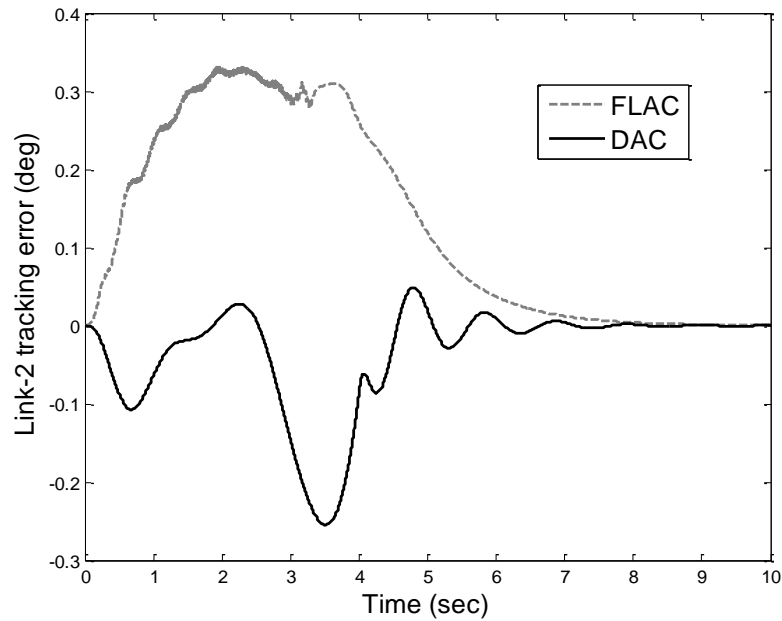


Fig.3.19 Simulation results (time domain) for tip trajectory tracking errors (Link-2) (0.457 kg)

DAC and FLAC

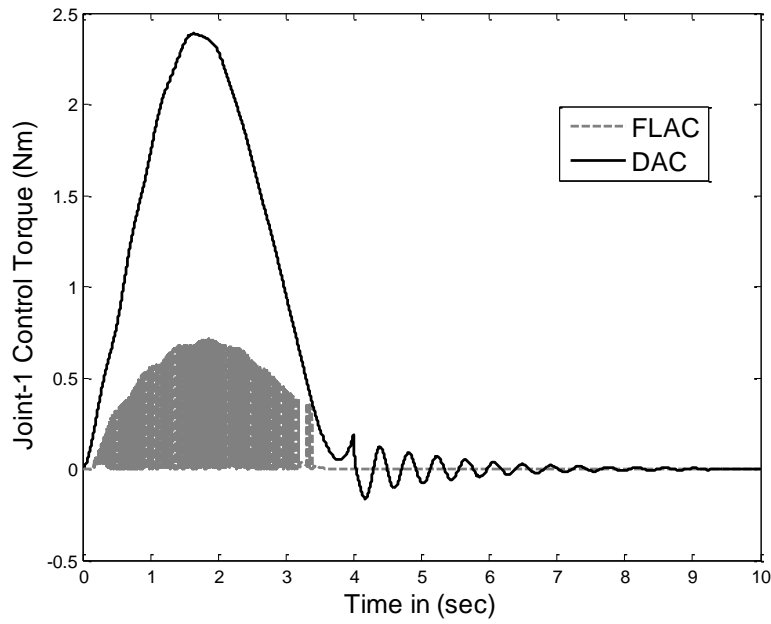


Fig.3.20 Simulation results (time domain) for torque profiles (joint-1) (0.457 kg): DAC and  
FLAC

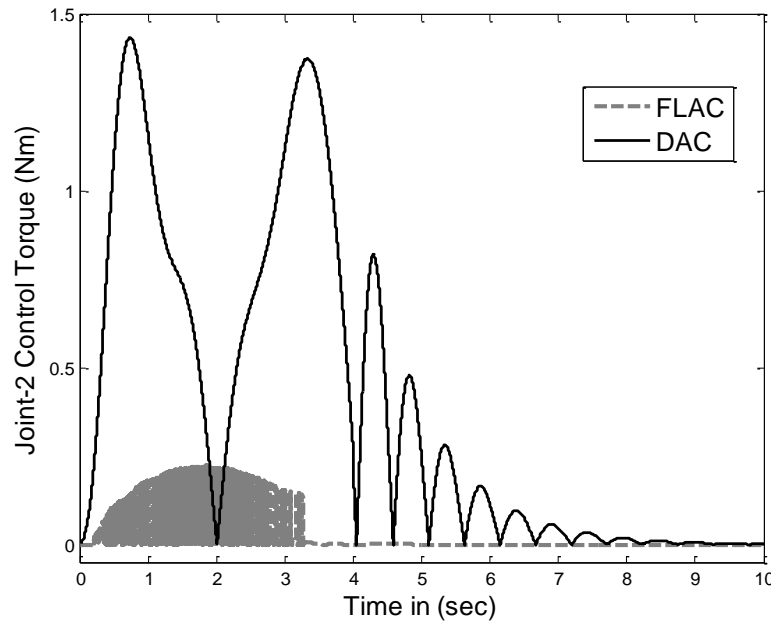


Fig.3.21 Simulation results (time domain) for torque profiles (joint-2) (0.457 kg): DAC and  
FLAC

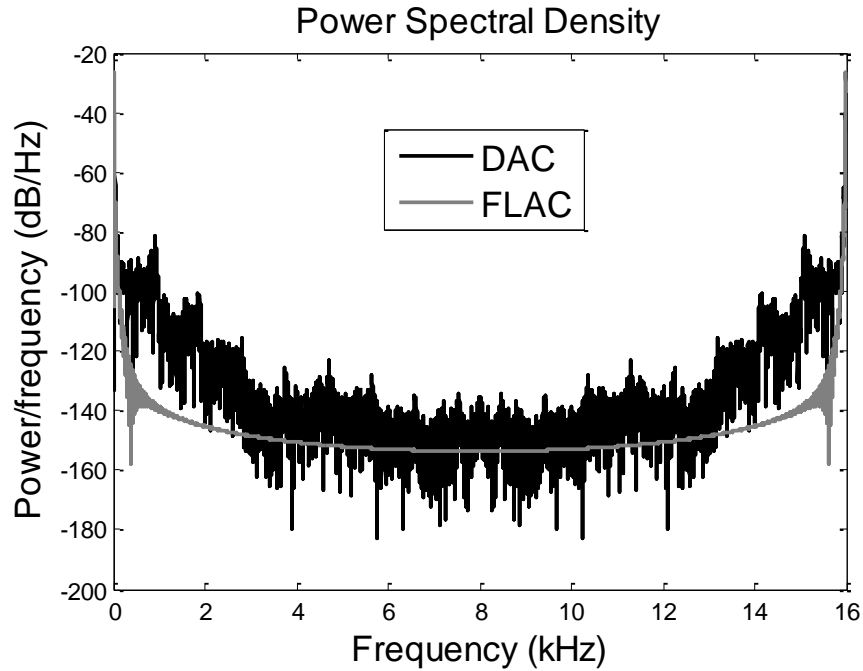


Fig.3.22 Simulation results (frequency domain) for link-1 tip deflection performances (0.457 kg):

DAC and FLAC

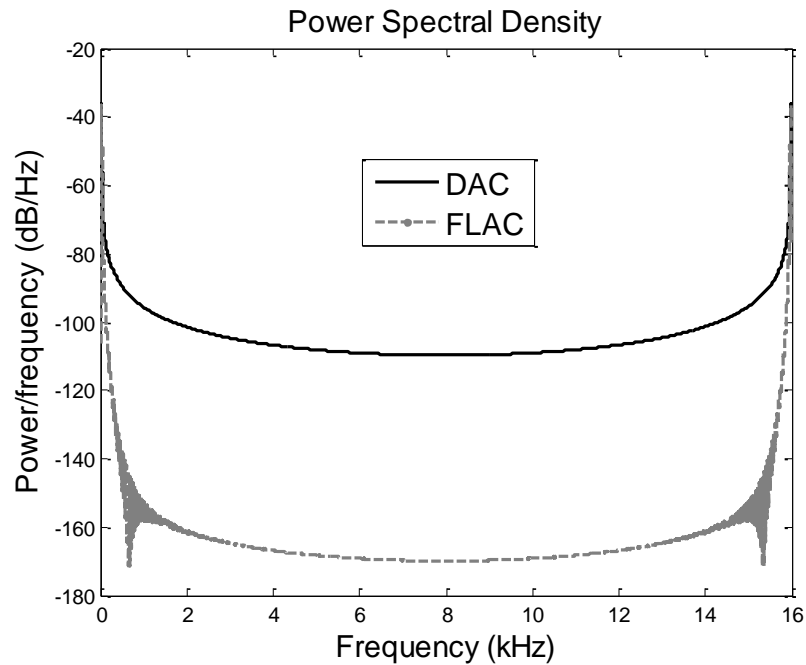


Fig.3.23 Simulation results (frequency domain) for link-1 tip deflection performances (0.457 kg):

DAC and FLAC



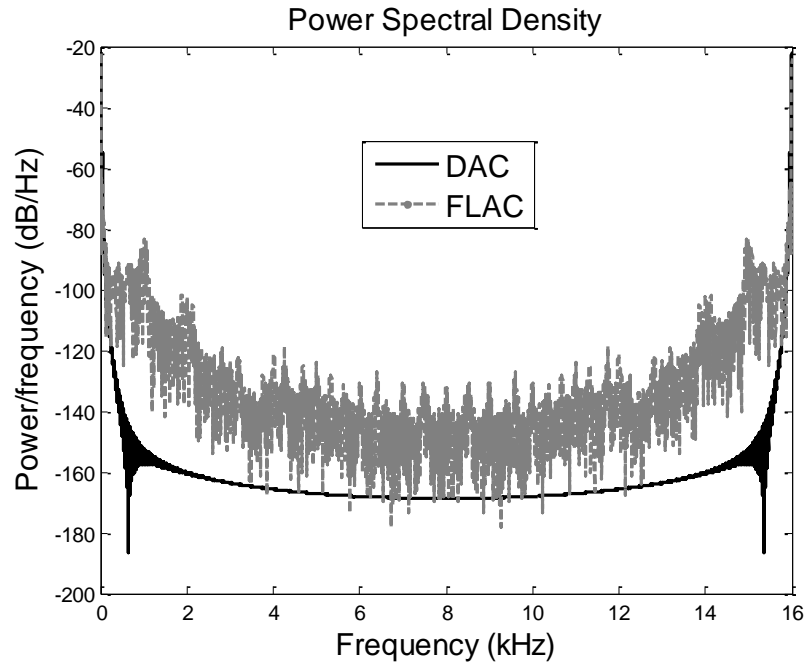


Fig.3.24 Simulation results (frequency domain) for tip trajectory tracking errors (Link-1) (0.457

kg) DAC and FLAC

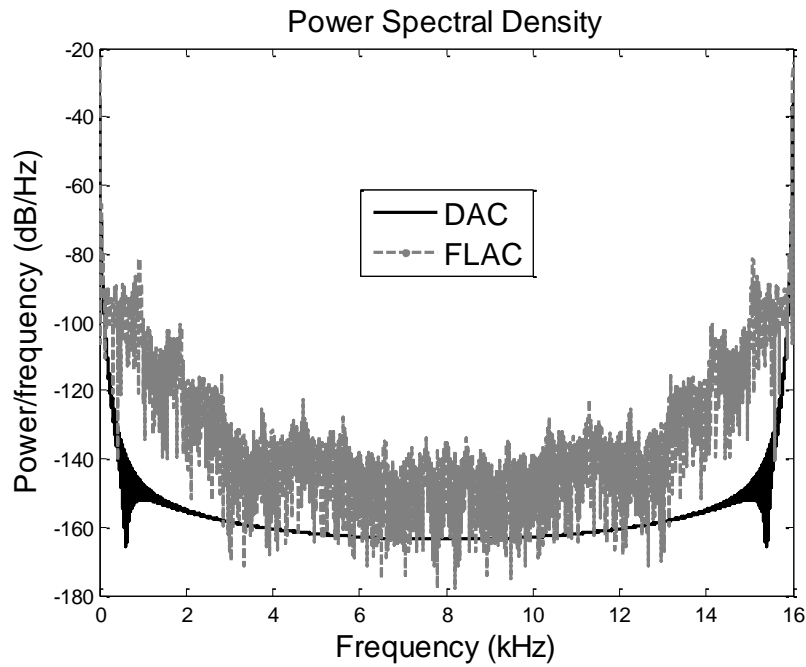


Fig.3.25 Simulation results (frequency domain) for tip trajectory tracking errors (Link-2) (0.457

kg) DAC and FLAC

### 3.4.3 Experimental results for an initial payload of 0.157

Fig.3.26-3.31 shows comparison of the experimental results for TLFM obtained by employing FLAC and DAC with an initial payload of 0.157 kg. Fig.3.26 and Fig.3.27 shows the tip deflection trajectories for the link-1 and link-2 when loaded for a 0.157 kg payload. From Fig.3.26, it can be seen that initial deviation for FLAC and DAC are 0.16 mm and 0.18 mm for link-1. Link-2 tip deflection characteristics are shown in Fig.3.27, from which it is seen that an initial deviation of 0.18 mm and 0.22 mm of for FLAC and DAC respectively.

Fig.3.28 and Fig.3.29 show the comparison of the tip trajectory tracking, after 4 sec when the tip attains the final position, the steady state error for DAC and FLAC are  $0.1^\circ$  and  $0.2^\circ$  for link-1 and link-2 respectively after 4sec. Although DAC show more amplitude in the tip deflection trajectory compared to FLAC, but manage to show better tip trajectory tracking error. Torque profiles for joint-1 generated by employing the DAC and FLAC controllers are shown in Fig.3.30, and that for joint-2 is shown in Fig.3.31. The joint torque control input for link-1 obtained by DAC reaches to a maximum value (9 Nm) at 2 sec when the tip reaches to the final position at 4 sec the control input reduces to 5 Nm. In case of FLAC where control input reaches to a maximum value (2 Nm) at 2 sec. From Fig.3.31, the joint control torque signals generated by DAC and FLAC for link-2 have maximum of 12 Nm and 10 Nm respectively. The reason of DAC being generating more torque compared to FLAC is that the parameters of the TLFM are updated using the error dynamics. PSDs (frequency domain) analysis was pursued and results presented in Figs. 3.32 to 3.35. From Fig. 3.32 and Fig. 3.33 it can be seen that the average power of the PSD for FLAC is -1dB and -0.6dB less compared to DAC for link-1 and link-2 respectively. The reduction in average power in case of FLAC signifies that a better damping is achieved for link deflection compared to DAC for the same payload. Also, the average power of

the tip trajectory error is calculated from its PSD in Fig. 3.34 and Fig. 3.35 respectively. From these figures it is observed that there is a reduction in average power of -1.5dB and -1.4dB for link-1 and link-2 respectively. Thus, FLAC suppresses the flexible mode vibration significantly.

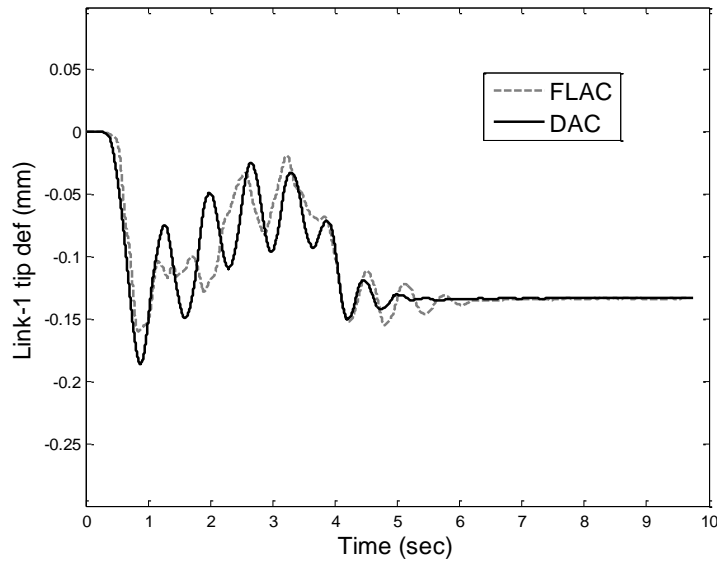


Fig.3.26 Experiment results (time domain) for link-1 tip deflection performances (0.157 kg):

DAC and FLAC

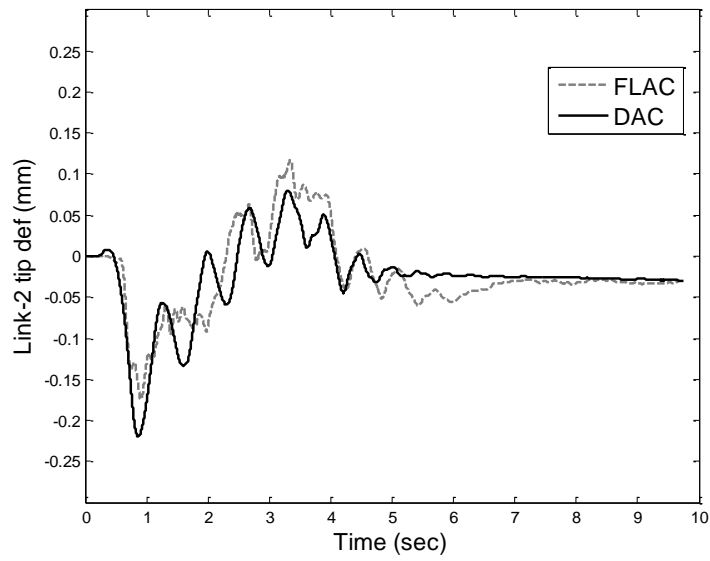


Fig.3.27 Experiment results (time domain) for link-2 tip deflection performances (0.157 kg):

DAC and FLAC

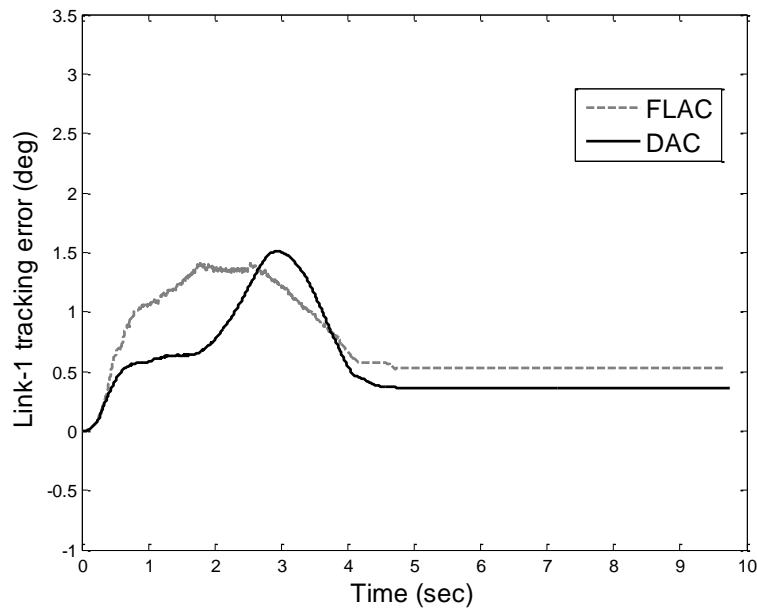


Fig.3.28 Experiment results (time domain) for tip trajectory tracking errors (Link-1) (0.157 kg):

DAC and FLAC

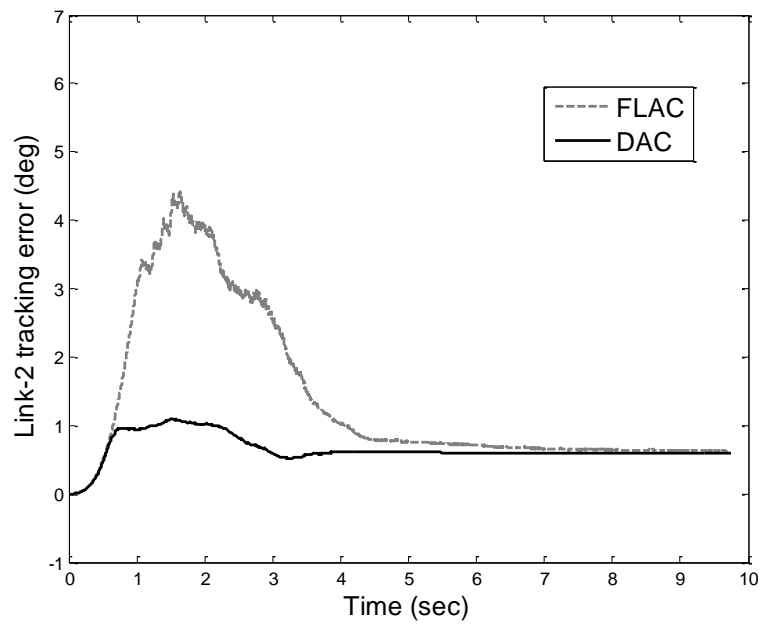


Fig.3.29 Experiment results (time domain) for tip trajectory tracking errors (Link-2) (0.157 kg):

DAC and FLAC

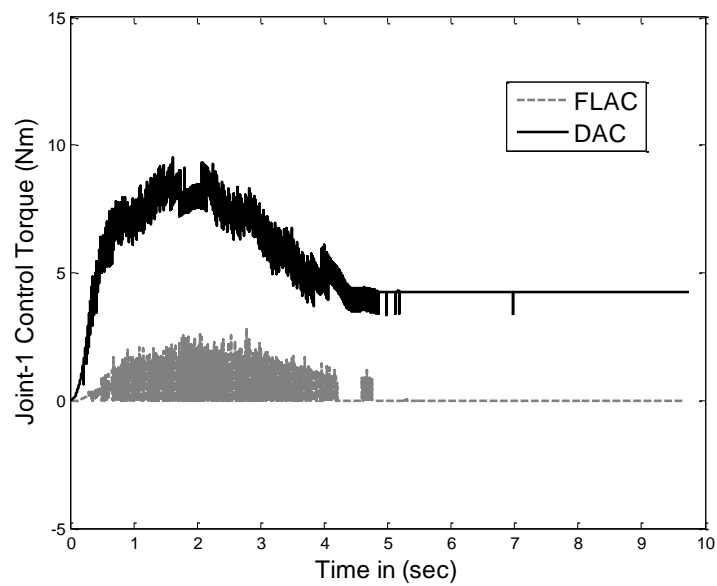


Fig.3.30 Experiment results (time domain) for torque profiles (joint-1) (0.157 kg): DAC and

FLAC

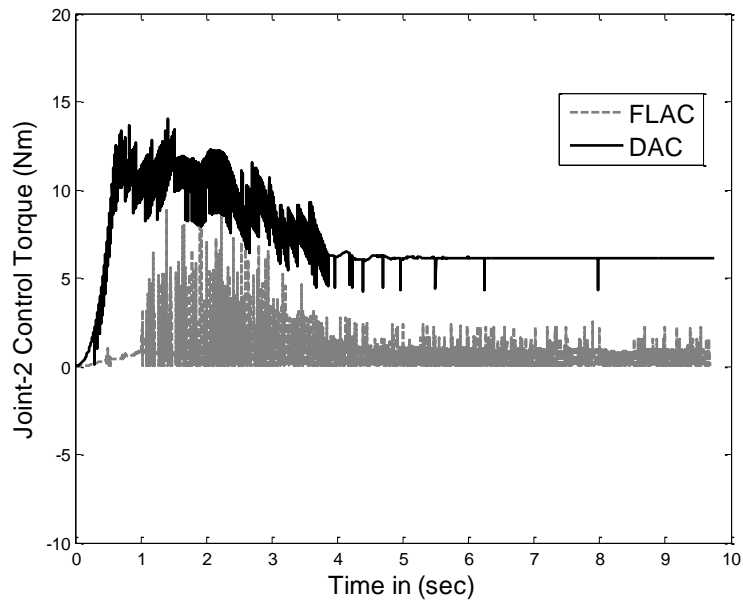


Fig.3.31 Experiment results (time domain) for torque profiles (joint-2) (0.157 kg): DAC and  
FLAC

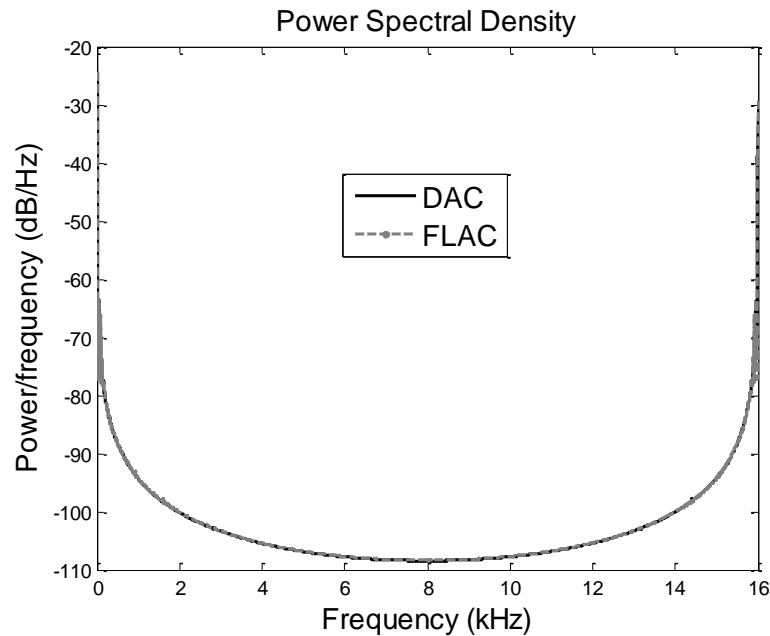


Fig.3.32 Experiment results (frequency domain) for link-1 tip deflection performances (0.157  
kg): DAC and FLAC

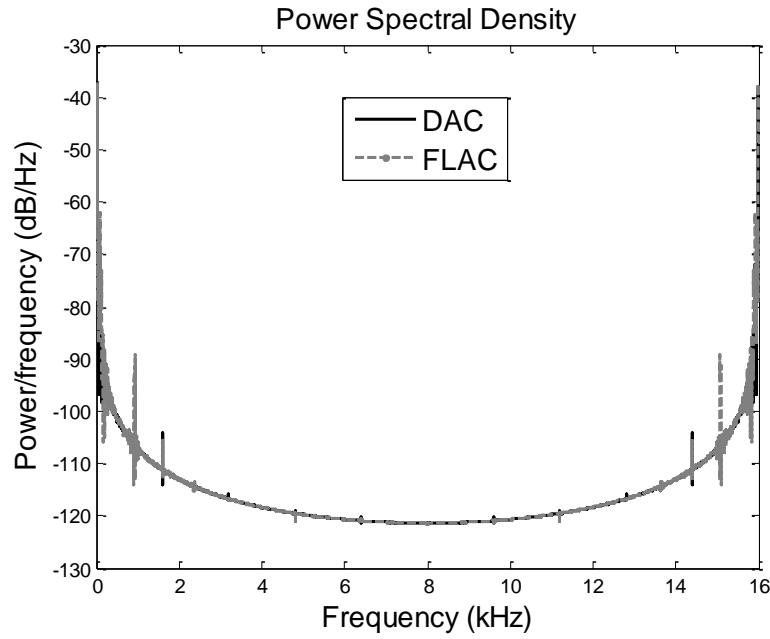


Fig.3.33 Experiment results (frequency domain) for link-2 tip deflection performances (0.157

kg): DAC and FLAC

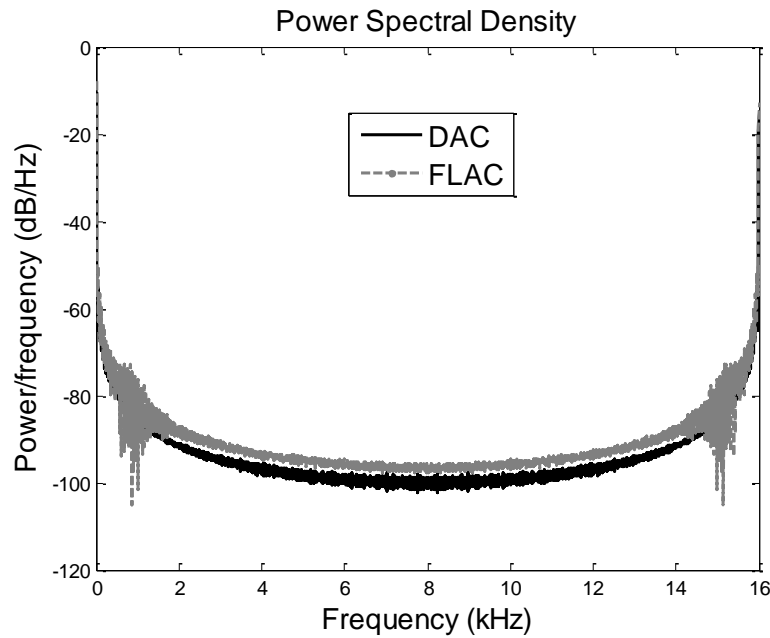


Fig.3.34 Experiment results (frequency domain) for tip trajectory tracking errors (Link-1) (0.157

kg): DAC and FLAC

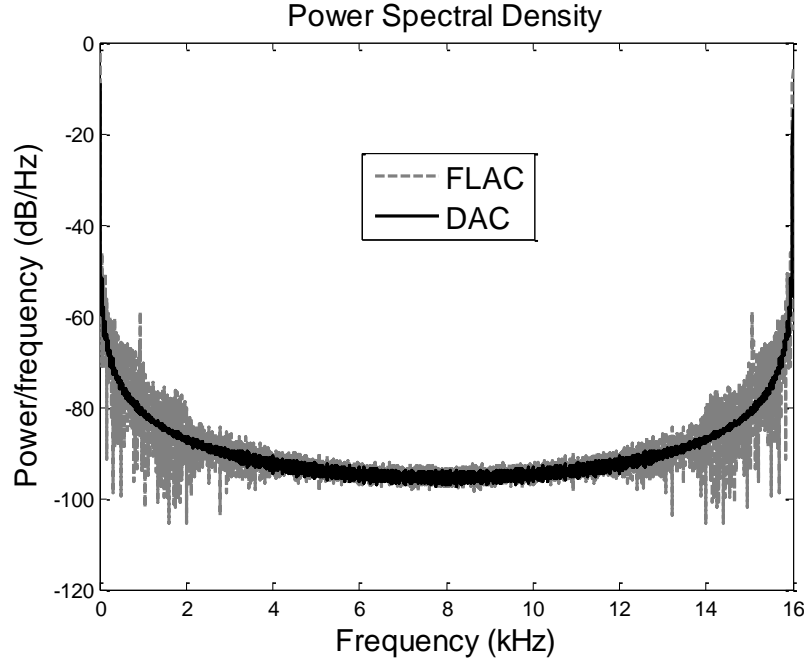


Fig.3.35 Experiment results (frequency domain) for tip trajectory tracking errors (Link-2) (0.157 kg): DAC and FLAC

#### 3.4.4 Experimental results for an additional payload of 0.3 kg:

The payload mass is now changed by adding an additional payload of 0.3 kg to the initial payload of 0.157 kg. Fig.3.36-41 shows comparison of the experimental results for TLFM obtained by employing FLAC and DAC with a payload of 0.457kg. Fig.3.36 and Fig.3.37 show the tip deflection trajectories for the link-1 and link-2 when the end effector carries a payload of 0.457 kg. From Fig.3.36 it is seen that in case of FLAC there exists an initial deviation of 0.2 mm for link-1 as compared to DAC which is 0.25 mm. Link-2 tip deflection responses obtained by using DAC and FLAC are shown in Fig.3.37. FLAC has 0.28 mm of maximum deviation as compared to DAC where a maximum deviation is 0.32 mm.



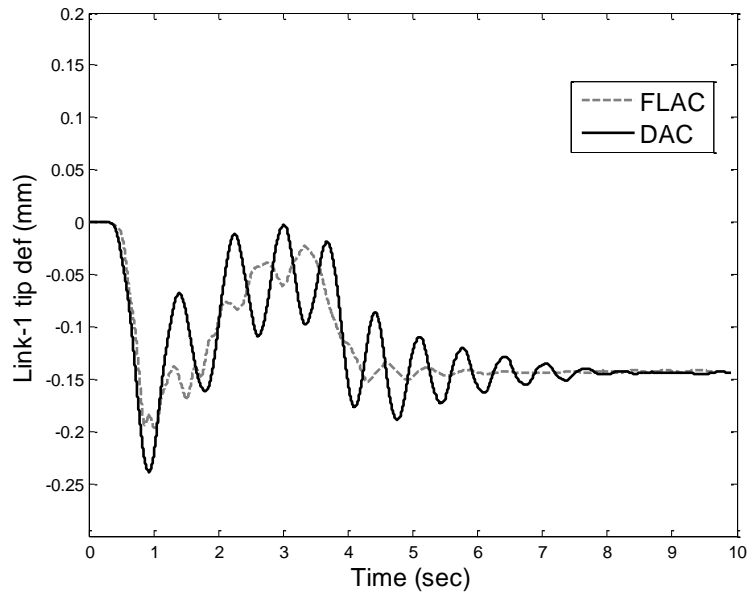


Fig.3.36 Experiment results (time domain) for link-1 tip deflection performances (0.457 kg):

DAC and FLAC

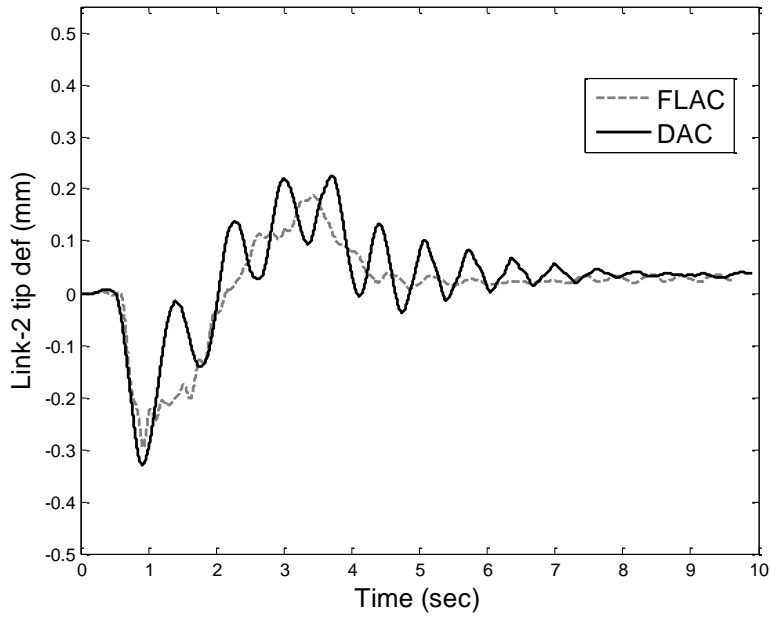


Fig.3.37 Experiment results (time domain) for link-2 tip deflection performances (0.457 kg):

DAC and FLAC

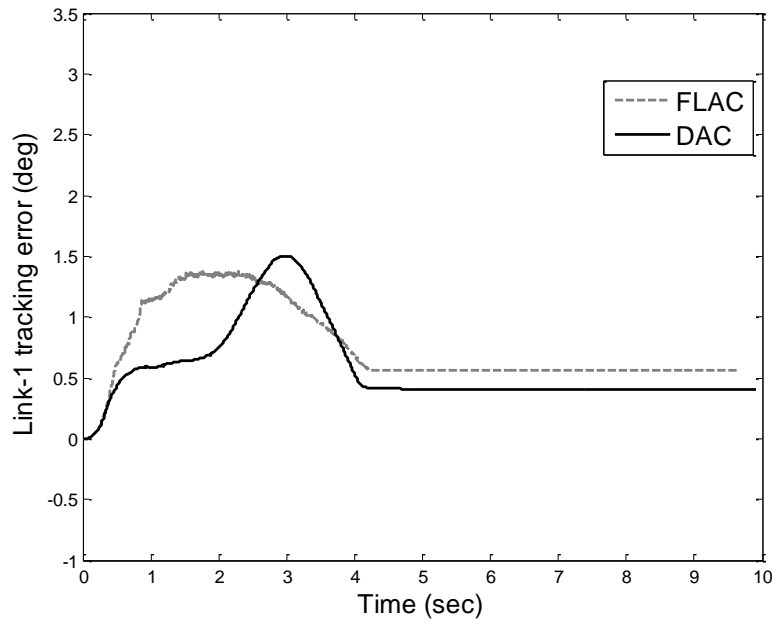


Fig.3.38 Experiment results (time domain) for Tip trajectory tracking errors (Link-1) (0.457 kg):

DAC and FLAC

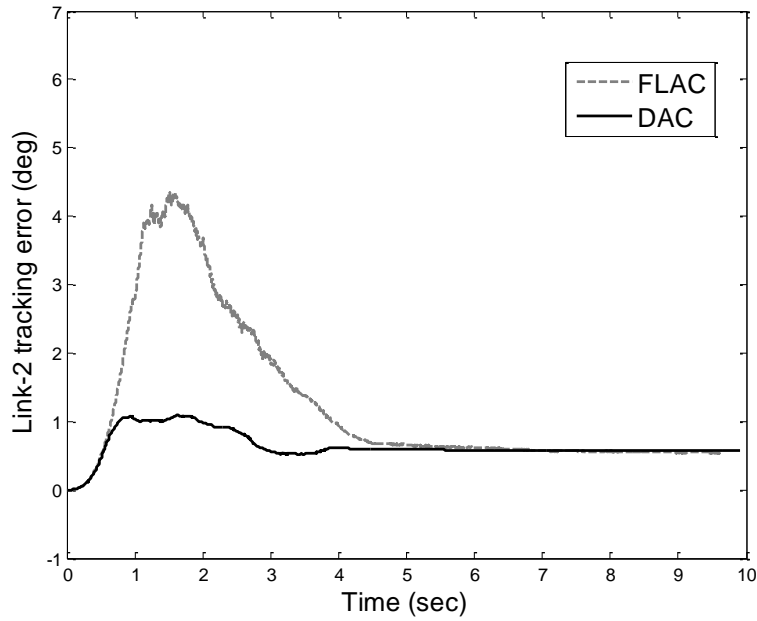


Fig.3.39 Experiment results (time domain) for tip trajectory tracking errors (Link-2) (0.457 kg):

DAC and FLAC

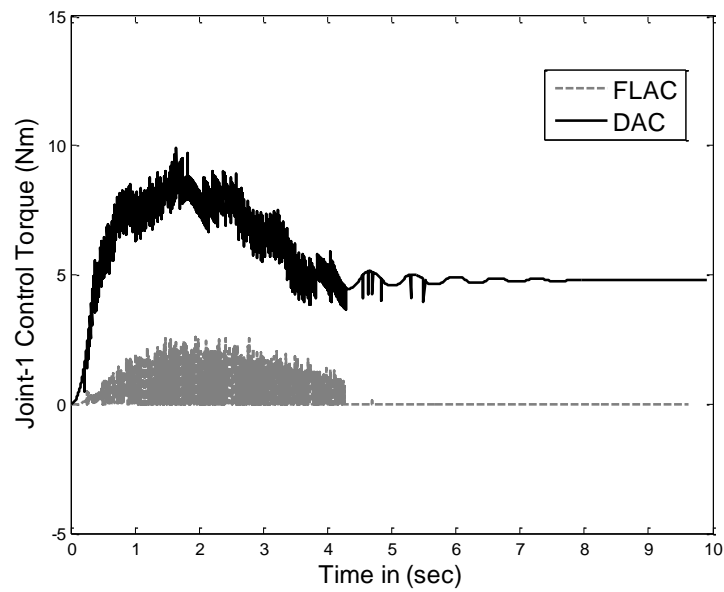


Fig.3.40 Experiment results (time domain) for torque profiles (joint-1) (0.457 kg): DAC and  
FLAC

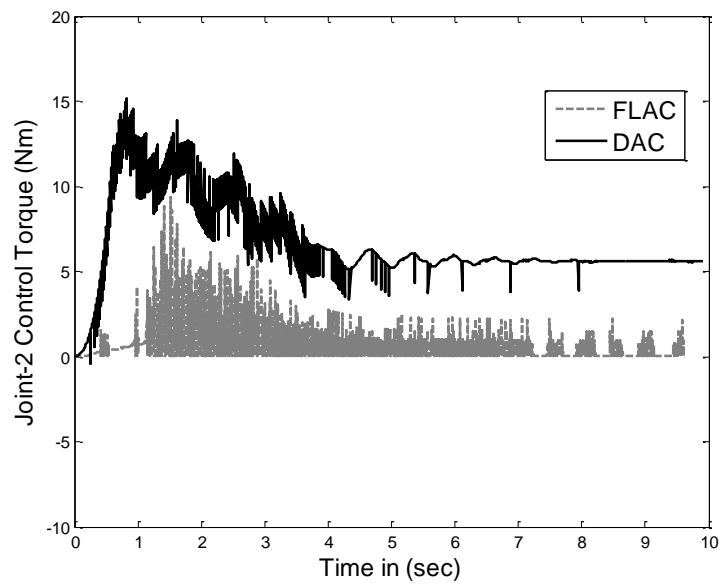


Fig.3.41 Experiment results (time domain) for torque profiles (joint-2) (0.457 kg): DAC and  
FLAC

Fig.3.38 and Fig.3.39 compare the tip trajectory tracking performances for link-1 and link-2 respectively. From Fig.3.38 and Fig.3.39 it is clear that when the final position is attained, FLAC and DAC show a finite steady state error of 0.7 sec and 0.4 sec respectively.

The TLFM is an infinite dimensional system due to distributed link flexure. Higher modes have been neglected in modeling therefore there is a difference in steady state error for simulation and experimental results.

Torque profile generated for joint-1 by the DAC and FLAC controllers are shown in Fig.3.39 and Fig.3.41. From Fig.3.39 it is seen that the DAC torque signal reaches to a maximum value of 9.5 Nm and reduces to 5 Nm at 4 sec when the final position is tracked. Torque signal generated in case of FLAC becomes maximum (2.5 Nm) at 2 sec and almost reduces to zero at the final position. From Fig.3.41, torque profile generated for joint-2, it is seen that the torque signal in case of DAC reaches to maximum value of 15 Nm at 1 sec and reduces to 6 Nm at 4 sec when the final position is tracked. Torque signal obtained by FLAC reaches to maximum value of 9 Nm at 1.5 sec and reduces to 2 Nm at 4 sec. The performance of the FLAC in time domain responses are again verified in frequency domain, from Fig. 3.42 and Fig. 3.43 the average power of the PSDs for FLAC was found to be -0.1dB and -2.3dB less compared to DAC for link-1 and link-2 respectively. Also, the average power of the tip trajectory error is calculated from its PSDs in Fig. 3.44 and Fig. 3.45 respectively. There is a reduction in average power of -1.5dB and -0.4dB for link-1 and link-2 respectively. By analyzing the frequency domain responses it can be concluded that there is a large reduction achieved in the average power resulting suppression of modal vibration effectively in case of FLAC compared to DAC.

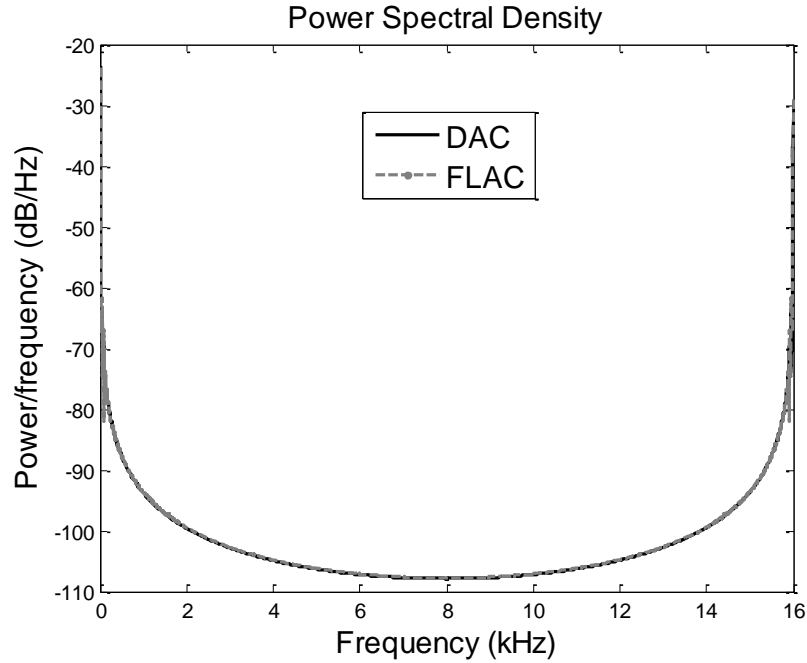


Fig.3.42 Experiment results (frequency domain) for link-1 tip deflection performances (0.457 kg): DAC and FLAC

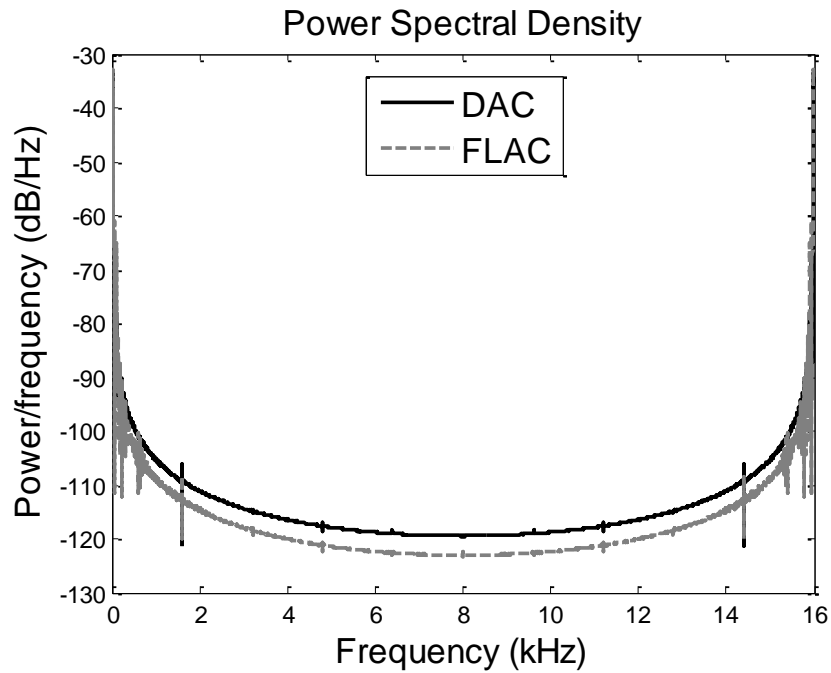


Fig.3.43 Experiment results (frequency domain) for link-2 tip deflection performances (0.457 kg): DAC and FLAC

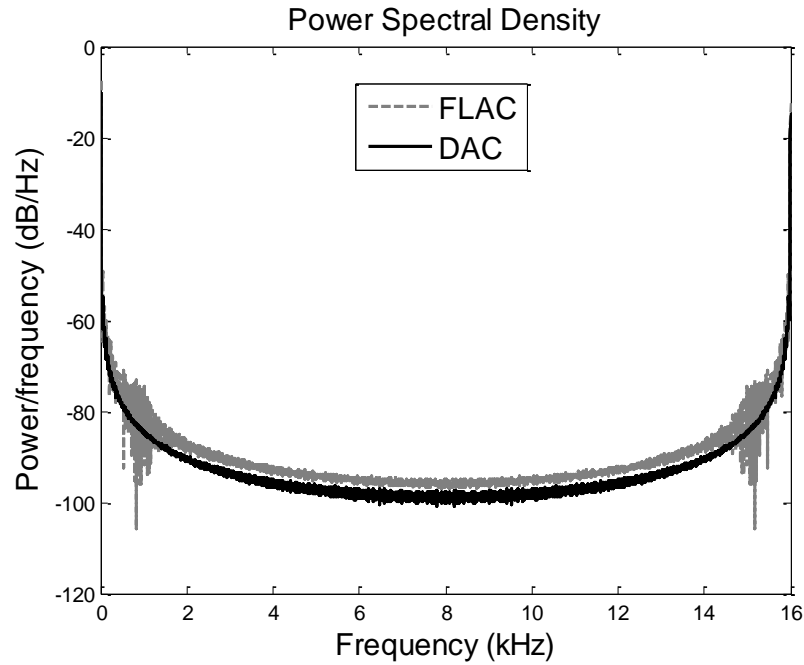


Fig.3.44 Experiment results (frequency domain) for Tip trajectory tracking errors (Link-1) (0.457

kg): DAC and FLAC

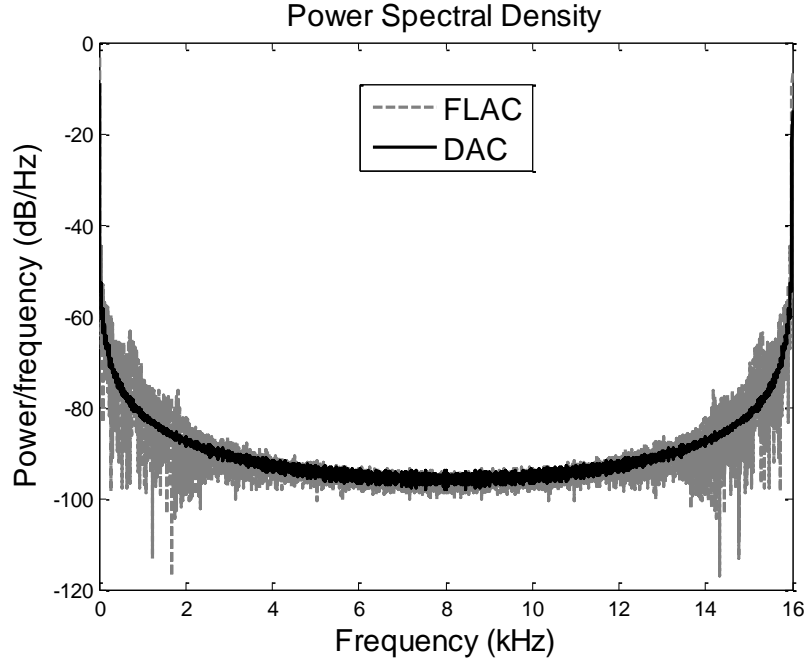


Fig.3.45 Experiment results (frequency domain) for tip trajectory tracking errors (Link-2) (0.457

kg): DAC and FLAC

### 3.5 Chapter Summary

This chapter has presented development, implementation and comparison performances of two adaptive control schemes i.e. direct adaptive control (DAC) and fuzzy learning based adaptive control (FLAC) for tip trajectory tracking and suppressing tip deflection of a two-link flexible manipulator (TLFM) while it is subjected to handle different unknown payload. The performances of the DAC and FLAC have been obtained after successfully implementing these control algorithms to both a physical flexible robot set-up in the Lab., and to the dynamic model of the TLFM. The simulation and experimental results obtained show that with change in payloads the DAC exhibited superior performance compared to the FLAC in real-time.

The superior performance of the DAC over FLAC may be due to the former's ability to incorporate the estimated TLFM parameters directly into the controller unlike in FLAC where the controller adapts based on a reference model output.

## Chapter 4

# Reinforcement Learning based Adaptive Control of a Two-Link Flexible Manipulator

Most of the intelligent controllers which are based on neural network, fuzzy logic and hybrid neuro-fuzzy for FLMs as discussed in *Chapter 1* are based on supervised learning [36-58], where the learning is driven by error signal (difference between desired and current response), whereas another learning method called reinforcement learning (RL), which occurs when an agent learns behavior through trial-and-error interaction with the environment based on “reinforcement” signals from the environment [59]. The benefits of RL based adaptive control are that it generates adaptive optimal control *online*. Also, in past RL is applied successfully for many complex systems such as in retail inventory management [80], intelligent databases [81], electrical power systems control [82], flight control studies [83], dynamic power management



[84], UAVs [85], robotics [86], traffic signal control and optimal adaptive control [87, 88]. This *Chapter* exploits RL technique for developing real-time adaptive control of tip trajectory and deflection of a two-link flexible manipulator handling variable payloads. This proposed adaptive controller consists of a proportional derivative (PD) tracking loop and an actor-critic based reinforcement learning loop that adapts the actor and critic weights in response to payload variations while suppressing the tip deflection and tracking the desired trajectory. Tip trajectory tracking and suppression of tip deflection performances of the proposed reinforcement learning based adaptive controller are compared with that of a nonlinear regression based direct adaptive controller and a fuzzy learning based adaptive controller developed in *Chapter 3*. The Chapter is organized as follows. In *Section 4.2* the development of the proposed reinforcement learning based adaptive controller is presented. Simulation and experimental results are discussed in *Section 4.3*. *Section 4.4* presents the chapter summary.

## 4.1. Introduction

In *Chapter 3*, adaptive controllers for flexible manipulators with variable payloads have been described using a direct adaptive controller (DAC) and also a fuzzy learning based adaptive control (FLAC). The DAC suffers from dependency on identification procedure and excessive tuning of adaptive gains. FLAC design depends upon proper formulation of control rule base. Also, intelligent controllers based on supervised learning using neural networks and fuzzy logic have been designed by some investigators [41] and [21] for flexible-link manipulators under parametric uncertainty. However, neural network based controllers require training of the synaptic weights to an optimal value which consume considerable amount of time and computational complexity. A hybrid neuro-fuzzy based adaptive controller has been proposed in

[54]. Although, the above hybrid neuro-fuzzy controller shows better performance compared to neural network and fuzzy logic based adaptive controllers but it needs a priori information about the input output relationship, i.e. supervised and off-line learning are essentially required. Also adaptive control of a multi-link flexible manipulator is more complex compared to a single-link flexible manipulator control problem owing to interlink coupling effects.

Thus, there is a need for a precise real-time adaptive control for flexible-link manipulators under payload variation. Hence, development of a real-time adaptive control for both tip trajectory tracking and suppression of tip deflection for a two-link flexible manipulator (TLFM) handling variable payload is the objective of this Chapter.

The contribution of this Chapter lies in developing a new reinforcement learning (RL) based real-time adaptive control for a TLFM. This work attempts to exploit actor-critic based reinforcement learning with modification in critic as well as in actor to develop an adaptive control for a TLFM. Many of the previous works on RL based control use least square (LS) approach to estimate the weights of the value function [89]. But as the LS are batch processing technique it is unsuitable for real-time control. Therefore, the proposed actor-critic reinforcement learning based adaptive control (RLAC) uses a recursive least-square based temporal difference learning to obtain the optimal weights of the value function in the critic. Further, a mechanism of eligibility trace [90] and adaptive memory are embedded to this temporal difference algorithm to enhance learning what we call as Recursive Least Square-Eligibility Trace-Adaptive Memory algorithm (RLS-ET-AM) algorithm. The proposed algorithm calculates the initial critic parameters off-line in order to reduce the computational overhead in real-time unlike previous approaches where either zero or random values were taken [91]. To ensure stability of the RLAC, a discrete time PD controller is supplemented with the above RL learning. The proposed

RLAC is compared with a nonlinear direct adaptive controller (DAC) and a fuzzy learning based adaptive controller (FLAC) to validate the performances of the proposed RLAC.

## 4.2. Reinforcement Learning based adaptive control

Reinforcement learning takes places when an agent (TLFM in this work) understands and learns by observing the environment workspace) based on a scalar internal reinforcement signal called reward  $r_k$  and  $\delta_{TD_k}$  (temporal difference error (TD error) at  $k^{\text{th}}$  instant. TD error is the external reinforcement signal that comes from the environment to minimize a long term value function described next. Fig.4.1 shows the actor-critic based reinforcement learning adaptive controller for real-time implementation of the TLFM carrying a variable payload. It consists of two important components such as an actor-critic block and a PD control loop.

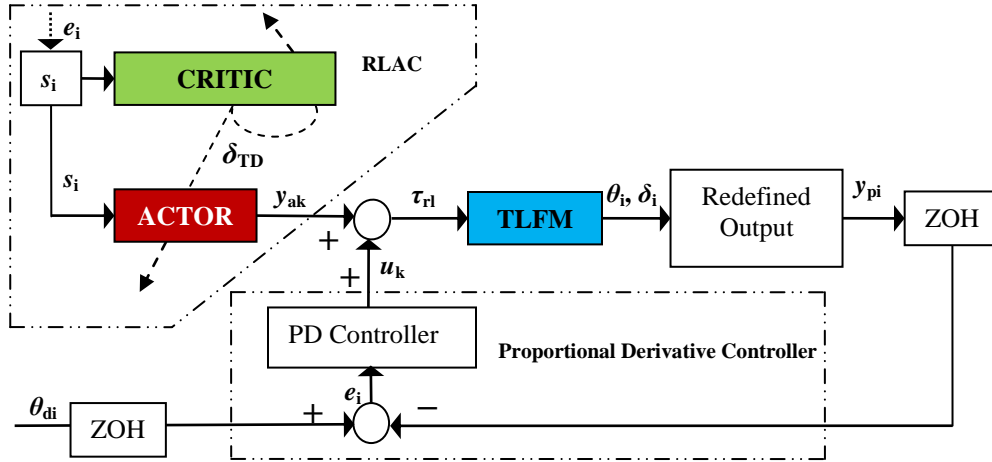


Fig.4.1 Structure of reinforcement learning based adaptive control for a TLFM

The actor-critic block adapts the actor and critic weights,  $w_{a_k}$  and  $w_{c_k}$  in order to compensate for the joint torque input under payload uncertainties. The PD controller provides stable closed loop performance by regulating the desired tip trajectory. A zero order hold (ZOH) block is used to achieve a discrete value of the desired tip trajectory  $y_{di}$  and redefined output  $y_{pi}$ . Thus, the net adaptive torque  $\tau_{ri}$  for  $i^{th}$  link is given by

$$\tau_{ri} = y_{a_k} + u_k \quad (4.1)$$

where  $u_k$  is the proportional derivative control action and  $y_{a_k}$  is the estimated actor output. The PD control law uses the past values of tip trajectory tracking error  $e_{i_{k-1}}$  for  $i^{th}$  link and the past value of the PD control output  $u_{i_{k-1}}$ . Thus, the  $i^{th}$  digital PD control action is generated using the following recursive law.

$$u_{i_k} = K_p (e_{i_k} - e_{i_{k-1}}) + K_d (e_{i_k} - 2e_{i_{k-1}} + e_{i_{k-2}}) + u_{i_{k-1}} \quad (4.2)$$

where  $K_p$  and  $K_d$  are proportional and derivative gain respectively and  $e_{i_{k-1}}$  and  $e_{i_{k-2}}$  are the tracking errors at sampling instants  $(k-1)$  and  $(k-2)$ , respectively,  $u_{i_{k-1}}$  is the control action at  $(k-1)^{th}$  instant for  $i^{th}$  link.

#### 4.2.1. Actor-Critic block

Fig.4.2 describes the actor-critic based reinforcement learning, where  $y_{a_k}$  denotes the control policy applied to the actuators of the TLFM,  $\zeta_{i_k} = y_{pi_k}$  represents the state vector comprising of measured redefined tip trajectory given in (2.6) for the  $i^{th}$  link at  $k^{th}$  instant. Reward at

$((k+1)^{\text{th}}$  instant,  $r_{k+1}$  is the result of the transition  $(\zeta_{i_k}, y_{ak}, \zeta_{i_{k+1}})$  where  $\zeta_{i_{k+1}}$  is the successive value of  $\zeta_{i_k}$  at  $(k+1)^{\text{th}}$  instant.

Let a value or cost be assigned to the total cumulative reward function say  $\mathfrak{R}_k(\zeta_k)$  expressed as

$$\mathfrak{R}_k(\zeta_k) = \sum_{k=0}^{\infty} \gamma^k r_{k+1} \quad (4.3)$$

where  $\gamma^k$  is the discount factor at the  $k^{\text{th}}$  instant. The value of the discount factor decides as how much weightage is to be given to future rewards. The reinforcement learning searches for a control policy,  $y_{ak}$  in the actor so that it minimizes the value function defined in eq. (4.4)

$$\mathfrak{R}_k(\zeta_k) = \min_{y_{ak}} \left( \sum_{k=0}^{\infty} \gamma^k r_{k+1} \right) \quad (4.4)$$

It is difficult to achieve minimization of the value function  $\mathfrak{R}_k(\zeta_k)$  in real-time as eq. (4.4) needs evaluation of an infinite sum backward in time. To provide forward in time solution of (4.4) approximation of the value function  $\mathfrak{R}_k(\zeta_k)$  is necessary.

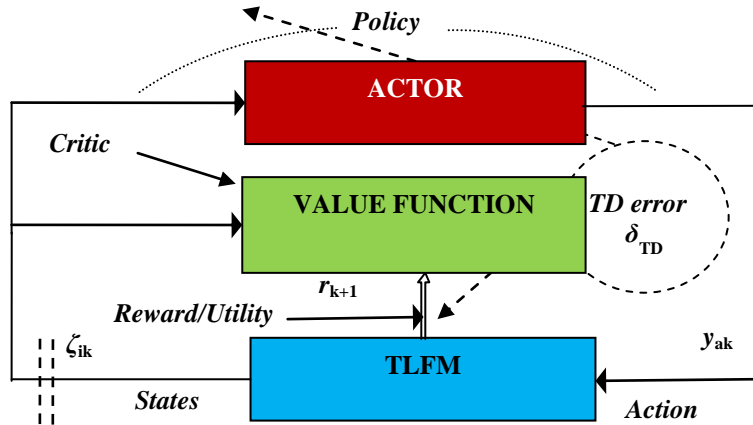


Fig.4.2 Actor-Critic based Reinforcement learning

In order to approximate the value function  $\mathfrak{R}_k(\zeta_k)$  Eq. (4.4) can be rewritten as sum of  $k^{\text{th}}$  step reward  $r_k$  and discount times infinite sum of the future value function in compact form as

$$\mathfrak{R}_k(\zeta_k) = r_k + \gamma \sum_{k=1}^{\infty} \gamma^{k-1} r_{k+1} \quad (4.5)$$

The difference equation equivalent of (4.5) is given by [9] as

$$\mathfrak{R}_k(\zeta_k) = r_k + \gamma \mathfrak{R}_k(\zeta_{k+1}) \quad (4.6)$$

where

$$\mathfrak{R}_k(\zeta_{k+1}) = \sum_{k=1}^{\infty} \gamma^{k-1} r_{k+1}$$

Eq. (4.6) is also known as Bellman equation [9]. Based on this equation,  $\delta_{TD_k}$  can be defined as

$$\delta_{TD_k} = r_k + \gamma \mathfrak{R}_k(\zeta_{k+1}) - \mathfrak{R}_k(\zeta_k) \quad (4.7)$$

$\delta_{TD_k}$  is a prediction error between predicted and observed performance. If (4.7) holds good for some value of  $y_{ak}$ , then  $\delta_{TD_k}$  must approach to zero. Thus, eq. (4.7) becomes

$$0 \cong r_k + \gamma \mathfrak{R}_k(\zeta_{k+1}) - \mathfrak{R}_k(\zeta_k) \quad (4.8)$$

The RLAC based actor-critic reinforcement learning consists of two separate blocks, actor and critic. In actor, the policy  $y_{ak}$  is updated and on critic, the value function  $\mathfrak{R}_k(\zeta_k)$  is updated using a linear function approximator based on recursive least square algorithm (RLS). Hence, the value function  $\mathfrak{R}_k(\zeta_k)$  relating the critic weights  $W_{ck}$  can be expressed as

$$\mathfrak{R}_k(x_k) = \Phi_{c_k}^T W_{c_k} \quad (4.9)$$

where  $\Phi_{c_k}^T$  is the regressor vector,  $\Phi_{c_k} = (x_k \otimes x_k)$ , where  $\otimes$  is the Kronecker product. Similarly,  $y_{ak}$  can be expressed in regressor form as

$$y_{ak} = \Phi_{a_k}^T W_{a_k} \quad (4.10)$$

where  $W_{a_k}$  is the matrix of actor weight estimates and  $\Phi_{a_k}^T$  is the actor regressor vector. Signals  $\delta_{TD_k}$  and  $r_k$  play vital role in determining the performance of the control policy by minimizing  $\delta_{TD_k}$  defined in (4.8). The performance measure of the TLFM control is attributed to achieve the desired tip trajectory tracking while simultaneously damping out the tip deflection. Therefore,  $s_i$  defined in Chapter 3 (3.7) which measures the accuracy of the tip trajectory tracking for  $i^{\text{th}}$  link is used to formulate the  $r_k$  and is given as

$$\left. \begin{aligned} r_k &= 0, \quad \text{if } (s_i^2 \leq \varepsilon) \\ \text{else} \\ r_k &= -0.5 \end{aligned} \right\} \quad (4.11)$$

where  $\varepsilon$  is a predefined tolerance value and a reward (negative) is taken in (4.11) to improve the closed loop performance. Substituting for  $\mathfrak{R}_k(\zeta_k)$  from (4.9) in (4.6), one obtains

$$\delta_{TD_k} = r_k + \gamma (\Phi_{c_{k+1}}^T W_{c_k}) - \Phi_{c_k}^T W_{c_k} \quad (4.12)$$

#### 4.2.2. Critic weight update using the proposed reinforcement learning algorithm

The objective of the critic is to estimate the value function  $\mathfrak{R}_k(\zeta_k)$  using proposed (RLS-ET-AM) algorithm. Let  $\hat{\mathfrak{R}}_k(\zeta_k)$  be the estimate of the value function  $\mathfrak{R}_k(\zeta_k)$  and a cost function  $J$

for N measurements is chosen so as to minimize the temporal difference error  $\delta_{TD_k}$  defined in (4.7). J is given as

$$J = \sum_{k=1}^{N-1} \left[ z_k \left( r_k + \gamma \hat{\mathfrak{R}}_k(\zeta_{k+1}) - \hat{\mathfrak{R}}_k(\zeta_k) \right) \right]^2 \quad (4.13)$$

where  $r_k$  is the reward function,  $\hat{\mathfrak{R}}_k(\zeta_k)$  is the estimate value of the value function  $\mathfrak{R}_k(\zeta_k)$  and  $z_k(\zeta_k)$  is the eligibility trace used to improve the temporal difference learning by selecting the eligible state embedded in  $(\zeta_k)$ . Let this algorithm be termed as RLS-ET algorithm. The eligibility trace is being defined as

$$z_k(\zeta_k) = \begin{cases} \gamma \lambda z_k(\zeta_k) + 1 & \text{if } \zeta_k = \theta_{di} \\ \gamma \lambda z_k(\zeta_k) & \text{if } \zeta_k \neq \theta_{di} \end{cases},$$

where  $\gamma$  is discount factor,  $\lambda$  is the value of the eligibility trace and  $\theta_{di}$  is the desired tip trajectory for  $i^{\text{th}}$  link, it is to be noted that both the values of  $\gamma$  and  $\lambda$  are less than unity. Substituting the value of  $\mathfrak{R}_k(\zeta_k)$  from (4.9) in (4.13) gives

$$J = \sum_{k=1}^{N-1} \left[ z_k \left( r_k + \gamma \Phi_{c_{k+1}}^T \hat{\mathbf{W}}_{c_{k+1}} - \Phi_{c_k}^T \hat{\mathbf{W}}_{c_k} \right) \right]^2 \quad (4.14)$$

Equation (4.14) can be modified in terms of predicted critic weights  $\hat{\mathbf{W}}_{c_{k+1}}$  as

$$J = \sum_{k=1}^{N-1} \left[ z_k \left( r_k + \hat{\mathbf{W}}_{c_{k+1}} \left( \gamma \Phi_{c_{k+1}}^T - \Phi_{c_k}^T \right) \right) \right]^2 \quad (4.15)$$

The least square solution [92] of (4.15) is given as

$$\hat{\mathbf{W}}_{c_{k+1}} = \left( \sum_{k=1}^N \left( \Phi_{c_k} \left( \Phi_{c_k} - \gamma \Phi_{c_k} \right)^T \right) \right)^{-1} \left( \sum_{k=1}^N \left( \Phi_{c_k} r_k z_k \right) \right) \quad (4.16)$$



A recursive form of the above equation with forgetting factor,  $\mu$  [92] can be obtained easily as follows.

$$\mathbf{W}_{c_{k+1}} = \mathbf{W}_{c_k} + \mathbf{G}_{k+1} \left[ \mathbf{r}_k + \left( \Phi_{c_k}^T - \gamma \Phi_{c_{k+1}}^T \right) \mathbf{W}_{c_k} \right] \quad (4.17)$$

with the Kalman gain  $\mathbf{G}_{k+1}$  and covariance matrix  $\mathbf{P}_{k+1}$  updation are given as follows.

$$\mathbf{P}_{k+1} = \frac{1}{\mu} \left[ \mathbf{P}_k - \mathbf{P}_k \mathbf{z}_k \left[ \mu + \left( \Phi_{c_k}^T - \gamma \Phi_{c_{k+1}}^T \right) \mathbf{P}_k \mathbf{z}_k \right]^{-1} \left( \Phi_{c_k}^T - \gamma \Phi_{c_{k+1}}^T \right) \mathbf{P}_k \right] \quad (4.18)$$

$$\mathbf{G}_{k+1} = \mathbf{P}_k \mathbf{z}_k \left( \mu + \left( \Phi_{c_k}^T - \gamma \Phi_{c_{k+1}}^T \right) \mathbf{P}_k \mathbf{z}_k \right)^{-1} \quad (4.19)$$

Equations (4.17)-(4.19) constitute the recursive least square based temporal difference learning with eligibility trace. Further, an incremental adaptive memory  $\mathbf{a}_m$  can be added to the above RLS-ET algorithm to enhance the learning speed of the critic. The resulting weight updation expressions with recursive least square based temporal difference learning with eligibility trace and an adaptive memory (RLS-ET-AM) are given in equations (4.20)-(4.23).

$$\mathbf{W}_{c_{k+1}} = \mathbf{W}_{c_k} + \mathbf{G}_{k+1} \left[ \mathbf{r}_k + \left( \Phi_{c_k}^T - \gamma \Phi_{c_{k+1}}^T \right) \mathbf{W}_{c_k} \right] \quad (4.20)$$

$$\mathbf{G}_{k+1} = \mathbf{P}_k \mathbf{z}_k \mathbf{a}_{m_k}^{-1} \left( \mu + \left( \Phi_{c_k}^T - \gamma \Phi_{c_{k+1}}^T \right) \mathbf{P}_k \mathbf{z}_k \mathbf{a}_{m_k}^{-1} \right)^{-1} \quad (4.21)$$

$$\mathbf{P}_{k+1} = \frac{1}{\mu} \left( \mathbf{a}_{m_k}^{-1} \left[ \mathbf{P}_k - \mathbf{P}_k \mathbf{z}_k \left[ \mu + \left( \Phi_{c_k}^T - \gamma \Phi_{c_{k+1}}^T \right) \mathbf{P}_k \mathbf{z}_k \right]^{-1} \right] \right) \quad (4.22)$$

$$\mathbf{a}_{m_k}^{-1} = \mathbf{a}_{m_k} + k_r \left[ \hat{\psi}_k^T \Phi_{c_k} \delta_{TD_k} \right] \quad (4.23)$$

The gradient vector  $\hat{\psi}_k$  is updated using following expression

$$\hat{\psi}_{k+1} = \left[ \mathbf{I} - \mathbf{G}_{k+1} \gamma \Phi_{c_{k+1}}^T \right] \hat{\psi}_k + \mathbf{S}_{k+1} \Phi_{c_{k+1}} \delta_{TD_k} \quad (4.24)$$

where  $I$  is the identity matrix and

$$S_{k+1} = \mathbf{a}_{m_{k+1}}^{-1} \left[ I - G_{k+1} \gamma \Phi_{c_{k+1}}^T \right] S_k \left[ I - \Phi_{c_k} G_{k+1} \right] + \mathbf{a}_{m_{k+1}}^{-1} \left[ G_{k+1} G_k^T P_{k+1} \right] \quad (4.25)$$

#### 4.2.3. Actor weight update using gradient based estimator and the proposed reinforcement learning algorithm

The actor weight vector  $W_{c_k}$  can be updated using gradient based estimator as described below.

The control policy  $y_{ak}$  can be written in parametric form as

$$y_{a_k} = \Phi_{a_k}^T W_{a_k} \quad (4.26)$$

and  $\hat{y}_{a_k} = \Phi_{a_k}^T \hat{W}_{a_k}$  be its estimate. Then the control policy estimation error can be written as

$$\tilde{y}_{a_k} = y_{a_k} - \hat{y}_{a_k} = \Phi_{a_k}^T (W_{a_k} - \hat{W}_{a_k}) \quad (4.27)$$

$$\hat{W}_{a_{k+1}} = \hat{W}_{a_k} - K_a \Phi_{a_k}^T (\hat{R}_k(\zeta_k) - \tilde{y}_{a_k}) \quad (4.28)$$

The control policy  $y_{ak}$  can also be rewritten in terms of the critic parameter  $W_{c_k}$  as follows

$$\hat{W}_{a_{k+1}} = \hat{W}_{a_k} - K_a \Phi_{a_k}^T (\Phi_{c_k}^T \hat{W}_{c_k} - \hat{y}_{a_k}) \quad (4.29)$$

$0 < K_a \leq 1$  is the adaptation gain.

Table 4.1: Proposed RLS-ET-AM algorithm

<b>Step 1:</b>	for k=0 <b>begin {</b> Define the performance index as given in (4.13)
<b>Step 2:</b>	Initialize initial values of $W_{c_k}, P_k, S_k, a_m, \mu, K_a, \gamma, z_k$
<b>Step 3:</b>	Observe the transition states of $y_{pi}, y_{di}, r_{k+1}$ and $\delta_{TD}$
<b>Step 4:</b>	Apply equations (4.20)-(4.25) to update critic weights
<b>Step 5:</b>	Apply equations (4.27)-(4.29) to update actor weights
<b>Step 6:</b>	Check the termination criteria from step: 1 update $k=k+1$ till criteria is satisfied <b>} end</b>

By measuring the external reinforcement signal  $\delta_{TD_k}$  and internal reinforcement signal  $r_k$ , the critic as well as actor weights are updated. The learning terminates as soon as approximation error tends towards zero. The proposed RLS-ET-AM algorithm is shown in Table 4.1.

#### 4.2.4. Convergence analysis of the critic weights using the proposed reinforcement learning algorithm

The existing RLS\_TD learning algorithm [103] is modified by adding an incremental adaptive memory to RLS based linear function approximator with off-line calculated critic weights. In order to prove the convergence of above RLS-ET-AM algorithm, certain assumptions are used. These are as follows.

*Assumption 1:* The discrete event of states  $\{\zeta_k\}$ , with transition probability matrix  $P$ , and distribution  $\chi$  satisfy

$$\chi^T P = \chi^T \quad (4.30)$$

*Assumption 2:* The transition reward  $r(\zeta_k, \zeta_{k+1})$  satisfies

$$E_0 \left[ r^2(\zeta_k, \zeta_{k+1}) \right] < \infty \quad (4.31)$$

where  $E_0[\cdot]$  is the expectation with respect to distribution  $\chi$ .

Assumption 3: The matrix  $\Phi_{ck}^T$  is linearly independent.

Assumption 4: For every 'k' the function  $\Phi_{ck}^T$  satisfies

$$E_0 \left[ \Phi_{ck}^2(\zeta_k) \right] < \infty \quad (4.32)$$

Assumption 5: The matrix  $\left[ P_k^{-1} + \frac{1}{k} \sum_{k=1}^K \Omega(\zeta_k) \right]$  is non-singular  $\forall k > 0$

**Theorem 1:** Considering the above assumptions (1-5) and using the proposed RLS-ET-AM algorithm given in (4.20)-(4.23), the critic weights  $W_{ck}$  converge to  $W_{ck}^*$  (optimal critic weights).

**Proof:** Applying matrix inversion Lemma  $(A+BC)^{-1} = A^{-1} - A^{-1}B(I+C A^{-1}B)^{-1}CA^{-1}$  (I is the identity matrix) to equation (4.21), it can be rewritten as

$$P_{k+1} = \mathbf{a}_{m_k}^{-1} \left[ P_k^{-1} + z_k \left( \Phi_{ck}^T - \gamma \Phi_{c_{k+1}}^T \right) \right]^{-1} \quad (4.33)$$

where  $A^{-1} = P_k$ ;  $B = z_k$ ,  $C = (\Phi_{ck}^T - \gamma \Phi_{c_{k+1}}^T)$  and assuming  $\mu=1$ . The Kalman gain vector  $G_k$  given in (4.20) is multiplied by  $P_k^{-1}$  giving

$$P_k^{-1} G_{k+1} = P_k^{-1} P_k z_k \mathbf{a}_{m_k}^{-1} \left( 1 + \left( \Phi_{ck}^T - \gamma \Phi_{c_{k+1}}^T \right) P_k z_k \right)^{-1} \quad (4.34)$$

$$G_{k+1} = z_k \mathbf{a}_{m_k}^{-1} \left( P_k^{-1} + \left( \Phi_{ck}^T - \gamma \Phi_{c_{k+1}}^T \right) z_k \right)^{-1} \quad (4.35)$$

Eq. (4.35) can be rewritten using the expression for  $P_{k+1}$  from (4.33) as

$$G_{k+1} = P_{k+1} z_k \mathbf{a}_{m_k}^{-1} \quad (4.36)$$

Using the results obtained for updatation of covariance matrix of the TD error  $P_{k+1}$  in (4.33) and Kalman gain vector  $G_{k+1}$  in (4.36), the updatation of the critic weights  $W_{c_{k+1}}$  defined in (4.20) can be rewritten as

$$\begin{aligned} W_{c_{k+1}} &= W_{c_k} + P_{k+1} z_k \mathbf{a}_{m_k}^{-1} \left[ r_k + (\Phi_{c_k}^T - \gamma \Phi_{c_{k+1}}^T) W_{c_k} \right] \\ &= W_{c_k} + P_{k+1} \left[ z_k r_k \mathbf{a}_{m_k}^{-1} + (\Phi_{c_k}^T - \gamma \Phi_{c_{k+1}}^T) W_{c_k} z_k \mathbf{a}_{m_k}^{-1} \right] \\ &= P_{k+1} \left[ (P_{k+1}^{-1} - z_k (\Phi_{c_k}^T - \gamma \Phi_{c_{k+1}}^T)) W_{c_k} + z_k r_k \mathbf{a}_{m_k}^{-1} \right] \end{aligned} \quad (4.37)$$

Substituting for  $P_{k+1}$  from (4.33) in (4.37) gives

$$= P_{k+1} \left( \left[ P_k^{-1} + z_k (\Phi_{c_k}^T - \gamma \Phi_{c_{k+1}}^T) \right] - z_k (\Phi_{c_k}^T - \gamma \Phi_{c_{k+1}}^T) \right) W_{c_k} + z_k r_k \mathbf{a}_{m_k}^{-1} \quad (4.38)$$

Using (4.33) in equation (4.38) gives

$$W_{c_{k+1}} = \left[ P_k^{-1} + z_k (\Phi_{c_k}^T - \gamma \Phi_{c_{k+1}}^T) \right]^{-1} (P_k^{-1} W_{c_k} + z_k r_k \mathbf{a}_{m_k}^{-1}) \quad (4.39)$$

denoting  $\Omega(\zeta_k) = z_k (\Phi_{c_k}^T - \gamma \Phi_{c_{k+1}}^T)$ ,  $p_k = z_k r_k \mathbf{a}_{m_k}^{-1}$  in (4.39) and  $W_{c_{k+1}}$  as  $W_{RLS-ET-AM}$  one obtains

$$\begin{aligned} W_{RLS-ET-AM} &= \left[ P_k^{-1} + \sum_{k=1}^K \Omega(\zeta_k) \right]^{-1} \left[ P_k^{-1} W_{c_k} + \sum_{k=1}^K p_k \right] \\ &= \left[ \frac{1}{N} P_k^{-1} + \frac{1}{N} \sum_{k=1}^N \Omega(\zeta_k) \right]^{-1} \left[ \frac{1}{N} P_k^{-1} W_{c_k} + \frac{1}{N} \sum_{k=1}^N p_k \right] \end{aligned} \quad (4.40)$$

since

$$E_0 [\Omega(\zeta_k)] = \lim_{k \rightarrow \infty} \frac{1}{N} \sum_{k=1}^N \Omega(\zeta_k) \quad (4.41)$$

$$E_0 [p_k] = \lim_{k \rightarrow \infty} \frac{1}{N} \sum_{k=1}^N p_k \quad (4.42)$$

where  $N$  denotes the number of measurements and from assumptions (1-5), it is known that

$E_0 [\Omega(\zeta_k)]$  is invertible i.e.

$$(E_0 [\Omega(\zeta_k)]) \lim_{k \rightarrow \infty} W_{RLS-ET-AM} = E_0 p_k = W^* \quad (4.43)$$

Thus, from (4.43) it is clear that  $W_{\text{RLS-ET-AM}}$  converges to  $W^*$  (optimal critic weights).

### 4.3. Results and Discussions

The numerical simulation of the DAC and FLAC controllers has been performed using MATLAB/SIMULINK<sup>®</sup>. To validate the tip trajectory tracking performances, the desired trajectory vector for two joints,  $\theta_{di}(t)$   $i=1,2$  are same as (3.14). The physical parameters of the studied TLFM are given in Table 2.2 and the controller parameters for RLAC are given in Table 4.2. Gains of the discrete PD controller for the RLAC were determined by assuming the manipulator's links to be rigid i.e. for  $d_i(l_i, t) = 0$ .

Table 4.2: Controller Parameters for RLAC

Controller Parameters	
Link-1	Link-2
$\omega_{n1} = 3.15\text{rad/sec}$ , (Link-1 natural frequency)	$\omega_{n2} = 10.054\text{rad/sec}$ , (Link-2 natural frequency)
$I_{eq1} = 0.17043\text{Kg/m}^2$ ,	$I_{eq2} = 0.0064\text{Kg/m}^2$
$K_{p1} = 1.75$ , $K_{d1} = 1.25$ ,	$K_{p2} = 0.65$ , $K_{d2} = 0.15$
$P_0 = 1000 \times I^{4 \times 4}$ , $\alpha = 0.5$ , $z = 0.25$ , $\gamma = 0.98$	

The gains were obtained from the following closed loop error equation knowing the values of

$\omega_{ni}$

$$I_{eqi} \ddot{e}_{i_k} + K_{di} \dot{e}_{i_k} + K_{pi} e_{i_k} = 0, i = 1, 2 \quad (4.44)$$

where  $I_{eqi}$  denotes the equivalent inertia of the  $i^{\text{th}}$  joint. From (4.44), assuming critical damping,

$K_{pi}$  and  $K_{di}$  can be determined as

$$\left. \begin{aligned} K_{pi} &= I_{eqi} \omega_{ni}^2 \\ K_{di} &= 2I_{eqi} \omega_{ni} \end{aligned} \right\} \quad (4.45)$$

where  $\omega_{ni}$  is the  $i^{\text{th}}$  link's natural frequency.

#### 4.3.1. Simulation results for an initial payload of 0.157 kg

Comparisons of performances exhibited by three adaptive control schemes (FLAC, DAC and RLAC) while carrying a 0.157 kg payload are shown in Figs 4.3-4.8. Fig.4.3 and Fig.4.4 show the tip trajectory tracking error curves for link-1 and link-2 respectively. From Fig.4.3, for link-1, it is seen that there exists a tracking error of  $0.4^\circ$  in case of the FLAC and  $1^\circ$  in case of DAC. However, the tracking error by the RLAC is almost zero. Link-2 tracking error profiles in Fig.4.4 reveal that the tracking errors are  $0.45^\circ$  for both DAC and FLAC whereas it is almost zero in case of the RLAC. Thus, RLAC provides excellent tracking performance. Fig.4.5 and Fig.4.6 show the tip deflection trajectories for link-1 and link-2 carrying 0.157 kg of payload. From these figures it is seen that the RLAC suppresses the tip deflection faster compared to the DAC and FLAC by damping it within 4 sec.

Fig.4.7 and Fig.4.8 show the control torque profiles generated by DAC, FLAC and RLAC for joint-1 and joint-2 respectively. From Fig. 4.7 and Fig.4.8, it is seen that the control input generated by the RLAC becomes zero compared to DAC and FLAC for link-1 and link-2 when the desired tip position is tracked. Thus, RLAC needs less control excitation for handling a payload of 0.157 kg compared to DAC and FLAC. In order to verify the performance of the RLAC compared to FLAC and DAC, further a frequency domain analysis has been performed. From Fig. 4.9 and Fig. 4.10 it is seen that the average power for RLAC is -15dB and -23dB less compared to DAC. The average power for RLAC is -18dB and -28dB less compared to FLAC for link-1 and link-2 respectively. Also, the average power of the tip trajectory error is calculated from its PSD. Fig. 4.11 and Fig. 4.12 indicate that there is a reduction in average power of -15dB and -22dB for

link-1 and -17dB and -16dB for link-2 less for RLAC compared to DAC and FLAC respectively. The reduction in average power in case of PSDs of link deflection and tip trajectory signifies that RLAC generates effective adaptive control to suppress the overall link deflection when subjected to 0.157 kg payload.

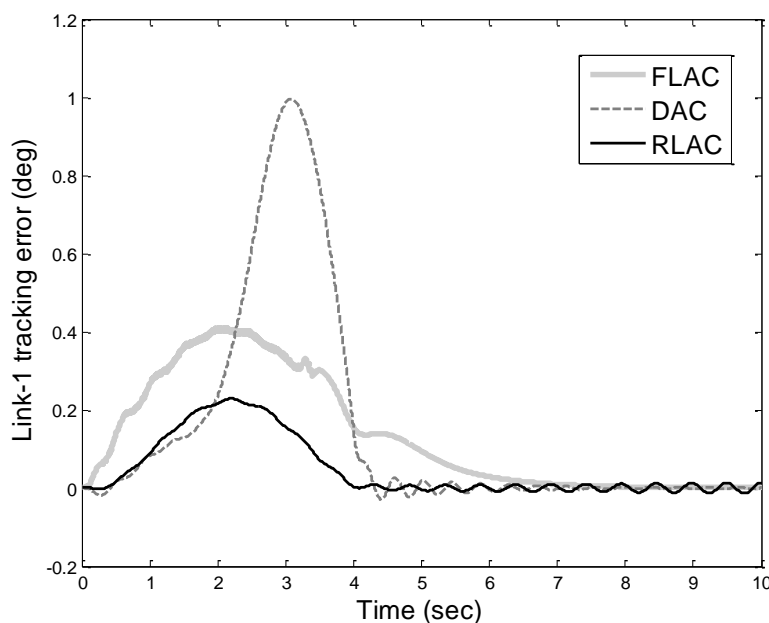


Fig.4.3 Simulation results (time domain) for tip trajectory tracking errors (Link-1) (0.157 kg):  
DAC, FLAC and RLAC



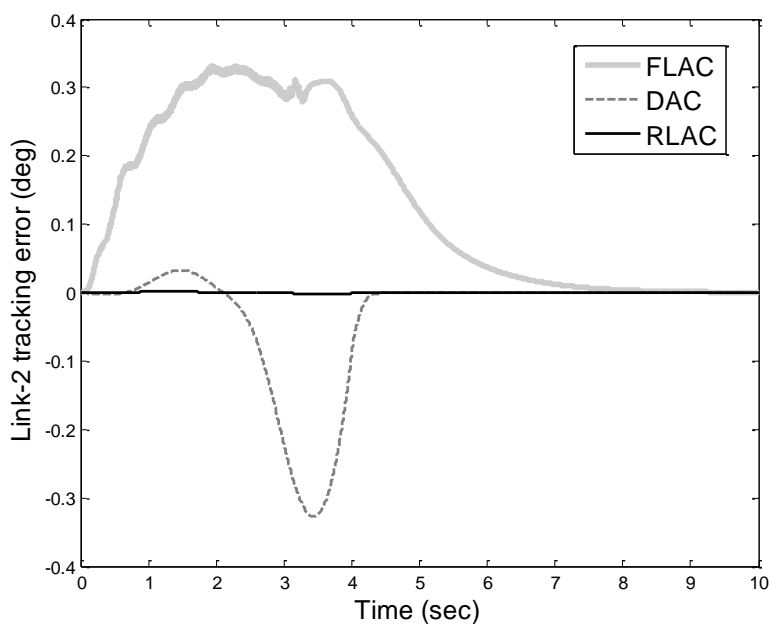


Fig.4.4 Simulation results (time domain) for tip trajectory tracking errors (Link-2) (0.157 kg):

DAC, FLAC and RLAC

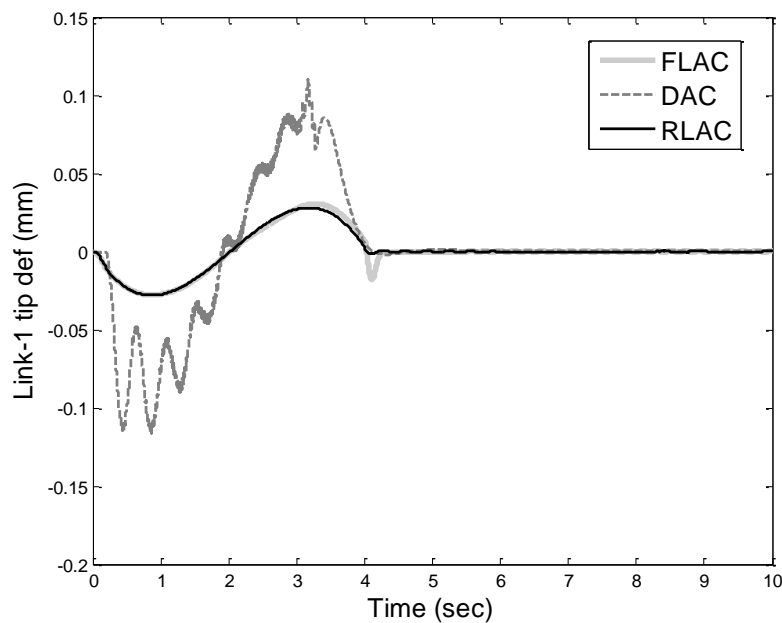


Fig.4.5 Simulation results (time domain) for comparison of link-1 tip deflection performances

(Link-1) (0.157 kg): DAC, FLAC and RLAC

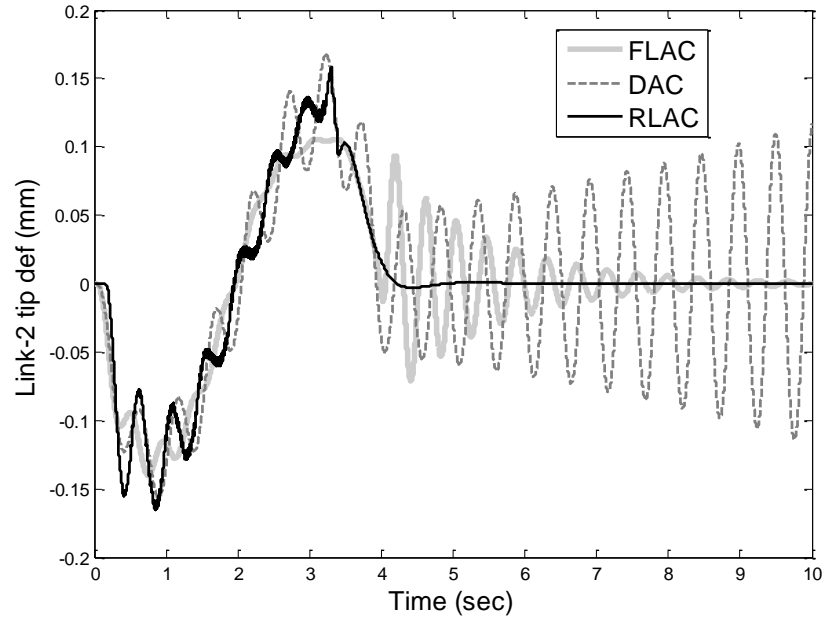


Fig.4.6 Simulation results (time domain) for comparison of link-2 tip deflection performances

(Link-1) (0.157 kg): DAC, FLAC and RLAC

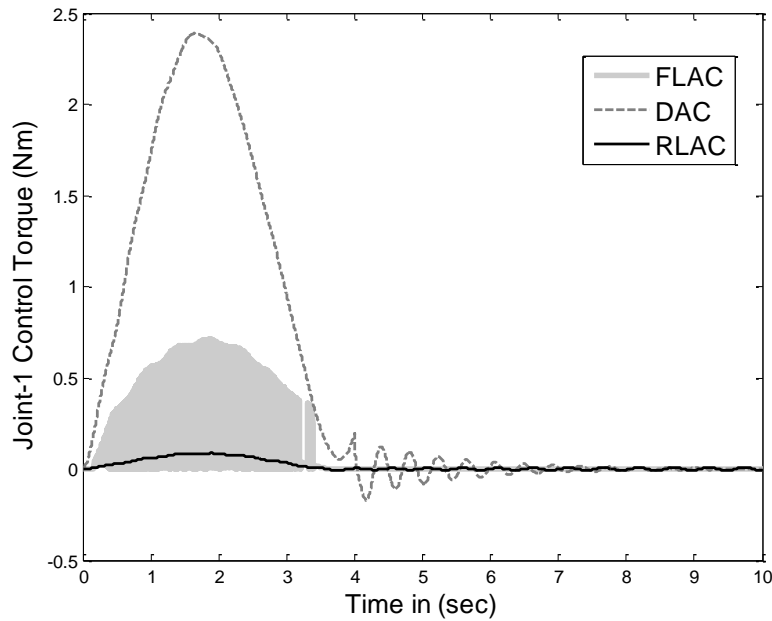


Fig.4.7 Simulation results (time domain) for torque profiles (joint-1) (Link-1) (0.157 kg): DAC,

FLAC and RLAC

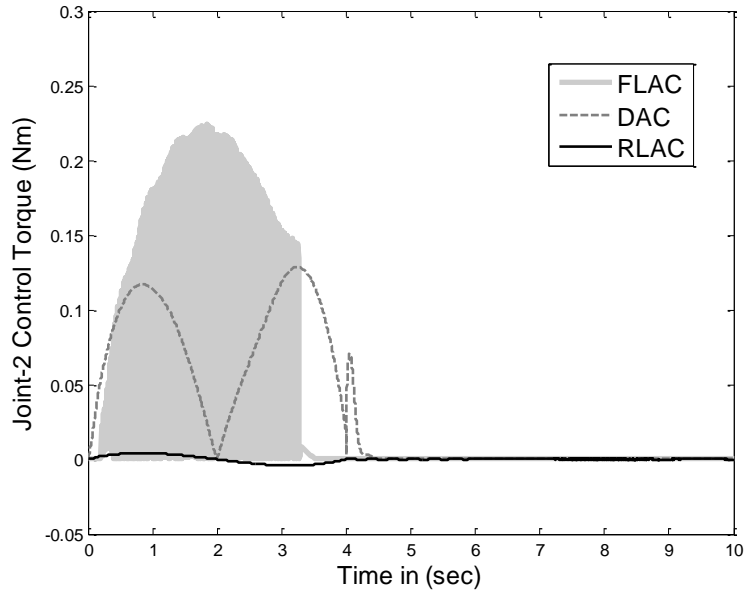


Fig.4.8 Simulation results (time domain) for torque profiles (joint-2) (Link-1) (0.157 kg): DAC, FLAC and RLAC

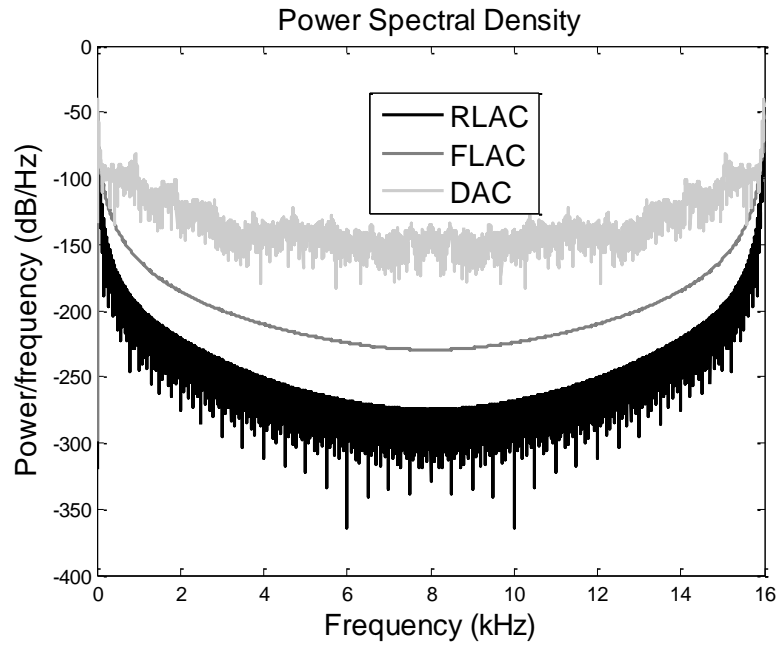


Fig.4.9 Simulation results (frequency domain) for tip trajectory tracking errors (Link-1) (0.157 kg): DAC, FLAC and RLAC

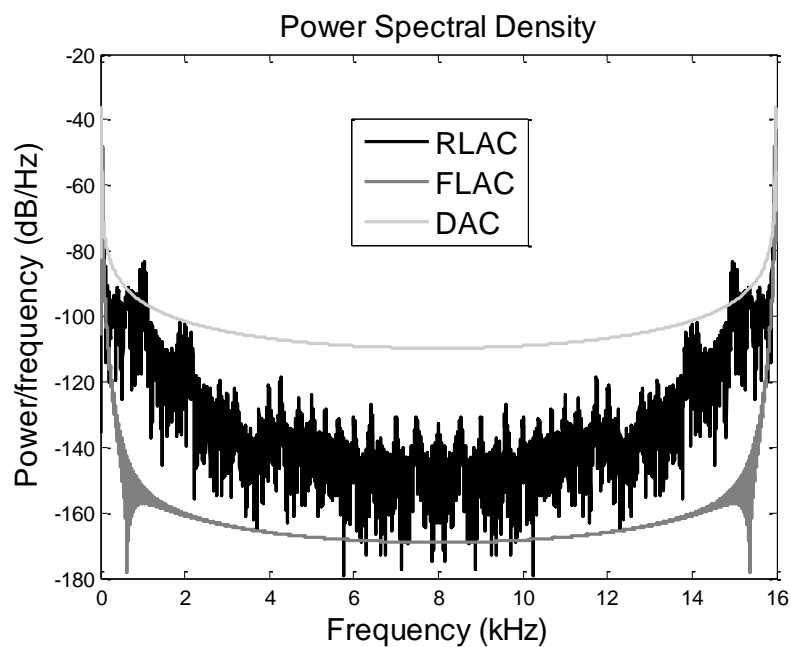


Fig.4.10 Simulation results (frequency domain) for tip trajectory tracking errors (Link-2) (0.157 kg): DAC, FLAC and RLAC

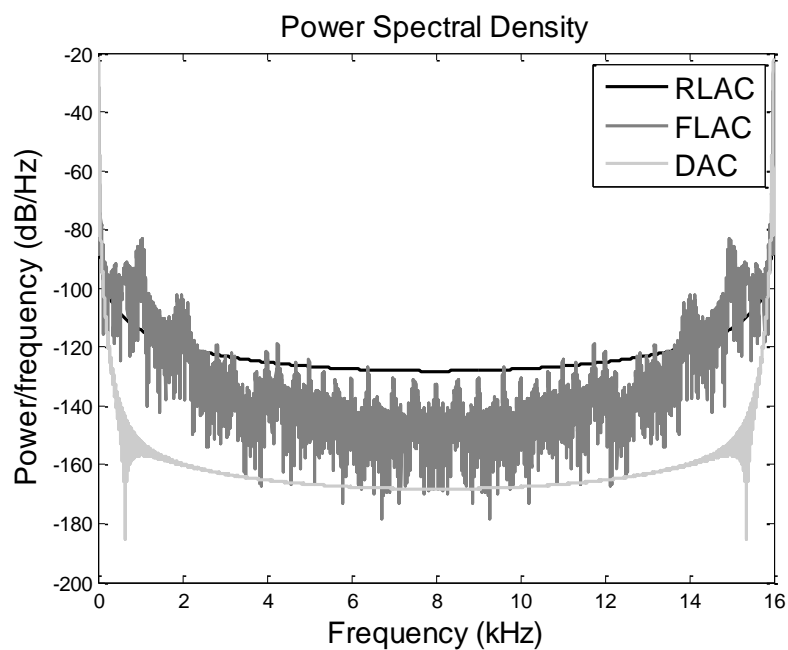


Fig.4.11 Simulation results (frequency domain) for comparison of link-1 tip deflection performances (Link-1) (0.157 kg): DAC, FLAC and RLAC

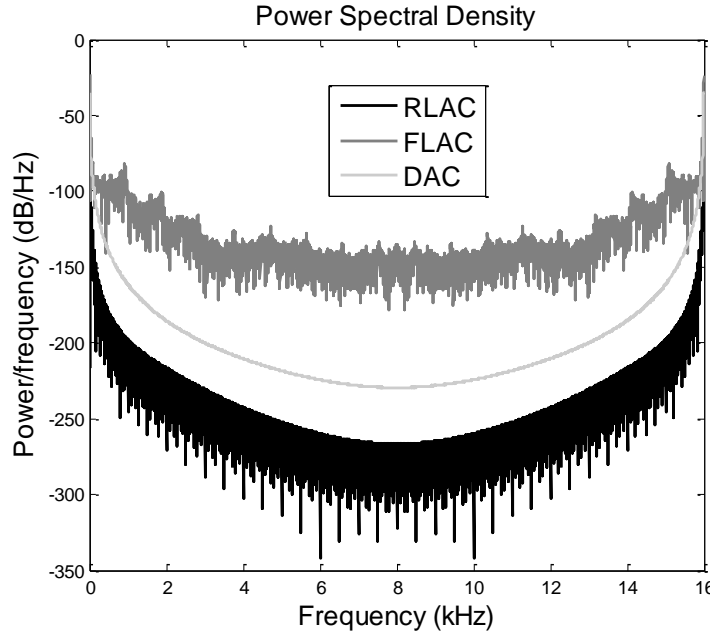


Fig.4.12 Simulation results (frequency domain) for comparison of link-2 tip deflection performances (Link-1) (0.157 kg): DAC, FLAC and RLAC

#### 4.3.2. Simulation results for an additional payload of 0.3 kg

An additional payload of 0.3 kg is now attached to the existing initial payload of 0.157 kg making the overall payload 0.457 kg. Performances of three controllers RLAC, FLAC and DAC for 0.457 kg payload were compared in Figs4.13-4.18. Fig.4.10 and Fig.4.14 depict the tip trajectory tracking performance for link-1 and link-2. From Fig.4.13, it can be seen that the time evolution of the error trajectory achieved by employing DAC has yielded maximum overshoot compared to the FLAC and RLAC. Fig.4.14 shows that FLAC has yielded maximum overshoot compared to the DAC and RLAC controllers.

Suppressing the tip deflection performances of RLAC, FLAC and DAC were compared in Fig.4.15 and Fig.4.16 for link-1 and link-2 respectively. From Fig.4.15, it is seen that tip

deflection is maximum in case of DAC compared to FLAC and also RLAC when a payload of 0.457 kg is attached for link-1. From Fig.4.16, it is seen that the tip deflection trajectories for link-2 is more oscillatory when carrying 0.457 kg of payload in case of DAC compared to FLAC and RLAC. Joint torque signals generated from DAC, FLAC and RLAC are compared in Fig. 4.17 and Fig.4.18. The adaptation of the actor and critic weights for RLAC carrying payload of 0.457 kg using simulation model is shown in Fig.4.19. The results show that as the learning progresses, the updated critic weights converge to their optimal values. RLAC performance is further analyzed by carrying out frequency domain analysis. The PSD of the time domain responses are given in Fig. 4.20 to Fig. 4.24. From Fig. 4.20 and Fig. 4.21 it can be seen that the average power of the PSD for RLAC is -5dB and -13dB less compared to DAC and is -18dB and -28dB less compared to FLAC for link-1 and link-2 respectively. The average power of the tip trajectory error is calculated from its PSDs in Fig. 4.22 and Fig. 4.23 respectively. The PSDs of tip trajectory errors show reduction in average power of -5.8dB and -7dB for link-1 and -7dB and -6dB for link-2 less for RLAC compared to DAC and FLAC respectively. Thus, a conclusion can be drawn that RLAC generates better adaptive control torques which damp the link deflections by effectively damping the mode excitations compared to FLAC and DAC.

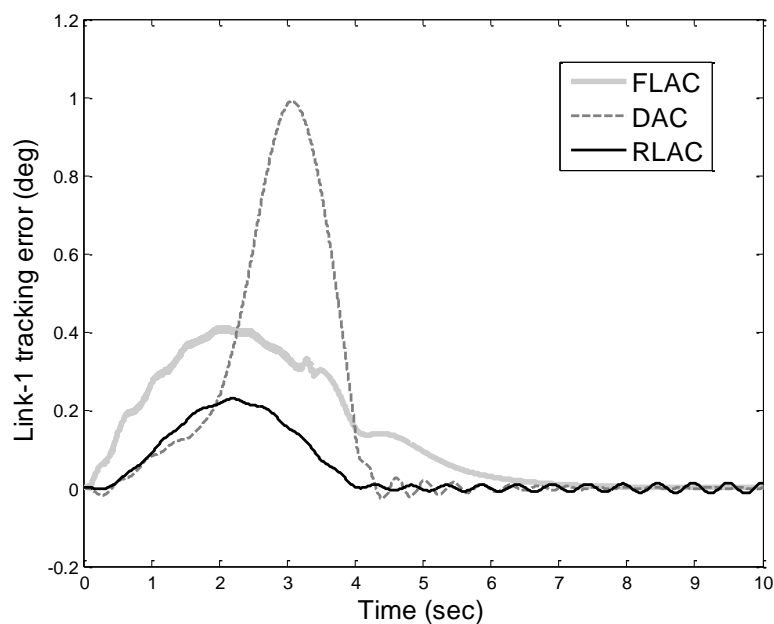


Fig.4.13 Simulation results (time domain) for tip trajectory tracking errors (Link-1) (0.457 kg):

DAC, FLAC and RLAC

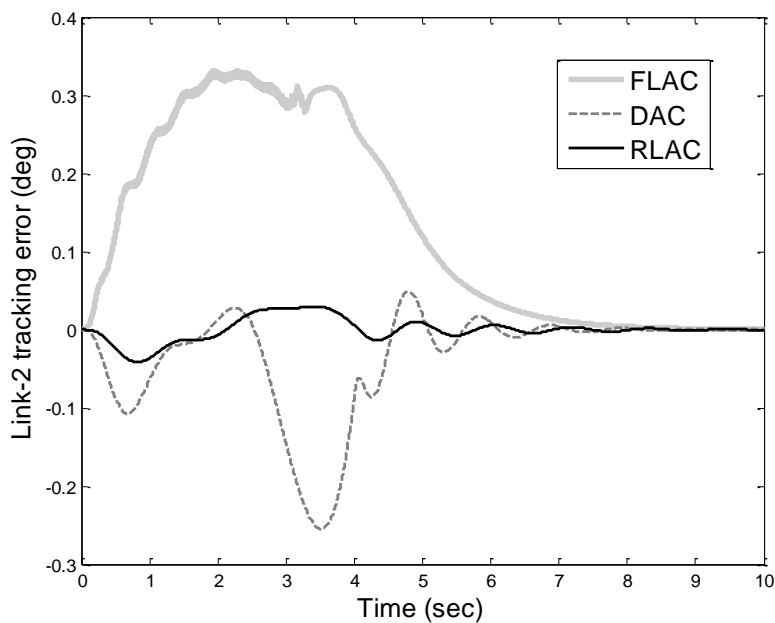


Fig.4.14 Simulation results (time domain) for tip trajectory tracking errors (Link-2) (0.457 kg):

DAC, FLAC and RLAC

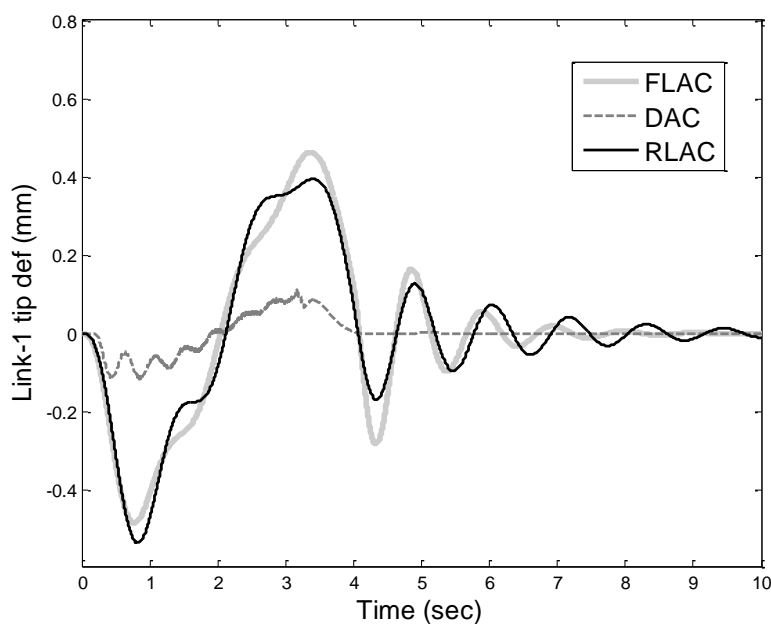


Fig.4.15 Simulation results (time domain) for comparison of link-1 tip deflection performances

(Link-1) (0.457 kg): DAC, FLAC and RLAC

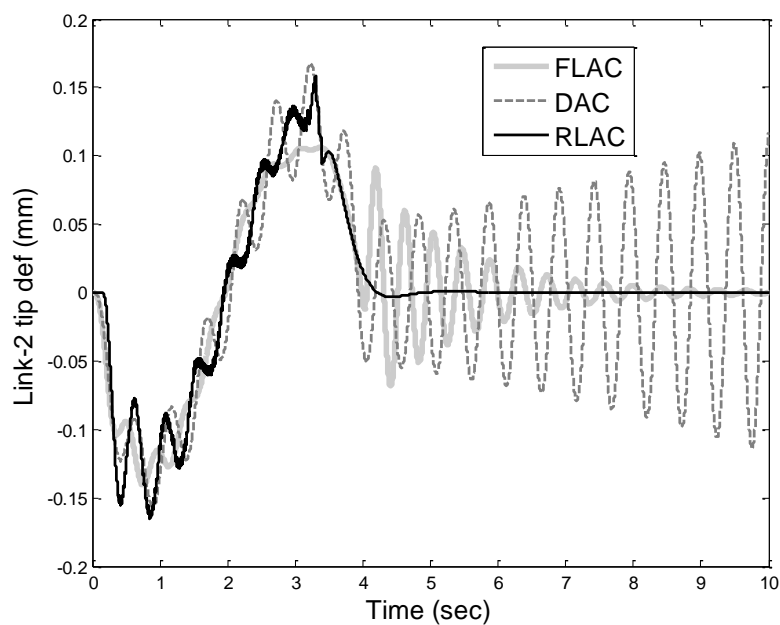


Fig.4.16 Simulation results (time domain) for comparison of link-2 tip deflection performances

(Link-1) (0.457 kg): DAC, FLAC and RLAC



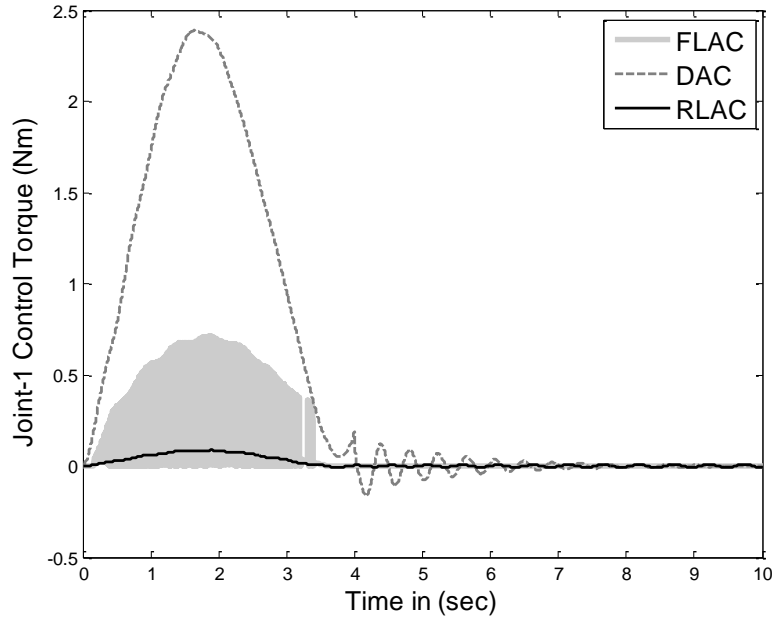


Fig.4.17 Simulation results (time domain) for torque profiles (joint-1) (0.457 kg): DAC, FLAC and RLAC

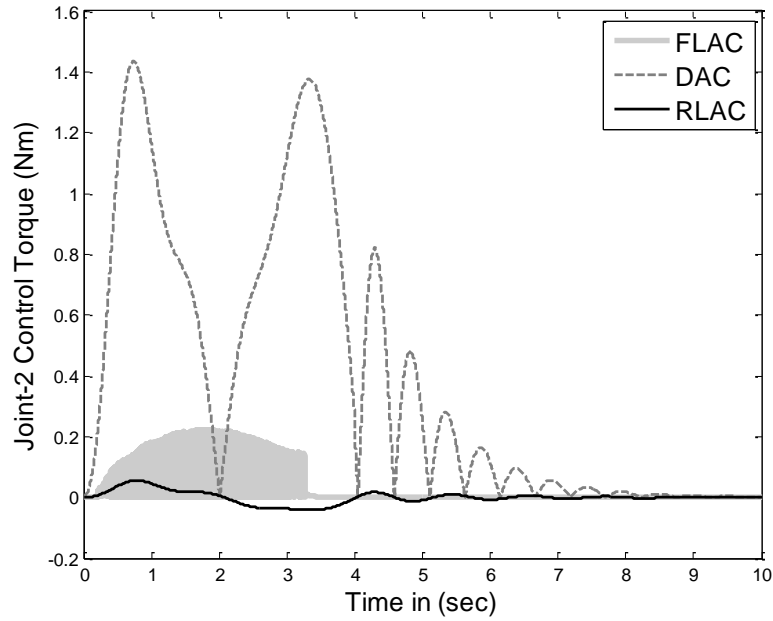


Fig.4.18 Simulation results (time domain) for torque profiles (joint-2) (0.457 kg): DAC, FLAC and RLAC

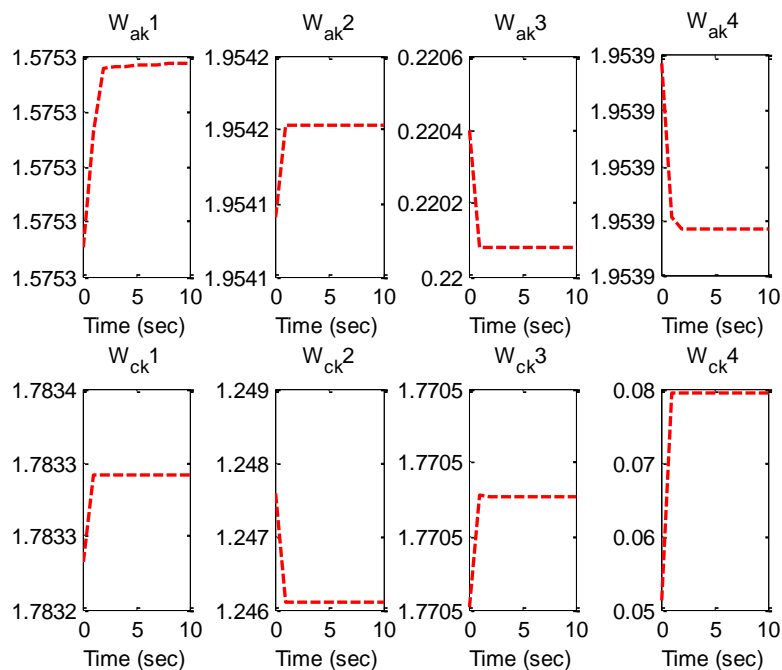


Fig.4.19 Simulation results for adaptation of the actor and critic weights to optimal values

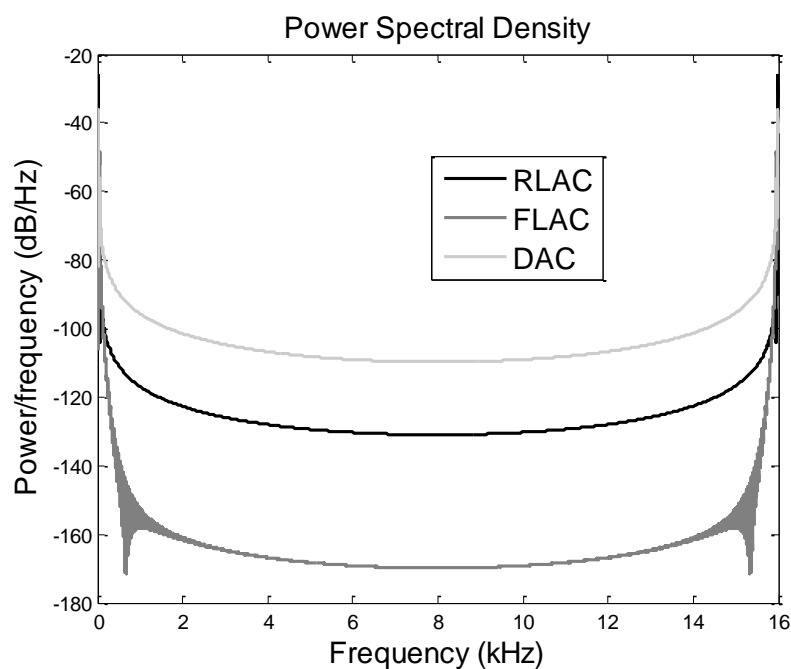


Fig.4.20 Simulation results (frequency domain) for tip trajectory tracking errors (Link-1) (0.457

kg): DAC, FLAC and RLAC

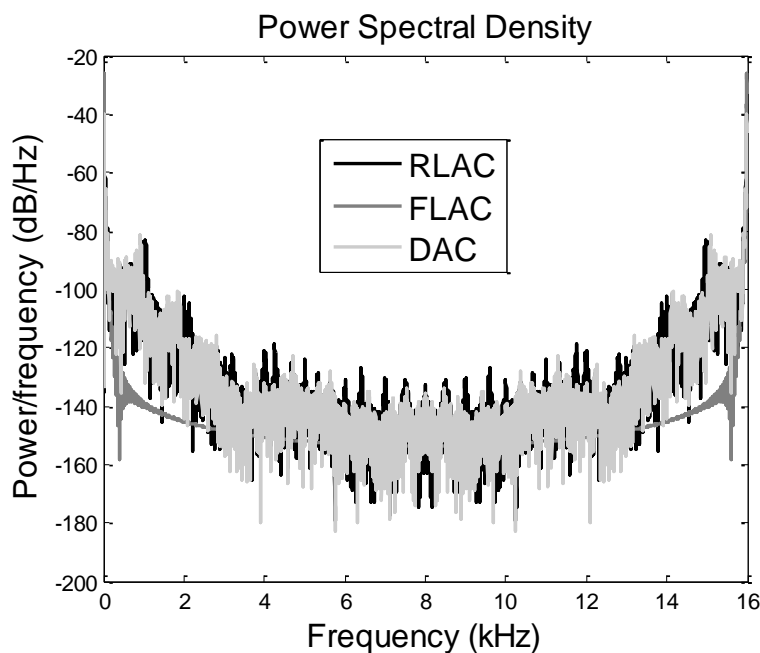


Fig.4.21 Simulation results (frequency domain) for tip trajectory tracking errors (Link-2) (Link-1) (0.457 kg): DAC, FLAC and RLAC

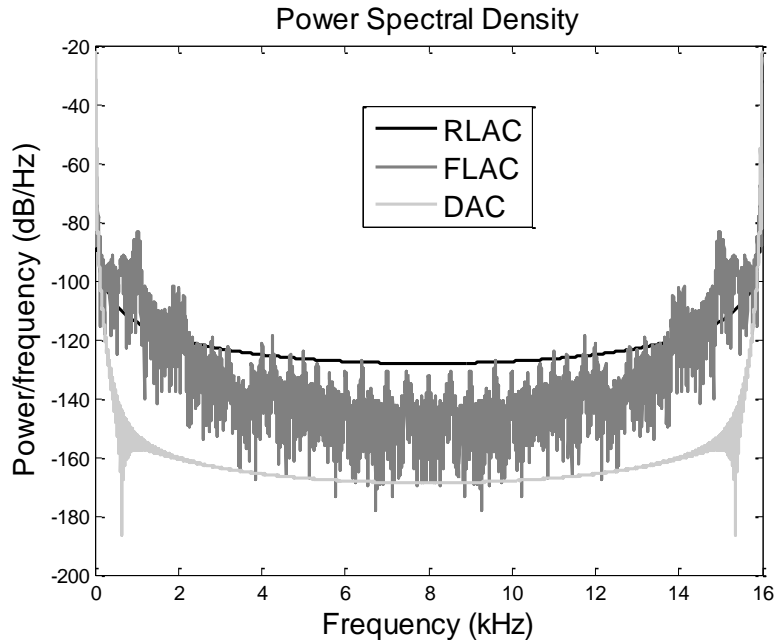


Fig.4.22 Simulation results (frequency domain) for comparison of link-1 tip deflection performances (Link-1) (0.457 kg): DAC, FLAC and RLAC

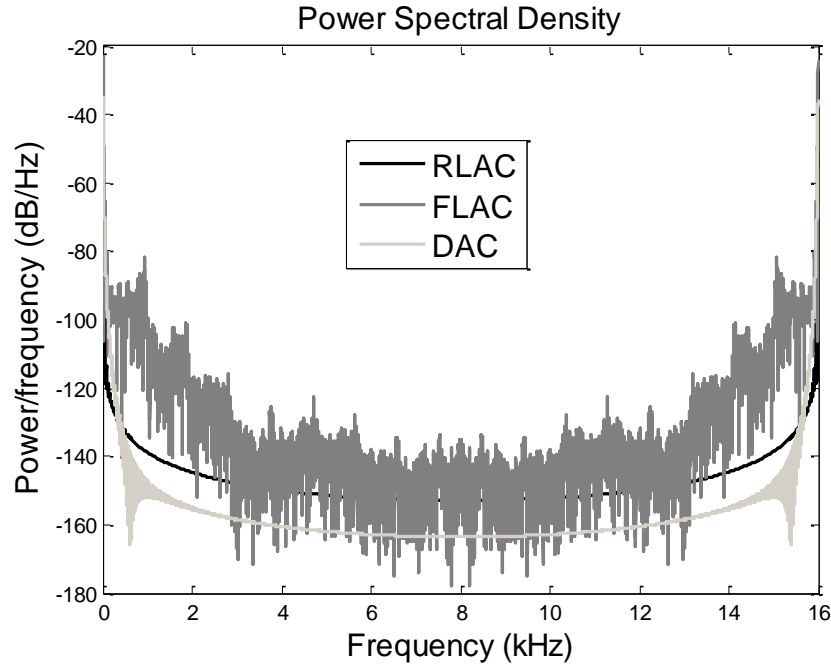


Fig.4.23 Simulation results (frequency domain) for comparison of link-2 tip deflection performances (Link-1) (0.457 kg): DAC, FLAC and RLAC

#### 4.3.3. Experiment results for an initial payload of 0.157 kg

Figs. 4.24-4.29 show comparison of the experimental results for TLFM obtained by employing RLAC, FLAC and DAC with an initial payload of 0.157 kg. Fig.4.24 and Fig.4.25 show the comparison of the tip trajectory tracking, after 4 sec when the tip attains the final position, the steady state error is almost zero in case of RLAC for link-1 and link-2, whereas the DAC and FLAC yield steady state errors of 0.1 and 0.2 for link-1 and link-2 respectively after 4 sec.

Fig.4.26 and Fig.4.27 show the tip deflection trajectories for the link-1 and link-2 when loaded for a 0.457 kg payload. From Fig.4.26, it can be seen that RLAC yields 0.1 mm of initial deviation as compared to FLAC and DAC where the deflection are 0.16 mm and 0.18 mm for link-1. Link-2 tip deflection characteristics are shown in Fig 4.27, from which it is seen that

RLAC has 0.15 mm of initial deviation as compared to who have 0.18 mm and 0.22 mm of initial deviation respectively for FLAC and DAC.

Torque profiles for joint-1 generated by employing the three controllers are shown in Fig. 4.28, and that for joint-2 is shown in Fig. 4.29. The joint torque control input for link-1 obtained by DAC reaches to a maximum value (9 Nm) at 2 sec when the tip reaches to the final position at 4 sec the control input reduces to 5 Nm. In case of FLAC where control input reaches to a maximum value (2 Nm) at 2 sec and 0.5 Nm for RLAC and torque becomes zero when the tip reaches the final position at 4sec. From Fig. 4.28 and Fig. 4.29, the joint control torque signals generated by DAC, FLAC and RLAC for link-2 have maximum of 12 Nm, 10 Nm, and 2.5 Nm respectively.

The time domain analysis show that the controller RLAC shows better performance compared to FLAC and DAC. Further in order to get more insight, a frequency domain analysis (PSDs) is carried out for the link deflection and tip trajectory error. From Fig. 4.30 and Fig. 4.31 it is seen that the average power of the PSD for RLAC is -0.5dB and -1.3dB less compared to DAC and is -1.4dB and -2.84dB less compared to FLAC for link-1 and link-2 respectively. Also, the average power of the tip trajectory error is calculated from its PSDs in Fig. 4.32 and Fig. 4.33 respectively, which shows reduction in average power of -1.8dB and -1.7dB for link-1 and -0.57dB and -0.26dB for link-2 less for RLAC compared to DAC and FLAC respectively. The results obtained signify that RLAC exhibits superior performance i.e. it provides damping the modal vibration by generating minimum average power signal compared to FLAC and DAC.

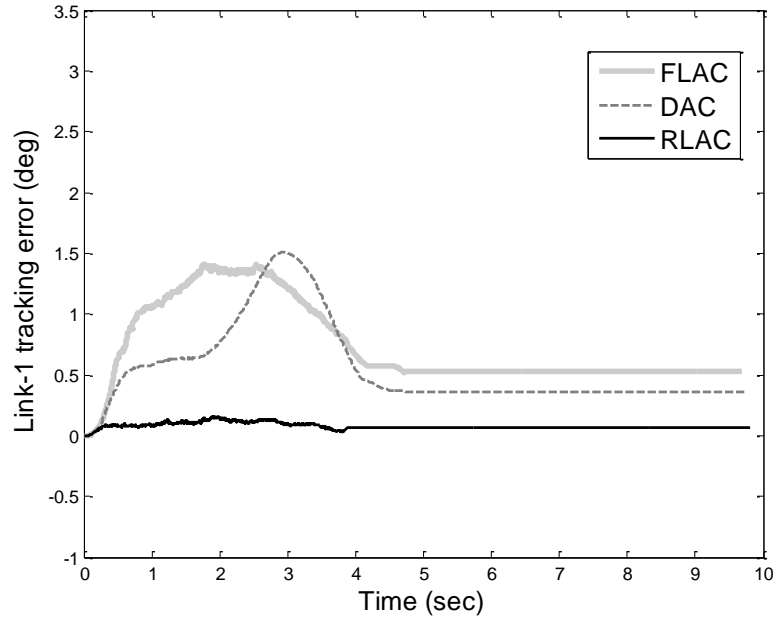


Fig.4.24Experiment results (time domain) for tip trajectory tracking errors (Link-1) (0.157 kg):

DAC, FLAC and RLAC

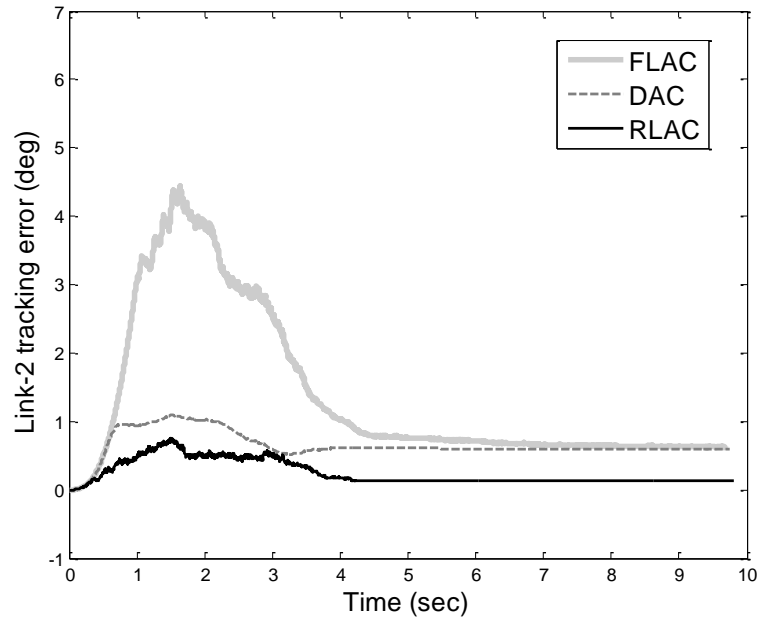


Fig.4.25Experiment results (time domain) for tip trajectory tracking errors (Link-2) (0.157 kg):

DAC, FLAC and RLAC

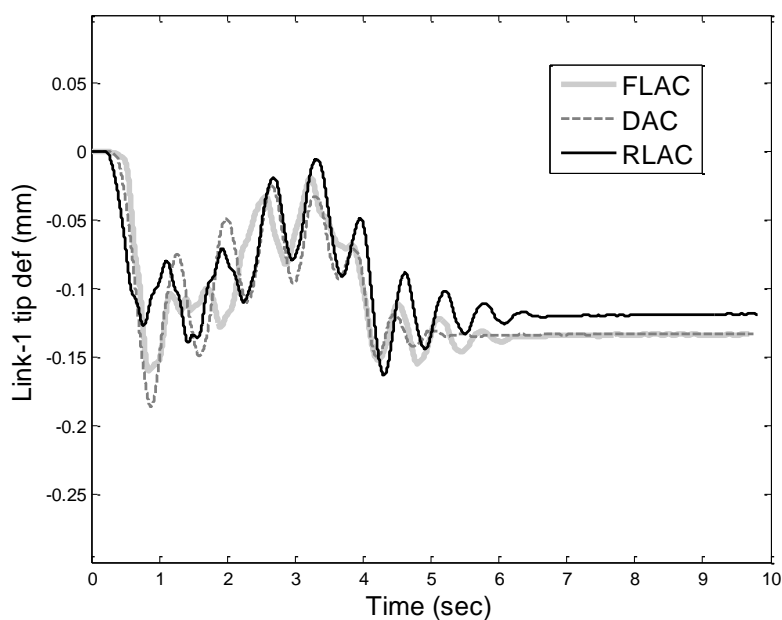


Fig.4.26 Experiment results (time domain) for comparison of link-1 tip deflection performances  
(0.157 kg): DAC, FLAC and RLAC

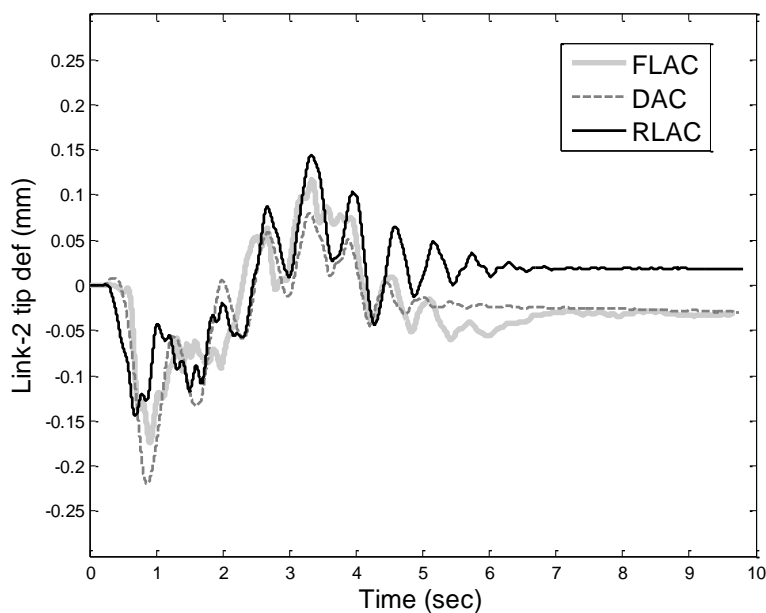


Fig.4.27 Experiment results (time domain) for comparison of link-2 tip deflection performances  
(0.157 kg): DAC, FLAC and RLAC

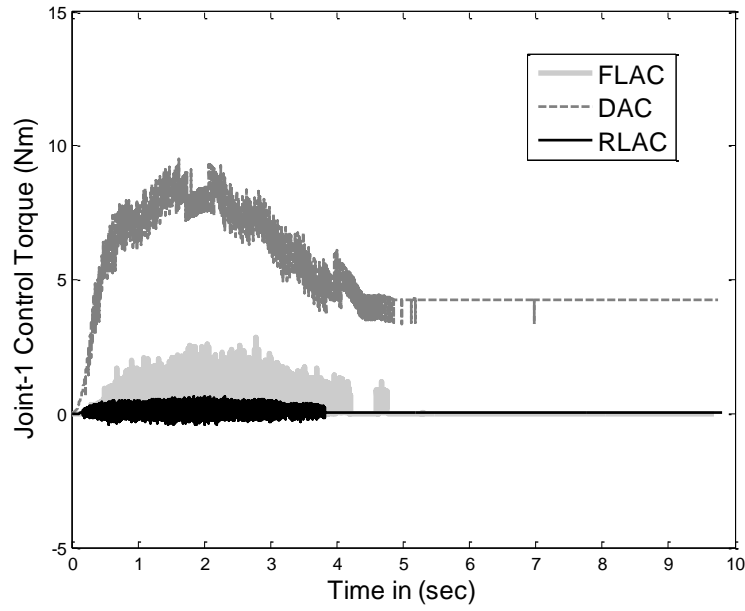


Fig.4.28 Experiment results (time domain) for torque profiles (joint-1) (0.157 kg): DAC, FLAC and RLAC

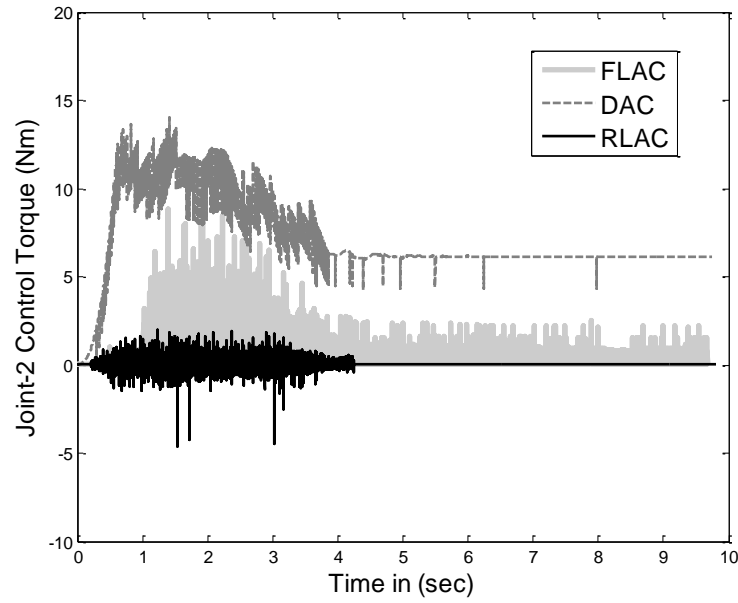


Fig.4.29 Experiment results (time domain) for torque profiles (joint-2) (0.157 kg): DAC, FLAC and RLAC



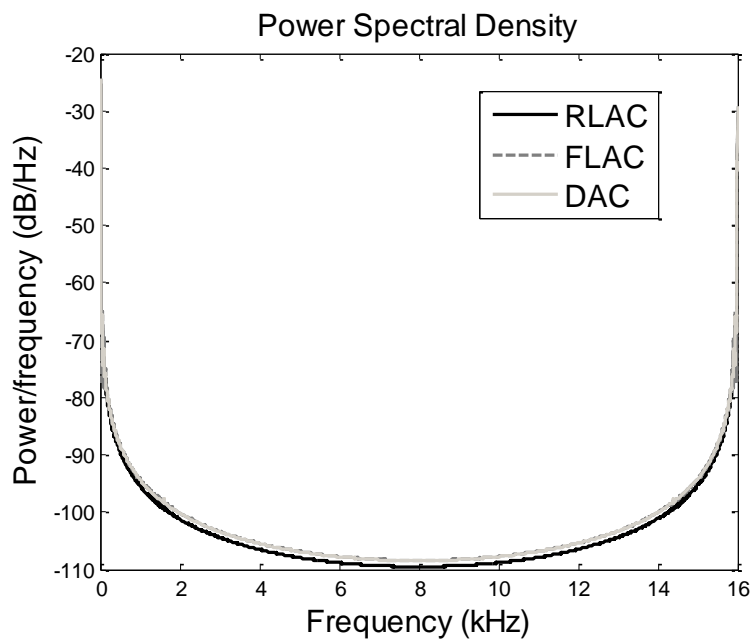


Fig.4.30 Experiment results (frequency domain) for tip trajectory tracking errors (Link-1)

(0.157 kg): DAC, FLAC and RLAC

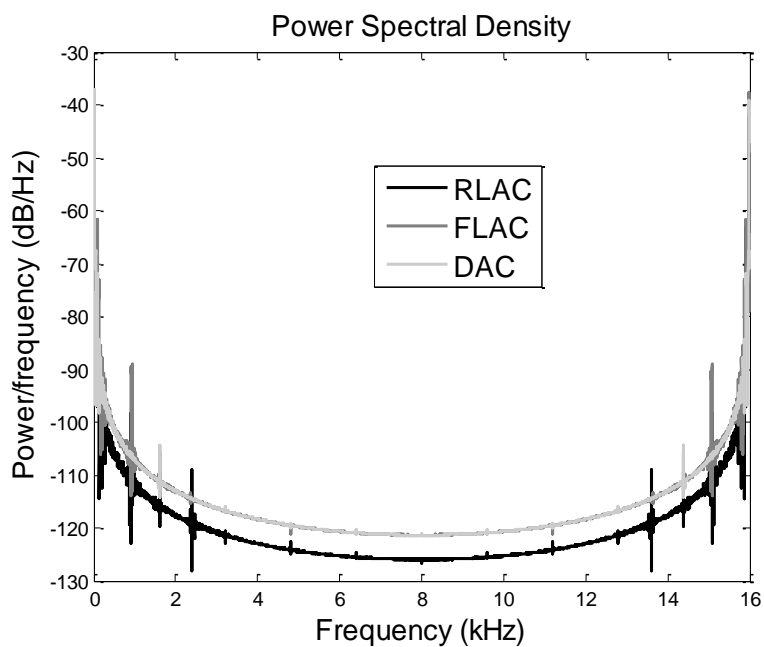


Fig.4.31 Experiment results (frequency domain) for tip trajectory tracking errors (Link-2)

(0.157 kg): DAC, FLAC and RLAC

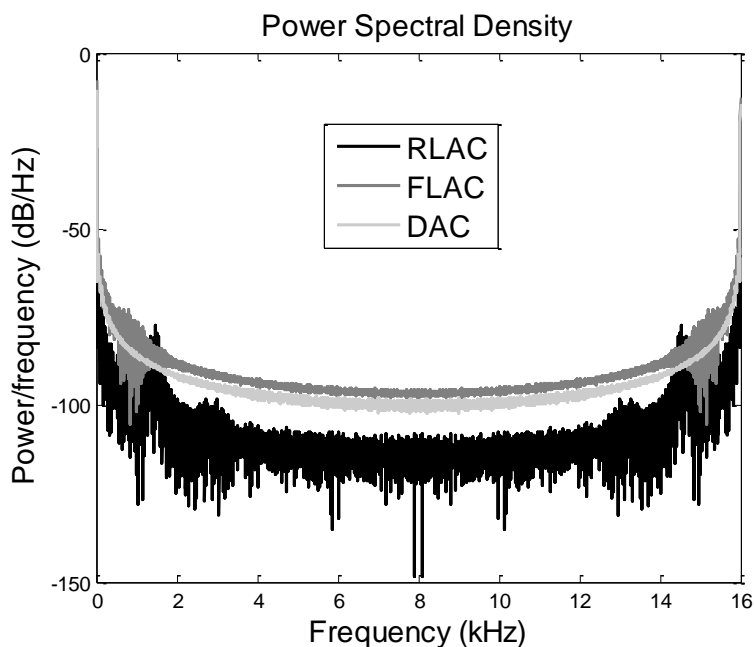


Fig.4.32 Experiment results (frequency domain) for comparison of link-1 tip deflection performances (0.157 kg): DAC, FLAC and RLAC

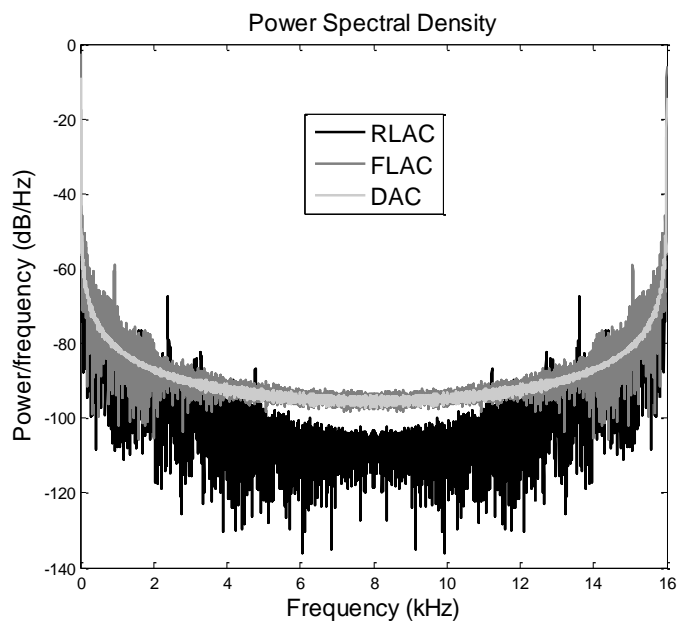


Fig.4.33 Experiment results (frequency domain) for comparison of link-2 tip deflection performances (0.157 kg): DAC, FLAC and RLAC

#### 4.3.4. Experiment results for an additional payload of 0.3 kg

An additional payload of 0.3 kg is added to the initial payload of 0.157 kg. Figs. 4.34-4.39 show comparison of the experimental results for TLFM obtained by employing RLAC, FLAC and DAC with a payload of 0.457 kg. Fig.4.34 and Fig.4.35 compare the tip trajectory tracking performances for link-1 and link-2 respectively. From Fig.4.34 and Fig.4.35 it is clear that when the final position is attained, the steady state error in case of RLAC is almost zero, whilst a finite steady state error exists in case of both DAC and FLAC. The TLFM is an infinite dimensional system due to distributed link flexure. Higher modes have been neglected in modeling therefore there is a difference in steady state error for simulation and experimental results. Fig.4.36 and Fig.4.37 show the tip deflection trajectories for the link-1 and link-2 when asked for a payload of 0.457 kg.

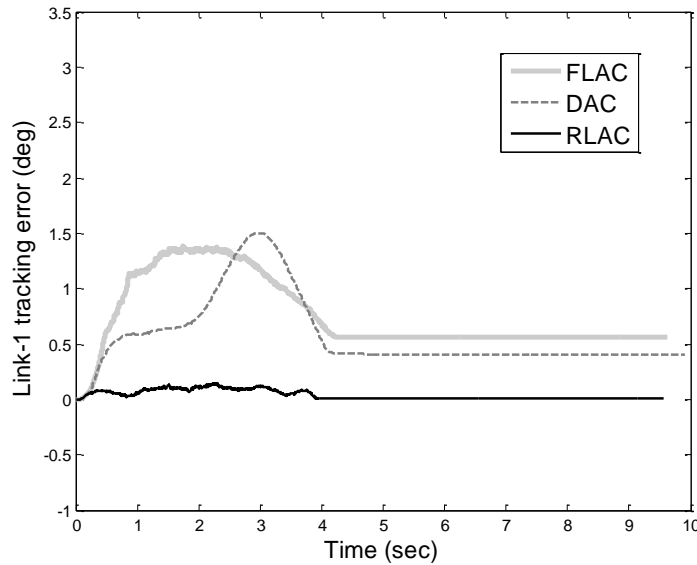


Fig.4.34 Experiment results (time domain) for tip trajectory tracking errors (Link-1) (0.457 kg):

DAC, FLAC and RLAC

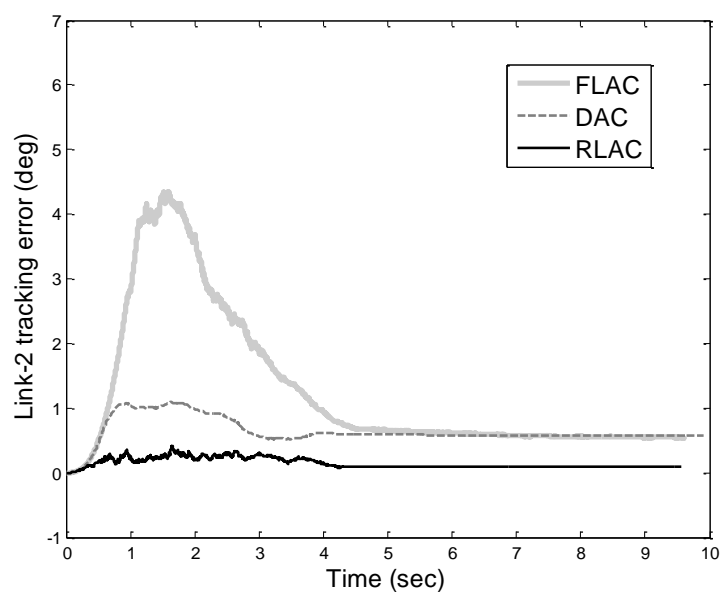


Fig.4.35 Experiment results (time domain) for tip trajectory tracking errors (Link-2) (0.457 kg):

DAC, FLAC and RLAC

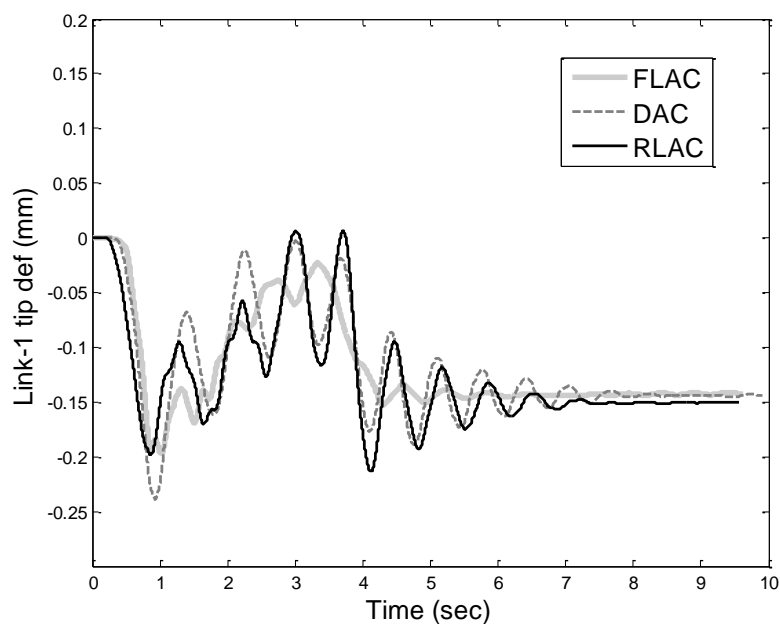


Fig.4.36 Experiment results (time domain) for comparison of link-1 tip deflection performances

(0.457 kg): DAC, FLAC and RLAC

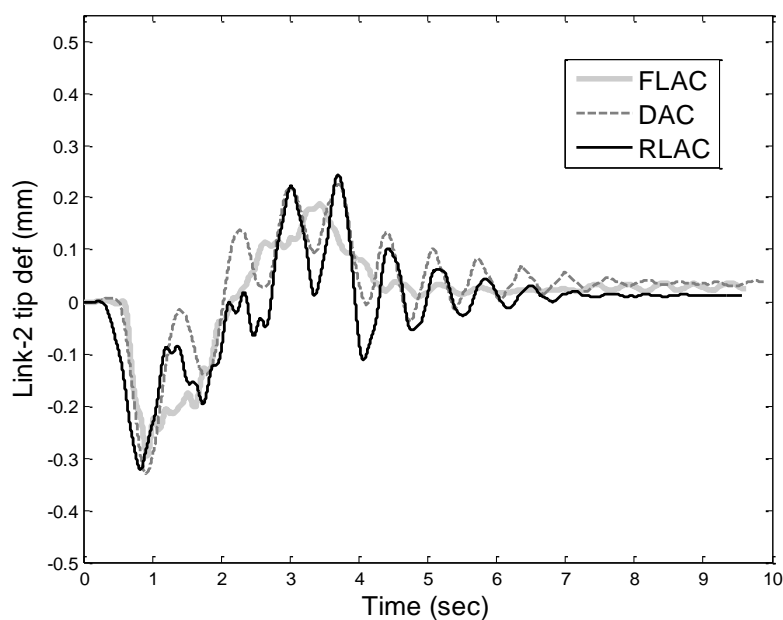


Fig.4.37Experiment results (time domain) for comparison of link-2 tip deflection performances

(0.457 kg): DAC, FLAC and RLAC

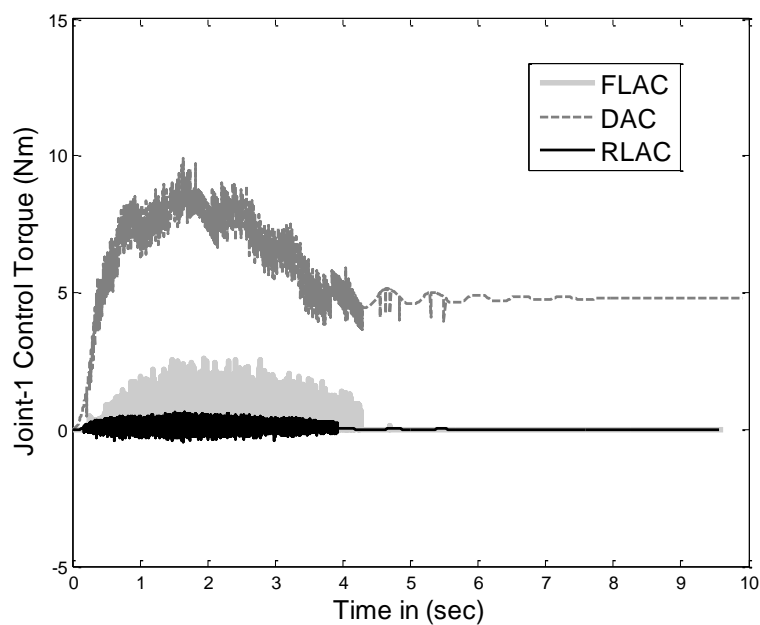


Fig.4.38Experiment results (time domain) for torque profiles (joint-1) (0.457 kg): DAC, FLAC

and RLAC

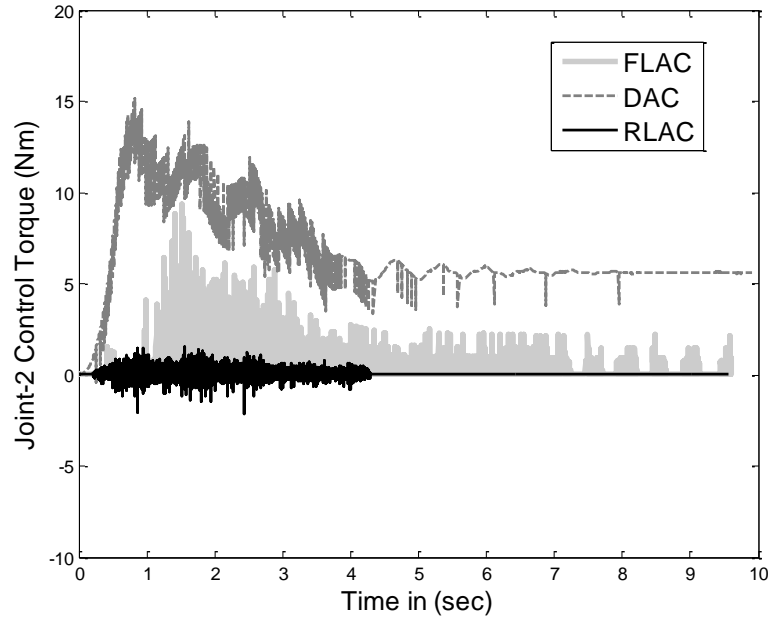
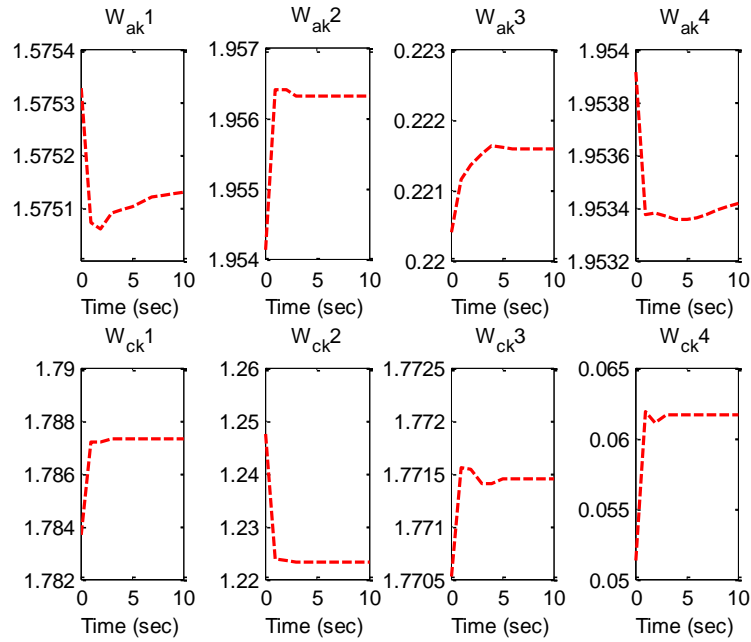


Fig.4.39 Experiment results (time domain) for torque profiles (joint-2) (0.457 kg): DAC, FLAC and RLAC



4.40 Experimental results for adaptation of the actor and critic weights to optimal values

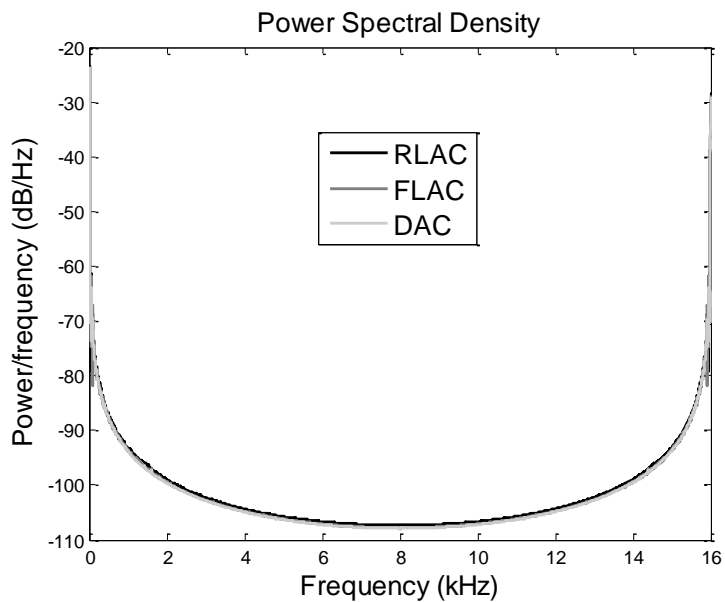


Fig.4.41 Experiment results (frequency domain) for tip trajectory tracking errors (Link-1) (0.457 kg): DAC, FLAC and RLAC

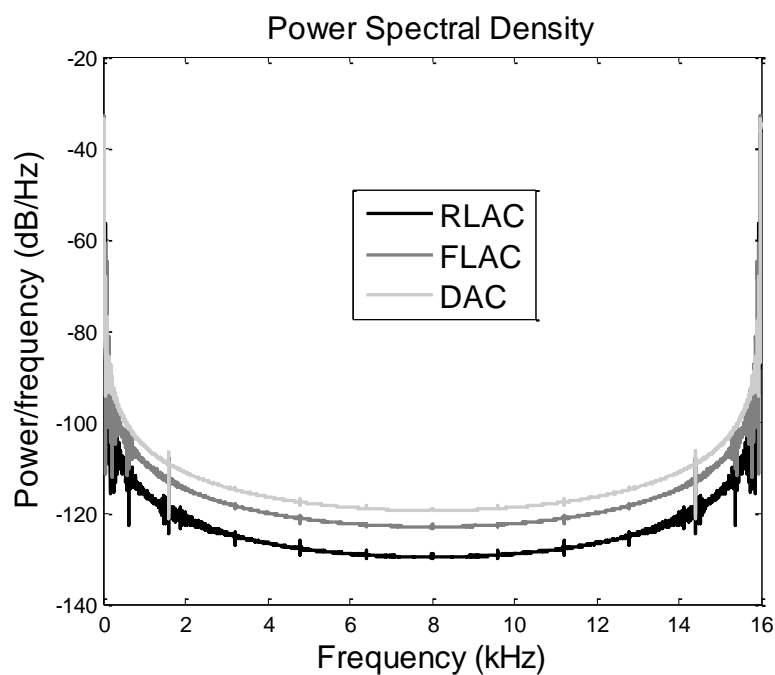


Fig.4.42 Experiment results (frequency domain) for tip trajectory tracking errors (Link-2) (0.457 kg): DAC, FLAC and RLAC

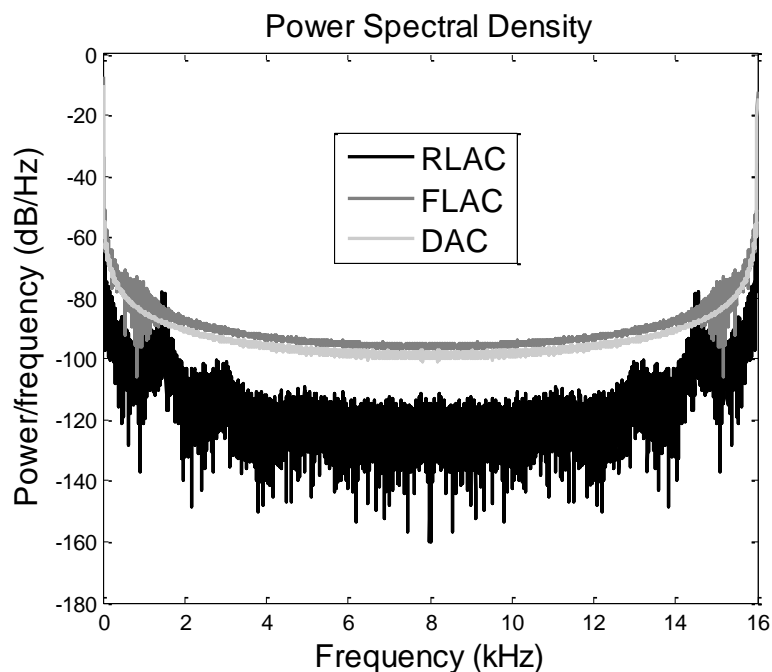


Fig.4.43 Experiment results (frequency domain) for comparison of link-1 tip deflection performances (0.457 kg): DAC, FLAC and RLAC

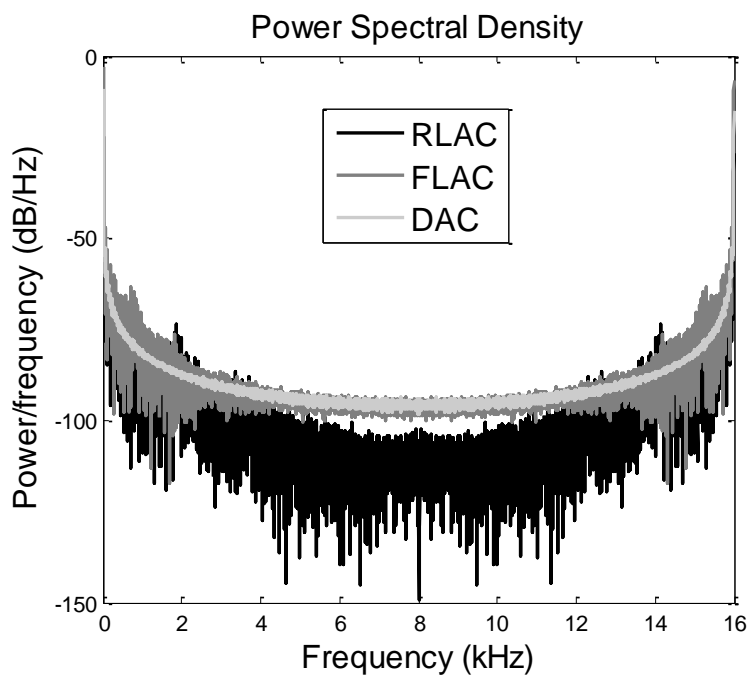


Fig.4.44 Experiment results (time domain) for comparison of link-1 tip deflection performances (0.457 kg): DAC, FLAC and RLAC



From Fig.4.36 it is seen in case of RLAC there exists an initial deviation of 0.2 mm as compared to FLAC and DAC in which deflections are 0.2 mm and 0.25 mm respectively for link-1. Link-2 tip deflection responses are shown in Fig.4.37. RLAC has 0.3 mm of initial deviation as compared to FLAC and DAC where initial deviations are 0.28 mm and 0.32 mm respectively. Torque profile generated for joint-1 by the three controllers is shown in Fig.4.38. From this figure it is seen that the DAC torque signal reaches to a maximum value of 9.5 Nm and reduces to 5 Nm at 4 sec when the final position is tracked. FLAC torque signal becomes the maximum (2.5 Nm) at 2 sec and almost reduces to zero at the final position. But RLAC generates control torque signal with less amplitude initially and zero magnitude while the desired position has been tracked. From Fig.4.39, torque profile generated for joint-2, it is seen that the DAC torque signal reaches to maximum value of 15 Nm at 1 sec and reduces to 6 Nm at 4 sec when the final position is tracked. FLAC torque signal reaches to maximum value of 9 Nm at 1.5 sec and reduces to 2 Nm at 4 sec, whereas RLAC generates appropriate control torques with maximum value of 2 Nm at 1.5 sec with almost zero value at the final position. The experimental values while updating the actor and critic weights under payload of 0.457 kg are shown in Fig.4.40. The results show that despite changes in payload, the critic weights converge to their optimal values. However, there is difference in critic weights in experiment and simulations. This is because of approximations in modeling of the TLFM. From Fig. 4.41 and Fig. 4.42 it is seen that the average power of the PSD for RLAC is -0.15dB and -0.12dB less compared to DAC and is -0.7dB and -0.4dB less compared to FLAC for link-1 and link-2 respectively. The average power of the tip trajectory error is calculated from its PSDs in Fig. 4.43 and Fig. 4.44 respectively, reduction in average power of -2.5dB and -2.5dB for link-1 and -2.7dB and -2.6dB for link-2 less for RLAC compared to DAC and FLAC respectively.

## 4.4. Chapter Summary

This *Chapter* has proposed a new real-time adaptive controller for tracking control of tip trajectory and suppressing tip deflection for a two-link flexible manipulator (TLFM) while subjected to handle variable payload based on reinforcement learning technique. The proposed RLAC provides better tracking and tip deflection damping performance compared to both a nonlinear direct adaptive controller (DAC) and a fuzzy learning based adaptive controller (FLAC) discussed in *Chapter 3*. The superiority of the RLAC over DAC and FLAC is its ability to adapt the actor and critic weights to an optimal value using the proposed Recursive Least Square-Eligibility Trace-Adaptive Memory algorithm (RLS-ET-AM) under variable payload.

The proposed RLAC has been applied successfully to a laboratory flexible robot set-up. The RLAC has exhibited excellent performance in real-time control of this manipulator which has distributed flexure along its links.

## Chapter 5

# Self-Tuning Control of a Two-Link Flexible Manipulator using NARMAX Model

An adaptive control scheme using RL technique (RLAC) discussed in *Chapter 4* exploits reinforcement learning for developing real-time adaptive control of tip trajectory and deflection of a two-link flexible manipulator handling variable payloads. However, RLAC depends upon a PD feedback loop for overall stability of the closed loop system. In this chapter a new adaptive controller is proposed to control the tip position and deflection of a flexible-link manipulator (FLM) while it is subjected to carry different payloads. The proposed adaptive controller uses a multivariable PID self-tuning control (STC) strategy. The parameters of the PID controller are adapted *on-line* using a nonlinear autoregressive moving average with exogenous-input (NARMAX) model of the two-link flexible manipulator (TLFM). The developed NATMAX

model based STC controller (NMSTC) is then compared with the RLAC. *Section 5.2* presents the identification of the TLFM dynamics using NARMAX model. The design of the proposed STC scheme is presented in *Section 5.3*. STC is applied to the developed mathematical model and to the physical TLFM; the simulation and experimental results are discussed in *Section 5.4*. The summary of the chapter is presented in *Section 5.5*.

## 5.1. Introduction

It is described in *Chapter 1* that due to sudden change in payload there may be large variation in manipulator parameters and that in turn adds further complexities to the FLM dynamics. Further, the dynamics of FLM is influenced by both rigid body motion and flexible motion. Usually while designing controllers for a flexible manipulator, its dynamics is derived by considering some finite number of flexible modes. When the payload changes, the mode shapes also change thus it is very difficult to obtain an accurate model of the FLM under varied payload conditions. Thus, the control problem of handling an unknown payload by a FLM is different and more complex than that of a rigid-link manipulator. In most of the reported adaptive controller schemes for FLM, linear identification is adopted, for example, a PID control law has been developed in [4] for a single-link flexible manipulator using an autoregressive moving average (ARMA) model with RLS algorithm to estimate parameters of the model. A simple decoupled self-tuning control law comprising of the estimation of link's natural frequency for a single link flexible manipulator with varied payloads is proposed in [9]. In [10], an adaptive pole placement control law is proposed using a finite dimensional ARMA model of a single-link flexible manipulator to control the tip trajectory and tip deflection with under unknown payloads.

In the past, a number of indirect adaptive control schemes using linear models have been suggested for FLMs. But indirect adaptive controllers using a linear model fail to achieve precise real-time adaptive controller for FLMs for different payloads. Hence, an indirect control design using a nonlinear estimated model using a NARMAX model and a self-tuning controller is the focus of this paper. The NARMAX model is a popular nonlinear modeling paradigm which is different from non-linear time series representation like Volterra and Hammerstein model in the sense that the later models require large number of parameters to describe nonlinear system dynamics, hence involve with more computational burden [93]. Also, there have been several examples where NARMAX model based system identification have been successfully accomplished for very complex nonlinear systems, for example, In [94], a NARMAX model is used for representing nonlinear ankle dynamics systems. A rigid manipulator dynamics has been identified using a NARMAX model in [95]. Also, soft computing approaches such as differential evolution based neural network have been used for system identification using a NARMAX model in [96]. STC based on estimated NARMAX model has been employed in different systems for example, a continuous stirred-tank reactor in [97], a pilot-scale level plus temperature control system in [98], a predictive control strategy for nonlinear NO<sub>x</sub> decomposition process in thermal power plants in [99] and a state-space self-tuning control for an active fault-tolerant pulse-width-modulation tracker for unknown nonlinear stochastic hybrid systems [100]. Hence, in this chapter of a new NARMAX model based self-tuning controller (NMSTC) for a TLFM is developed by exploiting NARMAX modeling when the manipulator tip is subjected to handle unknown payloads. The proposed NMSTC is compared with that of the RLAC derived in chapter 4.

## 5.2 Identification of the TLFM using NARMAX model

Equation (2.9) can be written after employing a forward difference discretization as

$$\dot{x}(k+1) = \frac{x(k+1) - x(k)}{T} \quad (5.1)$$

where  $T$  is the sampling-time,  $x(k)$  is the state vector, the TLFM dynamics derived in chapter 2 can be represented as follows. Discrete-time nonlinear form can be written as

$$Y(k) = F^n \begin{bmatrix} y_{p_i}(k-1), y_{p_i}(k-2), \dots, y_{p_i}(k-N_y), \\ u_i(k-1), u_i(k-2), \dots, u_i(k-N_u) \end{bmatrix} \quad (5.2)$$

where  $y_{p_i}(k)$  denotes the tip position of the  $i^{\text{th}}$  link,  $u_i(k)$  is the input to the  $i^{\text{th}}$  joint,  $N_y$  and  $N_u$  represent the maximum delay in the output and input vectors respectively, and  $F^n[\bullet]$  represents a multi-input multi-output (MIMO) nonlinear map of the TLFM input-output behavior. An additive noise term  $\xi_i(k)$  is added to (5.2) for representing the TLFM dynamics in form of NARMAX model. Hence, the NARMAX model for the TLFM is written as

$$Y(k) = F_i^n \begin{bmatrix} y_{p_i}(k-1), y_{p_i}(k-2), \dots, y_{p_i}(k-N_y), \\ u_i(k-1), u_i(k-2), \dots, u_i(k-N_u), \xi_i(k) \end{bmatrix} \quad (5.3)$$

The structure for discrete-time nonlinear MIMO representation of TLFM as a NARMAX model is shown in Fig.5.1, where

$Y_i(k)$	Nonlinear autoregressive (NAR) vector
$U_i(k)$	Exogenous (X) vector

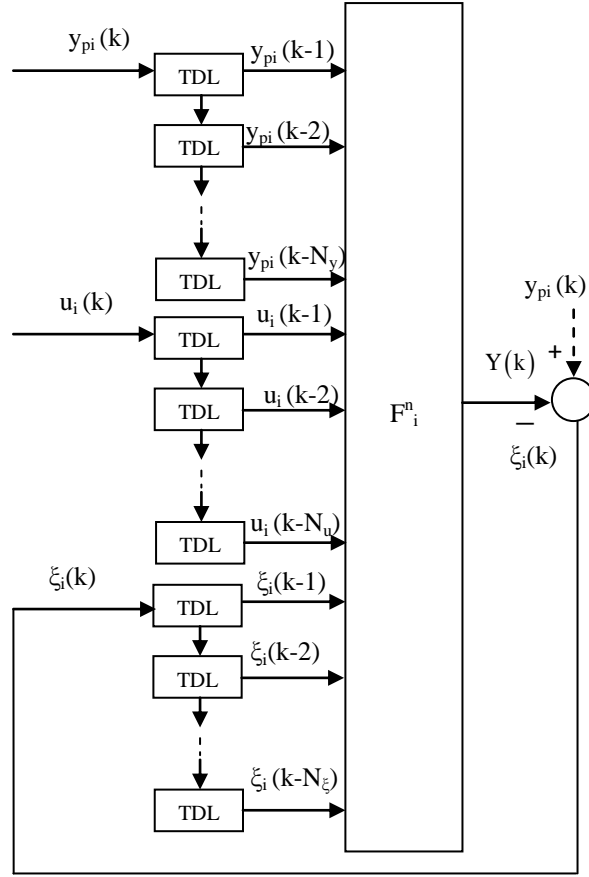


Fig.5.1 Structure of the NARMAX model of a planar TLFM

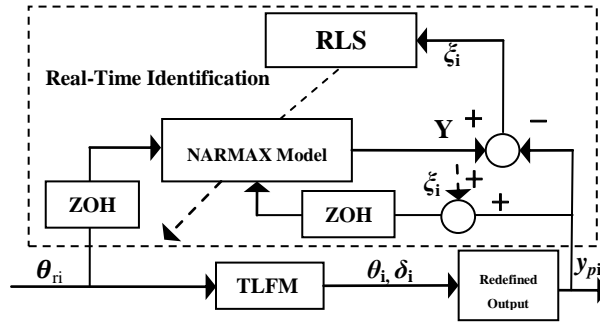


Fig.5.2 Structure for estimation of NARMAX parameters for TLFM

- $\xi_i(k)$  Moving average (MA) variable vector
- $F_i$  Nonlinear function with  $i^{\text{th}}$  input and output

N                      Order of the nonlinearity

$N_y$  and  $N_u$         Order of NAR, MA, and X respectively

The NARMAX model (5.3) can be rewritten using the *on-line* estimated parameters in its regressor form as

$$\hat{Y}(k) = \phi_i^T(k) \hat{w}(k) + \xi_i(k) \quad (5.4)$$

where

$$\phi_i^T(k) = \begin{bmatrix} y_{pi}(k-1), \dots, y_{pi}(k-n_y), y_{pi}^2(k-1), \dots, y_{pi}^2(k-n_y), \\ u_i(k-1), \dots, u_i(k-n_u), u_i^2(k-1), \dots, u_i^2(k-n_y), \\ \xi_i(k), y_i(k-1)u_i(k-1), \dots, \\ y_{pi}(k-n_y)u_i(k-n_u), y_{pi}^2(k-1)u_i(k-1), \dots, \\ y_{pi}^2(k-n_y)u_i(k-n_u), y_{pi}^2(k-1)u_i^2(k-1), \dots, \\ y_{pi}(k-n_y)u_i^2(k-n_u), y_{pi}^2(k-1)u_i^2(k-1), \dots, \\ y_{pi}^2(k-n_y)u_i^2(k-n_u) \end{bmatrix}^T, \quad \hat{w} = [\hat{w}_1, \hat{w}_2, \hat{w}_3, \hat{w}_4, \hat{w}_5, \hat{w}_6, \hat{w}_7]$$

$\hat{w}_1$  : Link-1 inertia.

$\hat{w}_2$  : Link-2 inertia.

$\hat{w}_3$  : Hub-1 inertia.

$\hat{w}_4$  : Hub-2 inertia.

$\hat{w}_5$  : Link-1 equivalent mass

$\hat{w}_6$  : Link-2 equivalent mass

$\hat{w}_7$  : Total coupling mass between the links

Fig.5.2 shows the structure for estimation of *on-line* NARMAX parameters where a ZOH is used to discretize the continuous signals. The estimated value of parameters  $\hat{w}(k)$  of the



NARMAX model is  $\hat{w}(k)$  which can be estimated using a RLS algorithm given in equations (5.6)-(5.7).

$$\hat{w}(k) = \hat{w}(k-1) + \frac{P_i(k-1)\phi_i(k)}{\lambda + \phi_i^T(k)P_i(k-1)\phi_i(k)} \xi_i(k) \quad (5.5)$$

$$\hat{P}_i(k) = \frac{1}{\lambda} \left\{ P_i(k-1) - \frac{P_i(k-1)\phi_i(k)\phi_i^T(k)P_i(k-1)}{\lambda + \phi_i^T(k)P_i(k-1)\phi_i(k)} \right\} \quad (5.6)$$

$$\hat{Y}_i(k) = \phi_i^T(k) \hat{w}(k-1) + \xi_i(k) \quad (5.7)$$

where  $\lambda$  is the forgetting factor and  $P_i(k)$  is the covariance matrix.

### 5.3 Self-tuning control using NARMAX model

A multivariable NMSTC has three main elements such as a control law generator in terms of multivariable difference equation, an *on-line* parameters estimator using NARMAX model that uses measured system output and input values and an algorithm that relates the estimated parameters and control parameters. The NMSTC algorithm for the TLFM is described as follows. Let us represent NARMAX output as

$$Y(k) = \frac{1}{A(z^{-1})} \left[ (b u_i(k - N_u) \phi(k)) + C(z^{-1}) \xi_i(k) \right] \quad (5.8)$$

where the polynomials  $A(z^{-1})$ ,  $C(z^{-1})$  and  $b$  for  $i^{\text{th}}$  link are given as

$$A(z^{-1}) = 1 + a_{i,1}z^{-1} + a_{i,2}z^{-2}, C(z^{-1}) = 1 + c_{i,1}z^{-1} + c_{i,2}z^{-2},$$

$$b = [b_1, \dots, b_n]^T$$

The discrete time multivariable PID control law is given by

$$\Delta u_i(k) = K_i \begin{bmatrix} e_i(k) - e_i(k-1) \\ + \frac{T}{2T_i} \{e_i(k) - e_i(k-1)\} \\ + \frac{T_D}{T} \{e_i(k) - e_i(k-1) + e_i(k-2)\} \end{bmatrix} \quad (5.9)$$

where  $\Delta u_i(k) = u_i(k) - u_i(k-1)$  and  $e_i(k) = y_{pi}(k)$  (TLFM tip position) -  $\theta_{di}(k)$  (desired tip position).

Further eq. (5.9) can be rewritten as

$$\begin{aligned} \Delta u_i(k) &= K_i \begin{bmatrix} \left(1 + \frac{T}{T_i} + \frac{T_D}{T}\right) e_i(k) - \left(1 + \frac{2T_D}{T}\right) e_i(k-1) + \frac{T_D}{T} e_i(k-2) \\ e_i(k-1) + \frac{T_D}{T} e_i(k-2) \end{bmatrix} \\ \Rightarrow \Delta u_i(k) &= \begin{bmatrix} K_i \left(1 + \frac{T}{T_i} + \frac{T_D}{T}\right) - \\ K_i \left(1 + \frac{2T_D}{T}\right) z^{-1} + \frac{K_i T_D}{T} z^{-2} \end{bmatrix} e_i(k) \end{aligned} \quad (5.10)$$

Let  $L_i(z^{-1})$  be a polynomial defined as

$$L_i(z^{-1}) = K_i \left(1 + \frac{T}{T_i} + \frac{T_D}{T}\right) - K_i \left(1 + \frac{2T_D}{T}\right) z^{-1} + \frac{K_i T_D}{T} z^{-2} \quad (5.11)$$

Then, using (5.11) in (5.10) one gets

$$\Delta u_i(k) = L_i(z^{-1}) (y_{pi}(k) - \theta_{di}(k)) \quad (5.12)$$

Eq. (5.12) can be rewritten as

$$L_i(z^{-1}) (\phi_i^T(k) w(k)) + \Delta u_i(k) - L_i(z^{-1}) \theta_{ri}(k) = 0 \quad (5.13)$$

The polynomial  $L_i(z^{-1})$  for the NMSTC law is tuned using minimum variance control law.

Fig.5.3 shows structure of the proposed NARMAX based NMSTC for TLFM. In order to tune the PID parameters based on the principle of minimum variance, a performance index  $J_1$  is considered as follows

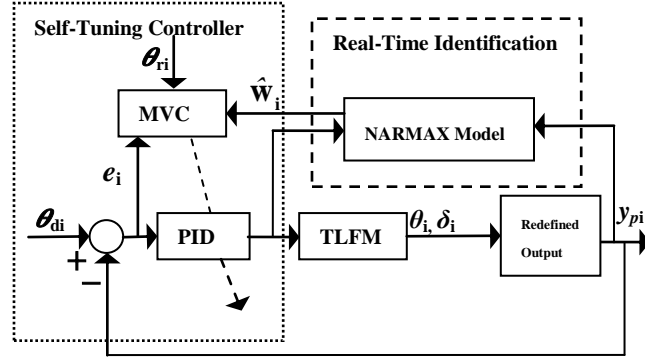


Fig.5.3 Structure of the NMSTC controller

$$J_1 = \sum \Xi \left[ Q_i(z^{-1}) \left( \phi_i^T(k) w(k) \right) + \Gamma_i \Delta u_i - R_i(z^{-1}) \theta_{ri} \right] \quad (5.14)$$

where  $\Xi$  is the expectation operator,  $\Gamma_i$  is the weighting factor with respect to the control input in eq. (5.12) and  $Q_i(z^{-1})$  user defined weighting polynomial with respect to the predicted input is the of the form

$$Q_i(z^{-1}) = 1 + q_{i,1}z^{-1} + q_{i,2}z^{-2} \quad (5.15)$$

The control law minimizing the performance index  $J_2$  in eq. (5.14) can be obtained as

$$F_i(z^{-1}) \left( \phi_i^T(k) w(k) \right) + \left\{ E_i(z^{-1}) C_i(z^{-1}) + \Gamma_i \right\} \Delta u_i - Q_i(z^{-1}) \theta_{ri} = 0 \quad (5.16)$$

where the  $E_i(z^{-1})$  and  $F_i(z^{-1})$  are found out by solving the following Diophantine equation

$$Q_i(z^{-1}) = A_i(z^{-1}) E_i(z^{-1}) + z^{-(d_i+1)} F_i(z^{-1}) \quad (5.17)$$

where

$$\begin{aligned} E_i(z^{-1}) &= 1 + e_{i,1}z^{-1} + \dots + e_{i,k_{m_i}}z^{-d_i} \\ F_i(z^{-1}) &= f_{i,0} + f_{i,1}z^{-1} + f_{i,2}z^{-2} \end{aligned} \quad (5.18)$$

Let  $E_i(z^{-1}) + C_i(z^{-1}) + \Lambda_i$  is defined as  $v_i$  in (5.17) and now multiplying by  $v_i^{-1}$  (5.18) becomes

$$\frac{F_i(z^{-1})}{v_i}(\phi_i^T(k)w(k)) + \Delta u_i - \frac{R_i(z^{-1})}{v_i}\theta_{ri} = 0 \quad (5.19)$$

Let  $R_i(z^{-1}) = F_i(z^{-1})$ , then (5.19) can be rewritten as

$$\frac{F_i(z^{-1})}{v_i}(\phi_i^T(k)w(k)) + \Delta u_i - \frac{F_i(z^{-1})}{v_i}\theta_{ri} = 0 \quad (5.20)$$

Equating (5.20) with (5.13) leads to

$$\frac{F_i(z^{-1})}{v_i} = L_i(z^{-1}) \quad (5.21)$$

and based on (5.11), (5.18) and (5.19), the PID parameters  $K_i, T_D, T_i$  can be calculated as follows.

$$\left. \begin{aligned} K_i &= -\frac{(f_{i,1} + 2f_{i,2})}{v_i} \\ T_{ri} &= -\frac{f_{i,1} + 2f_{i,2}}{f_{i,0} + f_{i,1} + f_{i,2}} T \\ T_{Di} &= -\frac{f_{i,2}}{f_{i,1} + 2f_{i,2}} T \end{aligned} \right\} \quad (5.22)$$

<b>Step 1:</b>	(a) Choose the polynomial $Q_i(z^{-1})$ for $i^{\text{th}}$ link as defined in (5.15) (b) Initialize the value of $\lambda_{i,0}, \Gamma_i$ used in (5.5) and (5.14) for $i^{\text{th}}$ link.
<b>Step 2:</b>	Apply RLS algorithm defined in (5.5)-(5.7) to estimate the NARMAX parameters $w_i^s$ for $i^{\text{th}}$ link.
<b>Step 3:</b>	Calculate the polynomials $F_i(z^{-1})$ and $E_i(z^{-1})$ of the Diophantine equation defined in (5.17) for $i^{\text{th}}$ link in order to calculate the predicted tip position
<b>Step 4:</b>	Using the estimated polynomials $F_i(z^{-1})$ and $E_i(z^{-1})$ , calculate the value of $v_i = E_i(z^{-1}) + C_i(z^{-1}) + \Lambda_i$ for $k^{\text{th}}$ instant
<b>Step 5:</b>	$K_i, T_D, T_i$ are calculated for $i^{\text{th}}$ link using (5.22)
<b>Step 6:</b>	Using the value of $K_i, T_D, T_i$ the self-tuning control law $u_i(k)$ is generated as input to the TLFM $i^{\text{th}}$ joint on solving (5.19) as $\Delta u_i(k) = \frac{Q_i(z^{-1})\theta_{ri} - F_i(z^{-1})(\phi_i^T(k)w_i(k))}{\{E_i(z^{-1})C_i(z^{-1}) + \Gamma_i\}}$

Fig.5.4 Algorithm for NMSTC

## 5.4 Results and Discussions

The numerical simulation of the NMSTC and RLAC controllers has been performed using MATLAB/SIMULINK®. To validate the tip trajectory tracking performances, the desired trajectory vector for two joints,  $\theta_{di}(t)$   $i=1,2$  are same as (3.16). The physical parameters of the studied TLFM are given in Table 2.2 in *Chapter 2*. And, the controller parameters for RLAC are given in Table 4.2 *whereas* gains of the discrete PD controller for the RLAC are taken from 4.44 and 4.45 given in *Chapter 4*.

### 5.4.1 Simulation results for an initial payload of 0.157 kg

Comparisons of performances exhibited by adaptive controllers (NMSTC and RLAC) while carrying a 0.157 kg payload are shown in Fig.5.5-5.10. Fig.5.5 and Fig.5.6 show the tip deflection trajectories for link-1 and link-2 carrying 0.157 kg of payload. From these figures it is seen that the NMSTC suppresses the tip deflection faster compared to the RLAC by damping it within 4 sec. Fig.5.7 and Fig.5.8 show the tip trajectory tracking error curves for link-1 and link-2 respectively. From Fig.5.7, it is seen that there is a tracking error of  $0.025^\circ$  in case of RLAC for link-1. However, the tracking error in case of NMSTC is  $0.03^\circ$ . Link-2 tracking error profiles in Fig.5.8 reveal that the tracking errors are  $0.15^\circ$  for RLAC whereas it is  $0.155^\circ$  in case of the NMSTC. Fig.5.9 and Fig.5.10 show the control torque profiles generated by RLAC and NMSTC for joint-1 and joint-2 respectively. From Fig.5.9 and Fig.5.10, it seen that the control input generated by the NMSTC becomes zero compared to RLAC for link-1 and link-2 when the desired tip position is tracked. Thus, NMSTC needs less control excitation for handling a payload of 0.157 kg compared to RLAC. Frequency domain analysis is carried out in order to further verify the performance of the NMSTC to suppress the overall link deflection. From Fig.

5.11 and Fig. 5.12 it is seen that the average power of the PSD for NMSTC is -10dB and -23dB less compared to RLAC for link-1 and link-2 respectively. Again the average power of the tip trajectory error is calculated from its PSDs in Fig. 5.13 and Fig. 5.14 respectively and they show reduction in average power of -15dB and -24dB for link-1 and link-2 respectively. The reductions of average power at the first and second mode by NMSTC compared to RLAC signify that the NMSTC exhibits better adaptive and optimal control performance.

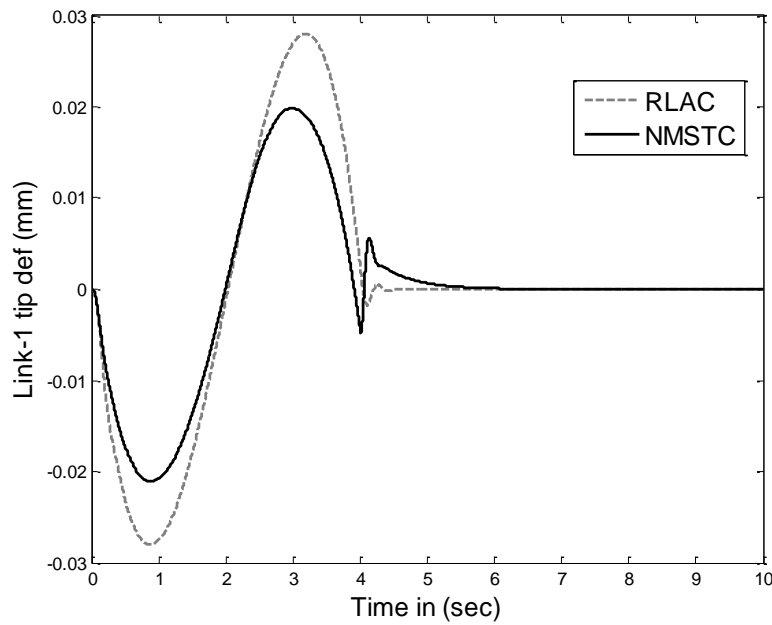


Fig.5.5 Simulation results (time domain) for comparison of link-1 tip deflection performances

(0.157 kg): RLAC and NMSTC

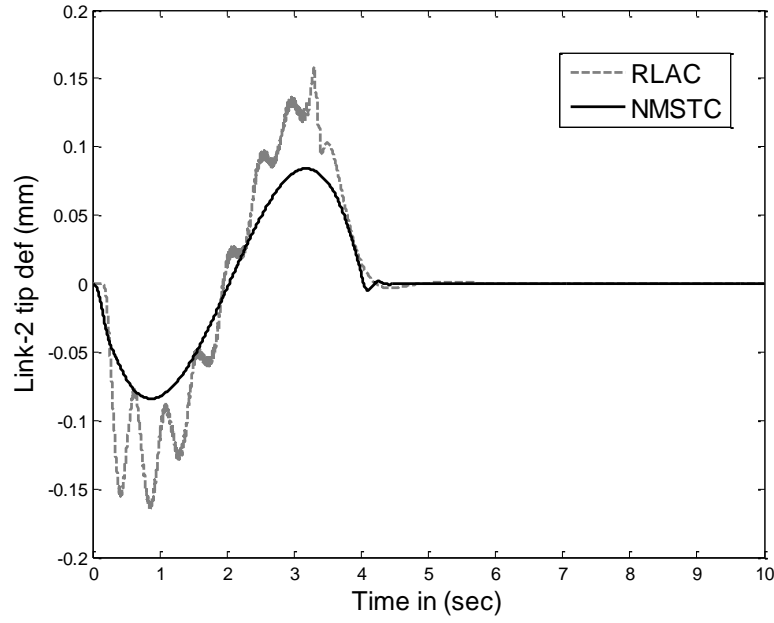


Fig.5.6 Simulation results (time domain) for comparison of link-2 tip deflection performances  
(0.157 kg): RLAC and NMSTC

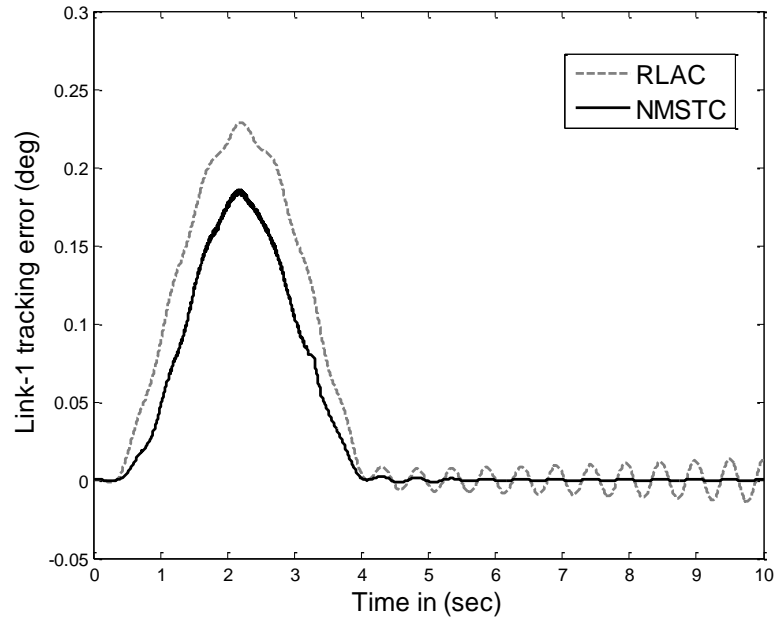


Fig.5.7 Simulation results (time domain) tip trajectory tracking errors (Link-1) (0.157 kg):  
RLAC and NMSTC

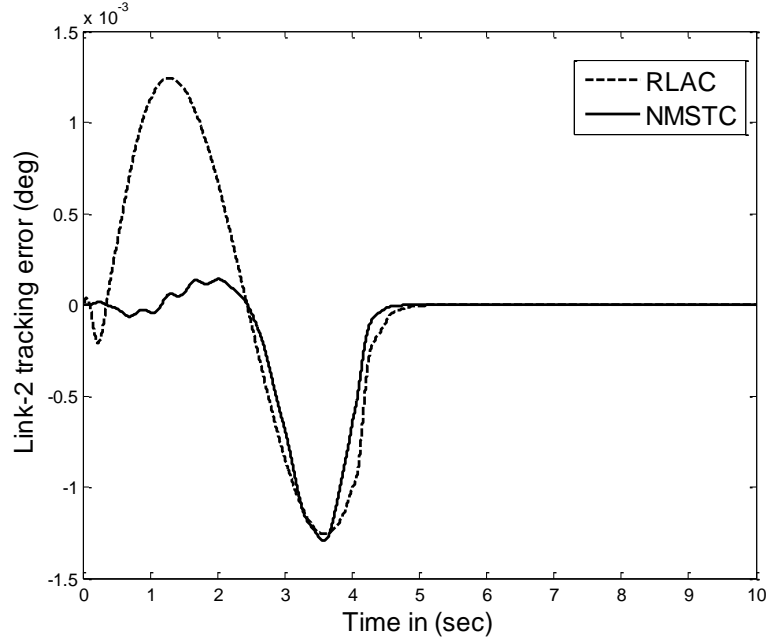


Fig.5.8 Simulation results (time domain) for tip trajectory tracking errors (Link-2) (0.157 kg):

RLAC and NMSTC

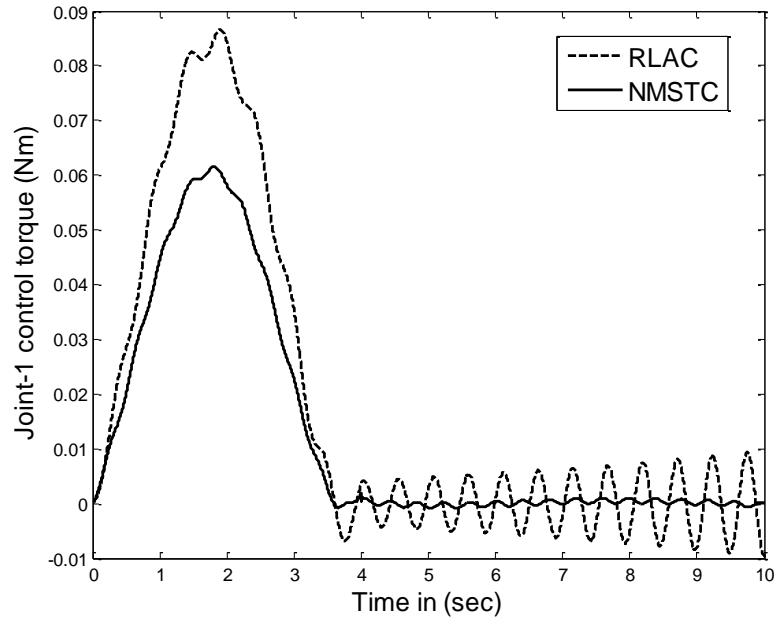


Fig.5.9 Simulation results (time domain) for torque profiles (joint-1) (0.157 kg): RLAC and

NMSTC



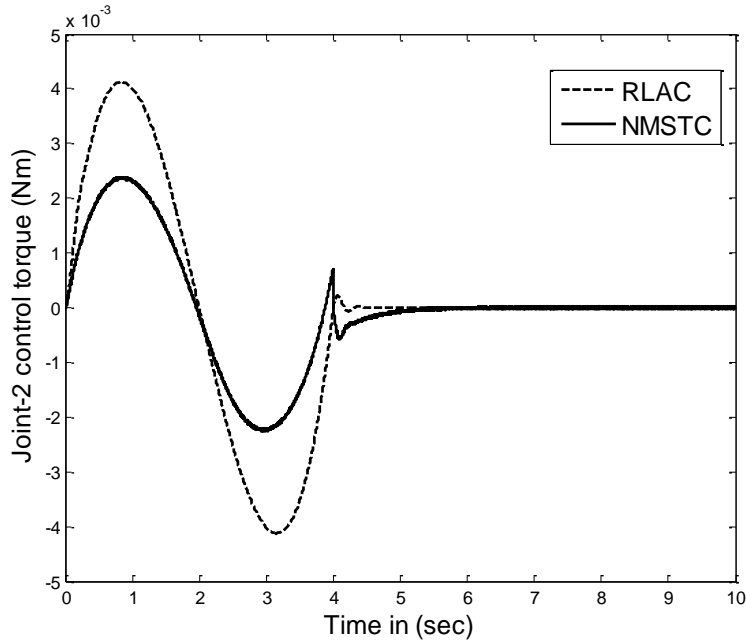


Fig.5.10 Simulation results (time domain) for torque profiles (joint-2) (0.157 kg): RLAC and NMSTC

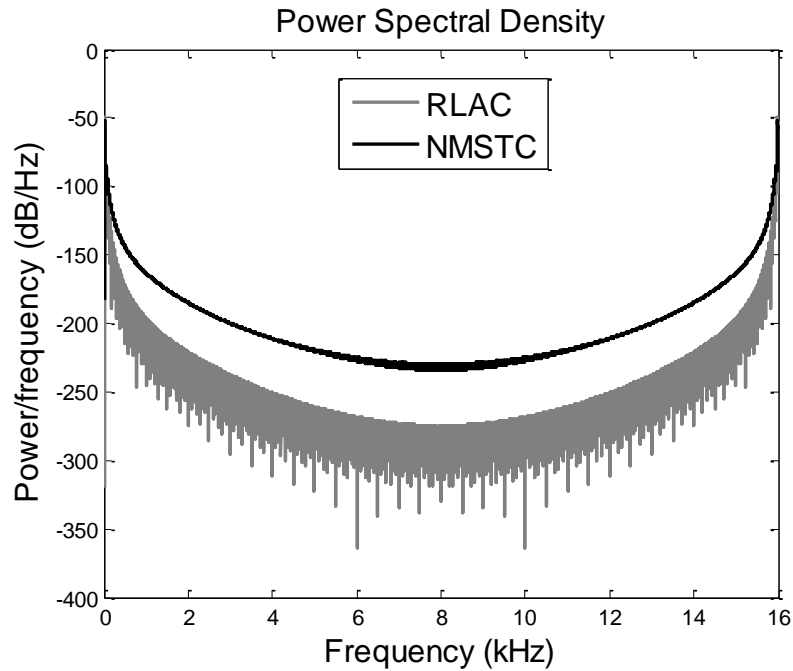


Fig.5.11 Simulation results (frequency domain) for comparison of link-1 tip deflection performances (0.157 kg): RLAC and NMSTC

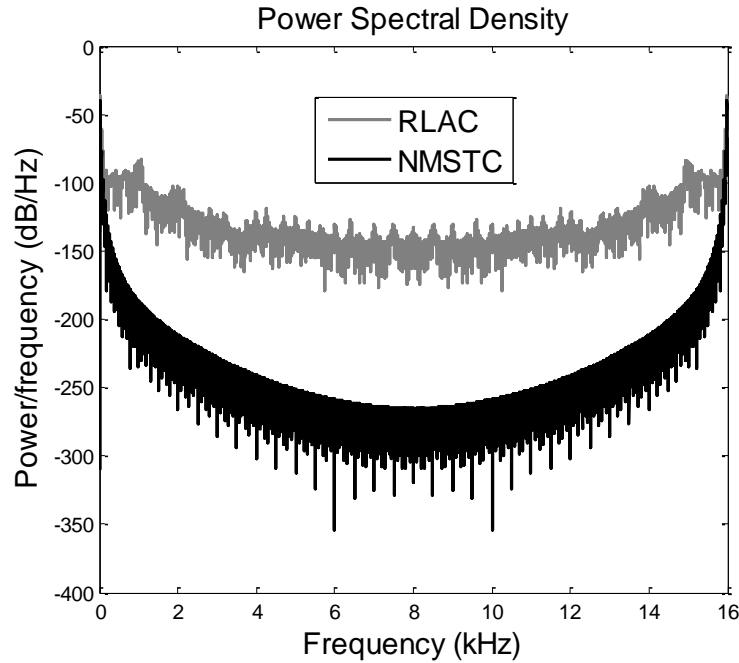


Fig.5.12 Simulation results (frequency domain) for comparison of link-2 tip deflection

performances (0.157 kg): RLAC and NMSTC

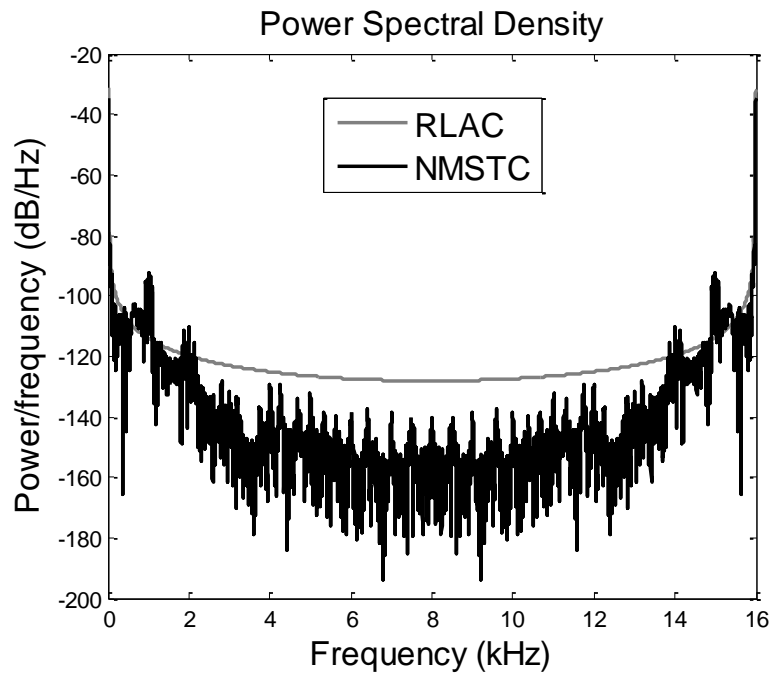


Fig.5.13 Simulation results (frequency domain) tip trajectory tracking errors (Link-1) (0.157 kg):

RLAC and NMSTC

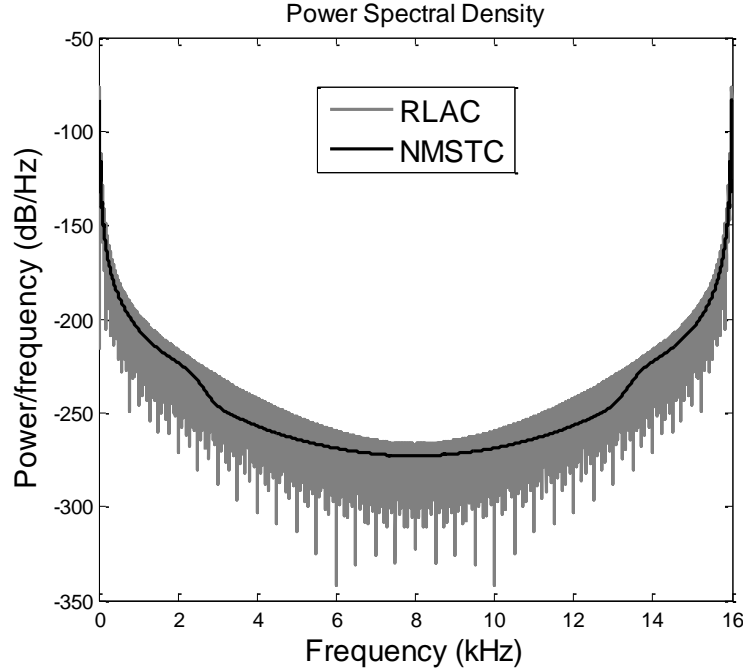


Fig.5.14 Simulation results (frequency domain) for tip trajectory tracking errors (Link-2) (0.157 kg): RLAC and NMSTC

#### 5.4.2 Simulation results for an additional payload of 0.3 kg

An additional payload of 0.3 kg is now attached to the existing initial payload of 0.157 kg making the overall payload 0.457 kg. Performances of NMSTC and RLAC for 0.457 kg payload were compared in Figs 5.15-5.20. Suppressing the tip deflection performances of NMSTC and RLAC were compared in Fig.5.15 and Fig.5.16 for link-1 and link-2 respectively. From Fig.5.15, it is seen that tip deflection is maximum in case of RLAC compared to NMSTC when a payload of 0.457 kg is attached for link-1. From Fig.5.16, it is seen that the tip deflection trajectories for link-2 is more oscillatory when carrying 0.457 kg of payload in case of RLAC compared to NMSTC. Fig.5.17 and Fig.5.18 depict the tip trajectory tracking performance for link-1 and link-2. From Fig.5.18, it can be seen that the time evolution of the error trajectory achieved by employing RLAC has yielded maximum overshoot compared to the NMSTC.

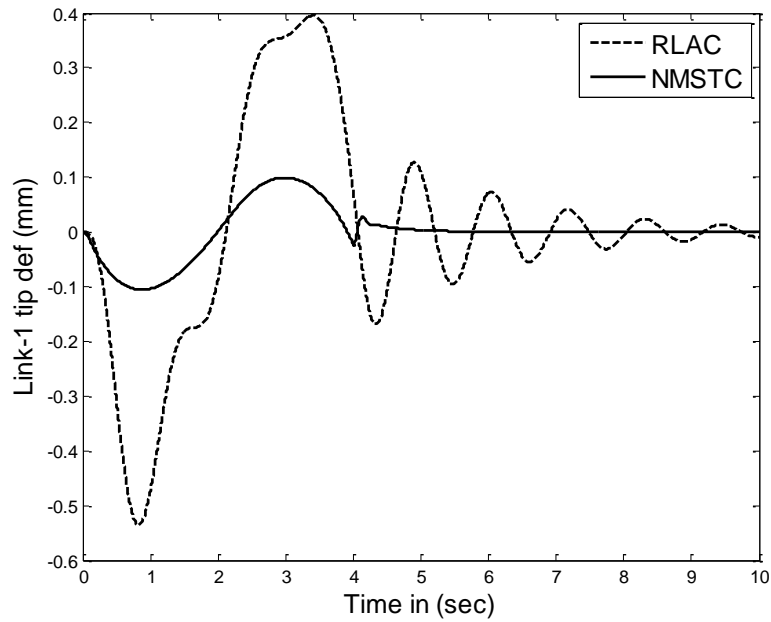


Fig.5.15 Simulation results (time domain) for comparison of link-1 tip deflection performances

(0.457 kg): RLAC and NMSTC

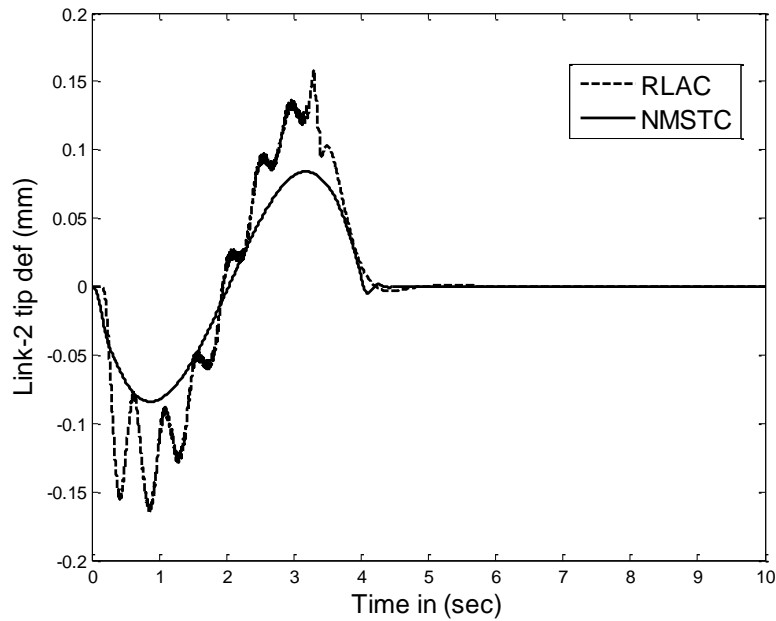


Fig.5.16 Simulation results (time domain) for comparison of link-2 tip deflection performances

(0.457 kg): RLAC and NMSTC

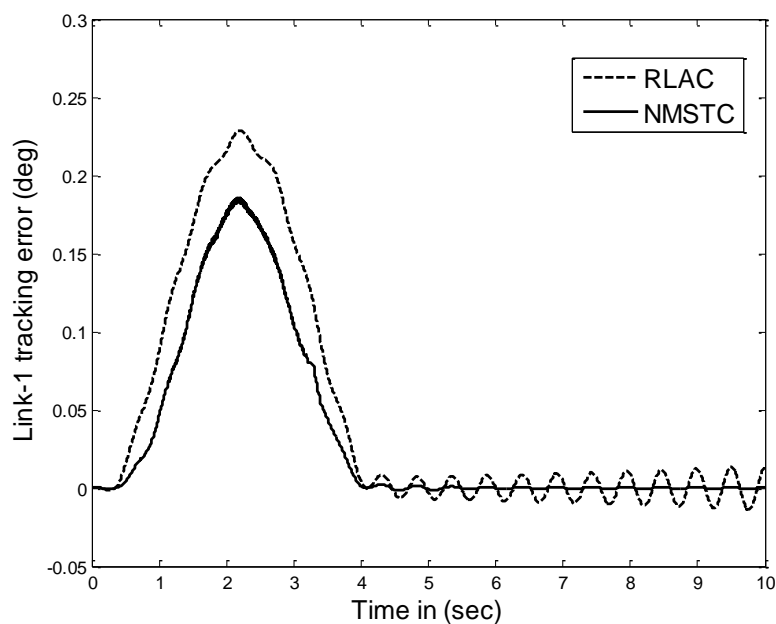


Fig.5.17 Simulation results (time domain) for tip trajectory tracking errors (Link-1) (0.457 kg):

RLAC and NMSTC

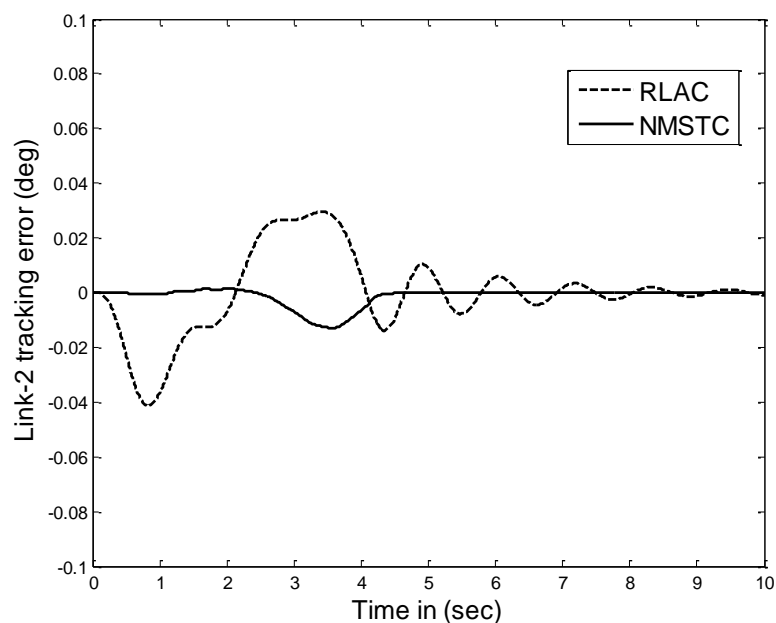


Fig.5.18 Simulation results (time domain) for tip trajectory tracking errors (Link-2) (0.457 kg):

RLAC and NMSTC

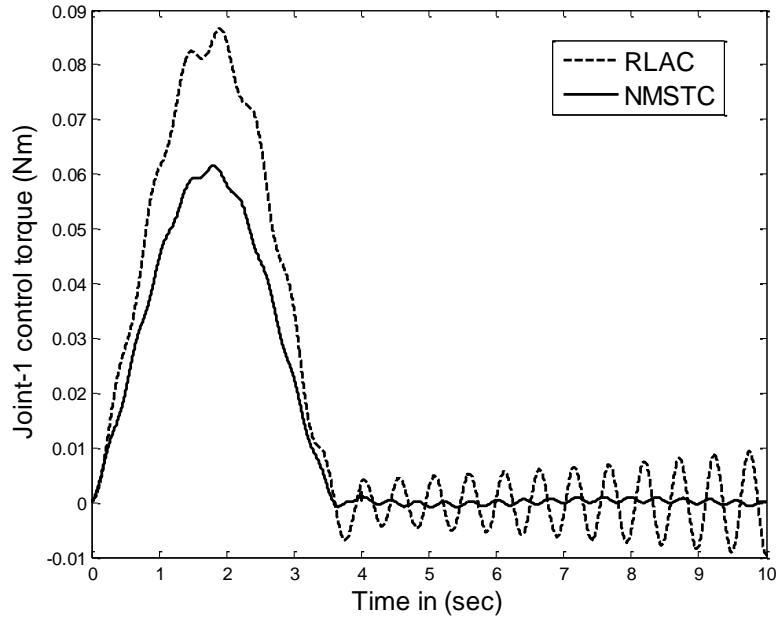


Fig.5.19 Simulation results (time domain) for torque profiles (joint-1) (0.457 kg): RLAC and NMSTC

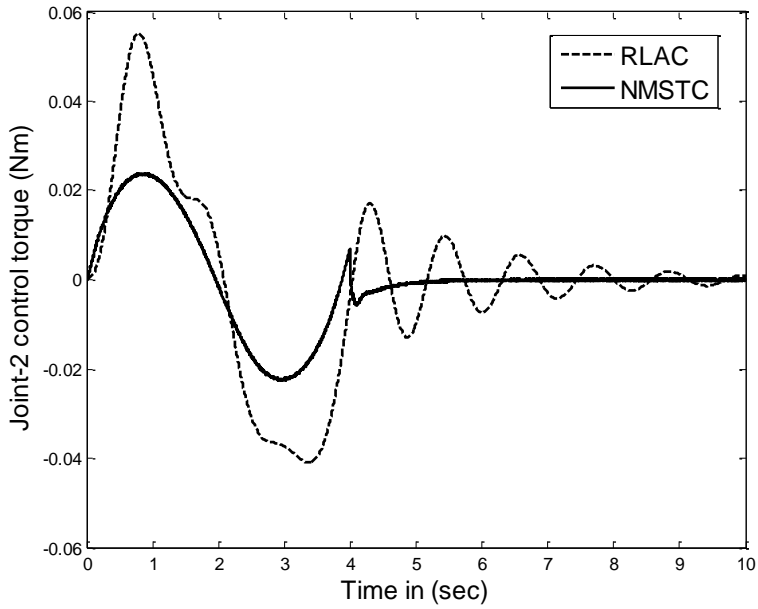


Fig.5.20 Simulation results (time domain) for torque profiles (joint-2) (0.457 kg): RLAC and NMSTC

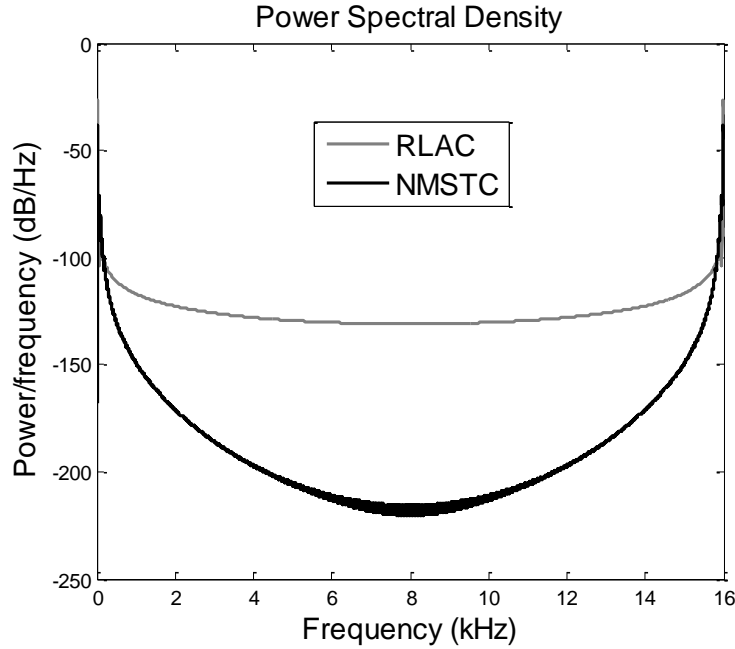


Fig.5.21 Simulation results (frequency domain) for comparison of link-1 tip deflection performances (0.457 kg): RLAC and NMSTC

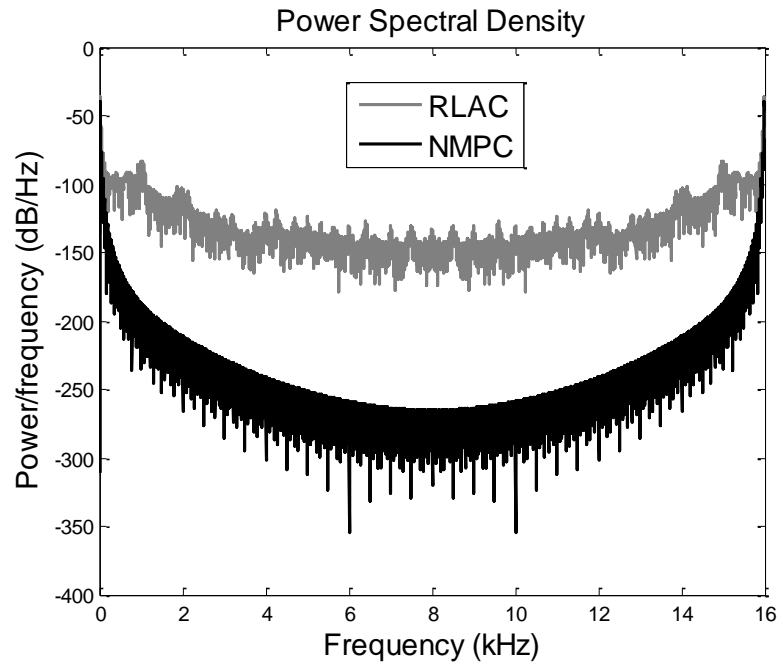


Fig.5.22 Simulation results (frequency domain) for comparison of link-2 tip deflection performances (0.457 kg): RLAC and NMSTC

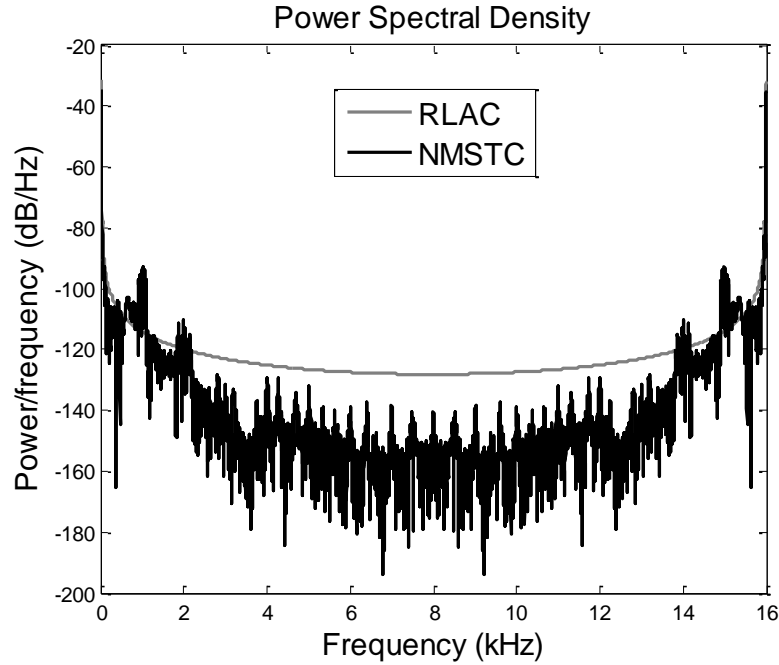


Fig.5.23 Simulation results (frequency domain) for tip trajectory tracking errors (Link-1)

(0.457 kg): RLAC and NMSTC

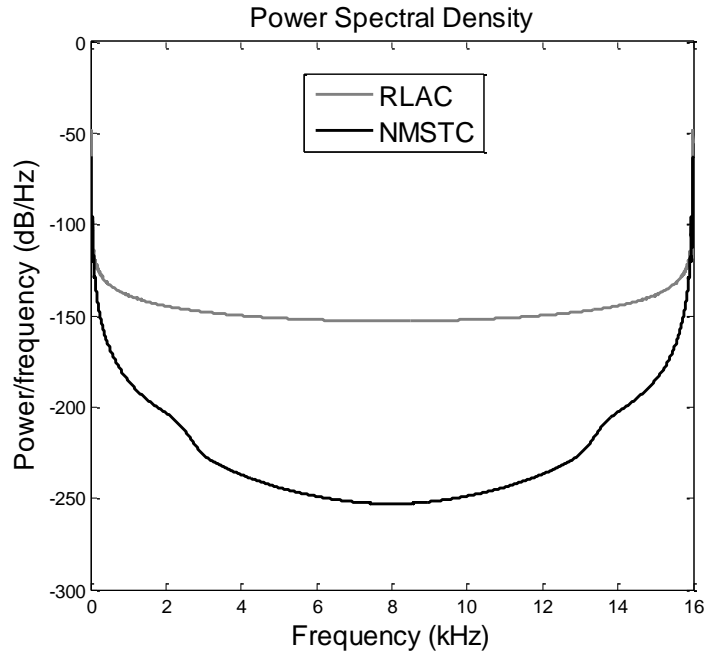


Fig.5.24 Simulation results (frequency domain) for tip trajectory tracking errors (Link-2)

(0.457 kg): RLAC and NMSTC



Fig.5.18 show that RLAC yields maximum overshoot compared to NMSTC controller. Joint torque signals generated from RLAC and NMSTC are compared in Fig.5.19 and Fig.5.20. From Fig. 5.21 and Fig. 5.22 it is seen that the average power of the PSD for NMSTC is -10dB and -23dB less compared to RLAC for link-1 and link-2 respectively. The average power of the tip trajectory error is calculated from its PSDs in Fig. 5.23 and Fig. 5.24 respectively and reduction in average power of -15dB and -24dB for link-1 and link-2 respectively. The simulation results for NMSTC and RLAC under 0.157 kg of nominal payload and with additional payload of 0.3 kg is summarized in Table 5.1. The comparison of performance indices such as settling time and maximum overshoot for tip trajectory tracking for NMSTC and RLAC were compared.

Table 5.1: Comparison of simulation results for the controllers (RLAC and NMSTC)

Controller Schemes	Payload (Kg)	Link	Overshoot (%)	Settling-Time ( $t_s$ ) in sec	Reference Figure
<b>RLAC</b>	0.157	Link-1	4.5	5.0	Fig.5.7
		Link-2	5.5	5.2	Fig.5.8
	0.457	Link-1	5.5	6.5	Fig.5.13
		Link-2	6.5	7.0	Fig.5.14
<b>NMSTC</b>	0.157	Link-1	<b>2</b>	<b>4.0</b>	Fig.5.5
		Link-2	<b>2.5</b>	<b>4.0</b>	Fig.5.8
	0.457	Link-1	<b>2.5</b>	<b>6.0</b>	Fig.5.13
		Link-2	<b>3</b>	<b>6.5</b>	Fig.5.14

From Table 5.1 it is observed that RLAC yields a 4.5% maximum overshoot for link-1 and 5.5 % for link-2 under a nominal payload of 0.157 kg and in case of NMSTC the maximum overshoot

percentage are 2% and 2.5% respectively for link-1 and link-2. When an additional payload of 0.3 kg is attached to tip, the maximum overshoots in case of NMSTC are 2.5% and 3% respectively for link-1 and link-2. But the RLAC yields 5.5% and 6.5% overshoots for link-1 and link-2.

#### 5.4.3 Experimental results for an initial payload of 0.157 kg

Figs. 5.25-5.30 compare experimental results obtained by NMSTC and RLAC with an initial payload of 0.157 kg. The tip deflection trajectories for the link-1 and link-2 when loaded for a 0.157 kg payload are shown in Fig 5.25 and Fig 5.26. From Fig.5.25, it can be seen that NMSTC yields 0.04 mm of initial deviation as compared to RLAC where the deflection is 0.18 mm for link-1. Link-2 tip deflection characteristics are shown in Fig.5.26, from which it is seen that NMSTC has 0.2 mm of initial deviation as compared to RLAC which has 0.6 mm of initial deviation. Fig.5.27 and Fig.5.28 show the comparison of the tip trajectory tracking, after 4 sec when the tip attains the final position, the steady state error is zero in case of NMSTC for link-1 and link-2, whereas the RLAC yield steady state error of  $0.12^\circ$  and  $0.6^\circ$  for link-1 link-2 respectively after 4 sec. Torque profiles for joint-1 generated by employing the controllers are shown in Fig.5.29 and that for joint-2 is shown in Fig. 5.30. In Fig.5.29 the joint torque control input for link-1 obtained by RLAC reaches to a maximum value (0.5 Nm) at 2 sec and as the tip reaches to the final position the control input reduces to 0.2 Nm. While in case of NMSTC there is 0.15 Nm initial torque and it becomes zero when the tip reaches the final position at 4 sec. From Fig. 5.31 and Fig. 5.32 shows the average power of the PSD for NMSTC is -1.7dB and -2.4dB less compared to RLAC for link-1 and link-2 respectively. The average power of the tip trajectory error is calculated from its PSDs in Fig. 5.33 and Fig. 5.34 respectively, reduction in average power of -1.6dB and -2.8dB for link-1 and link-2 respectively.

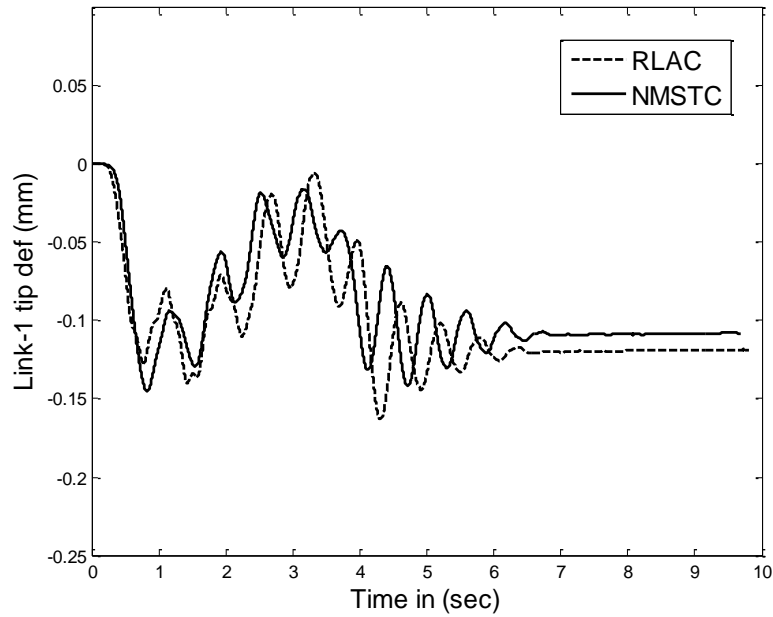


Fig.5.25 Experimental results (time domain) for comparison of link-1 tip deflection performances (0.157 kg): RLAC and NMSTC

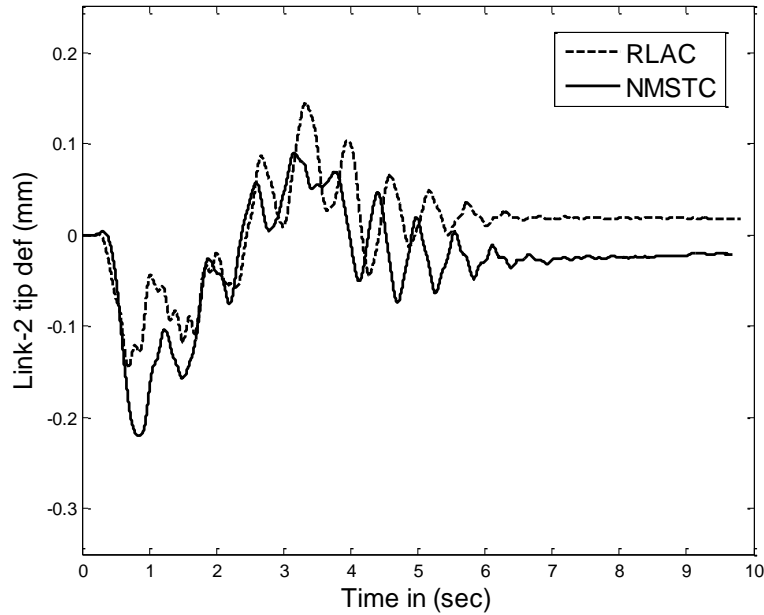


Fig.5.26 Experimental results (time domain) for comparison of link-2 tip deflection performances (0.157 kg): RLAC and NMSTC

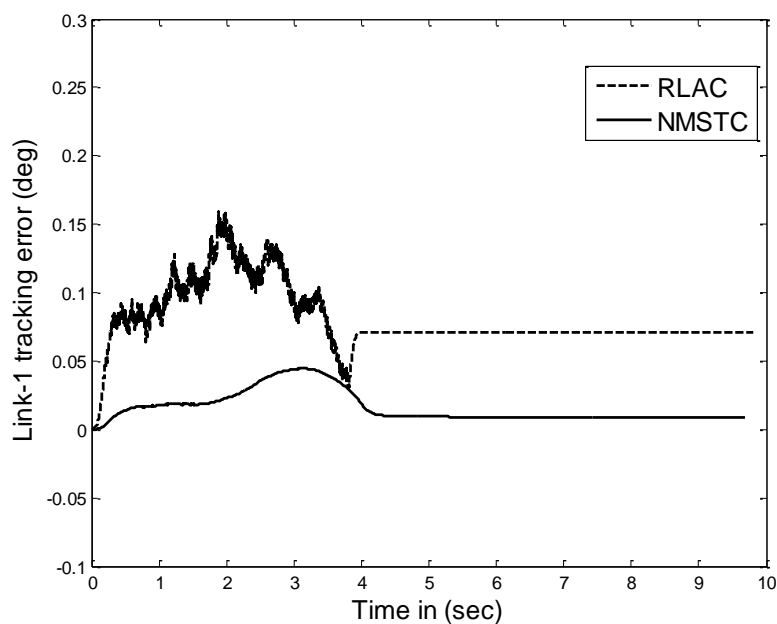


Fig.5.27 Experimental results (time domain) for tip trajectory tracking errors (Link-1) (0.157 kg): RLAC and NMSTC

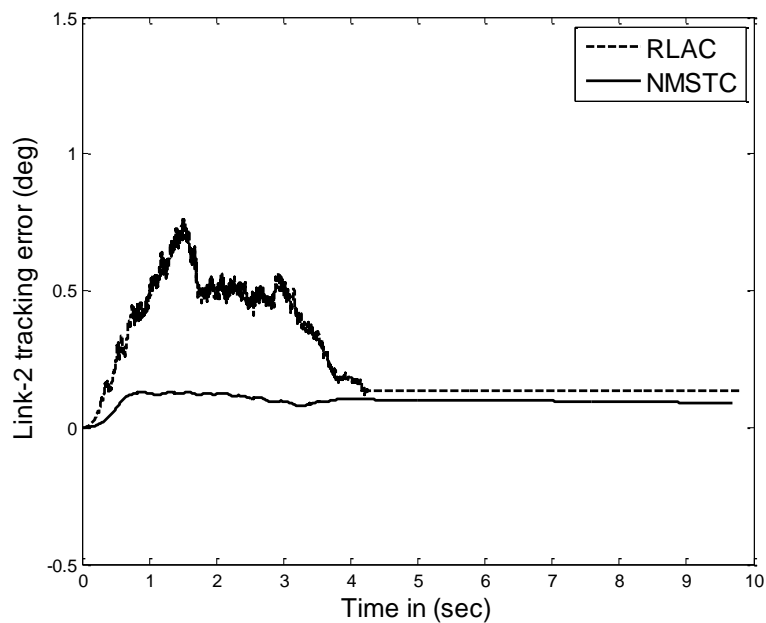


Fig.5.28 Experimental results (time domain) for tip trajectory tracking errors (Link-2) (0.157 kg): RLAC and NMSTC

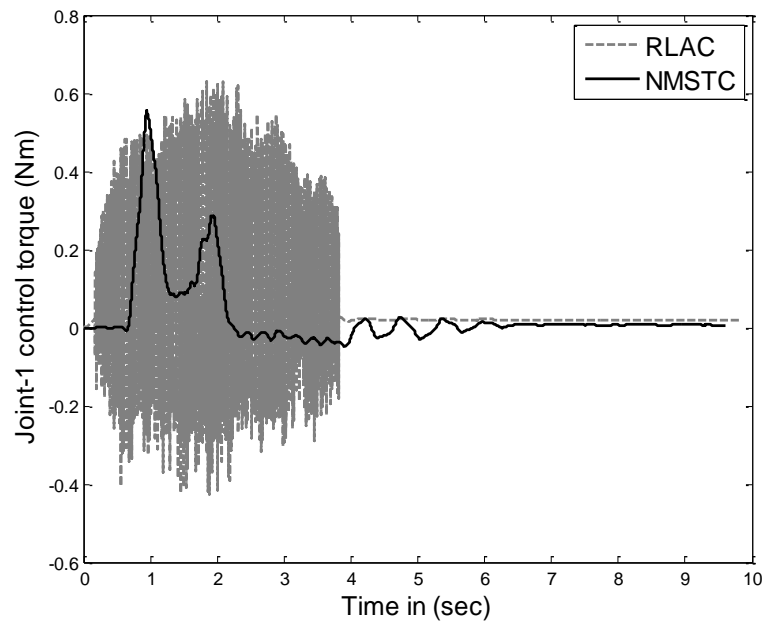


Fig.5.29 Experimental results (time domain) for torque profiles (joint-1) (0.157 kg): RLAC and NMSTC)

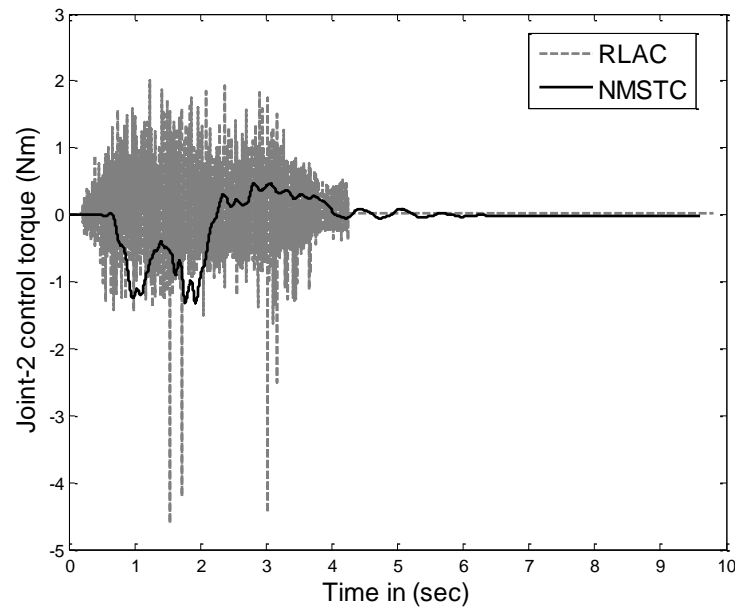


Fig.5.30 Experimental results (time domain) for torque profiles (joint-2) (0.157 kg): RLAC and NMSTC

Fig.5.22 shows the joint control torque signals generated by RLAC and NMSTC for link-2 have which has maximum of 2 Nm and 0.2 Nm and reduces to 0.2 Nm and zero respectively as the tip attains the final position.

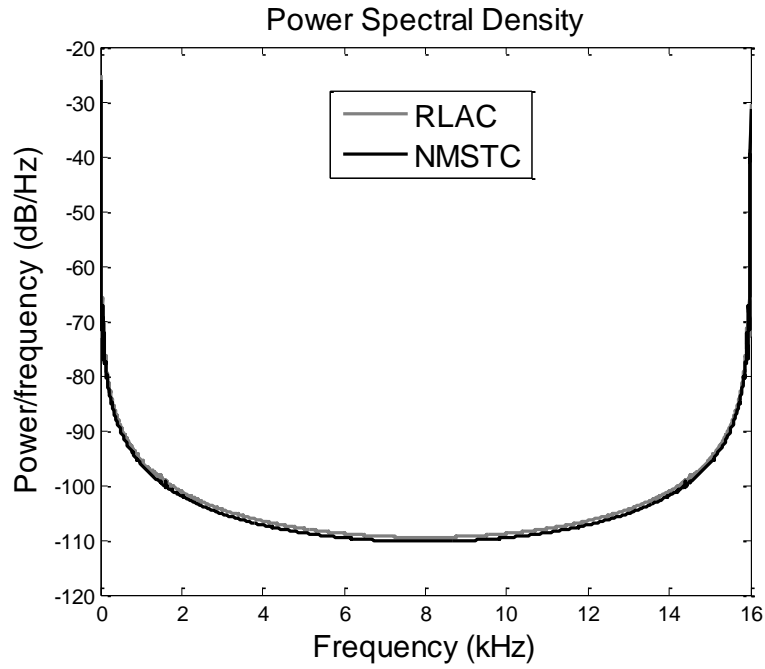


Fig.5.31 Experimental results (frequency domain) for comparison of link-1 tip deflection performances (0.157 kg): RLAC and NMSTC

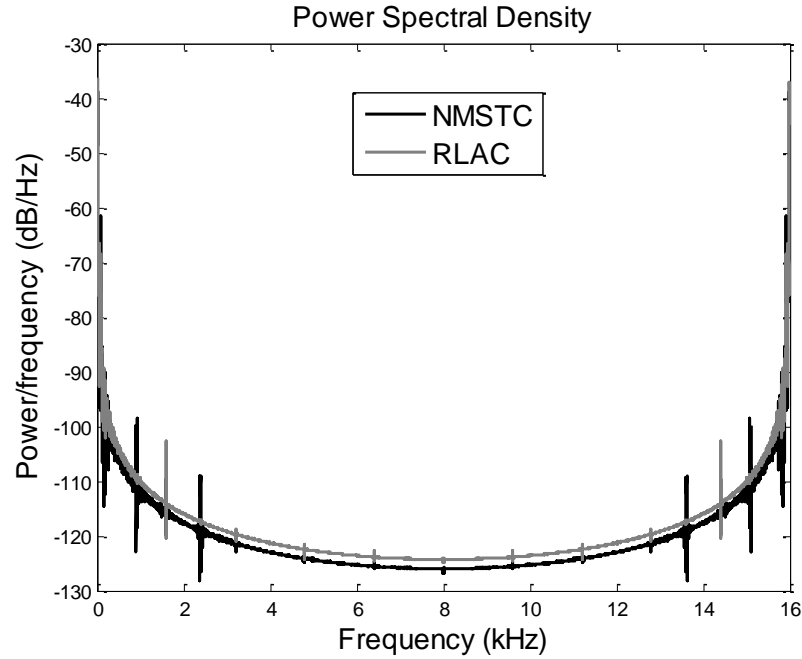


Fig.5.32 Experimental results (frequency domain) for comparison of link-2 tip deflection performances (0.157 kg): RLAC and NMSTC

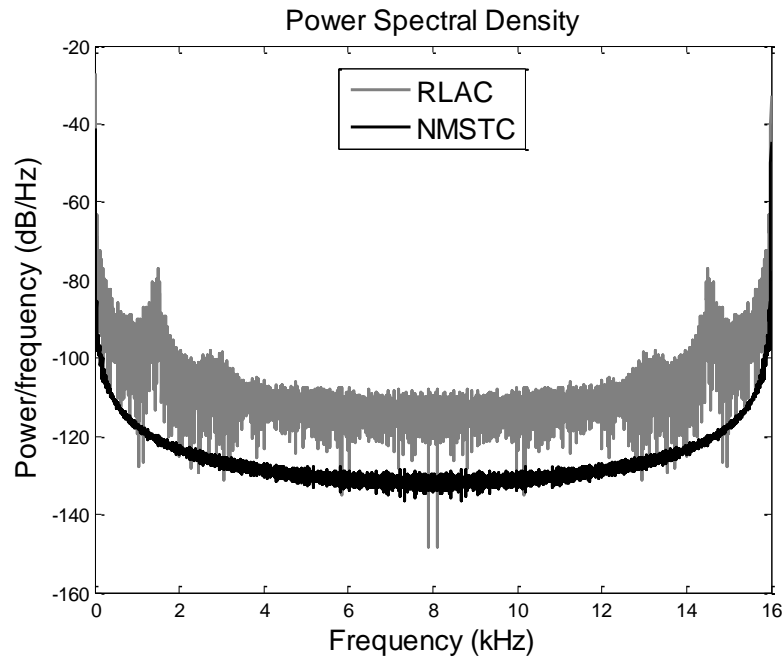


Fig.5.33 Experimental results (frequency domain) for tip trajectory tracking errors (Link-1) (0.157 kg): RLAC and NMSTC

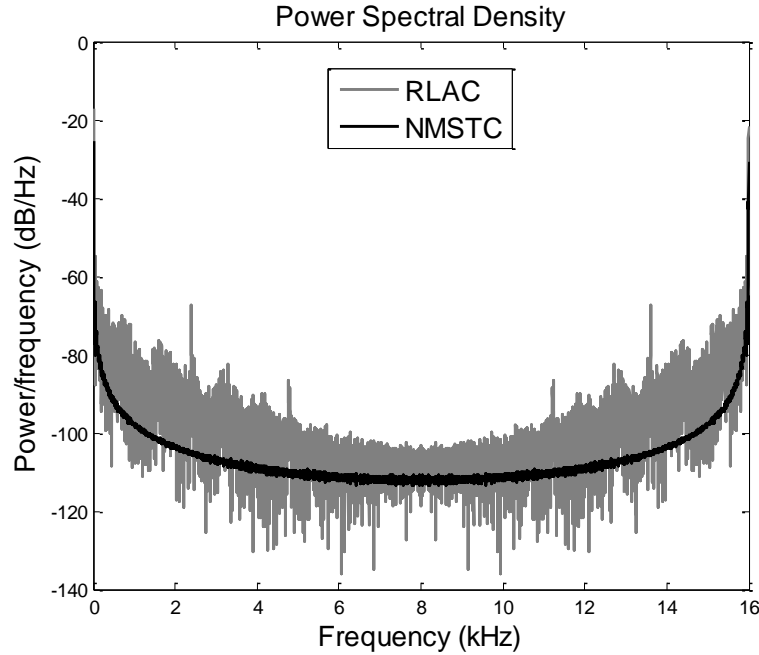


Fig.5.34 Experimental results (frequency domain) for tip trajectory tracking errors (Link-2)

(0.157 kg): RLAC and NMSTC

#### 5.4.4 Experimental results for an additional payload of 0.3 kg

An additional payload of 0.3 kg is added to the initial payload of 0.157 kg. Figures 5.35-5.40 show comparison of the experimental results for TLFM obtained by employing NMSTC and RLAC with a payload of 0.457 kg. Fig.5.35 and Fig.5.36 show the tip deflection trajectories for the link-1 and link-2 when asked for a payload of 0.457 kg. From Fig.5.35 it is seen in case of NMSTC there exists an initial deviation of 0.05 mm as compared to RLAC in which deflections 0.25 mm is for link-1. Link-2 tip deflection responses are shown in Fig.5.36.



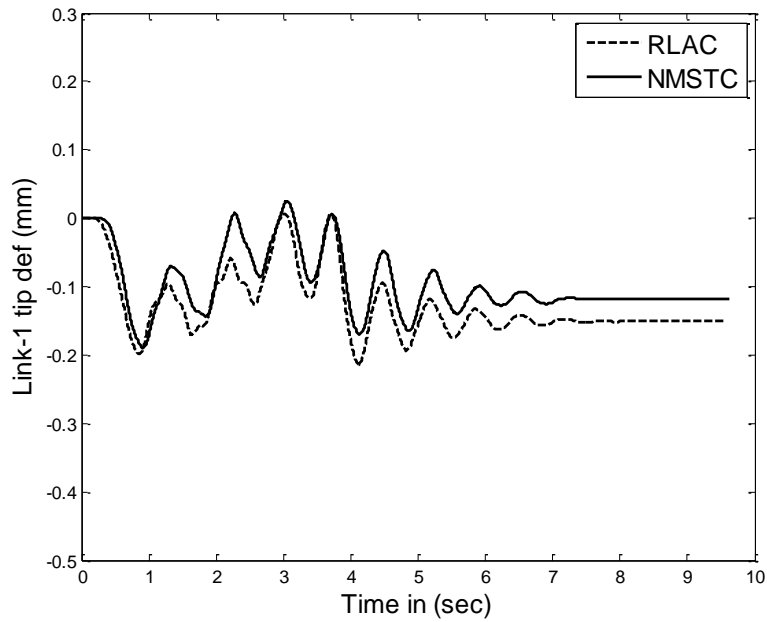


Fig.5.35 Experimental results (time domain) for comparison of link-1 tip deflection performances (0.457 kg): RLAC and NMSTC

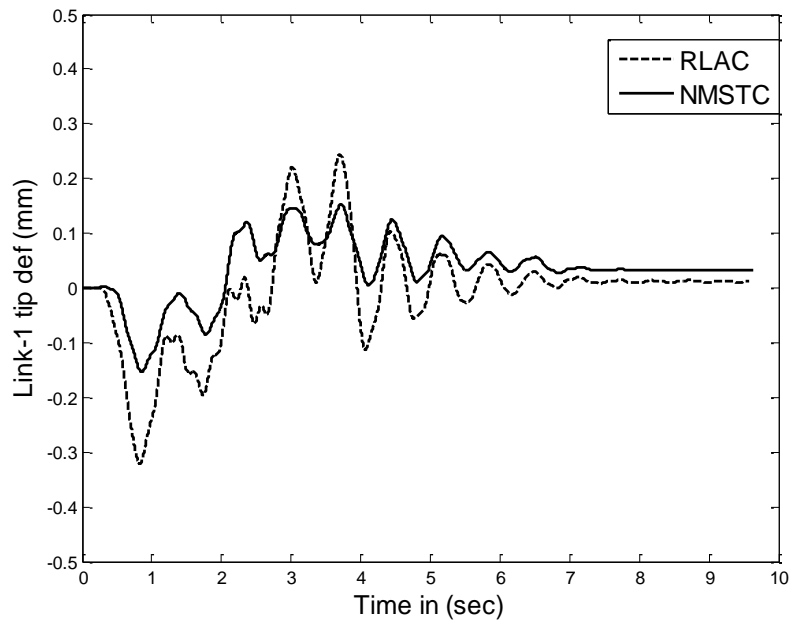


Fig.5.36 Experimental results (time domain) for comparison of link-2 tip deflection performances (0.457 kg): RLAC and NMSTC

NMSTC has 0.06 mm of initial deviation as compared to RLAC where an initial deviation is 0.25 mm. Fig.5.37 and Fig.5.38 compare the tip trajectory tracking performances for link-1 and link-2 respectively. From Fig.5.37 and Fig.5.38 it is clear that when the final position is attained, the steady state error in case of NMSTC is almost zero, whilst a finite steady state error exists in case of RLAC.

Torque profile generated for joint-1 by the controllers is shown in Fig.5.39. From this figure it is seen that the RLAC torque signal reaches to a maximum value of 0.55 Nm and reduces to 0.05 Nm at 4 sec when the final position is tracked. But NMSTC generates control torque signal with 0.2 Nm in amplitude initially and zero magnitude while the desired position has been tracked. From Fig.5.40, torque profile generated for joint-2, it is seen that the RLAC torque signal reaches to maximum value of 1.5 Nm at 1sec and reduces to 0.6 Nm at 4sec when the final position is tracked, whereas NMSTC generates appropriate control torques with maximum value of 0.5 Nm at 1.5 sec with 0.05 Nm value at the final position. Fig. 5.41 and Fig. 5.42 shows the average power of the PSD for NMSTC is -1.2dB and -2.4dB less compared to RLAC for link-1 and link-2 respectively. The average power of the tip trajectory error is calculated from its PSDs (Fig. 5.43 and Fig. 5.44 respectively). It is observed that there is a reduction in average power of -1.7dB and -1.8dB for link-1 and link-2 respectively. Table 5.2 shows the comparisons of the experiment results for NMSTC and RLAC under 0.157 kg of nominal payload and additional payload of 0.3 kg.

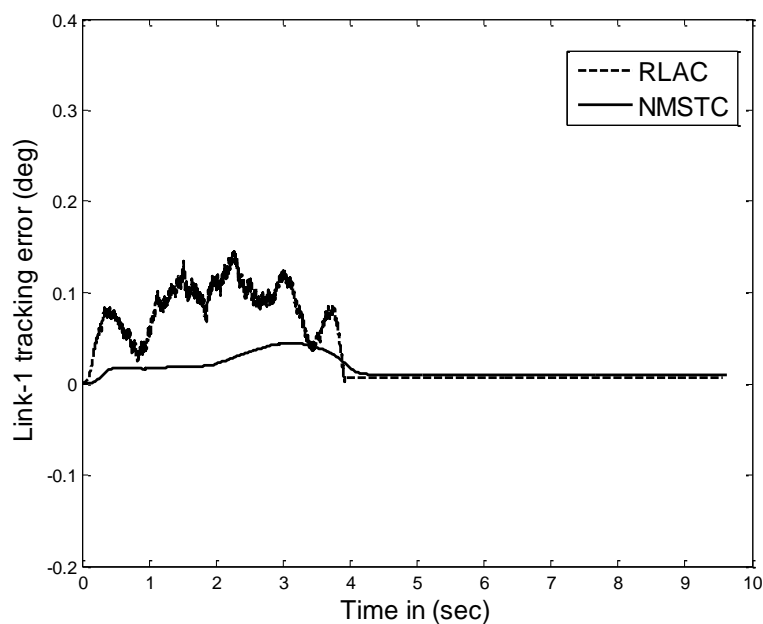


Fig.5.37 Experimental results (time domain) for tip trajectory tracking errors (Link-1) (0.457 kg): RLAC and NMSTC

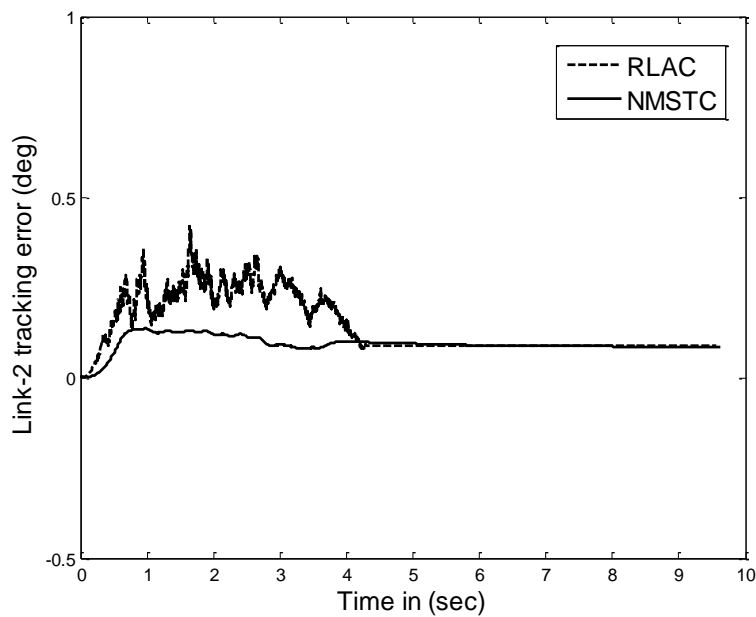


Fig.5.38 Experimental results (time domain) for tip trajectory tracking errors (Link-2) (0.457 kg): RLAC and NMSTC

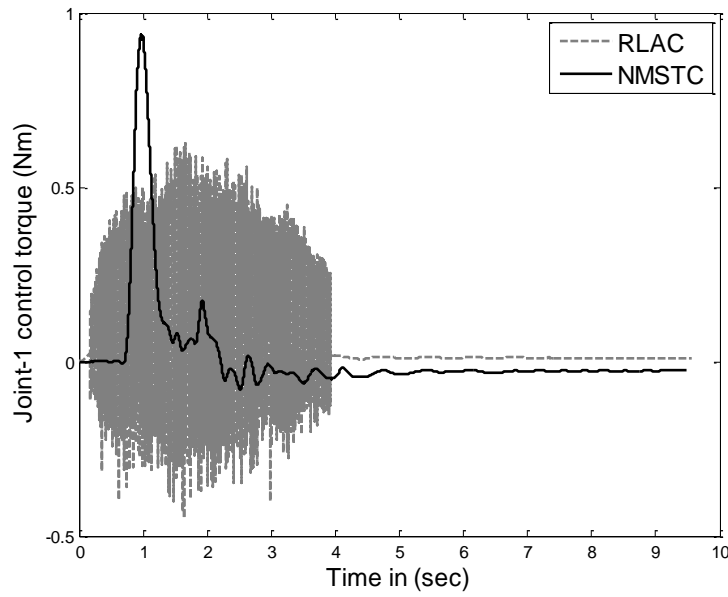


Fig.5.39 Experimental results (time domain) for torque profiles (joint-1) (0.457 kg): RLAC and NMSTC

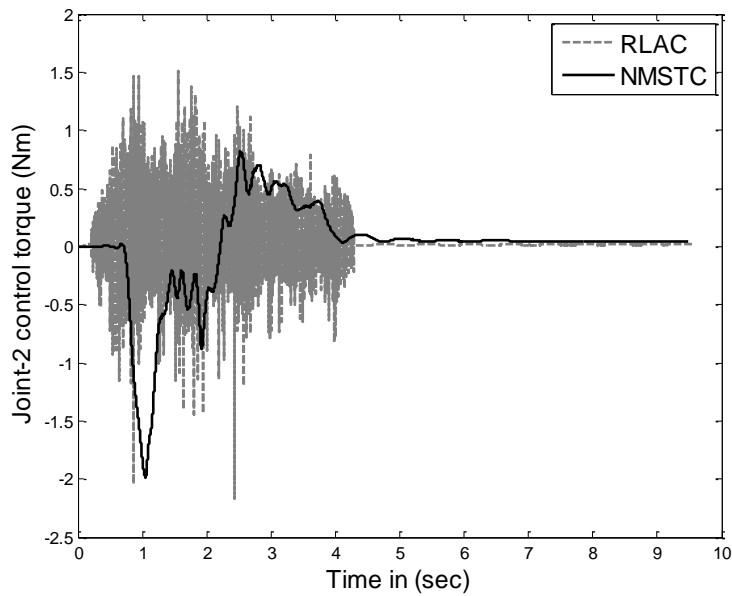


Fig.5.40 Experimental results (time domain) for torque profiles (joint-2) (0.457 kg): RLAC and NMSTC

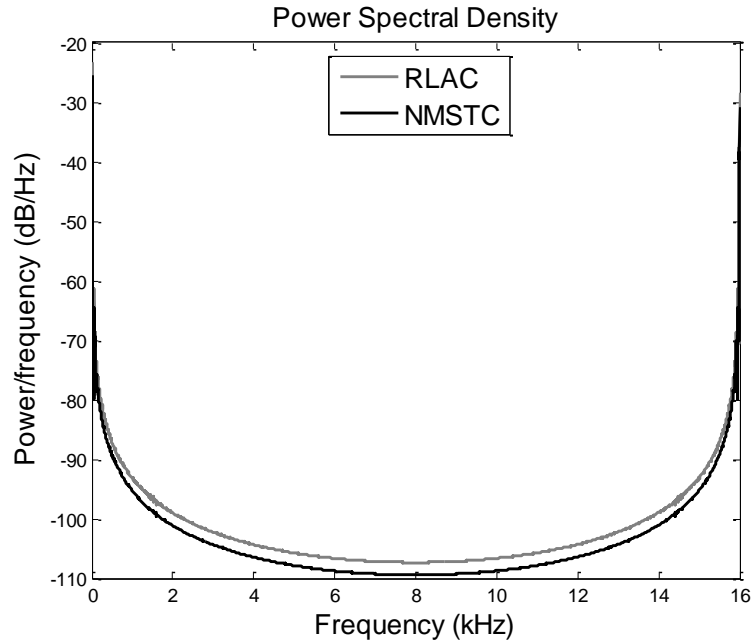


Fig.5.41 Experimental results (frequency domain) for comparison of link-1 tip deflection performances (0.457 kg): RLAC and NMSTC

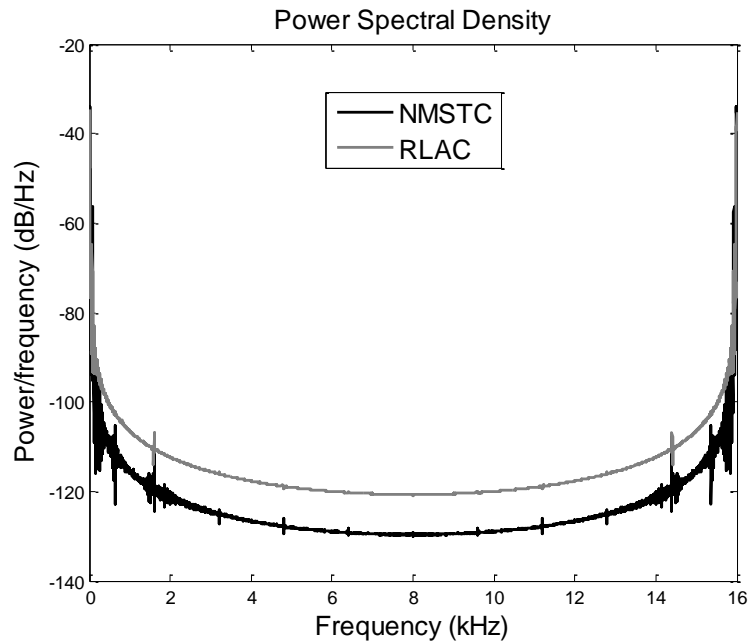


Fig.5.42 Experimental results (frequency domain) for comparison of link-2 tip deflection performances (0.457 kg): RLAC and NMSTC

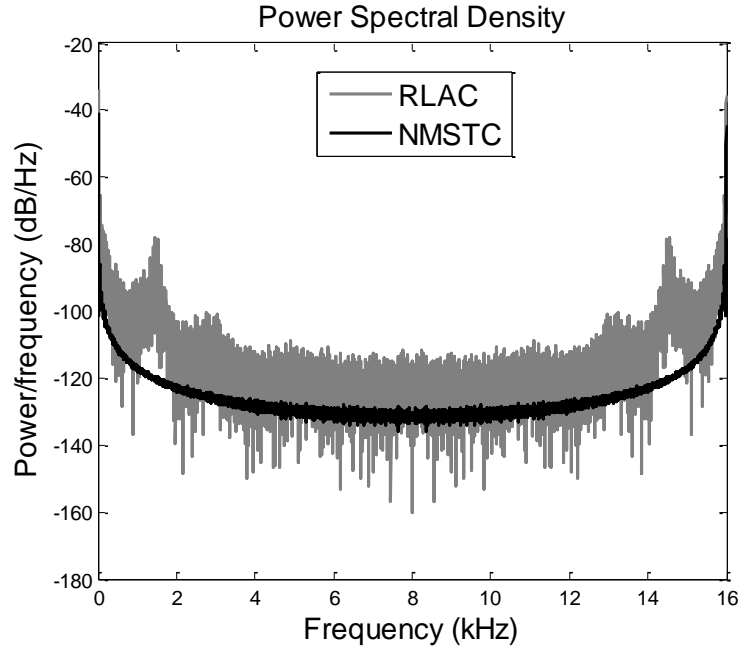


Fig.5.43 Experimental results (frequency domain) for tip trajectory tracking errors (Link-1)  
(0.457 kg): RLAC and NMSTC

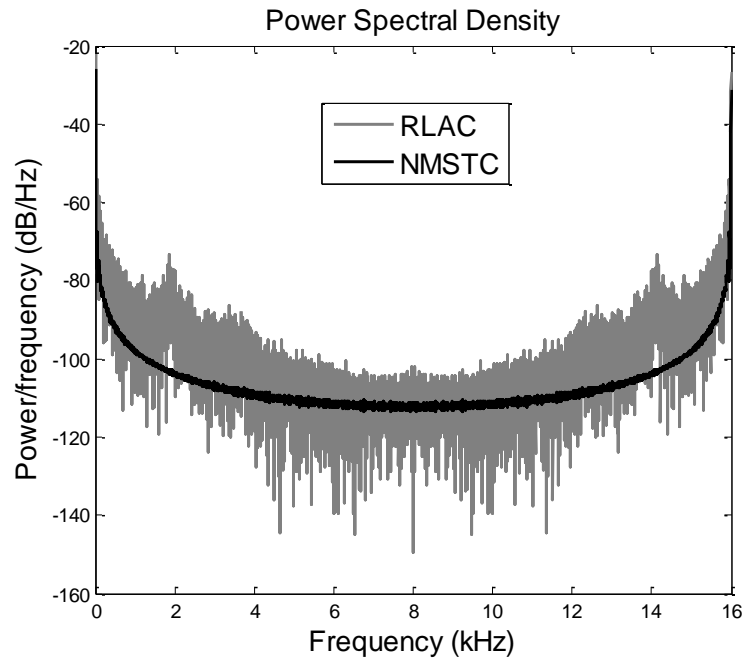


Fig.5.44 Experimental results (frequency domain) for tip trajectory tracking errors (Link-2)  
(0.457 kg): RLAC and NMSTC

The comparison of performance indices such as settling time and maximum overshoot for tip trajectory tracking for NMSTC and RLAC were compared. From Table 5.2 it is observed that RLAC yields a 6.5% maximum overshoot for link-1 and 5.5 % for link-2 under a nominal payload of 0.157 kg and in case of NMSTC the maximum overshoot percentage are 0.5% and 1% respectively for link-1 and link-2. When an additional payload of 0.3 kg is attached to tip, the maximum overshoots in case of NMSTC are 1% and 1.5% respectively for link-1 and link-2. But the RLAC yields 4.5% and 4% overshoots for link-1 and link-2.

Table 5.2: Comparison of experimental results for the controllers (RLAC and NMSTC)

Controller Schemes	Payload (Kg)	Link	Overshoot (%)	Settling-Time (t <sub>s</sub> )	Reference Figure
<b>RLAC</b>	0.157	Link-1	6.5	4.0	Fig.5.19
		Link-2	5.5	5.2	Fig.5.20
	0.457	Link-1	4.5	4.8	Fig.5.25
		Link-2	4.0	6.0	Fig.5.26
<b>NMSTC</b>	0.157	Link-1	<b>0.5</b>	<b>4.2</b>	Fig.5.19
		Link-2	<b>1</b>	<b>5.0</b>	Fig.5.20
	0.457	Link-1	<b>1</b>	<b>4.5</b>	Fig.5.25
		Link-2	<b>1.5</b>	<b>4.6</b>	Fig.5.26

## 5.5 Chapter Summary

The Chapter has presented a new self-tuning multivariable PID controller (NMSTC) to control tip trajectory and tip deflection of a two-link flexible manipulator while handling variable

payloads based on NARMAX model. The proposed NMSTC has been applied successfully to a flexible robot set-up in the laboratory. From the simulation and experimental results it is established that the proposed NMSTC generates appropriate adaptive torque when the manipulator is asked to handle additional payload of 0.3 kg compared to RLAC proposed in *Chapter 4*.

As in case of NMSTC, parameters are adapted due to change in payload by directly estimating the NARMAX model parameters *on-line* whereas in case of RLAC is based on the actor and critic weights adaptation using the Recursive Least Square-Eligibility Trace-Adaptive Memory algorithm (RLS-ET-AM).



## Chapter 6

# Nonlinear Adaptive Model Predictive Control of a Two-Link Flexible Manipulator using NARMAX Model

The adaptive control scheme described in *Chapter 5* uses a PID self-tuning control using NARMAX model to control the tip position and its deflection for a TLFM. However, in this control only *one-step* ahead prediction is used in the NMSTC but considerable time is needed to find an optimum tuning of control parameters. In this work a NARMAX model-based MPC control strategy is proposed i.e. NMPC which incorporates a nonlinear regressor and parameters in linear representation of the TLFM model. The *Chapter* is organized as follows. *Section 6.2* presents the design of the proposed NMPC scheme. NMPC is verified both through simulation

and experiment. The simulation and experimental results are discussed in *Section 6.4*. The summary of the chapter is presented in *Section 6.5*.

## 6.1 Introduction

In MPC, the current control action is obtained by solving a finite horizon open loop optimal control problem *online*, at each sampling instant. The optimization yields an optimal control sequence, and only the first control in this sequence is applied to the plant. MPC attracted attention of many researchers to exploit it as one of the most recommended advanced control algorithms [101-107]. This control methodology has been applied successfully in control of many complex systems such as inverse unstable systems, open loop unstable systems, and variable dead time processes [108-110]. From the results obtained in [111-114], it can be verified that MPC provide robustness with respect to modeling errors, over- and under parameterization, and sensor noise. Also recently nonlinear model predictive control is being applied to many nonlinear systems in [115-120]. Hence, in this *Chapter* a new NARMAX model based nonlinear adaptive multivariable model predictive control (NMPC) has been developed. The performances of the proposed controller are also compared with a nonlinear NMSTC using both simulation and experimental studies. Fig.6.1 shows the basic nonlinear model predictive control concept, where  $N_p$  is the prediction horizon and  $N_c$  is the control horizon. The basic idea in a model predictive control is to predict the vector of future outputs so that the norm of future error vector is minimized over a specific number of future control inputs.

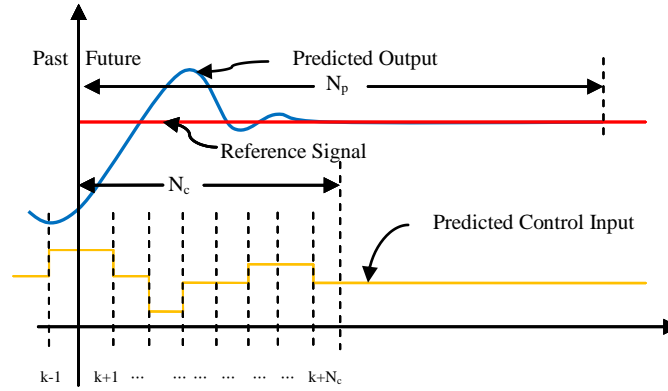


Fig.6.1 Basic Nonlinear model predictive control concept

## 6.2 Nonlinear Adaptive Model Predictive Control using NARMAX Model

The NARMAX model for the TLFM estimated in *Chapter 5* is

$$\mathbf{Y}(k) = \mathbf{F}_i^n \begin{bmatrix} y_{p_i}(k-1), y_{p_i}(k-2), \dots, y_{p_i}(k-N_y), \\ u_i(k-1), u_i(k-2), \dots, u_i(k-N_u), \xi_{s_i}(k) \end{bmatrix} \quad (6.1)$$

The  $j$ -step-ahead predicted output can be constructed with the available sequence of past inputs, past outputs and noise at sampling time  $T$  of the NARMAX model in (6.1) as

$$\hat{\mathbf{S}}(k) = \begin{bmatrix} \hat{\mathbf{Y}}(k+1) \\ \hat{\mathbf{Y}}(k+2) \\ \vdots \\ \hat{\mathbf{Y}}(k+j) \end{bmatrix} \quad (6.2)$$

Eq. (6.2) can be represented in a generalized form as

$$\hat{\mathbf{S}}(k) = \hat{\mathbf{G}}\phi(k) + \hat{\mathbf{H}}\mathbf{U}(k) \quad (6.3)$$

where

$$G = \begin{bmatrix} G_{11} & G_{12} & \cdots & G_{1N_y} \\ 0 & G_{22} & \cdots & G_{2N_y} \\ \vdots & \vdots & \vdots & \vdots \\ 0 & 0 & 0 & G_{N_y-1N_y} \end{bmatrix}, H = \begin{bmatrix} H_1 \\ H_2 \\ \vdots \\ H_{N_u} \end{bmatrix}$$

$$U(k) = \begin{bmatrix} u_i(k-1) \\ u_i(k-2) \\ \vdots \\ u_i(k-N_u) \end{bmatrix}$$

The predicted output (6.3) consists of control inputs  $U(k)$ (present values) and  $U(k-1), \dots, U(k-N_u)$ , (past values). The nonlinear functions  $\hat{G}\phi(k)$  and  $\hat{H}U(k)$  is written in parametric form as

$$\hat{G}\phi(k) = \sum_{k=1}^{N_i} \left[ \left( w_{if_{jk}} \psi_{i_{jk}} \right) \phi(k) \right] \quad (6.4)$$

$$\hat{H}U(k) = \sum_{k=1}^{N_{jl}} \left[ \left( w_{ig_{jlk}} \psi_{i_{jk}} \right) (\phi(k)) \right] \quad (6.5)$$

Hence, the  $j$ -step ahead prediction for the TLFM-NARMAX model (6.3) is rewritten using the parametric representation of  $\hat{G}\phi(k)$  and  $\hat{H}U(k)$  given in (6.4) and (6.5) respectively as

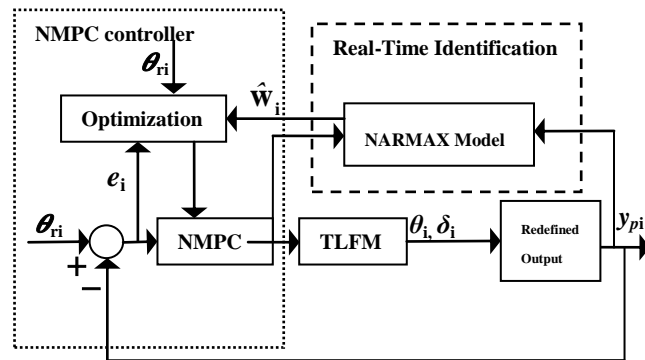


Fig.6.2 Structure of the proposed adaptive NMPC

$$\hat{Y}(k) = \sum_{k=1}^{N_j} \left[ \left( w_{if_{jk}} \psi_{i_{jk}} \right) (\phi(k)) \right] + \sum_{k=1}^{N_{jl}} \left[ \left( w_{ig_{jlk}} \psi_{i_{jlk}} \right) (\phi(k)) \right] \quad (6.6)$$

Eq. (6.6) can be rewritten as

$$\hat{Y}(k) = \sum_{k=1}^{N_j} w_{if_{jk}} \sum_{k=1}^{N_{jl}} w_{ig_{jlk}} \left[ \left( \psi_{i_{jk}} \right) \left( \psi_{i_{jlk}} \right) (\phi(k)) \right] = \hat{w}_{ip} \bar{\psi}_{ip} \quad (6.7)$$

where

$$\begin{aligned} \hat{w}_{ip} &= \sum_{k=1}^{N_j} \hat{w}_{if_{jk}} \sum_{k=1}^{N_{jl}} \hat{w}_{ig_{jlk}} \left[ \left( \psi_{i_{jk}} \right) \left( \psi_{i_{jlk}} \right) (\phi(k)) \right] \\ \bar{\psi}_{ip} &= \sum_{k=1}^{N_j} \sum_{k=1}^{N_{jl}} \left[ \left( \psi_{i_{jk}} \right) \left( \psi_{i_{jlk}} \right) (\phi(k)) \right] \end{aligned}$$

The structure of the proposed NMPC is shown in Fig. 6.2. Using the predicted output in (6.7) along with control input  $U(k)$  and the desired tip trajectory  $R(k)$  for  $i^{\text{th}}$  link, a cost function  $J_2$  is defined as

$$J_2 = \left[ R(k) - \hat{Y}(k) \right]^T K_Q \left[ R(k) - \hat{Y}(k) \right] + U^T(k) K_R U(k) \quad (6.8)$$

where

$$\begin{aligned} R(k) &= \begin{bmatrix} \theta_{r1}(k), \theta_{r1}(k+1), \dots, \theta_{r1}(k+N_p) \\ \theta_{r2}(k), \theta_{r2}(k+1), \dots, \theta_{r2}(k+N_p) \end{bmatrix}, K_Q = \text{diag} \left[ q_1 \dots q_{i_{N_p}} \right] \\ U(k) &= \begin{bmatrix} u_1(k), u_1(k+1), \dots, u_1(k+N_c-1) \\ u_2(k), u_2(k+1), \dots, u_2(k+N_c-1) \end{bmatrix}, K_R = \text{diag} \left[ r_1 \dots r_{i_{N_c}} \right] \end{aligned}$$

The optimal control sequence over the prediction horizon  $N_y$  can be obtained by minimizing the cost function  $J_1$  with respect to the control input  $U(k)$ , This can be achieved by setting  $\frac{\partial J_2}{\partial U} = 0$ .

Taking the derivative of the performance index (6.8) with respect to the control input, one gets

$$\begin{aligned} \frac{\partial J_2}{\partial U} = & \left[ \left( R(k) - \hat{Y}(k) \right)^T K_Q \frac{\partial}{\partial U} \left( R(k) - \hat{Y}(k) \right) \right] \\ & + \left[ \frac{\partial}{\partial U} \left( R(k) - \hat{Y}(k) \right) \right]^T K_Q \\ & + \left[ U^T \frac{\partial}{\partial U} K_R U \right]^T + \left[ \frac{\partial}{\partial U} U \right]^T K_R U \end{aligned} \quad (6.9)$$

Solving for the partial derivatives w.r.t.  $U(k)$  gives

$$\frac{\partial}{\partial U} \left( R(k) - \hat{Y}(k) \right) = -\frac{\partial}{\partial U} \hat{Y}(k) = -K_Y \quad (6.10)$$

$$\frac{\partial}{\partial U} \left( K_R U(k) \right) = K_R \quad (6.11)$$

and

$$\frac{\partial}{\partial U} \left( U(k)^T \right) = I \quad (6.12)$$

Using (6.10), (6.11) and (6.12) in (6.9) gives

$$\frac{\partial J_2}{\partial U} = -2K_Y^T K_Q \left( R(k) - \hat{Y}(k) \right) + 2K_R^T U(k) \quad (6.13)$$

Setting  $\frac{\partial J_2}{\partial U}$  to zero in order to minimize the performance index with respect to  $U(k)$ , and

substituting  $\hat{Y}(k)$  from (6.7) in (6.13), we have

$$-2K_Y^T K_Q \left( R(k) - \hat{w}_{ip} \bar{\psi}_{ip} \right) + 2K_R^T U = 0 \quad (6.14)$$

Hence, the control input  $U(k)$  can be obtained as

$$U(k) = \frac{K_Y^T K_Q \left( R(k) - \hat{w}_{ip} \bar{\psi}_{ip} \right)}{K_R^T} \quad (6.15)$$

Define a constant  $K_U$  as

$$\mathbf{K}_U = \frac{\mathbf{K}_Y^T \mathbf{K}_Q}{\mathbf{K}_R^T} \quad (6.16)$$

and the difference operator  $\Delta=1-q^{-1}$  to calculate the change in control input  $\Delta U(k)$ . Now, using (6.15) in (6.16), (6.14) can be rewritten in terms of  $\Delta U(k)$  as

$$\begin{aligned} \Delta U(k) &= \Delta \mathbf{K}_U \left( \mathbf{R}(k) - \hat{\mathbf{w}}_{ip} \bar{\boldsymbol{\Psi}}_{ip} \right) \\ U(k) &= \Delta \mathbf{K}_U \left( \mathbf{R}(k) - \hat{\mathbf{w}}_{ip} \bar{\boldsymbol{\Psi}}_{ip} \right) + U(k-1) \end{aligned} \quad (6.17)$$

The desired adaptive torque to the actuator of the  $i^{\text{th}}$  joint is given by (6.17). The proposed algorithm of the NMPC is described in Fig.6.3.

<b>Step 1:</b>	Initialize $\lambda_i$ , $\mathbf{K}_R$ and $\mathbf{K}_Q$ in (5.5) and (6.8) for $i^{\text{th}}$ link respectively.
<b>Step 2:</b>	Employ RLS algorithm (5.5)-(5.7) to estimate the NARMAX parameters $\mathbf{w}_i^s$ for $i^{\text{th}}$ link.
<b>Step 3:</b>	Calculate the j-step prediction of the redefined tip position using the NARMAX parameters and measured input and output values $\hat{\mathbf{Y}}(k) = \sum_{k=1}^{N_j} \mathbf{w}_{if_{jk}} \sum_{k=1}^{N_{jl}} \mathbf{w}_{ig_{jlk}} \left[ \left( \boldsymbol{\Psi}_{i_{jk}} \right) \left( \boldsymbol{\Psi}_{i_{jlk}} \right) \left( \phi(k) \right) \right] = \hat{\mathbf{w}}_{ip} \bar{\boldsymbol{\Psi}}_{ip}$
<b>Step 4:</b>	Calculate $\frac{\partial}{\partial \mathbf{u}_i} \left( \mathbf{R}_i(k) - \hat{\mathbf{Y}}(k) \right) = -\frac{\partial}{\partial \mathbf{u}_i} \hat{\mathbf{Y}}(k) = -\mathbf{K}_Y$
<b>Step 5:</b>	Calculate the gain matrix $\mathbf{K}_U = \frac{\mathbf{K}_Y^T \mathbf{K}_Q}{\mathbf{K}_R^T}$
<b>Step 6:</b>	Using the value of $\mathbf{K}_Y$ , the NMPC control law is generated as input to $i^{\text{th}}$ joint for $k^{\text{th}}$ instant till an control signal $U(k)$ is achieved else go to Step 2 $U(k) = \arg \min_{\Delta U(k)} [J_i]$ where $\Delta U(k)$ is the incremental control signal obtained by solving (6.17) as $\Delta U(k) = \Delta \mathbf{K}_U \left( \mathbf{R}(k) - \hat{\mathbf{w}}_{ip} \bar{\boldsymbol{\Psi}}_{ip} \right)$

Fig.6.3 Algorithm for proposed adaptive NMPC

## 6.3 Results and Discussions

The numerical simulation of the NMSTC and RLAC controllers has been performed using MATLAB/SIMULINK®. To validate the tip trajectory tracking performances, the desired trajectory vector for two joints,  $\theta_{di}(t)$   $i=1,2$  are same as (3.16). The physical parameters of the studied TLFM are given in Table 2.2.

### 6.3.1 Simulation results for an initial payload of 0.157 kg

The comparison of performances obtained using NMPC and NMSTC adaptive controllers while carrying a nominal payload of 0.157 kg are shown in Figs 6.4-6.9. Fig.6.4 and Fig.6.5 show the tip deflection trajectories respectively for link-1 and link-2 carrying a nominal payload 0.157 kg. From these figures it is seen that the tip deflection amplitude for link-1 is almost same for both NMPC and NMSTC. But in case of link-2, the maximum tip deflection amplitude is 0.035 mm in case of NMSTC and 0.01 mm for NMPC. The tip deflection is damped out within 4sec before the tip attains the final position.

Fig.6.6 and Fig.6.7 show the tip trajectory tracking error curves for link-1 and link-2 respectively with a nominal payload of 0.157 kg. From Fig.6.6, it is seen that there is a maximum tip tracking error of  $0.03^\circ$  in case of NMSTC for link-1 whereas in case of NMPC it is  $0.02^\circ$ . Link-2 tip trajectory tracking error is shown in Fig.6.7 from which it is seen that maximum tracking error amplitude is  $0.1^\circ$  for NMSTC and  $0.035^\circ$  for NMPC. Fig.6.8 and Fig.6.9 show the control torque profiles generated by NMSTC and NMPC for joint-1 and joint-2 respectively. From Fig.6.8 and Fig.6.9, it seen that the control input generated by the NMSTC becomes 0.858 Nm at 1 sec while on the other hand NMPC generates smooth control input with maximum amplitude of 0.6 Nm at 2 sec and then it goes to zero at 4 sec for link-1.



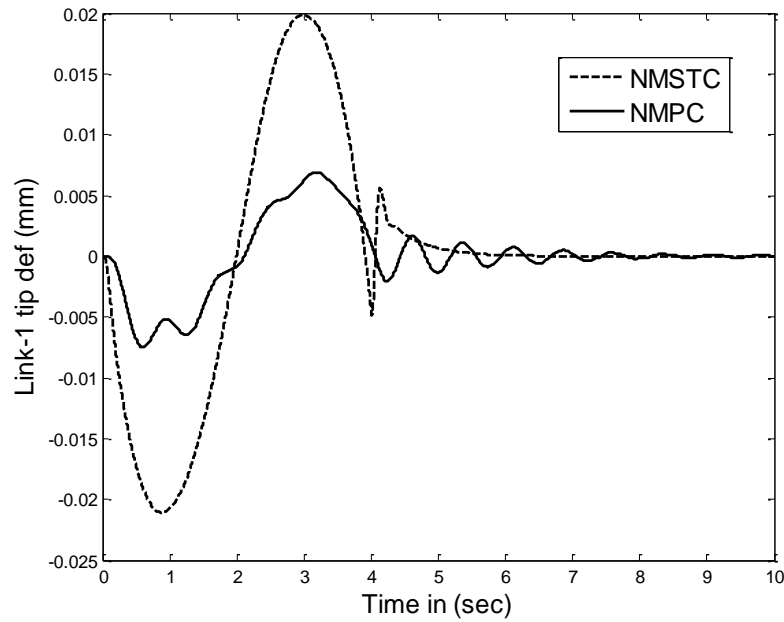


Fig.6.4 Simulation results (time domain) for comparison of link-1 tip deflection performances

(0.157 kg): NMSTC and NMMPC

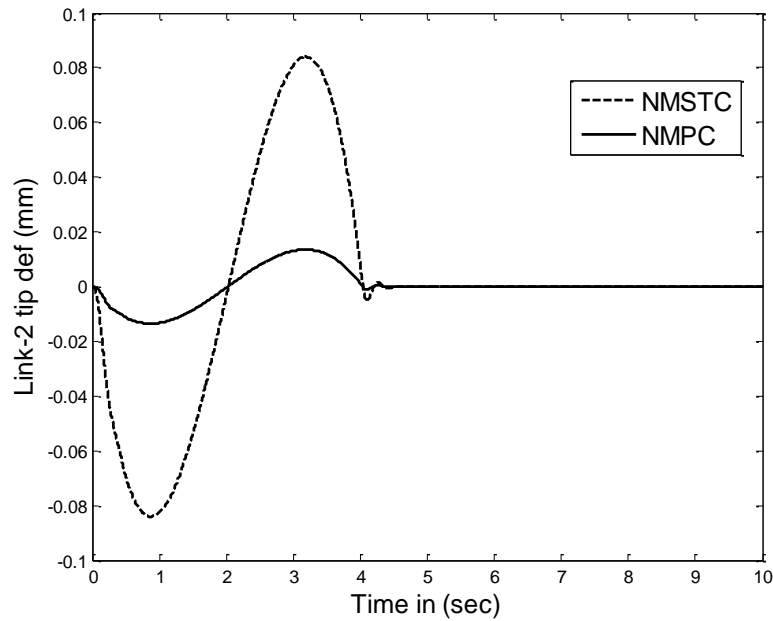


Fig.6.5 Simulation results (time domain) for comparison of link-2 tip deflection performances

(0.157 kg): NMSTC and NMMPC

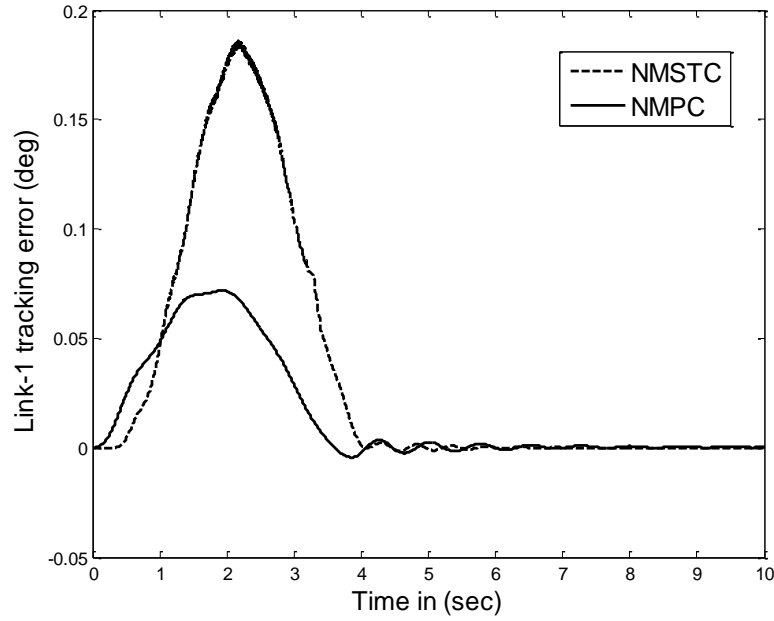


Fig.6.6 Simulation results (time domain) for tip trajectory tracking errors (Link-1) (0.157 kg):

NMSTC and NMPC

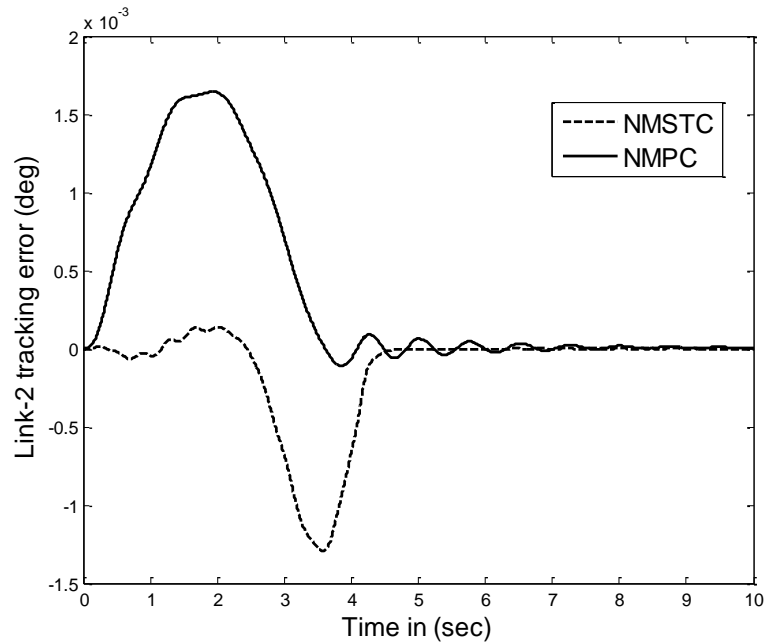


Fig.6.7 Simulation results (time domain) for tip trajectory tracking errors (Link-2) (0.157 kg):

NMSTC and NMPC

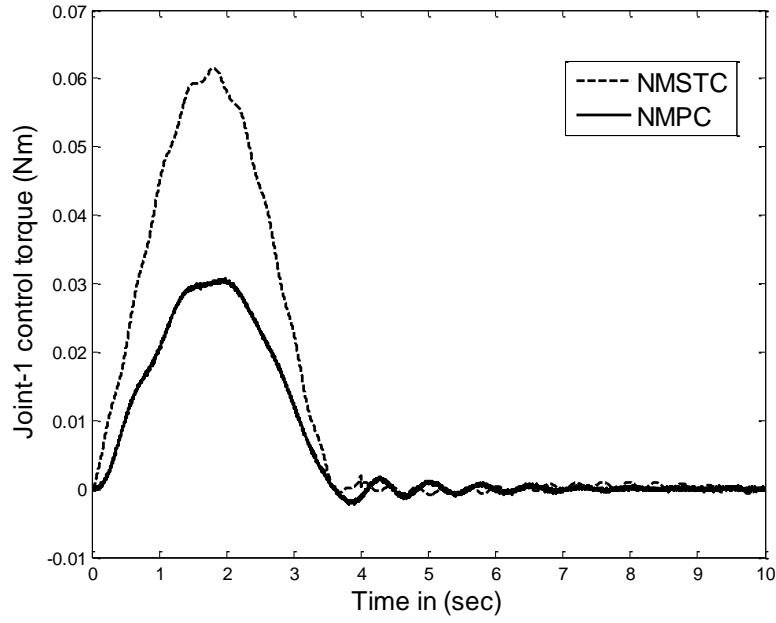


Fig.6.8 Simulation results (time domain) for torque profiles (joint-1) (0.157 kg): NMSTC and NMPC

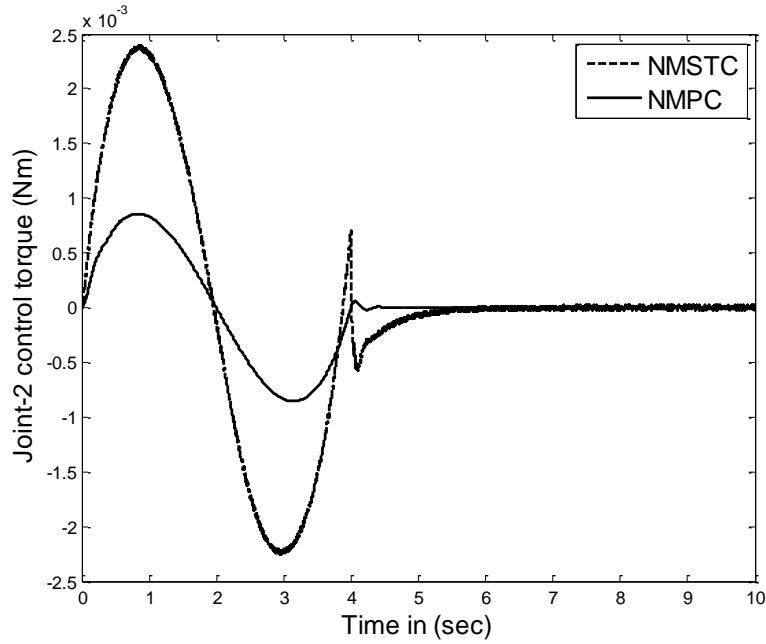


Fig.6.9 Simulation results (time domain) for torque profiles (joint-1) (0.157 kg): NMSTC and NMPC

For link-2, the control input is 1 Nm at 3 sec whereas for NMPC it is 0.5 Nm. Thus, NMPC needs less control excitation for handling a payload of 0.157kg compared to NMSTC. Fig. 6.10 and Fig. 6.11 show the average power of the PSD for NMPC is -10dB and -18dB less compared to NMSTC for link-1 and link-2 respectively. The average power of the tip trajectory error calculated from its PSDs shown in Fig. 6.12 and Fig. 6.13 envisage that there is a reduction in average power of -14dB and -24dB for link-1 and link-2 respectively.

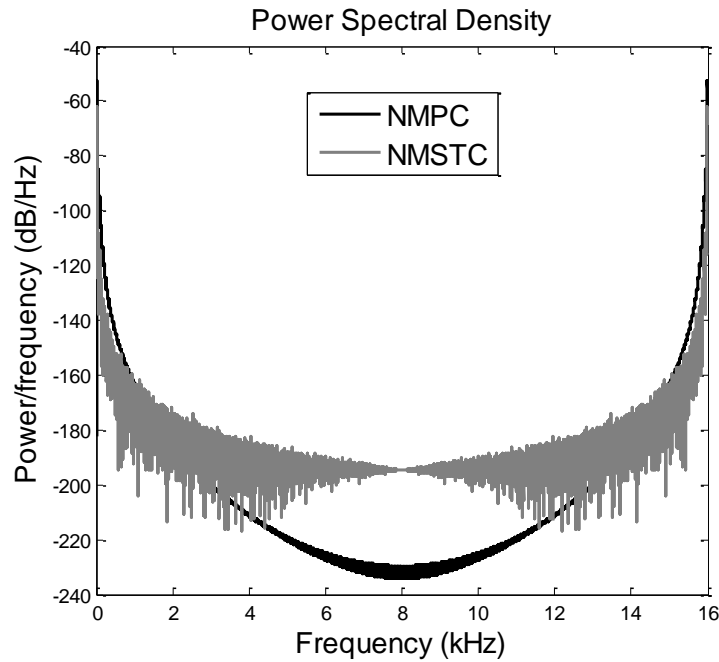


Fig.6.10 Simulation results (frequency domain) for comparison of link-1 tip deflection performances (0.157 kg): NMSTC and NMMP

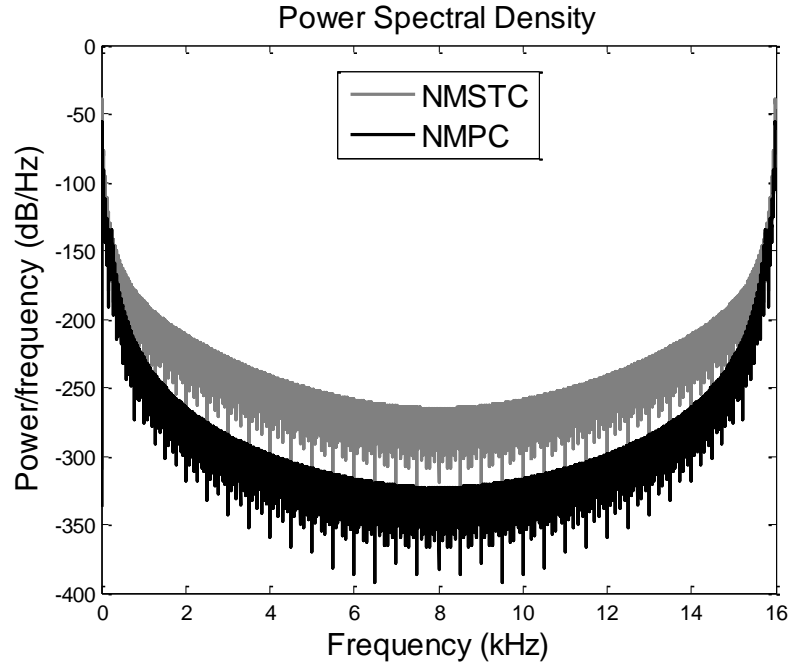


Fig.6.11 Simulation results (frequency domain) for comparison of link-2 tip deflection performances (0.157 kg): NMSTC and NMMPC

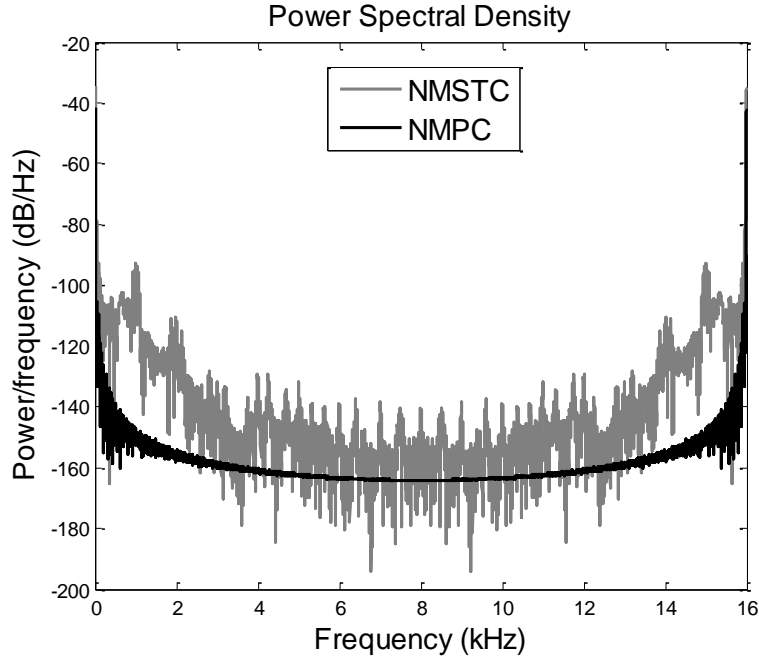


Fig.6.12 Simulation results (frequency domain) for tip trajectory tracking errors (Link-1) (0.157 kg): NMSTC and NMMPC

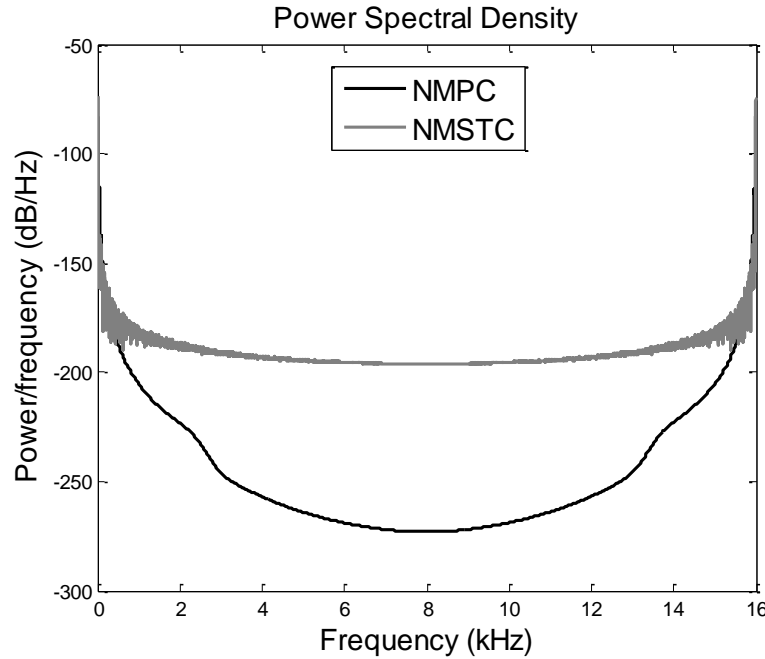


Fig.6.13 Simulation results (frequency domain) for tip trajectory tracking errors (Link-2) (0.157 kg): NMSTC and NMPC

### 6.3.2 Simulation results for an additional payload of 0.3 kg

In order to test the adaptive performance of the proposed NMPC compared to NMSTC an additional payload of 0.3 kg is now attached to the existing initial payload of 0.157 kg making the overall payload 0.457 kg. Performances of NMPC and NMSTC for a 0.457 kg payload are compared in Fig.6.14 to Fig.6.19. Fig 6.14 and Fig 6.15 show the tip deflections profile of the link-1 and link-2 respectively. From Fig 6.14 it is seen that in case of link-1, due to change in payload, the maximum tip deflection amplitude is 0.4 mm and NMSTC takes 8 sec to damp out the deflections whereas NMPC damps out the oscillation within 4 sec with tip deflection is 0.3 mm. Fig.6.16 and Fig.6.17 show the tip trajectory tracking error curves for link-1 and link-2 respectively. From Fig.6.16, it is seen that there is a maximum tracking error of  $0.25^\circ$  in case of NMSTC for link-1. However, the maximum tracking error in case of NMPC is  $0.15^\circ$ . Link-2

tracking error profiles in Fig.6.17 reveal that the tracking errors are  $0.05^\circ$  for NMSTC whereas it is  $0.02^\circ$  in case of the NMPC. Fig.6.18 and Fig.6.19 show the control torque profiles generated by NMSTC and NMPC for joint-1 and joint-2 respectively.

Fig.6.18 it seen that the control input generated by the NMSTC become maximum at 3 sec with amplitude of 0.8 Nm while on other hand in Fig.6.19 for link-2 with additional payload of 0.3 kg the maximum control input is 1.2 Nm for NMSTC while for NMPC it is 0.2 Nm only. Thus, NMPC needs show better performance with a payload of 0.157kg compared to NMSTC. Fig. 6.20 and Fig. 6.21 show the average power of the PSD for NMPC is -12dB and -28dB less compared to NMSTC for link-1and link-2 respectively. The average power of the tip trajectory error calculated from its PSDs (Fig. 6.22 and Fig. 6.23 respectively). It is seen that there is a reduction in average power of -24dB and -44dB for link-1 and link-2 respectively.

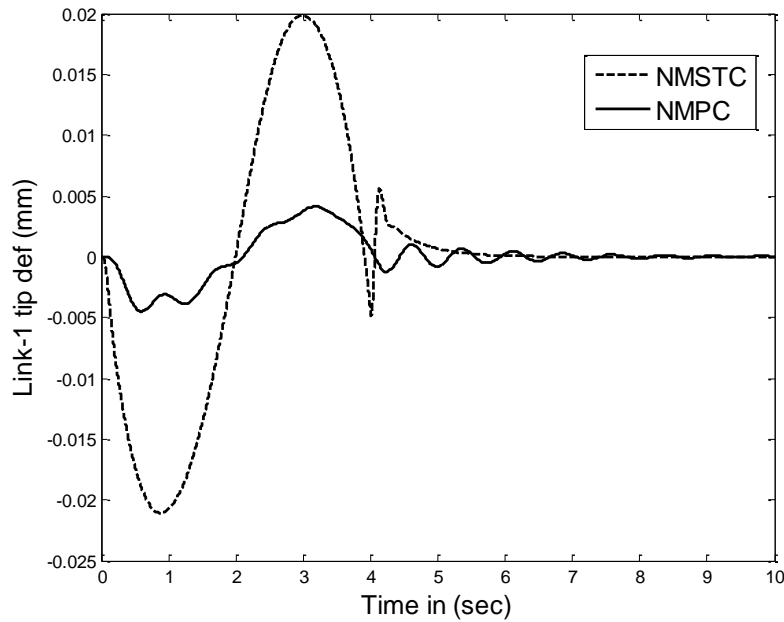


Fig.6.14Simulation results (time domain) for comparison of link-1 tip deflection performances  
(0.457 kg): NMSTC and NMMPC

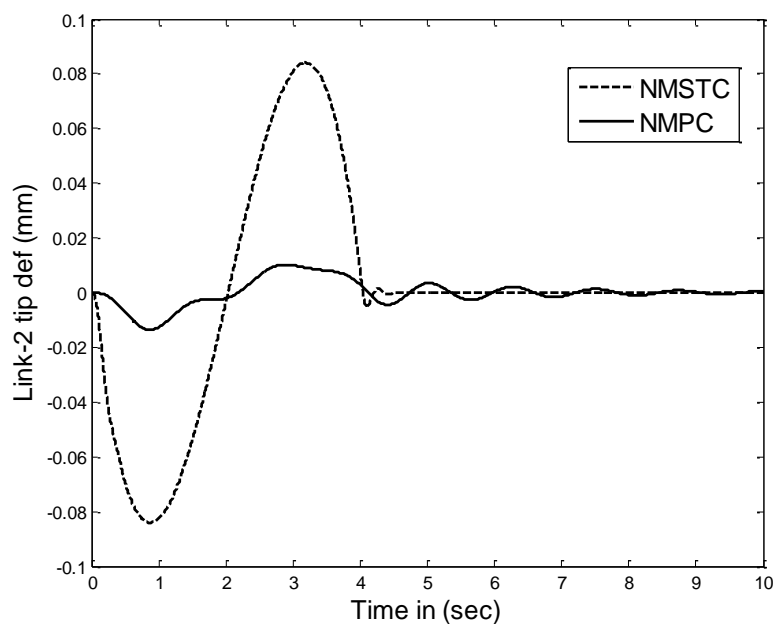


Fig.6.15 Simulation results (time domain) for comparison of link-2 tip deflection performances

(0.457 kg): NMSTC and NMPC

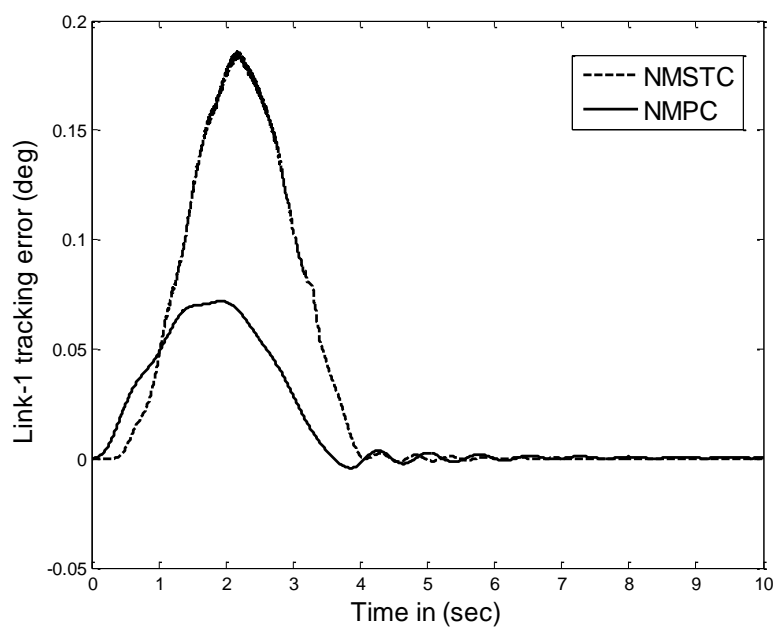




Fig.6.16 Simulation results (time domain) for tip trajectory tracking errors (Link-1) (0.457 kg):

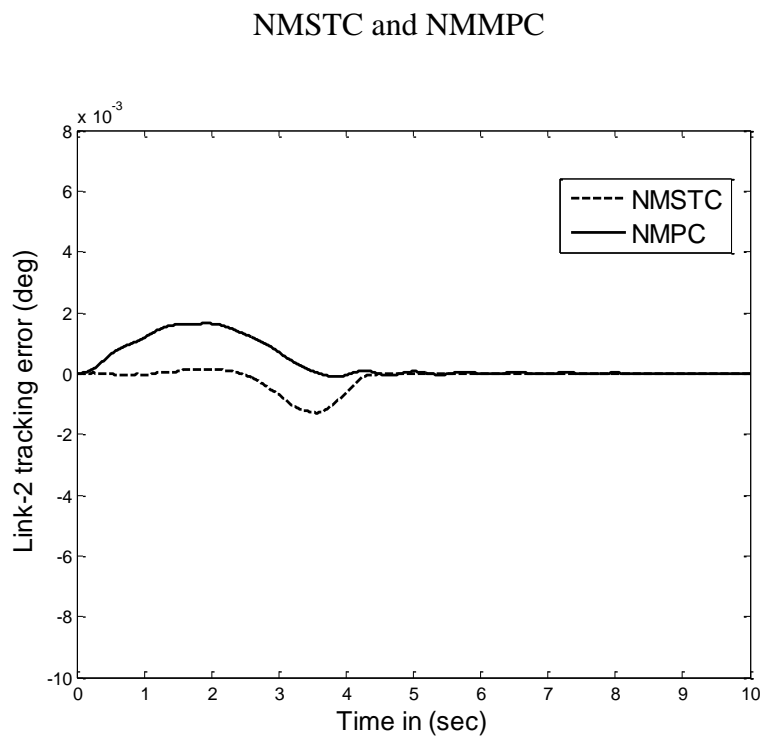


Fig.6.17 Simulation results (time domain) for tip trajectory tracking errors (Link-2) (0.457 kg):

NMSTC and NMPC

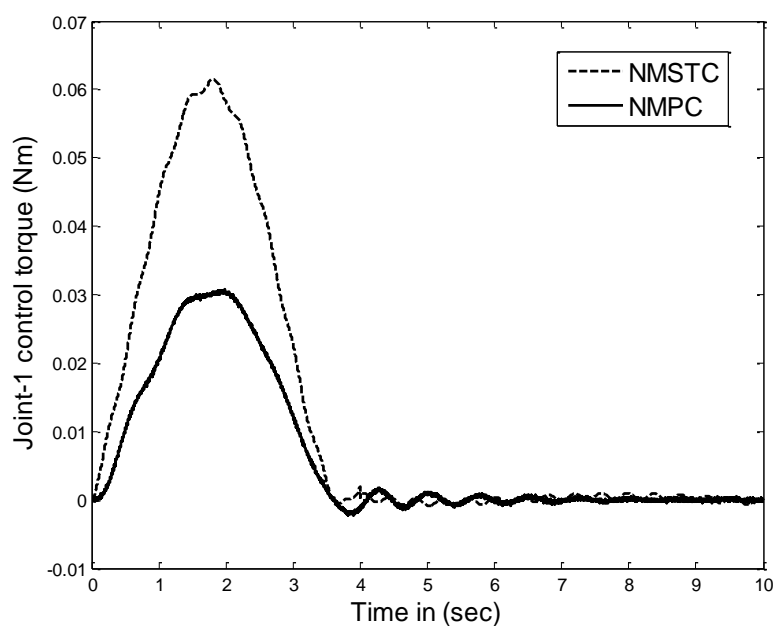


Fig.6.18 Simulation results (time domain) for torque profiles (joint-1) (0.457 kg): NMSTC and

NMPC

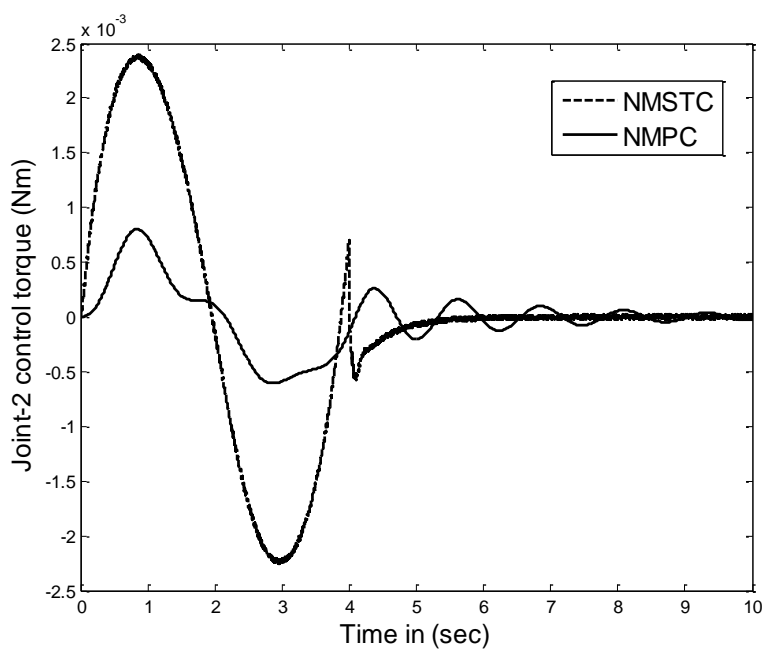


Fig.6.19 Simulation results (time domain) for torque profiles (joint-2) (0.457 kg): NMSTC and NMMPC

Table 6.1: Comparison of simulation results for the controllers (NMPC and NMSTC)

Controller Schemes	Payload (Kg)	Link	Overshoot (%)	Settling-Time ( $t_s$ ) in sec	Reference Figure
NMPC	0.157	Link-1	<b>0.25</b>	<b>4.0</b>	Fig.6.6
		Link-2	<b>0.65</b>	<b>4.0</b>	Fig.6.7
	0.457	Link-1	<b>0.5</b>	<b>4.0</b>	Fig.6.12
		Link-2	<b>0.75</b>	<b>4.5</b>	Fig.6.13
NMSTC	0.157	Link-1	2	4.0	Fig.6.6
		Link-2	2.5	4.0	Fig.6.7
	0.457	Link-1	2.5	6.0	Fig.6.12
		Link-2	3	6.5	Fig.6.13

The simulation results for NMSTC and NMPC under 0.157 kg of nominal payload and with additional payload of 0.3 kg is summarized in Table 6.1. The comparison of performance indices such as settling time and maximum overshoot for tip trajectory tracking for NMSTC and NMPC were compared. From Table 6.1 it is observed that NMPC yields a 0.25% maximum overshoot for link-1 and 0.65 % for link-2 under a nominal payload of 0.157 kg and in case of NMSTC the maximum overshoot percentage is 2% and 2.5% respectively for link-1 and link-2. When an additional payload of 0.3 kg is attached to tip, the maximum overshoots in case of NMSTC are 2% and 2.5% respectively for link-1 and link-2. But the NMPC yield 0.5% and 0.75% overshoots for link-1 and link-2.

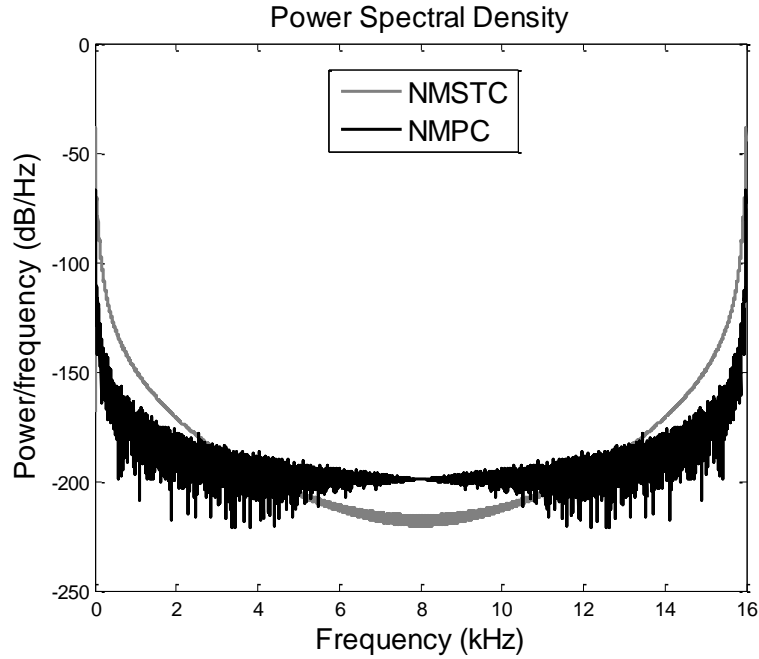


Fig.6.20 Simulation results (frequency domain) for comparison of link-1 tip deflection performances (0.457 kg): NMSTC and NMMPC

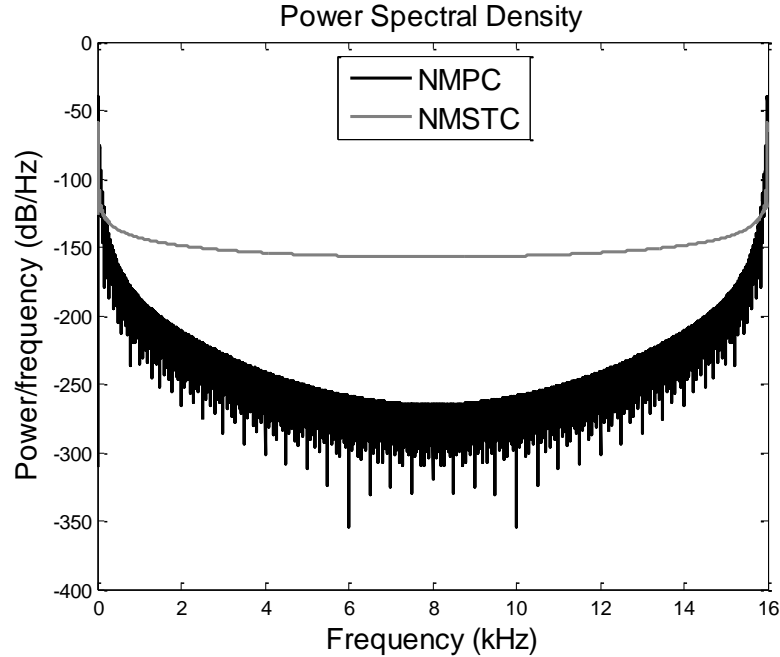


Fig.6.21 Simulation results (frequency domain) for comparison of link-2 tip deflection performances (0.457 kg): NMSTC and NMMPC

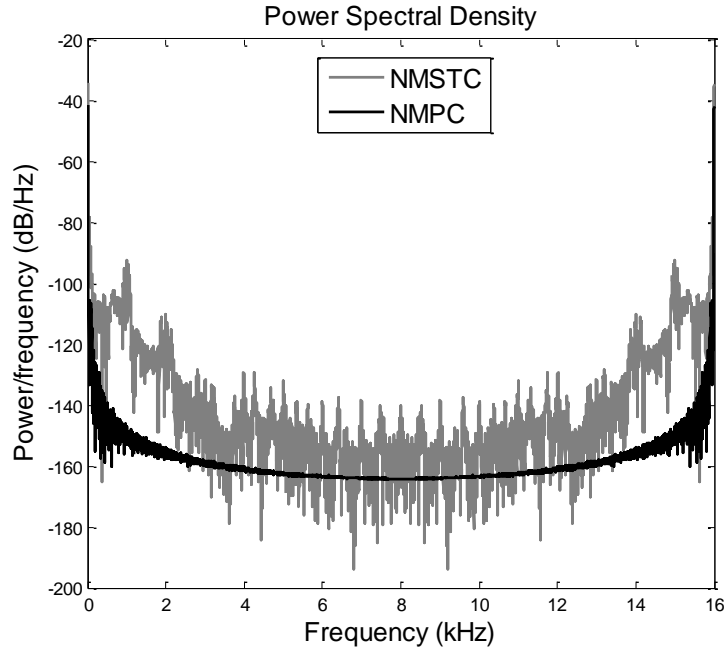


Fig.6.22 Simulation results (frequency domain) for tip trajectory tracking errors (Link-1) (0.457

kg): NMSTC and NMPC

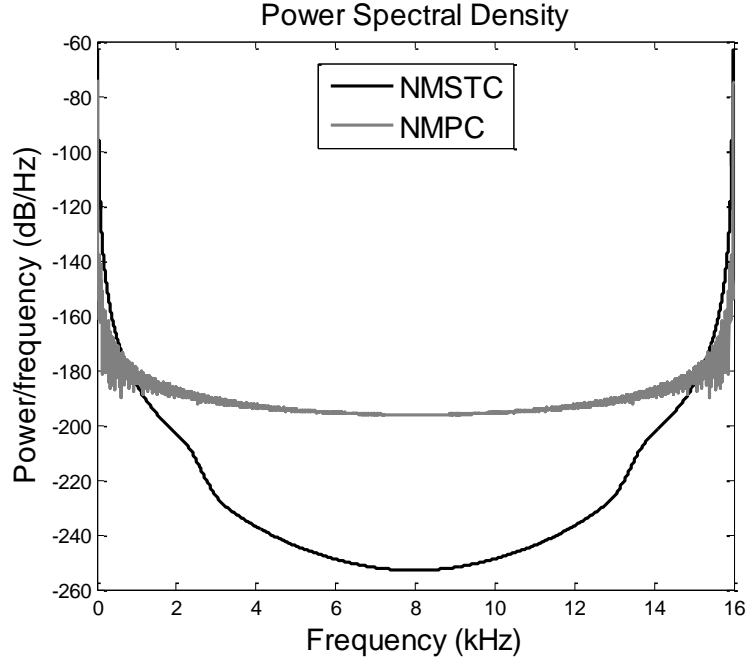


Fig.6.23 Simulation results (frequency domain) for tip trajectory tracking errors (Link-2) (0.457

kg): NMSTC and NMPC

### 6.3.3 Experimental results for an initial payload of 0.157 kg

Experimental results under a nominal payload of 0.157 kg are shown in Fig.6.24 to Fig.6.29. The experimental results showing the tip deflection obtained by NMPC and NMSTC with a nominal payload of 0.157 kg are shown in Fig.6.24 and Fig. 6.25 for link-1 and link-2 respectively. From Fig.6.24 it is observed that maximum tip deflection of 0.25 mm in case of NMSTC while the maximum deflection is 0.05 mm is seen in case of NMPC. Fig.6.25 shows that the maximum tip deflection amplitude is 0.1 mm for link-2 in case of NMPC whereas in case of NMSTC it is 0.15 mm. Fig.6.26 and Fig.6.27 shows the tip trajectory tracking error curves for link-1 and link-2 respectively. From Fig.6.26, it is seen that there is a tracking error of  $0.015^\circ$  in case of NMSTC for link-1. However, the tracking error in case of NMPC is  $0.005^\circ$ . Link-2 tracking error profiles in Fig.6.27 reveal that the tracking errors is  $0.6^\circ$  for NMSTC whereas it is  $0.1^\circ$  in case of the NMPC. Fig.6.28 and Fig.6.29 show the control torque profiles generated by NMSTC and NMPC for joint-1 and joint-2 respectively. The maximum value of control torque is 0.5 Nm and reduces to almost zero after 2 sec in case of NMPC, whereas for NMSTC the maximum value is 0.6 Nm and it is maintained till the tip attains its final position, consequently reducing to zero after 4 sec. On the other hand, the torque profiles for joint-2, the NMPC attains 1.5 Nm and reduces to almost zero after 4 sec whereas in case of NMSTC the maximum input control torque is 2 Nm initially, then rises to about 2.5 Nm and it is maintained till the tip attains its final position, consequently reducing to zero after 4 sec. Fig. 6.30 and Fig. 6.31 show the average power of the PSD for NMPC is -2.6dB and -1.8dB less compared to NMSTC for link-1 and link-2 respectively. There is a reduction in average power of -4dB and -3dB for tracking errors of link-1 and link-2 respectively (Fig. 6.32 and Fig. 6.33).

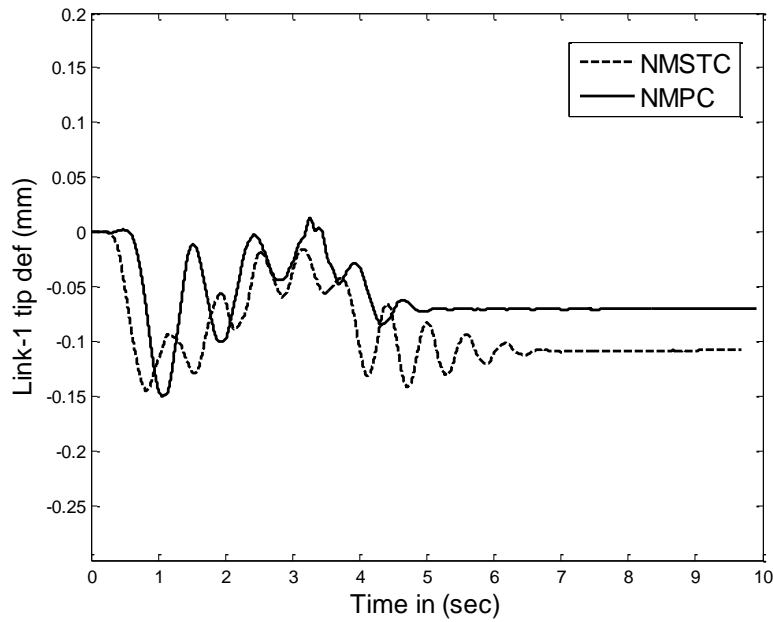


Fig.6.24 Experimental results (time domain) for comparison of link-1 tip deflection performances (0.157 kg): NMSTC and NMPC

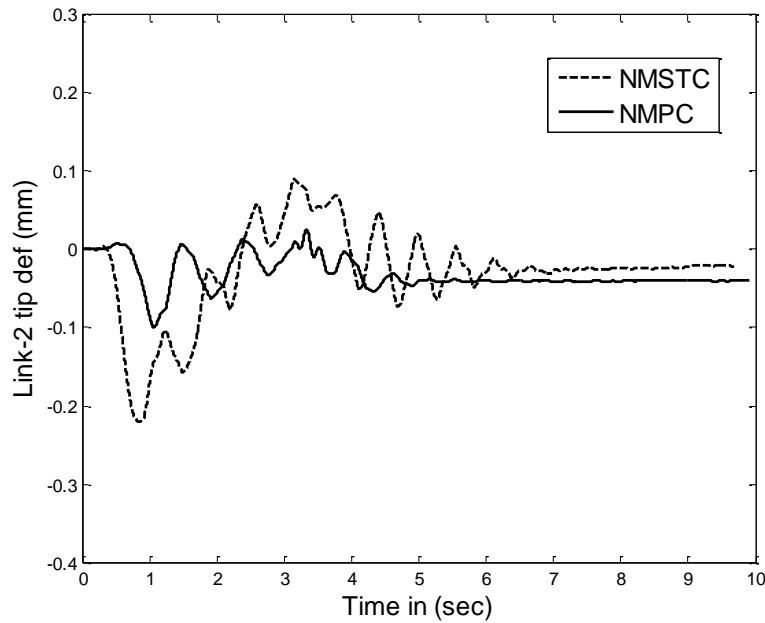


Fig.6.25 Experimental results (time domain) for comparison of link-2 tip deflection performances (0.157 kg): NMSTC and NMPC

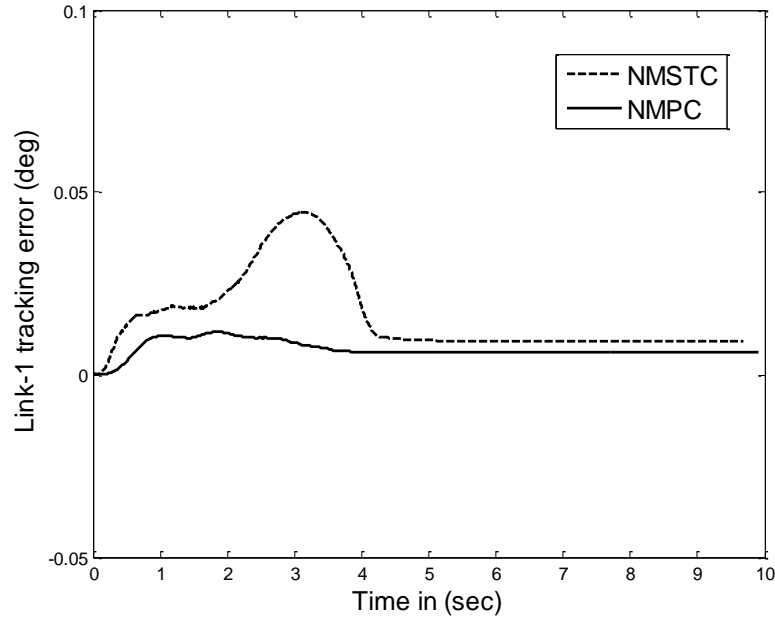


Fig.6.26 Experimental results (time domain) for tip trajectory tracking errors (Link-1) (0.157 kg): NMSTC and NMPC

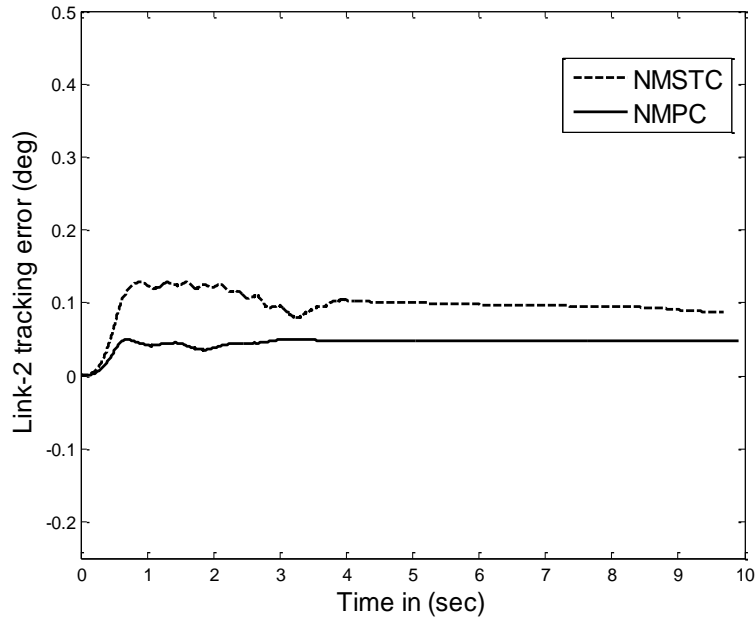


Fig.6.27 Experimental results (time domain) for tip trajectory tracking errors (Link-2) (0.157 kg): NMSTC and NMPC



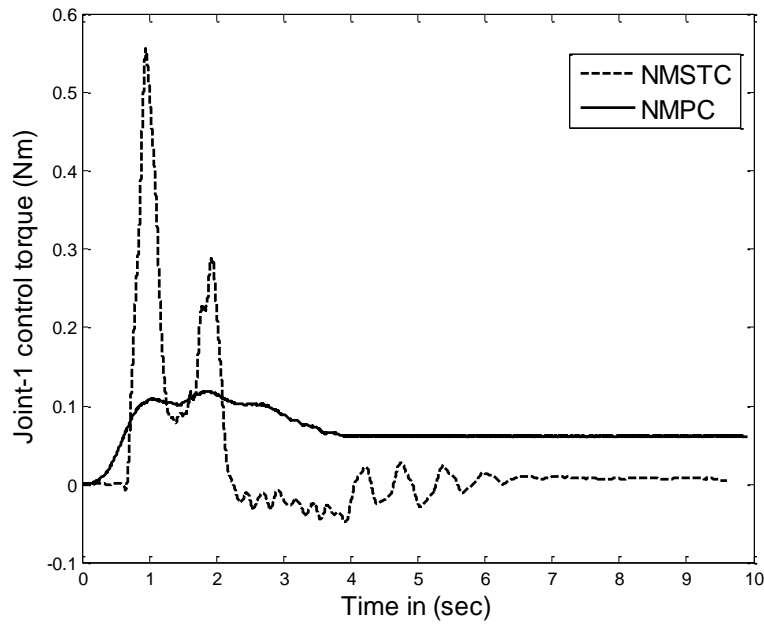


Fig.6.28 Experimental results (time domain) for torque profiles (joint-1) (0.157 kg): NMSTC and NMMPC

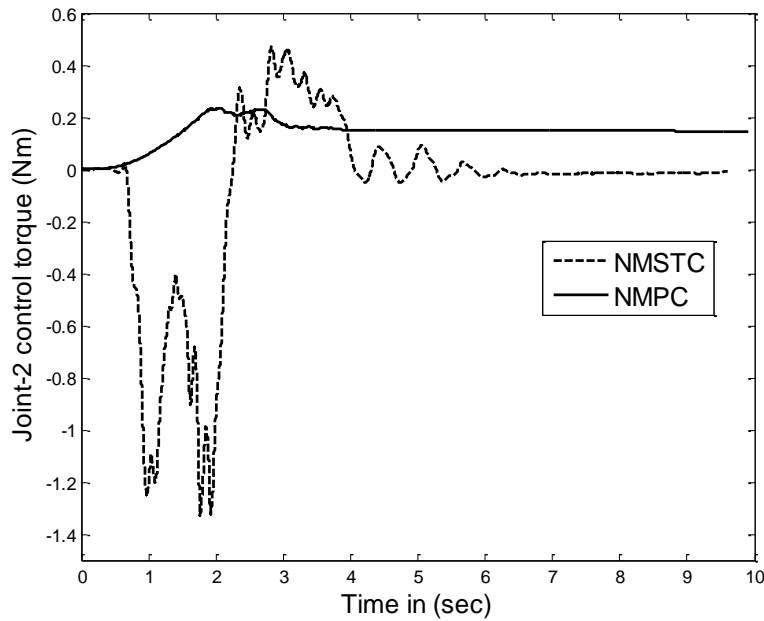


Fig.6.29 Experimental results (time domain) for torque profiles (joint-2) (0.157 kg): NMSTC and NMMPC

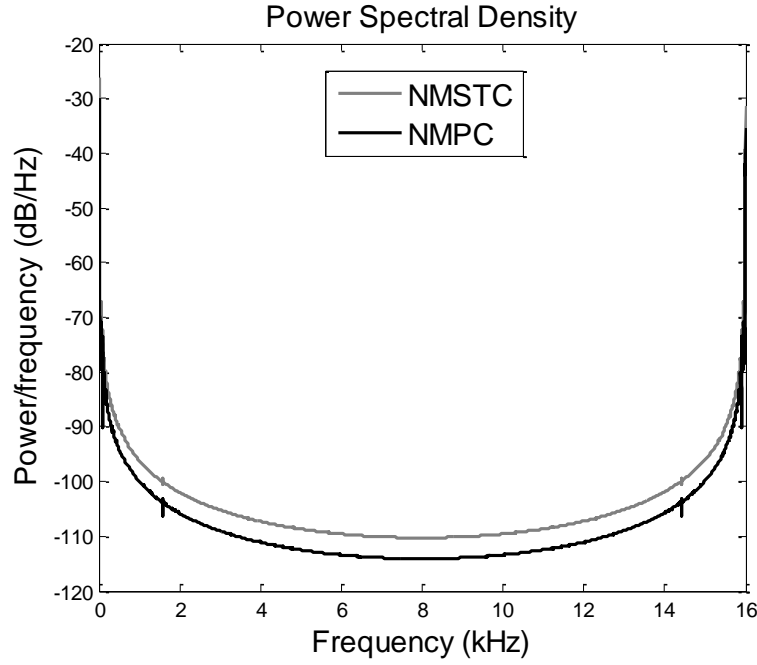


Fig.6.30 Experimental results (frequency domain) for comparison of link-1 tip deflection performances (0.157 kg): NMSTC and NMMP

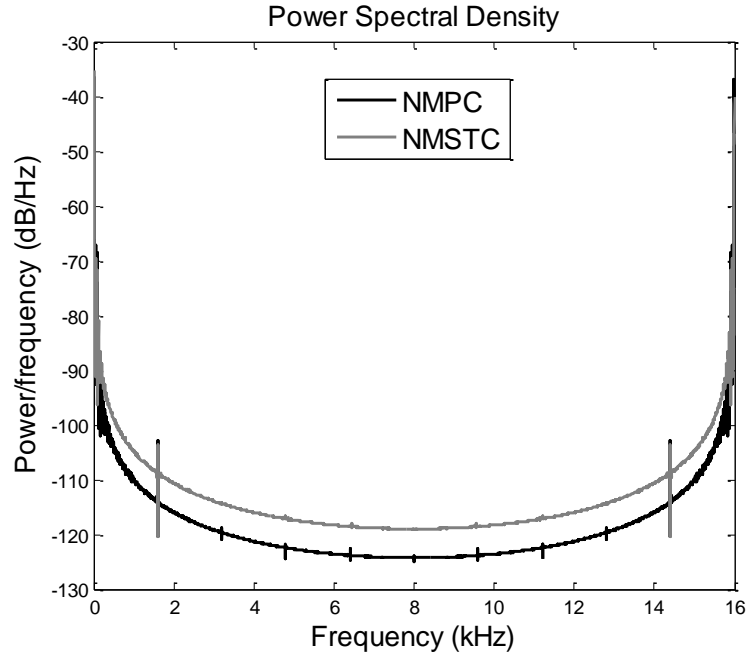


Fig.6.31 Experimental results (frequency domain) for comparison of link-2 tip deflection performances (0.157 kg): NMSTC and NMMP

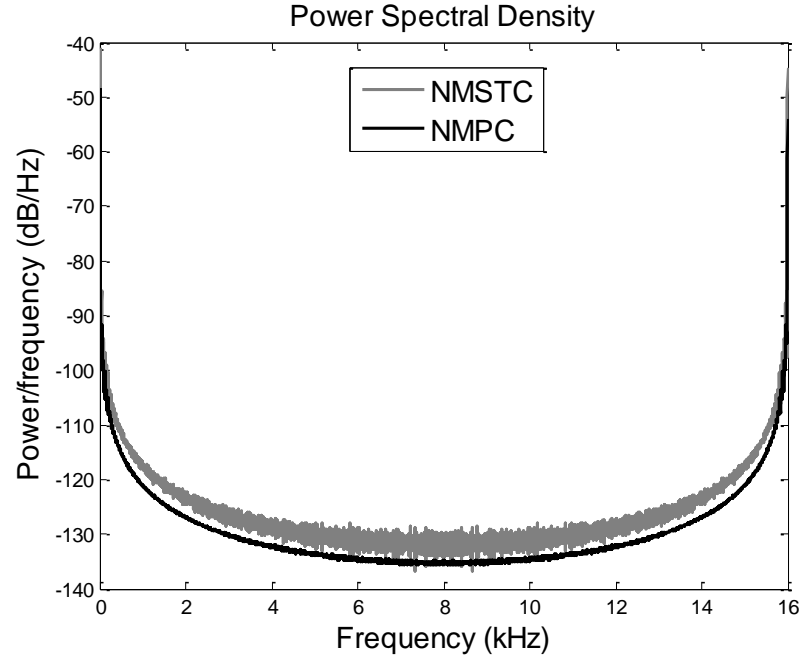


Fig.6.32 Experimental results (frequency domain) for tip trajectory tracking errors (Link-1)

(0.157 kg): NMSTC and NMPC

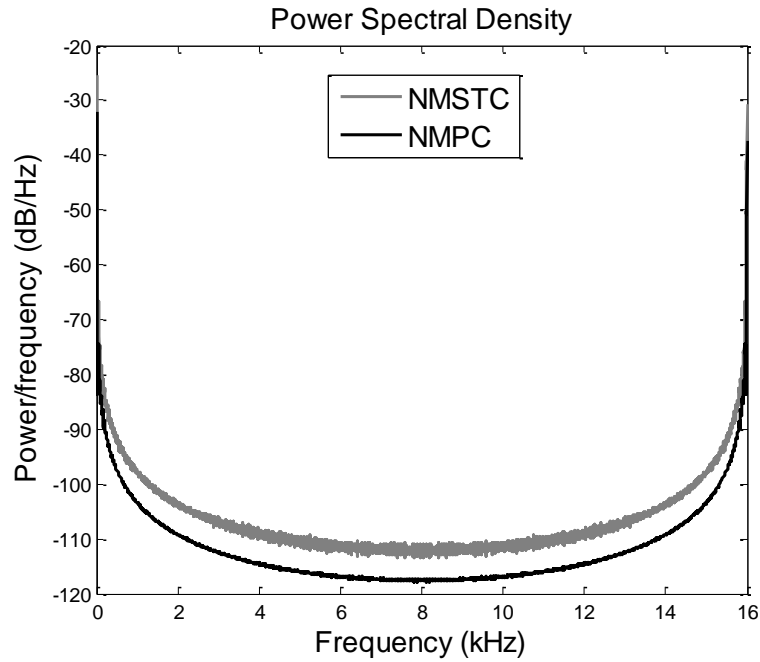


Fig.6.33 Experimental results (frequency domain) for tip trajectory tracking errors (Link-2)

(0.157 kg): NMSTC and NMPC

#### 6.3.4 Experimental results for an additional payload of 0.3 kg

An additional payload of 0.3 kg was added making the overall payload to 0.457 kg. Performances of NMPC and NMSTC with 0.457 kg payload were compared in Fig.6.34 to Fig.6.39. Fig.6.34 and Fig.6.35 show the tip deflections profile of the link-1 and link-2 respectively. From Fig.6.34 it is revealed that in case of link-1, due to change in payload of 0.3 kg, the maximum tip deflection amplitude becomes 0.25 mm and it takes 8 sec to damp out the tip deflection by the NMSTC, whereas NMPC damps out the tip deflection within 5 sec and the maximum tip deflection amplitude is 0.15 mm. Compensating of tip deflection performances for link-2 by the two controllers is shown in Fig.6.35. This figure depicts that NMSTC yields a maximum deflection up to 0.3 mm and damps out tip deflection at 8 sec whereas NMPC yields maximum deflection of 0.15mm and takes 6 sec to damp out link-2 tip deflection. Fig.6.36 and Fig.6.37 show the tip trajectory tracking error curves for link-1 and link-2 respectively. From Fig.6.36, it is seen that there is a maximum tracking error of  $0.15^\circ$  in case of NMSTC for link-1, however, the maximum tracking error in case of NMPC is  $0.05^\circ$  while carrying an additional payload of 0.3 kg. Link-2 tracking error profiles are shown in Fig.6.37 reveal that the maximum tracking error is  $0.5^\circ$  for NMSTC whereas it is  $0.2^\circ$  in case of the NMPC. Fig.6.38 and Fig.6.39 show the control torque profiles generated by NMSTC and NMPC for joint-1 and joint-2 respectively. From Fig.6.26 and Fig.6.27 it seen that the maximum control input generated by NMSTC is 0.6 Nm and 1.5 Nm respectively, whereas the NMPC generate smooth control moves with maximum control input of 0.15 Nm and 0.1 Nm for both link-1 and link-2 respectively. Thus, it can be conclude from Fig.6.38 and Fig.6.39 that NMPC needs less control excitation to control tip position and suppress the tip deflection with an additional payload of 0.3 kg compared to NMSTC.

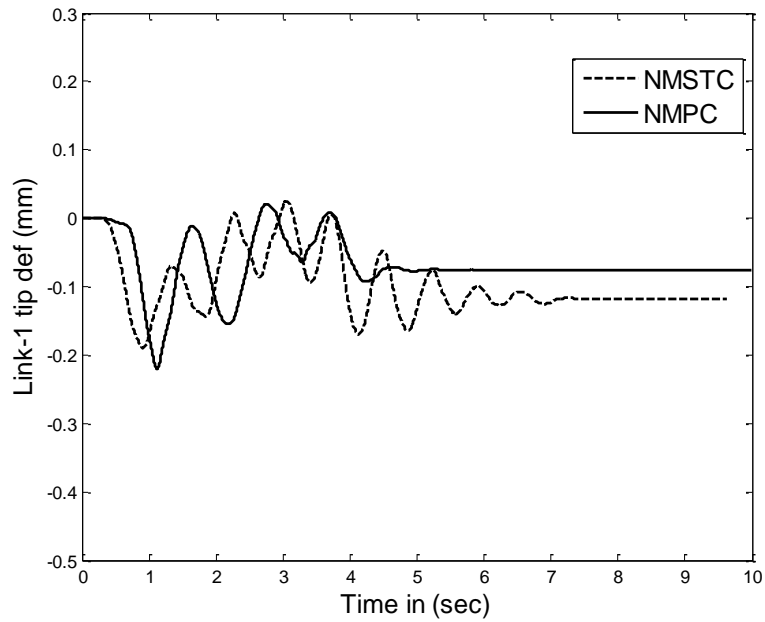


Fig.6.34 Experimental results (time domain) for comparison of link-1 tip deflection performances (0.457 kg): NMSTC and NMMPC

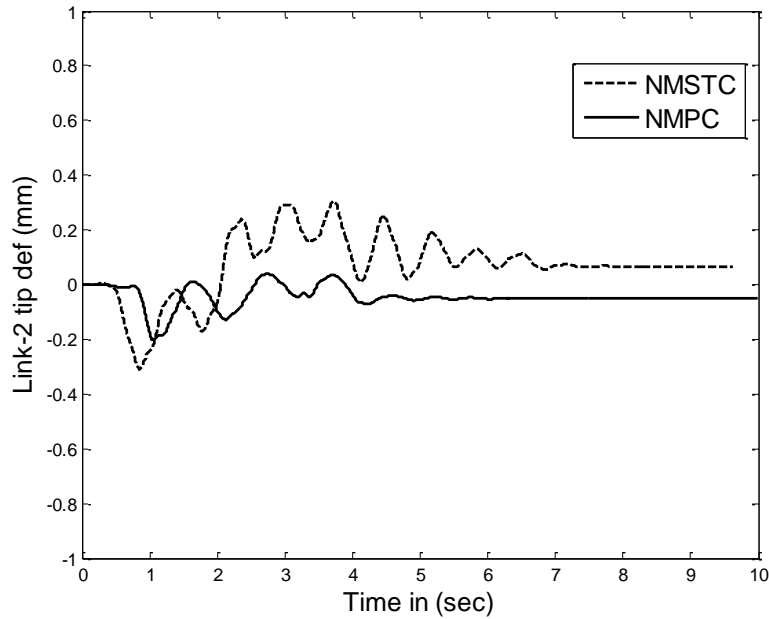


Fig.6.35 Experimental results (time domain) for comparison of link-2 tip deflection performances (0.457 kg): NMSTC and NMMPC

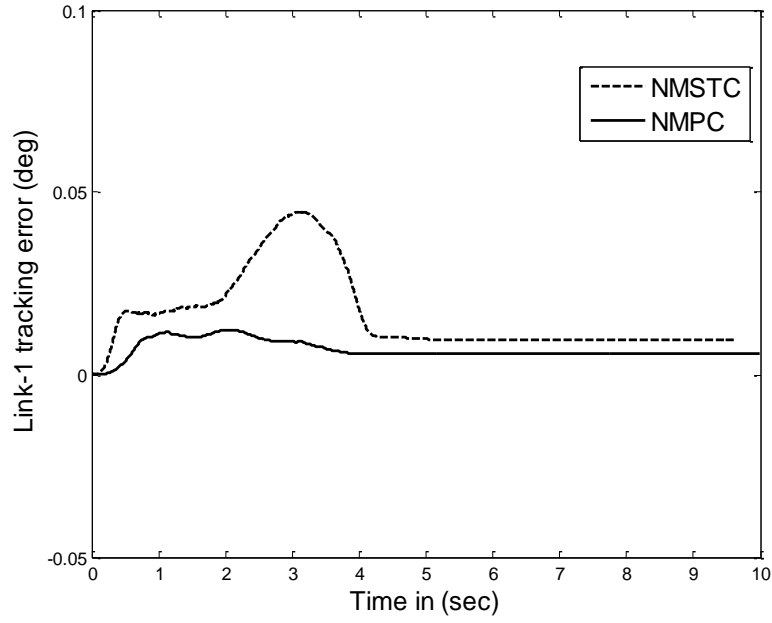


Fig.6.36 Experimental results (time domain) for tip trajectory tracking errors (Link-1) (0.457 kg): NMSTC and NMPC

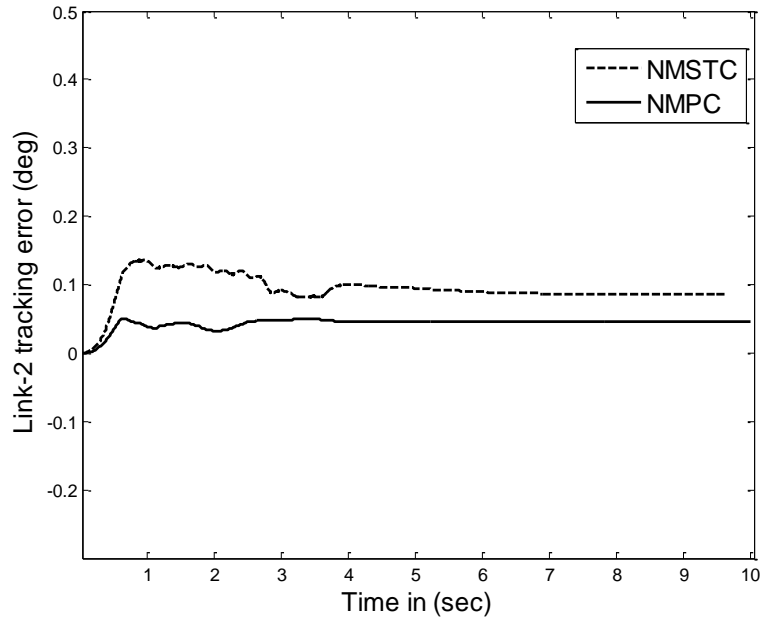


Fig.6.37 Experimental results (time domain) for tip trajectory tracking errors (Link-2) (0.457 kg): NMSTC and NMPC

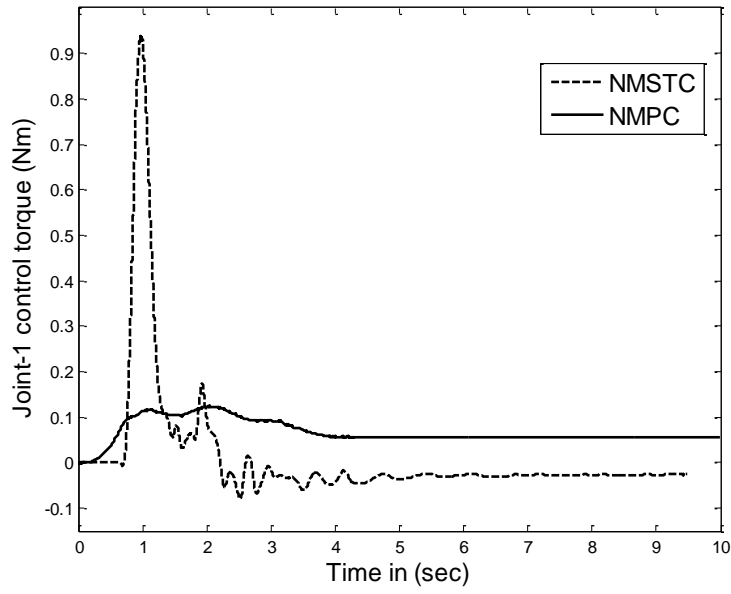


Fig.6.38 Experimental results (time domain) for torque profiles (joint-1) (0.457 kg): NMSTC and NMMPC

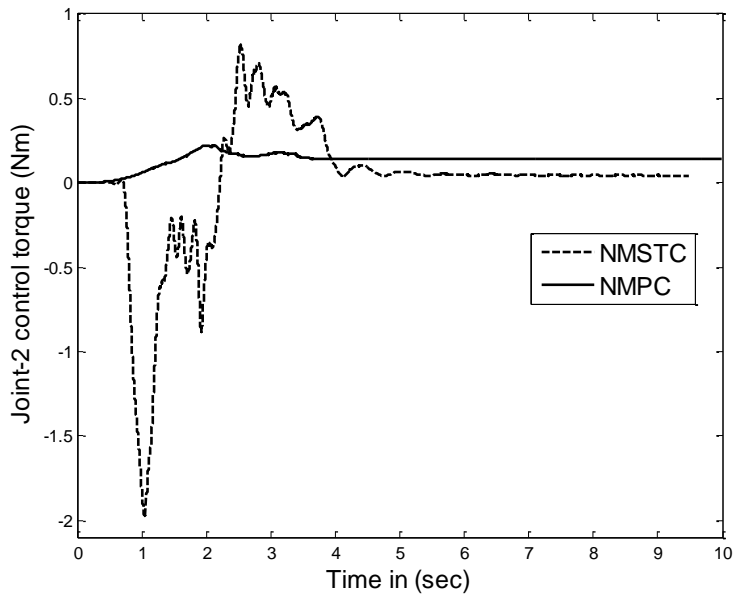


Fig.6.39 Experimental results (time domain) for torque profiles (joint-2) (0.457 kg): NMSTC and NMMPC

Fig. 6.40 and Fig. 6.41 show the average power of the PSD for NMPC is -2.6dB and -1.8dB less compared to NMSTC for link-1 and link-2 respectively. There is a reduction in average power of -4dB and -3dB for tracking errors of link-1 and link-2 respectively (Fig. 6.42 and Fig. 6.43). Table 6.2 shows the comparisons of the experiment results for NMSTC and RLAC under 0.157 kg of nominal payload and additional payload of 0.3 kg. From Table 6.2 it is observed that NMPC yields a 0.15% maximum overshoot for link-1 and 0.5 % for link-2 under a nominal payload of 0.157 kg and in case of NMSTC the maximum overshoot percentage is 0.5% and 1% respectively for link-1 and link-2. When an additional payload of 0.3 kg is attached to tip, the maximum overshoots in case of NMSTC are 1% and 1.5% respectively for link-1 and link-2. But the NMPC yield 0.5% and 0.6% overshoots for link-1 and link-2.

Table 6.2: Comparison of experimental results for the controllers (NMPC and NMSTC)

Controller Schemes	Payload (Kg)	Link	Overshoot (%)	Settling-Time (t <sub>s</sub> )	Reference Figure
NMPC	0.157	Link-1	<b>0.15</b>	<b>4.0</b>	Fig.6.18
		Link-2	<b>0.5</b>	<b>4.0</b>	Fig.6.19
	0.457	Link-1	<b>0.5</b>	<b>4.0</b>	Fig.6.24
		Link-2	<b>0.6</b>	<b>4.5</b>	Fig.6.25
NMSTC	0.157	Link-1	0.5	4.2	Fig.5.19
		Link-2	1	5.0	Fig.5.20
	0.457	Link-1	1	4.5	Fig.5.25
		Link-2	1.5	4.6	Fig.5.26



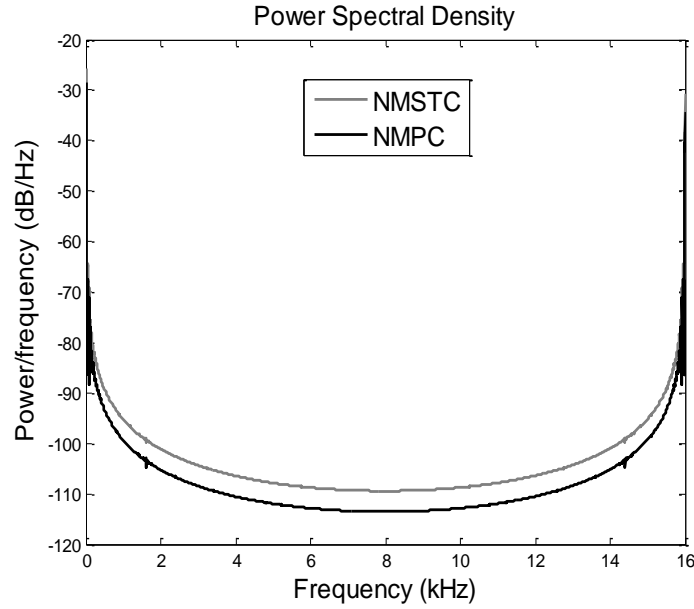


Fig.6.40 Experimental results (frequency domain) for comparison of link-1 tip deflection performances (0.457 kg): NMSTC and NMMPC

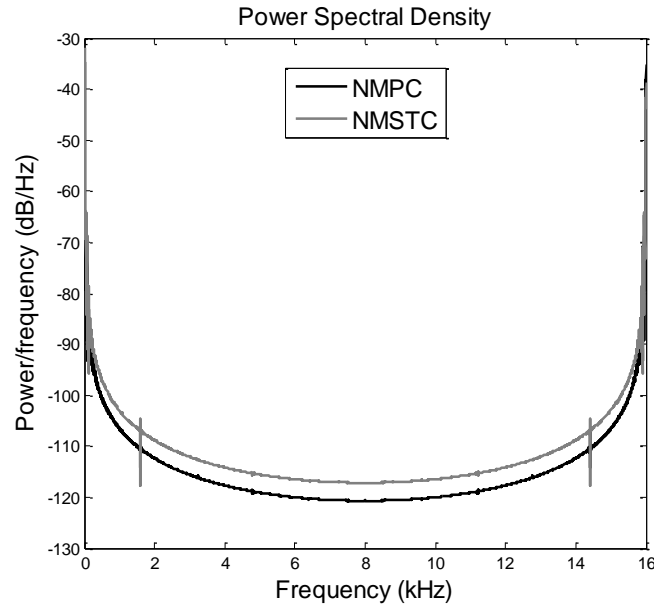


Fig.6.41 Experimental results (frequency domain) for comparison of link-2 tip deflection performances (0.457 kg): NMSTC and NMMPC

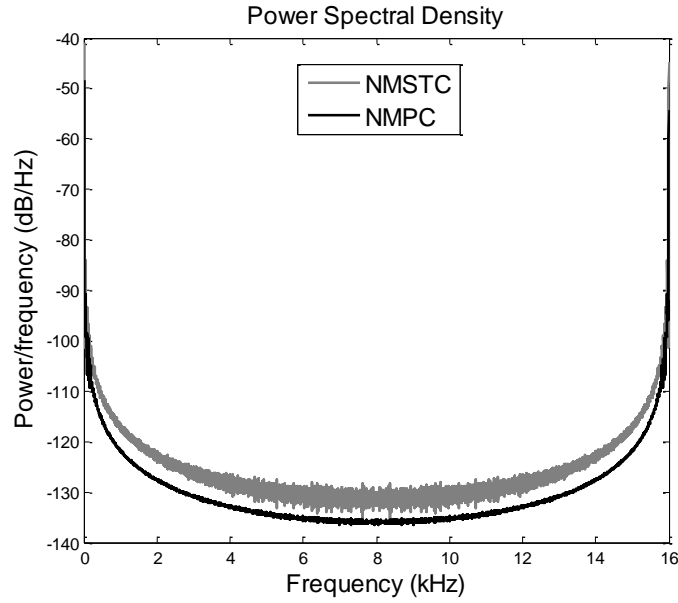


Fig.6.42 Experimental results (frequency domain) for tip trajectory tracking errors (Link-1)  
(0.457 kg): NMSTC and NMPC

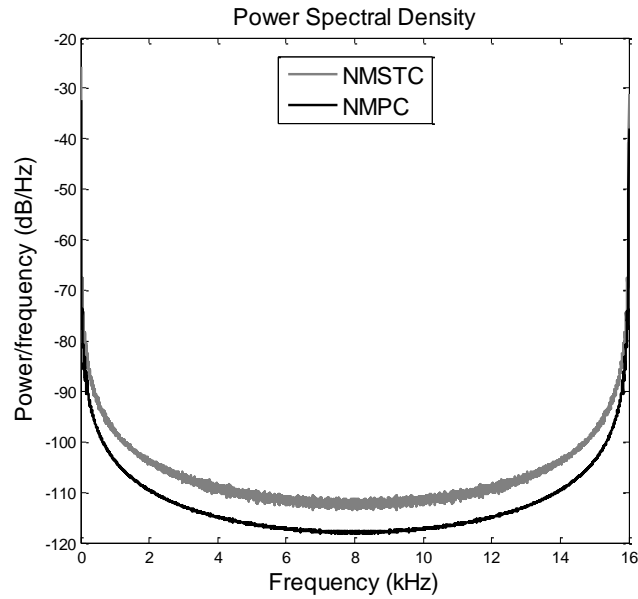


Fig.6.43 Experimental results (frequency domain) for tip trajectory tracking errors (Link-2)  
(0.457 kg): NMSTC and NMPC

## 6.4 Chapter Summary

The *Chapter* has presented a new nonlinear adaptive model predictive controller (NMPC) to control tip trajectory and suppression of tip deflection for a two-link flexible manipulator while handling variable payloads. The design of the proposed nonlinear adaptive model predictive controller is based on the *on-line* identified NARMAX model. Both a self-tuning controller (NMSTC) and the proposed NMPC have been applied successfully to a flexible robot set-up in the laboratory. From the simulation and experimental results it is established that the proposed NMPC generates appropriate adaptive torque to control tip trajectory tracking and suppression of tip deflection for the TLFM compared to NMSTC, when the manipulator is asked to handle a variable payload. The reason for its superiority is because NMPC generates optimal control sequence by optimum tuning of its control parameters in real time adaptively.

## Chapter 7

### Conclusions and Suggestions for Future Work

There has been great deal of interest for researchers in adaptive control of FLMs. In spite of advances from a control design perspective, this issue will remain an open research area in the years to come. As discussed previously that several factors contribute to the complexity of tip position tracking of a FLM under unknown payload mass. The distributed link flexibility, which makes the system under-actuated and infinite dimensional are the major factors. This thesis focused on the development of new adaptive control strategies to control the tip position and while simultaneously suppressing its tip deflection when subjected to unknown payloads. The adaptive control strategies were implemented and tested on an experimental physical two-link flexible manipulator setup and to the developed mathematical model. This *Chapter* concludes the

thesis and some future scope of extension of the work described in the thesis are also highlighted.

## 7.1 Summary of the Thesis Work

This thesis has mainly investigated on development of new adaptive control schemes to control the tip trajectory while quickly suppressing its deflection when subjected to handle unknown payloads for a two-link flexible manipulator (TLFM). A number of new adaptive control strategies namely direct adaptive control (DAC), fuzzy learning based adaptive control (FLAC), reinforcement learning based adaptive control (RLAC), NARMAX model based self-tuning control (NMSTC) and NARMAX model based nonlinear adaptive model predictive control (NMPC) have been developed. A summary of the developed controllers is presented here,

- Complexities encountered for controlling a FLM and literature survey on its adaptive control schemes are described in *Chapter 1*.
- A detailed study of a physical flexible robot with its hardware and software components was made in *Chapter 2*. Subsequently a dynamic model of the TLFM is derived using Euler-Lagrange approach together with the concept of assume mode, the mathematical model is validated using open-loop response of the physical TLFM by exciting its joint with different bang-bang input signals. From the responses i.e. Fig. obtained, it is confirmed that the derived model is appropriate enough to represent the dynamics of the physical TLFM.

- A new direct adaptive control (DAC) is developed to control the tip position of a TLFM while simultaneously suppressing its deflection quickly when subjected to carry different payloads in *Chapter 3*. The developed DAC uses a Lyapunov criterion ensuring the closed-loop system stability. The performance of the developed DAC is then compared with a fuzzy learning based adaptive controller (FLAC). The dynamics of a FLM being uncertain owing to distributed link flexure and payload variation, a fuzzy logic approach was chosen for controlling the TLFM. The performances of the DAC are compared both through simulation and experiments for different payloads i.e. with an initial payload of 0.157 kg and an additional payload of 0.3 kg.
- A new real-time adaptive control of tip trajectory tracking and deflection of a TLFM handling variable payloads using reinforcement learning techniques has been presented in *Chapter 4*. This proposed adaptive controller consists of a proportional derivative (PD) tracking loop and an actor-critic based reinforcement learning loop that adapts the actor and critic weights in response to payload variations while suppressing the tip deflection and tracking the desired trajectory. Tip trajectory tracking and suppression of tip deflection performances of the proposed reinforcement learning based adaptive controller are compared with that of a direct adaptive controller (DAC) and a fuzzy learning based adaptive controller (FLAC) developed in *Chapter 3*. Unlike supervised learning, where the learning is driven by error signal (difference between desired and current response), reinforcement learning, this occurs when an agent learns behavior through trial-and-error interaction with the environment based on “reinforcement” signals from the environment. The benefits of RL based adaptive control are that it generates adaptive optimal control

*online*. The simulation and experimental results show that RLAC indicate excellent accuracy (in terms of tip trajectory tracking and suppression of tip deflections) compared to DAC and FLAC. The superiority of the RLAC over DAC and FLAC is its ability to adapt the actor and critic weights to an optimal value using the proposed Recursive Least Square-Eligibility Trace-Adaptive Memory algorithm (RLS-ET-AM) under variable payload. The convergence critic weights of the RLAC using RLS-ET-AM algorithm have been proved.

- A new multivariable PID self-tuning control (NMSTC) strategy using NARMAX model of the TLFM have been proposed in *Chapter 5* to control the tip trajectory tracking and suppression of tip deflections under unknown payload. The parameters of the PID are adapted *on-line* using a nonlinear autoregressive moving average with exogenous-input (NARMAX) model of the two-link flexible manipulator (TLFM). Advantage of representing the TLFM dynamics as NARMAX model is that the noise term is in the form of coupled function unlike linear model. The developed controller is then compared with the developed reinforcement learning based adaptive controller (RLAC). The advantage of NMSTC is that its parameters are adapted due to change in payload by directly estimating the NARMAX model parameters *on-line* whereas in case of RLAC is based on the actor and critic weights adaptation using the Recursive Least Square-Eligibility Trace-Adaptive Memory algorithm (RLS-ET-AM). The experimental and simulation results envisage that NMSTC outperforms RLAC.
- Subsequently, a NARMAX model-based MPC control strategy is proposed in *Chapter 6* i.e. NMPC which incorporates a nonlinear linear representation of the TLFM model. The proposed NMPC the optimization problem is solved to obtain a new nonlinear model

*online*. NARMAX model based NMSTC uses only *one-step* ahead prediction and considerable time is needed to find an optimum tuning of control parameters. In MPC, the current control action is obtained by solving a finite horizon open loop optimal control problem *online*, at each sampling instant. Hence, the optimization yields an optimal control sequence. From the simulation and experimental results it is established that the proposed NMPC generates appropriate adaptive torque to control tip trajectory tracking and suppression of tip deflection for the TLFM compared to NMSTC, when the manipulator is asked to handle a variable payload. The reason for its superiority is because NMPC generates optimal control sequence by optimum tuning of its control parameters in real time adaptively.

The objectives of the thesis proposed in *Section 1.4* have been achieved by developing new *real-time* adaptive control strategies to alleviate the difficulties of existing adaptive controllers.

## 7.2 Thesis Contributions

- Development of the mathematical model of the physical TLFM and its model validation.
- Development of direct adaptive control (DAC) and a fuzzy learning based adaptive control (FLAC) for the TLFM and their implementations on both simulation and experiment to verify the control performances on achieving simultaneously tip position tracking and suppression of tip deflection while the manipulator is handling different payloads [123].



- Development and real-time implementation of a new RL based adaptive control (RLAC) scheme using RLS-ET-AM algorithm to control the tip trajectory and its deflection when subjected to handle varying payloads for a TLFM. Also comparative assessment of performances of DAC, FLAC and RLAC [121, 122, 123].
- Development of new self-tuning PID control (NMSTC) by exploiting the NARMAX model of the TLFM to control the tip trajectory while suppressing its deflection when subjected to varying payloads and compared its performances with that of the RLAC [124, 125].
- Development of new nonlinear adaptive model predictive control (NMPC) based on NARMAX model of the TLFM and its performance verification of tip trajectory tracking and its deflection with varying payloads with that of NMSTC.

## 7.3 Suggestions for Future Work

### 7.3.1 Adaptive Iterative Learning Control for a TLFM

The proposed research work can be extended to design and develop an adaptive iterative learning controller (AILC) to control the tip trajectory while quickly suppressing its deflection when subjected to handle unknown payloads, and compare its performance with that of NMPC.

In iterative learning control (ILC), learning process uses information from previous repetitions to improve the control signal ultimately enabling a suitable control action. Some previous work show that ILC gives superior performances for systems that operate in a repetitive manner include rigid robot manipulators [126] and point-to-point motion [127]. There lies opportunity to

design an AILC for a TLFM in real-time. The advantage of AILC over ILC is that, unlike the conventional iterative learning control that require some preconditions on the learning gain to stabilize the dynamic systems, the adaptive iterative learning control can achieve the convergence through a learning gain in real-time.

### 7.3.2 Adaptive Visual-Servo Control for a TLFM

In order to increase the performance of the proposed adaptive control strategies for a TLFM one can use a visual-feedback based adaptive control loop for perfect tip trajectory tracking. The closed-loop position control for a robot end-effector using machine vision is known as visual servoing [128]. Visual servoing is the fusion of results from many elemental areas including high speed image processing, kinematics, dynamics, control theory and real-time computing.

Hence, proposed research work can be extended to design a visual servoing based high performance nonlinear adaptive control by giving real-time visual feedback of the tip position.

# Publications

## Journals

- [1] S. K. Pradhan and B. Subudhi, “Real-Time Adaptive Control of a Flexible Manipulator Using Reinforcement Learning,” *IEEE Trans. On Automation Science and Engineering*, vol. 9, no. 2, pp. 237–249, 2012.
- [2] S. K. Pradhan and B. Subudhi, “Nonlinear Adaptive Model Predictive Controller for a Flexible Manipulator: An Experimental Study,” (Revised) *IEEE Trans. on Control System Technology*, April, 2012.
- [3] S. K. Pradhan and B. Subudhi, “Multivariable Self-Tuning PID Control of a Flexible Manipulator Using a NARMAX Model,” (Under Review) *IEEE Trans. on Automation Science and Engineering*, Sep., 2012.

## Conferences

- [1] B. Subudhi, S. K. Pradhan, “Direct adaptive control of a flexible robot using reinforcement learning,” *Proceedings of the IEEE sponsored International Conference on Industrial Electronics, Control & Robotics (IECR), 2010, Rourkela, India, 27-29 Dec. 2010.*
- [2] B. Subudhi and S. K. Pradhan, “Reinforcement Learning Based Adaptive Control of a Two-Link Flexible Manipulator,” *Proceedings of the National System Conference (NSC), 2010, Mangalore, India 10-12 Dec. 2010.*
- [3] S. K. Pradhan and B. Subudhi, “Identification of a Two-Link Flexible Manipulator using NARMAX model,” *Proceedings of India Conference (INDICON), 2011 Annual IEEE, 2011, Hyderabad, India 16-18 Dec. 2011.*

- [4] S. K. Pradhan and B. Subudhi, “Nonlinear Self-Tuning PID control for a Flexible Manipulator based on NARMAX Model,” *Proceedings of Advances in Control and Optimization of Dynamic Systems ACODS-2012, 2012 , IISc Bangaluru, India* 16-8 Feb. 2012.

# Appendix A

## Dynamic Equations of the Two-Link Flexible Manipulator

### A.1 Dynamic Model of the Two-Link Flexible Manipulator

The dynamic model of the two-link flexible manipulator (TLFM) used in designing the adaptive controller for the physical setup is derived based on the assumed modes method with clamped-mass shape functions given by (2.7) is rewritten as

$$\begin{aligned}\varphi_i(l_i) = & C_{1,i} \sin(\beta_i, l_i) + C_{2,i} \cos(\beta_i, l_i) + C_{3,i} \sinh(\beta_i, l_i) \\ & + C_{4,i} \cosh(\beta_i, l_i)\end{aligned}\quad (\text{A.1})$$

where  $\omega_i$  natural frequency of the  $i^{\text{th}}$  link. By applying the boundary condition given in Fig.2.5 (a) the constant coefficients in (A.1) can be determined according to (2.8) and from Fig.2.5 (b) one gets (2.9). The solution for  $\beta_{ij}$  are obtained from (2.9)

$$\det[f(\beta_i, l_i)] = 0 \quad (\text{A.2})$$

which gives a transcendental equation given as

$$\begin{aligned}& (1 + \cos(\beta_i, l_i) \cosh(\beta_i, l_i)) \\ & - \frac{M_{\text{eq}_i} \beta_i}{\rho_i} (\sin(\beta_i, l_i) \cosh(\beta_i, l_i) - \cos(\beta_i, l_i) \sinh(\beta_i, l_i)) \\ & + \frac{J_{\text{eq}_i} \beta_i^3}{\rho_i} (\sin(\beta_i, l_i) \cosh(\beta_i, l_i) + \cos(\beta_i, l_i) \sinh(\beta_i, l_i)) \\ & + \frac{M_{\text{eq}_i} J_{\text{eq}_i} \beta_i^4}{\rho_i^2} (1 - \cos(\beta_i, l_i) \cosh(\beta_i, l_i)) = 0\end{aligned}\quad (\text{A.3})$$

where

$M_{eqi}$  : Equivalent mass of  $i^{th}$  link.

$J_{eqi}$  : Equivalent inertia of  $i^{th}$  link.

On the basis of the discretization introduced in (A.3), and utilizing the Lagrangian formulation defined in (2.1) we drive the dynamic equation of the physical TLFM. In order to solve (2.1) we need generalized coordinate's  $q_i$  comprise of joint angles, joint velocities and modal coordinates. The total kinetic energy of the  $i^{th}$  link which can be expressed as  $(K_T)_i =$  (Total kinetic energy due to  $i^{th}$  joint= $(K_{Th})_i$ ) + (Total kinetic energy due to  $i^{th}$  link= $(K_{Ti})_i$ ) + (Total kinetic energy due to payload  $M_p$ = $(K_{Tp})_i$ ) and the potential energy due to  $i^{th}$  link= $(U_T)_i$ . First the total kinetic energy  $(K_T)_i$  is calculated.

Let us consider the schematic diagram of the TLFM given in Fig.2.4. Let  $A_{li}$  be the cross sectional area of the  $i^{th}$  link. Also, let us assume a point on link-1 by  $p_1(l_1, t)$  as

$$p_1(l_1, t) = R_1(\theta_1) \begin{bmatrix} l_1 \\ \varphi_1(l_1) \delta_1(t) \end{bmatrix} \quad (A.4)$$

where

$$R_1(\theta_1) = \begin{bmatrix} \cos \theta_1 & -\sin \theta_1 \\ \sin \theta_1 & \cos \theta_1 \end{bmatrix}$$

Hence kinetic energy due to link-1 is given as

$$(K_{Ti})_1 = \frac{\rho_1}{2} \int (A l_1 \dot{p}_1^T \dot{p}_1) dl_1 \quad (A.5)$$

Similarly for link-2

$$p_2(l_2, t) = R_1(\theta_1) \left( \begin{bmatrix} l_1 \\ d_1(l_1, t) \end{bmatrix} + R_2(\theta_2) \begin{bmatrix} l_2 \\ d_2(l_2, t) \end{bmatrix} \right) \quad (A.6)$$

where

$$R_2(\theta_2) = \begin{bmatrix} \cos \bar{\theta}_2 & -\sin \bar{\theta}_2 \\ \sin \bar{\theta}_2 & \cos \bar{\theta}_2 \end{bmatrix}$$

$$\bar{\theta}_2 = \theta_2 + d_1(l_1, t)$$

Therefore kinetic energy due to link-2 is

$$(K_{T_1})_2 = \frac{\rho_2}{2} \int (Al_2 \dot{p}_2^T \dot{p}_2) dl_2 \quad (A.7)$$

The kinetic energy due to  $i^{\text{th}}$  joint is

$$(K_{T_h})_i = \frac{J_{h_i} \theta_i^2}{2} + \frac{m_{h_i} \dot{p}_i^T \dot{p}_i}{2} \quad (A.8)$$

The kinetic energy due to payload mass  $M_p$

$$K_{T_p} = \frac{J_p \sum_{i=1}^2 y_{p_i}^2}{2} + \frac{M_p \dot{p}_2^T \dot{p}_2}{2} \quad (A.9)$$

where

$M_{hi}$  : Mass of  $i^{\text{th}}$  joint.

$J_{hi}$  : Equivalent inertia of  $i^{\text{th}}$  joint.

$M_p$  : Payload mass.

$J_p$  : Moment of inertia due to payload mass.

$y_{pi}$  : Redefined tip position of the  $i^{\text{th}}$  link.

Thus the total kinetic energy is obtained as

$$(K_T)_i = \frac{1}{2} \left[ \begin{aligned} &\rho_1 \int (A l_1 \dot{p}_1^T \dot{p}_1) dl_1 \\ &+ \rho_2 \int (A l_2 \dot{p}_2^T \dot{p}_2) dl_2 \\ &+ J_{h_i} \dot{\theta}_i^2 + m_{h_i} \dot{p}_i^T \dot{p}_i \\ &+ J_p \sum_{i=1}^2 y_{p_i}^2 + M_p \dot{p}_2^T \dot{p}_2 \end{aligned} \right] \quad (\text{A.10})$$

and, the total potential energy is given as

$$(U_T)_i = \sum_{i=1}^2 \int_0^{l_i} (EI)_i(l_i) \left[ \frac{d^2 d_i(l_i, t)}{dl_i^2} \right]^2 dl_i \quad (\text{A.11})$$

As a result, taking  $q_i$  as the generalized coordinates i.e.  $q_i = [\theta_i, \dot{\theta}_i, \delta_i, \dot{\delta}_i]^T$  ii along with total kinetic energy and total potential energy from (A.10) and (A.11) respectively the Lagrangian equation given in (2.1) can be rewritten as

$$\frac{d}{dt} \frac{\partial [(K_T)_i - (U_T)_i]}{\partial \dot{q}_i} - \frac{\partial [(K_T)_i - (U_T)_i]}{\partial q_i} = \tau_i \quad (\text{A.12})$$

where,  $\tau_i$  is the generalized vector of torques which, for the case of damped mode shapes is given by

$$\tau_i = \begin{bmatrix} I_{2 \times 2} \\ 0_{2 \times 2} \end{bmatrix} u_i \quad (\text{A.13})$$

a matrix representation for the dynamic model as given in (2.9) of the TLFM is



$$\mathbf{M}(\theta_i, \delta_i) \begin{bmatrix} \ddot{\theta}_i \\ \ddot{\delta}_i \end{bmatrix} + \begin{bmatrix} \mathbf{c}_1(\theta_i, \delta_i, \dot{\theta}_i, \dot{\delta}_i) \\ \mathbf{c}_2(\theta_i, \delta_i, \dot{\theta}_i, \dot{\delta}_i) \end{bmatrix} + \mathbf{K} \begin{bmatrix} 0 \\ \delta_i \end{bmatrix} + \mathbf{D} \begin{bmatrix} 0 \\ \dot{\delta}_i \end{bmatrix} = \begin{bmatrix} \tau_i \\ 0 \end{bmatrix} \quad (\text{A.14})$$

# References

- [1] M. O. Tokhi and A. K. M. Azad, *Flexible Robot Manipulators: Modeling, Simulation and Control*. London, U.K.: IET, 2008.
- [2] H. Geniele, R. V. Patel, and K. Khorasani, “End-point control of a flexible- link manipulator: An experimental study,” *IEEE Trans. Contr. Syst. Technol.*, vol. 5, pp. 556–570, 1997.
- [3] A. J. Koivo and K. S. Lee, “Self-Tuning Control of Planar Two-Link Manipulator with Non-Rigid Arm,” *Proceedings of the International Conference on Robotics and Automation*, Scottsdale, Arizona, USA, May 1989.
- [4] V. Feliu, K. S. Rattan, and B. H. Brown, “Adaptive control of a single-link flexible manipulator,” *IEEE Control System Magazine*, vol. 10, no. 2, pp. 29–33, 1990.
- [5] S. Yurkovich and A. P. Tzes, “Experiments in Identification and Control of Flexible-Link Manipulator,” *IEEE Control System Magazine*, vol. 10, no. 2, pp. 41–46, 1990.
- [6] S Yurkovich, K. L. Hillsley and A. P. Tzes, “Identification and Control for a Manipulator with Two Flexible Links,” *Proceedings of the 29<sup>th</sup> Conference on Decision and Control*, Honolulu, Hawaii, USA, Dec. 1990.
- [7] P. Lucibello, and F. Bellezza, “Nonlinear Adaptive Control of a Two Link Flexible Robot Arm,” *Proceedings of the 29<sup>th</sup> Conference on Decision and Control*, Honolulu, Hawaii, USA, Dec. 1990.

- 
- [8] Y. S. Kim, and J. S. Gibson, "A Variable-Order Adaptive Controller for a Manipulator with a Sliding Flexible Link," *IEEE Trans. on Robotics and Automation*, vol. 7, no. 6, pp. 818–827, 1991.
- [9] T. C. Yang, J.C. S.Yang, and P., Kudva, "Adaptive control of a single-link flexible manipulator with unknown load," *IEE Proceedings D. Control Theory & App.*, vol. 138, no. 2, pp. 153–159, 1991.
- [10] T. C. Yang, J.C. S.Yang, and P., Kudva, "Load Adaptive Control of a Single-Link Flexible Manipulator," *IEEE Trans. Syst. Man and Cybernetics*, vol. 22, no. 1, pp. 85–91, 1992.
- [11] M. Teshnehlab and K. Watanabe, "Self tuning of computed torque gains by using neural networks with flexible structures," *IEE Proceedings Control Theory & App.*, vol. 141, no. 4, pp. 235–242, 1994.
- [12] L. J. Alder, and S. M. Rock, "Experiments in Control of a Flexible-Link Robotic Manipulator with Unknown Payload Dynamics: An Adaptive Approach". *International Journal on Robotics Research*, vol. 13, pp. 481–495, 1993.
- [13] M. Bai, D. H. Zhou and H. Schwarz, "Adaptive Augmented State Feedback Control for an Experimental Planar Two-Link Flexible Manipulator," *IEEE Trans. on Robotics and Automation*, vol. 14, no. 6, pp. 940–950, 1998.
- [14] M.R. Rokui, and K. Khorsani, "Experimental Results on Discrete Time Nonlinear Adaptive Tracking Control of a Flexible-Link Manipulator," *IEEE Trans. on Syst. Man and Cybernetics*, vol. 30, no. 1, pp. 151–164, 2000.

- 
- [15] C.A. Monje, F. Ramos, V. Feliu and B.M. Vinagre, "Tip Position Control of a Lightweight Flexible Manipulator using a Fractional Order Controller," *IET Control Theory Appl.*, vol. 1, no. 5, pp. 1451–1460, 2007.
- [16] J. Becedas, J. R. Trapero, V. Feliu, and H. Sira-Ramírez, "Adaptive Controller for Single-Link Flexible Manipulators Based on Algebraic Identification and Generalized Proportional Integral Control," *IEEE Trans. on Syst. Man and Cybernetics*, vol. 39, no. 3, pp. 735–751, 2009.
- [17] R. Morales, V. Feliu, and V. Jaramillo, "Position control of very lightweight single-link flexible arms with large payload variations by using disturbance observers," *Robotics and Autonomous Systems*, vol. 60, no. 4, pp. 532–547, 2012.
- [18] B. Siciliano, B. S. Yuan and W.J. Book, "Model Reference Adaptive Control of a One Link Flexible Arm," *Proceedings of the 25th IEEE Conference on Decision and Control. Athens, Greece*, 1986.
- [19] J. Yuh, "The Effect of Unmolded Flexible Dynamics in a Discrete-Time Model Reference Adaptive Control of a Flexible Single-Link Robot," *Proceedings of the 25th IEEE Conference on Decision and Control. Los Angeles, California, USA, Dec.* 1987.
- [20] J. M. Skowronski, "Algorithm for Adaptive Control of Two-Arm Flexible Manipulators Under Uncertainty," *IEEE Trans. on Aerospace and Electronic Systems*, vol. 24, no. 5, pp. 562–570, 1988.

- 
- [21] V. G. Moudgal, W. A. Kwong, K. M. Passino and S. Yurkovich, "Fuzzy Learning Control for a Flexible-Link Robot," *IEEE Trans. on Fuzzy Systems*, vol. 3, no. 2, pp. 199–210, 1995.
- [22] A. T. Zaremba, "Adaptive Control of Flexible Link Manipulators Using a Pseudolink Dynamic Model," *Dynamics and Control*, vol. 6, pp. 179–198, 1996.
- [23] J. H. Yang, F. L. Lian, and L. C. Fu, "Nonlinear Adaptive Control for Flexible-Link Manipulators," *IEEE Trans. on Robotics and Automation*, vol. 13, no. 1, pp. 140–148, 1997.
- [24] M. S. de Queiroz, D. M. Dawson, M. Agarwal, and F. Zhang "Adaptive Nonlinear Boundary Control of a Flexible Link Robot Arm," *IEEE Trans. on Robotics and Automation*, vol. 15, no. 4, pp. 779–787, 1999.
- [25] I. Lizarraga, V. Etxebarria, and A. Sanz, "Sliding-Mode Adaptive Control for Flexible-Link Manipulators Using a Composite Design," *Cybernetics and Systems: An International Journal*, vol. 38, pp. 471–490, 2005.
- [26] M. Dogan and Y. Istefannopulos, "Optimal Nonlinear Control Design for Flexible Robot Manipulators with Adaptive Internal Model," *IET Control Theory & Appl.*, vol. 1, no. 3, pp. 770–778, 2007.
- [27] M. Azadi, S. A. Fazelzadeh, M. Eghtesad, and E. Azadi, "Vibration Suppression and Adaptive-Robust Control of a Smart Flexible Satellite with Three Axes Maneuvering," *Acta Astronautica*, vol. 69, pp. 307–322, 2011.

- 
- [28] Z. Mohamed, and M.O. Tokhi, "Vibration control of a single-link flexible manipulator using command shaping techniques," *Proceedings of IMech E-I:Journal of Systems and Control Engineering*, vol. 216, no. 2, pp. 191–210, 2002
- [29] A. Tzes, and S. Yurkovich, "An Adaptive Input Shaping Control Scheme for Vibration Suppression in Slewing Flexible Structures," *IEEE Trans. on Control System Technology*, vol. 1, no. 2, pp. 114–121, 1993.
- [30] M. R. Rokui, and K. Khorasani, "Experimental Results on Adaptive Nonlinear control and Input Preshaping for Multi-Link Flexible Manipulators," *Automatica*, vol. 31, no. 1, pp. 83–97, 1995.
- [31] Y-G Sung, "Adaptive Robust Vibration Control with Input Shaping as a Flexible Maneuver Strategy," *KSME International Journal*, vol. 13, no. 11, pp. 807–817, 1999.
- [32] S. Rhim, and W. J. Book, "Adaptive Time-Delay Command Shaping Filter for Flexible Manipulator Control," *IEEE Trans. on Mechatronics*, vol. 9, no. 4, pp. 619–626, 2004.
- [33] M. Z. Md Zain, M. O. Tokhi, and Z. Mohamed, "Hybrid Learning Control Schemes with Input Shaping of a Flexible Manipulator System," *Mechatronics*, vol. 16, pp. 209–219, 2006.
- [34] M. H. Shaheed and O. Tokhi, "Adaptive closed-loop control of a single-link flexible manipulator," *Journal of Vibration and Control*, DOI: 10.1177/1077546312453066, 2012.

- 
- [35] M. O. T. Cole, and T. Wongratanaphisan, "A Direct Method of Adaptive FIR Input Shaping for Motion Control With Zero Residual Vibration," *IEEE/ASME Trans. on Mechatronics*, vol. 18, no. 1, pp. 316–327, 2013.
- [36] A. Ramakalyan, and M. Gopal, "A Robust Hybrid Controller for Robotic Manipulators using Neural and  $H_\infty$  techniques," *Proceedings of the International Conference on Neural Networks ICNN 96, Washington, USA, Proc.* vol. 2, pp. 120–1208, 1996.
- [37] L. Cheng, Z. G.Hou, and M. Tan, "Adaptive Neural Network Tracking Control for Manipulators with Uncertain Kinematics, Dynamics and actuator Model," *Automatica*, vol. 45, no. 10, pp. 2312–2318, 2009.
- [38] B. K. Roy, A. Patra, S. Mukhopadhyay, and D. C. Saha, "Fault Detection and Diagnosis of a Chemical Reactor by Direct Physical Parameter Estimation," *Paritantra*, vol. 6, no. 1, pp. 37–45, 2001.
- [39] L. B. Gutierrez, F. L. Lewis, and J. A. Lowe, and N. Ahmad, "Implementation of a Neural Network Tracking Controller for a Single Flexible Link: Comparison with PD and PID Controllers," *IEEE Trans. on Industrial Electronics*, vol. 45, no. 2, pp. 307–318, 1998.
- [40] H. A. Talebi, K. Khorasani and, R. V. Patel "Neural Network based Control Schemes for Flexible-Link Manipulators: Simulations and Experiments," *Neural Networks*, vol. 11, pp. 1357–1377, 1998.

- [41] Z. Su and K. Khorasani, "A Neural-Network-Based Controller for a Single-Link Flexible Manipulator Using the Inverse Dynamics Approach," *IEEE Trans. on Industrial Electronics*, vol. 48, no. 6, pp. 1074–1086, 2001.
- [42] L. Tian, J. Wang, and Z. Mao, "Constrained Motion Control of Flexible Robot Manipulators Based on Recurrent Neural Networks," *IEEE Trans. on Syst. Man and Cybernetics-Part B: Cybernetics*, vol. 34, no. 3, pp. 1541–1552, 2004.
- [43] S. C. P. Gomes, V. S. da Rosa, and Bruno de C. Albertini, "Active Control to Flexible Manipulator," *IEEE Trans. on Mechatronics*, vol. 11, no. 1, pp. 75–83, 2006.
- [44] Y. Tang, F. Sun and, Z. Sun "Neural Network Control of Flexible-Link Manipulators using Sliding Mode," *Neurocomputing*, vol. 70, pp. 288-295, 2006.
- [45] S. Kamalasadan and Ade A. Ghandakly, "A Neural Network Parallel Adaptive Controller for Dynamic System Control," *IEEE Trans. on Instrument and Measurement*, vol. 56, no. 5, pp. 1786–1796, 2007.
- [46] A. de A. Neto, L. C. S. Goes, and C. L. Nascimento Jr., "Accumulative Learning using Multiple ANN for Flexible Link Control," *IEEE Trans. on Aerospace and Electronic Systems*, vol. 46, no. 2, pp. 508–524, 2010.
- [47] V. G. Moudgal, K. M. Passino and S. Yurkovich, "Rule-Based Control for a Flexible-Link Robot," *IEEE Trans. on Control System Technology*, vol. 2, no. 4, pp. 392–405, 1994.



- 
- [48] A. Tzes, and K. Kyriakides, "A Hybrid Frequency-Time Domain Adaptive Fuzzy Control Scheme for Flexible Link Manipulators," *Journal of Intelligent and Robotic Systems*, vol. 10, pp. 283–300, 1994.
- [49] J. Lin, and F. L. Lewis, "Fuzzy Controller for Flexible-Link Robot Arm by Reduced-Order Techniques," *IEE Proc-Control Theory Appl.*, vol. 147, no. 3, pp. 177–187, 2002.
- [50] A. Green, and J. Z. Sasiadek, "Heuristic Design of a Fuzzy Control for a Flexible Robot," *IEEE Trans. on Control System Technology*, vol. 14, no. 2, pp. 293–300, 2006.
- [51] Yongming Li, Shaocheng Tong, and Tieshan Li, "Adaptive Fuzzy Output feedback Control for a Single-Link Flexible robot Manipulator Driven DC Motor via Backstepping," *Nonlinear Analysis: Real World Application*, vol. 14, no. 1, pp. 483–494, 2012.
- [52] M. F. Azeem, M. Hanmandlu, and N. Ahmad, "Generalization of adaptive neuro-fuzzy inference systems," *IEEE Trans. on Neural Networks*, vol. 11, pp. 1332–1346, 2000.
- [53] A. E. Merchan-Cruz and A. S. Morris, "Fuzzy-GA-based trajectory planner for robot manipulators sharing a common workspace," *IEEE Trans. on Robotics*, vol. 22, no. 4, pp. 613–624, 2006.
- [54] B. Subudhi and A. S. Morris, "Soft Computing Methods Applied to the Control of a Flexible Robot Manipulator," *Applied Soft Computing*, vol. 9, no. 1, pp. 149–158, 2009.

- 
- [55] F. M. Caswara, and H. Unbehauen “A Neurofuzzy Approach to the Control of a Flexible-Link Manipulator,” *IEEE Trans. on Robotics and Automation*, vol. 18, no. 6, pp. 932–944, 2002.
- [56] R. J. Wai and M-C Lee, “Intelligent Optimal Control of Single-Link Flexible Robot Arm,” *IEEE Trans. on Industrial Electronics*, vol. 51, no. 1, pp. 201–220, 2004.
- [57] S. Kamalasadan and Ade A. Ghandakly, “A Neural Network Parallel Adaptive Controller for Dynamic System Control,” *IEEE Trans. on Instrument and Measurement*, vol. 56, no. 5, pp. 1786–1796, 2005.
- [58] A. Madkour, M. A. Hossain, K. P. Dahal and, H. Yu, “Intelligent Control for Active Vibration Control,” *IEEE Trans. on System, Man, and Cybernetics-Part C: Application and Reviews*, vol. 37, no. 5, pp. 1022–1033, 2007.
- [59] A. G. Barto, R. S. Sutton, and C. W. Anderson, “Neuron like Adaptive Elements that can Solve Difficult Learning Control Problems,” *IEEE Trans. on Syst. Man and Cybernetics*, vol. 13, pp. 834–846, 1983.
- [60] R. S Sutton, and A. G Barto, *Reinforcement Learning: An Introduction*. Cambridge, MA: MIT Press. 1998.
- [61] W. J. Book, “Recursive Lagrangian dynamics of flexible manipulator arms”, *Int. Journal. of Robotics Research*, vol. 3, no. 3, pp. 87-101, 1984.
- [62] M. J. Balas, “Trends in large space structures control theory: Fondest hopes, wildest dreams”, *IEEE Trans. on Automatic Control*, vol. 27, no. 3, pp. 522-535, 1982.

- 
- [63] R. H. Cannon, Jr. and E. Schmitz, "Initial experiments on the end-point control of a flexible one-link robot," *Int. Journal. of Robotics Research* vol. 3, no. 3, 1984.
- [64] W. Wang, S. Lu, and, C. Hsu, "Experiments on the position control of a one-link flexible robot arm," *IEEE Transactions on Robotics and Automation*, vol. 5, no. 3, pp.131-138, 1989.
- [65] D. Wang, "Modelling and control of multi-link manipulators with one flexible link," Ph. D. Thesis, Department of Electrical Engineering, University of Waterloo, Canada, 1989.
- [66] D. Wang, and, M. Vidyasagar, "Transfer functions for a single flexible link," *International Journal of Robotics Research*, vol. 10, no. 5, pp. 540–549, 1991.
- [67] A. De Luca, and, B. Siciliano, "Trajectory control of a non-linear one-link flexible arm," *International Journal of Control*, vol. 50, no. 5, pp. 1699–1715, 1989.
- [68] –, "Closed-form dynamic model of planar multi-link lightweight robots," *IEEE Transactions on Systems, Man, and Cybernetics*, vol. 21, no. 4, pp. 826–839, 1991.
- [69] M. A. Ahmad, Z. Mohamed and, N. Hambali, "Dynamic modelling of a two-link flexible manipulator system incorporating payload," *Proceedings of 3rd IEEE Conference on Industrial Electronics and Applications (ICIEA 2008)*, 3–5 June 2008, Singapore.
- [70] B.Subudhi and, A.S.Morris, "Dynamic modelling, simulation and control of a manipulator with flexible links and joints," *Robotics and Autonomous Systems*, vol.41, No.4, pp.257–270, 2002.

- 
- [71] Quanser Consulting Inc., Markham, ON, Canada, “2-DOF Serial Flexible Link Robot Reference Manual,” Doc. No. 763, Rev. 1, 2008.
- [72] W. J. Book, “*Modeling, Design and Control of flexible manipulator arms*,” Ph. D. Thesis, Department of Mechanical Engineering, Massachusetts Institute of Technology, Cambridge MA, 1974.
- [73] O. Maizza-Neto, “*Modal analysis and control of flexible manipulator arms*,” Ph. D. Thesis, Department of Mechanical Engineering, Massachusetts Institute of Technology, Cambridge MA, 1974.
- [74] W. J. Book, O. Maizza-Neto, and, D. E. Whitney, “Feedback control of two beams, twojoint systems with distributed flexibility,” *Journal of Dynamic Systems, Measurement and Control, Transactions of the ASME*, vol. 97G, no. 4, pp. 424–431, 1975.
- [75] W. J. Book, and, M. Majette, “Controller design for flexible, distributed parametermechanical arms via combined state space and frequency domain techniques,” *Journal of Dynamic Systems, Measurement and Control, Transactions of the ASME*, vol. 105, no. 4, pp. 245–254, 1983.
- [76] W. J. Book, “Controlled motion in an elastic world,” *Journal of Dynamic Systems, Measurement and Control, Transactions of the ASME*, vol. 115, no. 2, pp. 252–261, 1993.

- [77] M. Moallem, K. Khorasani, and R. V. Patel, "Inversion-based sliding control of a flexible-link manipulator," *International Journal of Control*, vol. 71, no. 3, pp. 477–490, 1998.
- [78] B.Subudhi and A.S.Morris, "Singular perturbation approach to trajectory tracking of flexible robot with joint elasticity," *International Journal of Systems Science*, vol.34, no.3, pp.167–179, 2003.
- [79] J. J. E. Slotine and L. Weiping, "Adaptive Manipulator Control: A Case Study," *IEEE Trans. on Automatic Control*, vol. 33, no. 11, pp. 995–1003, 1988.
- [80] B. Van Roy, B., D. Bertsekas, Y. Lee, and, J. Tsitsiklis, J, "A neuro-dynamic programming approach to retailer inventory management," *Proceedings of the 36th IEEE conference on decision and control*, 1997.
- [81] I. Rudowsky, M. Kulyba, M. Kunin, S. Parsons, and, T. Raphan, "Reinforcement learning interfaces for biomedical database systems," *Proceedings of the 28th IEEE EMBS annual international conference*, New York City, USA, 2006.
- [82] D. Ernst, M. Glavic, P. Geurts, and, L. Wehenkel, "Approximate value iteration in the reinforcement learning context: Application to electrical power system control," *International Journal of Emerging Electric Power Systems*, vol. 3, no. 1, pp. 1066.1–1066.37, 2005.
- [83] E. Kampen, Q. Chu, and, J. Mulder, "Online adaptive critic flight control using approximated plant dynamics," *Proceedings of the International conference on machine learning and cybernetics*, 2006.

- 
- [84] W. Liu, Y. Tan, and Q. Qiu, "Enhanced Q-learning algorithm for dynamic power management with performance constraint," *In Design, automation test in Europe conference exhibition (DATE)*, 2010.
- [85] P. Stingu, and, F. Lewis, "Adaptive dynamic programming applied to a 6dof quad-rotor," *In B. Igel'nik (Ed.), Computational modeling and simulation of intellect: Current state and future perspectives. IGI Global*, 2010
- [86] W. Smart, and, L. Kaelbling, "Reinforcement learning for robot control," *In D. Gage, & H. Choset (Eds.), Society of photo-optical instrumentation engineers (SPIE) conference series*, vol. 4573, pp. 92–103, 2002.
- [87] L. A Prashanth and, S. Bhatnagar, "Reinforcement Learning with Function Approximation for Traffic Signal Control," *IEEE Trans. on Intelligent transportation Systems*, vol. 12, pp. 412–421, 2011.
- [88] Q. Yang and S. Jagannathan, "Reinforcement Learning Control for Affine Nonlinear Discrete-Time Systems using Online Approximators," *IEEE Trans. on Syst. Man and Cybernetics-Part B: Cybernetics*, pp. 1–14, 2011.
- [89] S. J. Bradtke and A. G. Barto, "Linear Least-Squares Algorithms for Temporal Difference learning," *Machine Learning*, vol. 22, pp. 33-57, 1996.
- [90] X. Xu, D. Hu, and, X. Lu, "Kernel-based least squares policy iteration for reinforcement learning," *IEEE Transactions on Neural Networks*, vol. 18, no. 4, pp. 973–992, 2007.

- 
- [91] D. Vrabie, O. Pastravanu, M. Abu-Khalaf, and, F. Lewis, "Adaptive optimal control for continuous-time linear systems based on policy iteration," *Automatica*, vol. 45, no. 2, pp. 477–484, 2009.
- [92] F. L. Lewis, and, D. Vrabie, "Reinforcement learning and adaptive dynamic programming for feedback control," *Circuits and Systems Magazine*, vol. 9, no. 3, pp. 32–50, 2009.
- [93] S. Chen and S. A. Billings, "Representations of nonlinear systems: the NARMAX model," *Int. Journal of Control*, vol. 49, no. 3, pp. 1013–1032, 1989.
- [94] S. Kukreja, L. H. L. Galiana, and Kearney, R. E. , "NARMAX Representation and Identification of Ankle Dynamics," *IEEE Trans. on Biomedical Eng.*, vol. 50, no. 1, pp. 70-81, 2003.
- [95] J. S. H. Tsai, C. T. Yang, C. C. Kuang, S. M. Guo, L. S. Shieh, and C. W. Chen, "NARMAX model-based state-space self-tuning control for nonlinear stochastic hybrid systems.," *Journal of Applied Mathematical Modelling*, vol. 31, no. 1, pp. 3030-3054, 2010.
- [96] B. Subudhi, and D. Jena, "A differential evolution based neural network approach to nonlinear system identification," *Applied Soft Computing*, vol. 1, no. 1, pp. 861–871, 2011.
- [97] M. Agarwal, and D. E. Seborg, "Self-tuning Controllers for Nonlinear Systems," *Automatica*, vol. 23, no. 1, pp. 2009–2014, 1987.

- 
- [98] T. Yamamoto, and S. L. Shah, "Design and experimental evaluation of a multivariable self-tuning PID controller," *IEEE Proc. Control Theory Appl.*, vol. 151, no. 5, pp. 645–652, 2004.
- [99] H. Peing, W. Gui, H. Shioya, and R. A Zou, "Predictive Control Strategy for Nonlinear NO<sub>x</sub> Decomposition Process in Thermal Power Plants," *IEEE Trans. on Syst. Man and Cybernetics-Part A: Systems and Humans*, vol. 36, no. 5, pp. 904–921, 2006.
- [100] C. T. Wang, J. S. H. Tsai, C. W. Chen, Y. Lin, S. M. Guo, and L. S. Shieh, "An Active Fault-Tolerant PWM Tracker for Unknown Nonlinear Stochastic Hybrid Systems: NARMAX Model and OKID Based State-Space Self-Tuning Control," *Journal of Control Science and Engineering*, vol. 1, pp. 1–22, 2010.
- [101] D. W. Clarke, C. P. S. Mohtadi, and Tuffs, "Generalized predictive control-Part I. The basic algorithm," *Automatica*, vol. 23, no. 2, pp. 137–148, 1987.
- [102] C. E. Garcia, D. M. Prett, and M. Morari, "Model Predictive Control: Theory and practice-a survey," *Automatica*, vol. 25, no. 3, pp. 335–348, 1989.
- [103] M. Morari and J. H. Lee, "Model Predictive Control: Past, Present and Future," *Computer and Chemical Engineering*, vol. 23, pp. 667–682, 1999.
- [104] S. Piche, B. Sayyar-Rodsari, D. Johnson, and M. Gerules, "Nonlinear Model Predictive Control using Neural Network," *IEEE Control System Magazine*, vol. 20, no. 3, pp. 55–62, 2000.



- 
- [105] J. B. Rawlings, and K. R. Muske, "Stability of constrained receding horizon control," *IEEE Transaction on Automatic Control*, vol. 38, no. 10, pp. 1512–1516, 1993.
- [106] J.M. Maciejowski, *Predictive Control with Constraints*. Prentice Hall, Englewood Cliffs, 2002.
- [107] H. H. J. Bloemen, M. Cannon, and B. Kouvaritakis, "An interpolation strategy for discrete-time bilinear MPC problems," *IEEE Transactions on Automatic Control*, vol. 45, no. 5, pp. 775–778, 2002.
- [108] D. Nagrath, V. Prasad, and B. W. Bequette, "A Model Predictive Formulation for control of Open-Loop Unstable Cascade Systems," *Chemical Engineering Science*, vol. 57, pp. 365–378, 2002.
- [109] R. Srhriddhar, and D. J. Cooper, "A Novel Tuning Strategy for Multivariable Model predictive Control," *ISA Transactions*, vol. 36, no. 4, pp. 273–280, 1998.
- [110] J. Yang, S. Li, X. Chen, and Q. Li, "Disturbance Rejection of Dead-time Process Using Disturbance Observer and Model Predictive control," *Chemical Engineering Research and Design*, vol. 89, pp. 125–135, 2011.
- [111] A. A. Patwardhan, G. T. Wright, and T. F. Edgar, "Nonlinear Model Predictive Control of a Distributed-Parameter Systems," *Chemical Engineering Science*, vol. 47, pp. 721–735, 1992.
- [112] C-H Lu, and C-C Tsai, "Adaptive Predictive Control with Recurrent Neural Network for Industrial Processes: An Application to Temperature Control of a Variable-Frequency

- 
- Oil-Cooling Machine,” *IEEE Transactions on Industrial Electronics*, vol. 55, no. 3, pp. 1366–1375, 2008.
- [113] M. Hassan, R. Dubay, C. Li, R. Wang, “Active vibration control of a flexible one-link manipulator using a multivariable predictive controller,” *Mechatronics*, vol. 17, pp. 311–323, 2007.
- [114] P. Boscariol, A. Gasparetto, and V. Zanutto, “Model Predictive Control of a Flexible Links Mechanism,” *Journal of Intelligence Robot System*, vol. 58, pp. 125–147, 2010.
- [115] M. Hassan, R. Dubay, C. Li, and, R. Wang, “Active vibration control of a flexible one-link manipulator using a multivariable predictive controller,” *Mechatronics*, vol. 17, pp. 311–323, 2007.
- [116] P. Boscariol, A. Gasparetto, and, V. Zanutto, “Vibration reduction in a single-link flexible mechanism through the synthesis of an MPC controller,” *Proceedings of IEEE Int. Conf. on Mechatronics*, Malaga, Spain, 2009.
- [117] L. He, T. Shen, L. Yu, N. Feng, and, J. Song, “A Model Predictive Control-based Torque Demand Control Approach for Parallel Hybrid Power trains,” *IEEE Trans. on Vehicular Technology*, (doi: 10.1109/TVT.2012.2218291), 2012.
- [118] M. Richter, M. E. Magana, O. Sawodny, and, T. K. A. Brekken, “Nonlinear Model Predictive Control of a Point Absorber Wave Energy Converter,” *IEEE Trans. on Sustainable Energy*, (doi: 10.1109/TSTE.2012.2202929), 2012.

- 
- [119] M. Preindl, and, S. Bolognani, "Model Predictive Direct Torque Control with Finite Control Set for PMSM Drive Systems, Part 2: Field Weakening Operation," *IEEE Trans. on Industrial Informatics*, (doi: 10.1109/TII.2012.2220353), 2012.
- [120] M. A. S. Kamal, M. Mukai, J. Murata, and, T. Kawabe, "Model Predictive Control of Vehicles on Urban Roads for Improved Fuel Economy," *IEEE Trans. on Control Systems Technology*, (doi: 10.1109/TCST.2012.2198478), 2012.
- [121] B. Subudhi, S. K. Pradhan, "Direct adaptive control of a flexible robot using reinforcement learning," *Proceedings of the IEEE sponsored International Conference on Industrial Electronics, Control & Robotics (IECR), 2010, Rourkela, India, 27-29 Dec. 2010.*
- [122] B. Subudhi and S. K. Pradhan, "Reinforcement Learning Based Adaptive Control of a Two-Link Flexible Manipulator," *Proceedings of the National System Conference (NSC), 2010, Mangalore, India 10-12 Dec. 2010.*
- [123] S. K. Pradhan and B. Subudhi, "Real-Time Adaptive Control of a Flexible Manipulator Using Reinforcement Learning," *IEEE Trans. On Automation Science and Engineering*, vol. 9, no. 2, pp. 237–249, 2012.
- [124] S. K. Pradhan and B. Subudhi, "Identification of a Two-Link Flexible Manipulator using NARMAX model," *Proceedings of India Conference (INDICON), 2011 Annual IEEE, 2011, Hyderabad, India 16-18 Dec. 2011.*
- [125] S. K. Pradhan and B. Subudhi, "Nonlinear Self-Tuning PID control for a Flexible Manipulator based on NARMAX Model," *Proceedings of Advances in Control and*

- Optimization of Dynamic Systems ACODS-2012, 2012 , IISc Bangaluru, India 16-8 Feb. 2012.*
- [126] B. Bukkems, D. Kostic, B. de Jager, and, M. Steinbuch, “Learning-based identification and iterative learning control of direct-drive robots,” *IEEE Trans. On Control Systems Technology*, vol.13, no.4, pp. 537- 549, 2005.
- [127] C. T. Freeman, C. Zhonglun, E. Rogers, and, P. L. Lewin, “Iterative Learning Control for Multiple Point-to-Point Tracking Application,” *IEEE Trans. On Control Systems Technology*, vol.19, no.3, pp.590-600, 2011.
- [128] S. Hutchinson, G. D. Hager, and, P. I. Corke, “A tutorial on visual servo control,” *IEEE Trans. on Robotics and Automation*, vol.12, no.5, pp.651-670, 1996.

# Santanu Kumar Pradhan

Assistant Professor

Department of Electrical & Electronics Engineering

Birla Institute of Technology, Mesra, Ranchi

Ranchi-835215, India

E-mail: [santanupradhan.nitrkl@gmail.com](mailto:santanupradhan.nitrkl@gmail.com)

## Qualification

- Ph.D. (Continuing)(2009-till date)  
Electrical Department, NIT Rourkela
- M.Tech. (Energy System)(2007-2009)[First division]  
Indian Institute of Technology, Roorkee
- B.E (Electrical and Electronics Engineering)(2002-2006)[First division]  
Biju Patnaik University of Technology, Orissa

## Publications

- 01 Journal Articles
- 04 Conference Papers

## Permanent Address

Village-Kurulua, P.O-Chakradharpur,

Singhbhum (West), 833102, Jharkhand, India

## Date of Birth

March 21, 1980